COLLISIONAL - RADIATIVE MODEL FOR NON - LTE HELIUM PLASMAS

A Thesis Submitted
In Partial Fulfilment of the Requirements
for the Degree of

DOCTOR OF PHILOSOPHY

by

HARISH CHANDRA SRIVASTAVA

to the

DEPARTMENT OF CHEMISTRY

INDIAN INSTITUTE OF TECHNOLOGY, KANPUR

JULY, 1982

TO FOND MEMORIES OF MY FATHER

DEPARTMENT OF CHEMISTRY
INDIAN INSTITUTE OF TECHNOLOGY, KANPUR

CERTIFICATE I

This is to certify that Mr. H.C. Srivastava has satisfactorily completed all the courses required for the Ph.D. degree programme. These courses include:

Chm	500	Mathematics for Chemists I
Chm	521	Chemical Binding
Chm	524	Modern Physical Methods in Chemistry
Chm	541	Advanced Inorganic Chemistry I
Chm	800	General Seminar
Chm	801	Graduate Seminar
Chm	900	Graduate Research

Mr. H.C. Srivastava successfully completed his Ph.D. Qualifying Examination in January 1979.
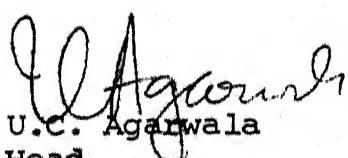
U.C. Agarwala
Head
Department of Chemistry
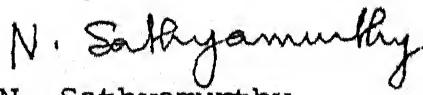
N. Sathyamurthy
Convener
Departmental Postgraduate Committe
Department of Chemistry

CERTIFICATE II

Certified that the work 'Collisional-Radiative Model for non-LTE Helium Plasmas' has been carried out by Mr. H.C. Srivastava under my supervision and the same has not been submitted elsewhere for a degree.

P.K. Ghosh
Thesis Supervisor

ACKNOWLEDGEMENTS

CONTENTS

LIST OF TABLES

LIST OF FIGURES

LIST OF SYMBOLS

a_i	Zeros of Laguerre polynomial
$a_{i,j}$	Element of ith row and jth column of matrix A
a_o	Bohr radius
A,B,C,D,E,F,X	Matrices representing collisional-radiative processes
$A^{-1}(i,j)$	Element of the ith row and jth column of the inverse of matrix A
$A(p,q)_{p>q}$ $A(i,j)_{i>j}^{p>q}$	Spontaneous transition probabilities of HeI(p-q) and HeII(i,j) transitions
$B(p,q), B(q,p)$	Einstein coefficients
B'	Ratio $n(2^1S)/n(1^1S)$
c	First continuum, velocity of light
C'	Defined in Eq. (2.35)
D'	Ratio $n(2^3S)/n(1^1S)$
E_e	Electron energy
E_H^1	Ionization potential of hydrogen
E_p	Energy (cm^{-1}) of the pth level of HeI
E_i	Energy (cm^{-1}) of the ith level of HeII
$E_p', E'(j)$	Ionization energies (eV) of HeI and HeII levels
E_1^+	Ionization potential of ground state of HeII
$\Delta E'(j)$	Lowering of ionization energy due to electric microfields
$E_{p,q}, E_{i,j}$	Excitation energies of HeI(p-q) and HeII(i-j) transitions
E_{pi}	Excitation energy from pth level of HeI to ith level of HeII
$E_p(t)$	Enhancement in population density of level p at time t

$f(p,q), f(i,j)$	Oscillator strengths of HeI (p-q) and HeII(i-j) transitions
$f(v)$	Velocity distribution function
g_p, g_i	Weight factors of pth level of HeI and ith level of HeII
$g(\nu)$	Free bound Gaunt factor
$g(\nu - \nu_o)$	Normalized Gaussian line shape function
$g(U_{p,q})$	Term defined by Eq. (2.17)
h	Planck's constant
HeI, HeII	Neutral helium and singly charged helium ion
H_i	Weight factors of Laguerre polynomials
i,j	Energy levels of HeII
i_{ep}	Probe electron current
I_o, I_B	Intensities of a spectral line at zero and B magnetic fields
J_+	Probe ion saturation current
k	Boltzmann constant
$^\circ K$	Degree Kelvin
$K(p,q), K(q,p)$	Electron impact excitation, (p-q), deexcitation (q-p) rate coefficients for HeI
$K(i,j), K(j,i)$	Electron impact excitation (i-j), deexcitation (j-i) rate coefficients for HeII
$K(p,i)$, $K(i,p)_{i=1}$	Electron impact ionization (p-i), three body recombination (i-p) rate coefficients
$K(i,c), K(c,i)$	Electron impact ionization, recombination rate coefficients for HeII
$KN(p,q)$, $KN(q,p)$	Neutral-neutral excitation (p-q), deexcitation (q-p) rate coefficients
$KN(p,i)$, $KN(i,p)$	Neutral-neutral ionization (p-i), recombination (i-p) rate coefficients
$L(t)$	Shape function of the laser pulse
m_e	Electron mass

m_{He}	Mass of helium atom
n	Principal quantum number
n_e	Electron density (cm^{-3})
$n(1), n^+(1), n^{++}$	Ground state population densities of HeI, HeII and doubly charged helium ion
$n(p), n^+(i)$	Population densities of HeI (level p) and HeII (level i)
$n_E(p), n_E^+(i)$	Saha equilibrium population densities of HeI (level p) and HeII (level i)
p, q	Energy levels of HeI
$q_{p,q}$	Electron impact cross sections (p - q)
q_{pi}	Direct ionization excitation cross section (p-i)
$r_o(p), r_1(p)$	Population coefficients for HeI (level p)
$r_o^+(i), r_1^+(i), r_2^+(i)$	Population coefficients for HeII (level i)
R_B	Ratio I_B/I_o
T_e	Electron temperature
T_g	Gas temperature
T_{excit}	Excitation temperature
T_{kin}	Kinetic temperature
T_{rad}	Radiation temperature
T_{react}	Reaction temperature
T_{wall}	Wall temperature
U_{ij}	Defined in Eq. (2.32)
$U_{p,q}$	Defined as $E_e/E_{p,q}$
v_k^l	Relative velocity between the particles of kind k and l
w_p'	Ionization energy of level p of HeI in units of kT_g
$W_{p,q}$	Excitation energy in units of kT_g

$W(p,q), W(q,p)$	Rates of induced absorption and emission
x	Defined as E_e/E_p', $E_e/E_{p i}$
$x_{11}^{2 \times 2}$ etc.	Element of first row and first column of matrix X
x_{ij}	Element of ith row and jth column of matrix X
$\bar{x}$	Ratio $n_e/n^+(1)$
x_o, x_{casc}	Line intensity ratios without and with cascade corrections
$\bar{Y}$	Ratio n_e/n^{++}
Y	Term $(U_{pq} - 1)$
z	Nuclear charge
Z	Term αY
α	Ratio $E_{p,q}/kT_e$, E_p/kT_e
$\alpha_{p,q}, \beta_{p,q}$	Constants in Eq. (2.17)
α_{ij}	Defined in Eq. (2.32)
$\beta(p), \beta(i)$	Radiative recombination coefficients for HeI (level p) and HeII (level i)
λ_{ij}	Wavelength of transition $i \to j$
$\Lambda_{p,q}, \Lambda_{i,j}$	Optical escape factors for HeI($p \to q$) and HeII ($i \to j$) transitions
$\hat{\tau}$	Optical depth
$\rho(p), \rho^+(i)$	Reduced population coefficients for HeI (level p) and HeII (level i)
$\rho(\nu)$	Radiation density per unit frequency interval
Θ	Reduced electron temperature
$\eta(c)$	Reduced electron density
$\eta(p)$	Reduced population density
ν, ν_o	Frequency, central frequency
$\Delta\nu$	Spectral line width
σ	cross section
ξ_p	Number of equivalent electrons in shell p
τ	FWHM (nsec) of laser pulse

ABSTRACT

A theoretical study of a collisional-radiative model of low temperature (kT_e = 1-20 eV) helium plasmas has been carried out. The model treats HeI and HeII levels together, includes the processes of direct ionization-excitation, heavy particle collisions and the effect of optical pumping by a laser pulse. Comparisons have been made between calculated population densities of excited states and those available in the literature from experiments of other workers.

A comparison of the theoretical results of the present work with the results of the steady state experiments on helium plasmas shows that agreement is good at low electron temperatures. The direct ionization-excitation process has been found to be important in populating HeII levels at $kT_e > 2$ eV and $n_e < 10^{12}$ cm^{-3}. A procedure for simplification of the elaborate model has also been worked out, and by application of this procedure it has been shown that with suitable neglect of even 70% of the atomic processes, population densities can be predicted within 20% of the results obtained from elaborate models. This simplified model works satisfactorily in the range kT_e = 4-20 eV and $n_e = 10^6$-10^{12} cm^{-3}. Application of the model used in the present work to several recent pulsed laser excitation studies on helium plasmas (at torr range gas pressures) indicate a need of lower values of heavy particle rate coefficients and higher values of optical escape factors at torr range pressures than those used in recent

literature. On the basis of calculations carried out on the method of determining electron temperature from line intensity ratios, it has been concluded that at electron densities $> 10^9$ cm^{-3}, the line intensity ratio method is not suitable for determination of electron temperature.

CHAPTER 1

INTRODUCTION

The study of instantaneous population densities of excited atoms and ions in gaseous plasmas is of considerable importance from the viewpoint of spectroscopic diagnosis. Emission of line radiation associated with cooling of plasma constitutes an important source of information on the various collisional-radiative processes occurring therein. These processes include electron impact excitation, deexcitation, ionization, recombination, neutral-neutral collisions etc. Besides low-temperature laboratory plasmas, there is also much interest in astrophysical plasmas, fusion plasmas, afterglow plasmas and laser plasmas. A study of laboratory plasmas can provide insight into the various processes that occur in astrophysical plasmas. In almost all types of plasmas the study of the population densities of excited atomic and ionic species are of much importance.

As a result of various excitation processes in a plasma, the higher energy states of atoms and ions are populated which in turn depopulate by various mechanisms e.g. spontaneous emission, collisional transfer etc. Emission of radiation is perhaps the most easily noted plasma phenomenon. Plasma emissivity can be used for identification of plasma constituents as well as determining plasma conditions in laboratory as well as in remote astrophysical plasmas.

The concept of complete/local thermodynamic equilibrium (CTE/LTE) is of great importance in plasma spectroscopy.[1,2] In complete thermodynamic equilibrium, all the properties of a plasma, enclosed in a black body of wall temperature T_{wall} can be uniquely described by this temperature. In CTE, the kinetic energy distribution of all plasma particles is given by Maxwell-Boltzmann distribution function of kinetic temperature T_{kin}, the Planck's law determines the distribution of the radiation field with a radiation temperature T_{rad}, excited states are populated according to the Boltzmann distribution law with the excitation temperature T_{excit} and the atoms, molecules, ions, and electrons are distributed according to the mass action law with reaction temperature T_{react}. In CTE, all these temperatures are equal to one another, hence

$$T = T_{wall} = T_{kin} = T_{rad} = T_{excit} = T_{react}.$$

The condition of CTE is realized under very special conditions. The core of plasmas formed during the short time interval of strong explosions, the state of plasma in interior of stars are examples of plasmas in CTE. It is practically very difficult to realize plasmas in CTE under laboratory conditions. However, a large class of plasmas exists in what is known as local thermodynamic equilibrium (LTE). Except Planck's radiation law, the plasmas in LTE obey all thermodynamic distribution laws applicable to CTE plasmas. However, the role of radiation in the establishment of local thermodynamic equilibrium is important at low electron densities. Here, the radiation field produced by the plasma (given by Kirchoff's law) interacts with

the plasma constituents and this interaction contributes to radiative transfer processes. LTE plasmas exist only when the following condition[3,4] is satisfied

$$n_e \geq 1.2 \times 10^{12} \, T_e^{1/2} \, E_{p,q}^3 \qquad (1.1)$$

where n_e is the electron density, T_e the electron temperature in °K and $E_{p,q}$ is the excitation energy from level p to level q in electron volts. For helium the values of n_e above which LTE will exist at electron temperatures of 1, 10 and 20 eV are respectively 1.9×10^{18} cm^{-3}, 6.08×10^{18} cm^{-3} and 8.59×10^{18} cm^{-3}.

In LTE plasmas, the Saha-Eggert equation is valid and correlates the population density of a species having charge z-1 to the population density of its next ionic species with charge z as follows[1,4]:

$$\frac{n_z(1)n_e}{n_{E_{z-1}}(j)} = \frac{2g_z(1)}{g_{z-1}(j)} \left(\frac{2\pi \, m_e kT_e}{h^2}\right)^{3/2} \exp\left(-\frac{E'_{z-1}(j) - \Delta E'_{z-1}}{kT_e}\right)$$

$$(1.2)$$

where $n_z(1)$ and $n_{E_{z-1}}(j)$ are respectively the population density of the ground state of ion of charge z and Saha equilibrium population density of the jth level of species of charge z-1, n_e and T_e are respectively the electron density and electron temperature. $E'_{z-1}(j)$ is the ideal ionization energy of level j and $\Delta E'_{z-1}$ is the lowering of ideal ionization energy due to electric micro fields, $g_z(1)$ and $g_{z-1}(j)$ are the multiplicities of the levels. The Boltzmann equation correlates $n_{E_{z-1}}(j)$ with $n_{E_{z-1}}(1)$ as follows:

$$\frac{n_{E_{z-1}}(j)}{n_{E_{z-1}}(1)} = \frac{g_{z-1}(j)}{g_{z-1}(1)} \exp\left(-\frac{E'_{z-1}(1) - E'_{z-1}(j)}{kT_e}\right) \qquad (1.3)$$

Under laboratory and many native conditions, however, most plasmas neither follow the classical thermodynamic equilibrium relations[5] nor satisfy CTE conditions. They are even far from being in LTE and represent an open system having temperature and density gradients. The reabsorption is very weak and most of the photons may escape. Under such conditions the populations of discrete levels are not described by T_e alone and cannot be calculated simply by applying Boltzmann distribution law. This class of plasmas,which does not obey classical thermodynamic equilibrium relations is termed as non-LTE plasmas.

The properties of non-LTE plasmas can only be described by taking into consideration the various processes involving (a) electron impact excitation, deexcitation, ionization, recombination (b) photo-excitation, deexcitation, ionization, and (c) diffusion etc. By considering all the processes responsible for population and depopulation of all individual levels, coupled rate equations describing the rate of change of populations of the levels with respect to time can be written[1] in terms of Einstein coefficients for spontaneous emission and absorption, $A(p,q)$ and $B(p,q)$ besides various collisional excitation and deexcitation rate coefficients K's. The collisional coefficient K of particles of kind k and l is given by

$$K = \int_V \sigma_k^l(v_k^l) \, f_k(v_k^l) \, v_k^l \, dv \qquad (1.4)$$

where $f_k(v_k^l)$ represents the velocity distribution function of the relative velocity v_k^l between the particles of kind k and l. $\sigma_k^l(v_k^l)$ is the cross section as a function of v_k^l. The distribution function $f(v)$ is obtained by solving the Boltzmann collision equation[2] with the proper initial and final conditions.

In non-LTE plasmas the excited state populations deviate from the Saha equilibrium populations due to radiation losses and diffusion fluxes. The departures of the population densities of excited states from Saha population densities are generally expressed in terms of reduced population coefficients (Saha decrements[1,6,7]) $\rho(j)$ and defined as

$$\rho(j) = \frac{n(j)}{n_E(j)} \qquad (1.5)$$

where $n(j)$ denotes the non-LTE population density of the jth level and $n_E(j)$ represents the Saha equilibrium population density.

Thus in non-LTE conditions the population densities of excited states can be calculated only by simultaneously solving the coupled rate equations obtained on the basis of a collisional-radiative model. The role of electron impact processes depend on the magnitudes of electron density, electron temperature and electron impact cross sections. Similarly cross sections of photon induced processes and the magnitude of the photon flux in the plasma decide the role of photon-induced processes. From the viewpoint of photon induced processes, one can classify plasmas in two categories. When the plasma conditions are such that all radiations can freely escape from the plasma without absorption, the plasma is called optically thin plasma. In contrast, when

the plasma reabsorbs the escaping photons either completely or partially, one has either optically thick or partially optically thick plasma. This absorption phenomenon is quantitatively incorporated in the collisional-radiative model through optical escape factors.[8,9,10] In optically thin case, the optical escape factors of all radiations can be taken as unity but in partially optically thick case, the optical escape factors are less than one, the magnitude depending on the nature of excitation transition, electron density, gas pressure etc. In case of complete absorption, the optical escape factor is taken as zero.

A collisional-radiative model is a versatile and convenient aid in understanding the nature of non-LTE plasmas. It may be used for prediction of population densities of various levels under different plasma conditions. When applied to an experiment, it can be used[11] to interpret experimental data and for deriving plasma parameters.[12,13] A collisional-radiative model simulation for a laser induced selective excitation experiment[14] can also help in estimating cross sections of elementary processes. In a laser generated plasma[15], relaxation times can also be estimated with the help of a collisional-radiative model. A collisional-radiative model along with experimental plasma emissivities can be used for determining plasma parameters of remote astrophysical plasmas.

There has been considerable amount of work on collisional-radiative models applied to various systems. Bates, Kingston and McWhirter[16] proposed a collisional-radiative model for hydrogenic plasmas and calculated the reduced population coefficients $\rho(p)$ for hydrogen atom and hydrogenic ions in optically thin plasmas.

The processes considered include electron impact excitation, deexcitation, electron impact ionization, three-body recombination, radiative recombination and radiative deexcitation. The coupled differential equations describing the time development of the population densities of the excited states were solved numerically under the quasi-steady state approximation. The assumption of quasi-steady state is valid because of the fact that for a wide range of plasmas, the Saha equilibrium population densities of excited levels are much less than the electron density and the population density of the bare nuclei.[16] This implies that for a still wider range

$$n(p) << n_e \qquad (p \neq 1) \qquad\qquad (1.6)$$

where $n(p)$ is the population density of the pth level and n_e is the electron density. This condition is violated only in very dense plasmas. Moreover, if the mean thermal energy is much less than the first excitation energy, $n(p)$ is much less than $n(1)$, the ground state population density, when the steady state is attained. In such plasmas, the excited states attain quasi-steady state population densities almost instantaneously and the electron density and the density of bare nuclei are not significantly changed. The relaxation times for the excited levels are significantly shorter compared to the relaxation times of the ground level or of the free electrons. Thus all the rate equations, except that for the ground state, can be set equal to zero and can be conveniently solved numerically. Bates et al[16] suggested that the number of coupled differential equations could be limited in number by making use of the fact that for higher lying levels,

collisional processes are much more important than radiative processes and n(p) satisfies the Saha equation. The levels with p greater than some value s may be grouped together such that $\rho(s)$ is very close to unity and the finite number of coupled differential equations may be solved to obtain $\rho(p)$'s. If s is chosen correctly and is large enough, then the line $\rho(p) = 1$ will be tangential to the curve obtained by plotting $\rho(p)$ against p.

McWhirter and Hearn[17] presented values of reduced population coefficients and relaxation times for hydrogenic systems and used the reduced variables $\theta = T/z^2$, $\eta(c) = n_e/z^7$ and $\eta(p) = \bar{X} n(p)/z^{11}$ where z is the nuclear charge and $\bar{X}$ is the ratio of electron density and the population density of singly charged ion of charge z. Drawin[18] solved a system of coupled collisional-radiative rate equations for a homogeneous and steady state hydrogen plasma. It was found that hydrogen plasmas are totally optically thick towards all Lyman lines and partially optically thick towards H_α; equilibrium populations are establish at electron densities greater than 10^{16} cm^{-3}. Drawin[19] also calculated the relaxation times for the ground and excited states of hydrogen atoms and hydrogen like ions. The relaxation times were found to be sensitive to the number of reabsorbed photons from the resonance lines and the resonance continuum in collision dominated plasmas. Even under LTE conditions, in the presence of strong resonance absorption, the relaxation times of hydrogen were found to be of the order of 1-50 μs for $n_e \oplus 10^{16}$ cm^{-3} at temperatures lying between 8×10^3 and 1.6×10^4 °K.

Johnson and Hinnov[20] used a new set of transition rates and calculated the population coefficients, ionization and

recombination coefficients for the excited levels of hydrogen in the electron density range 10^5-10^{18} cm^{-3} and in the electron temperature range 2.5×10^2-8.2×10^6 °K.

Drawin and Emard[21] investigated the role of particular collision and radiative processes in the final solution of coupled rate equations for atomic hydrogen levels. The results were found to be sensitive to the processes as well as number of levels indicated in the model. They showed that the critical quantum number n^* defining the limit of partial LTE could not be considered as the critical number of rate equations above which the population coefficients become independent of p. Drawin and Emard[22] also discussed the role of cross section data and recalculated the population coefficients, collisional-radiative recombination and ionization coefficients for hydrogen atom and hydrogen like ions for optically thin and three different sets of partially optically thick conditions. They[23] also obtained the homogeneous stationary state solution and calculated the ground state populations of atomic hydrogen and hydrogen like ions in non thermal plasmas and presented the Saha decrement for ground state population, ionization and recombination coefficients in the electron density range 10^8-10^{18} cm^{-3} and electron temperature range 8×10^3 °K-2.56×10^5 °K for optically thin and partially optically thick conditions.

The present work is on the collisional-radiative model of helium. Before we discuss collisional-radiative models of helium, we might mention the collisional-radiative models of other polyelectronic systems. In polyelectronic systems lack of cross section and other data and large number of energy levels

make computations more difficult. Here, we mention a few models applied to non hydrogenic systems other than helium.

Park[24] has applied a collisional-radiative model to nitrogen plasmas to calculate spectral line intensities. He used 41 groups of the bound states of atomic nitrogen and calculated the population densities of excited states as a function of electron density and electron temperature following the method of Bates et al.[16] The objective of this work was to use intensities of two atomic nitrogen lines to determine electron temperatures in nitrogen plasmas. He found that if the equilibrium relation is used for determination of T_e, non equilibrium effects cause the apparent T_e to be higher than the true T_e in an expanding plasma.

Cartwright[25], using a collisional-radiative model, calculated vibrational populations of triplet excited states of N_2 under auroral conditions and predicted the relative contributions of various cascade and intersystem cascade processes. Ashraf et al[26] developed a collisional-radiative model to calculate the population densities of the triplet states of N_2 using quasi-steady state conditions and Maxwellian electron energy distribution.

Giannaris and Incropera[27] explored the effect of collisional and radiative processes on electronic state population densities in a cylindrically confined argon arc plasma on the basis of a collisional-radiative model following the method of Bates et al.[16] They coalesced the allowed energy levels having same electronic configuration and assumed levels with p > 15 to be in equilibrium with free electrons and compared their calculated population densities with the experimental results.

Van Der Sijde et al [28,29] developed a collisional-radiative model of the argon ion laser system and compared the calculated population densities of 4s and 4p groups with the experimental results of their continuous hollow cathode arc discharge experiment.

Helium plasmas have been of much interest for a number of reasons. Among the polyelectronic atoms, helium is the simplest one and has attracted considerable theoretical attention. Higher levels of helium can be approximated as hydrogenic levels. It has two metastable states 2^1S and 2^3S, which are not radiatively coupled to the ground state and require a collisional mechanism for depopulation to the ground state. The study of helium plasmas is also interesting due to the fact that helium shows largest deviation from LTE[30] amongst all neutral particles under given values of electron temperature and electron density. The large energy gap between the ground level and the first excited state, the non-emitting nature of the 2^3S state, and the presence of autoionizing states causing dielectronic recombination at high electron temperatures and low electron densities are responsible for this deviation of He from LTE. Experimentally, because of the monatomic nature of helium, it is quite simple to ascertain neutral concentration in plasmas. Further, collisional-radiative model already worked out for hydrogenic ions can be easily applied to He^+ ions in a helium plasma.

It will be appropriate to mention briefly a few experiments in helium plasmas before discussing in detail the theoretical calculations that have been carried out. Hinnov and Hirschberg[31,32] studied the rate of disappearance of electrons and the characteristics of the afterglow spectrum in a quiescent

helium plasma produced in the B-1 Stellarator. They determined the electron density and electron temperature from absolute measurements of line intensities. They also made brief calculations on the population densities and recombination coefficients in which only collisions with $\Delta n = \pm 1$ were considered; collisions involving optically forbidden transitions were neglected. Also, energy sublevels were not considered separately. Motley and Kuckes[33] studied plasma loss in helium afterglow discharges in B-1 Stellarator and found that the three-body recombination reaction is the principal mechanism for the charge removal in low temperature highly ionized helium plasma of the experiment.

Johnson[34] compared the results of his experiment on afterglow and ohmic heating of discharges with results of theoretical calculations from a collisional-radiative model. The measurements were done in the electron density range of 10^{12}-10^{13} cm^{-3} and electron temperature range of 0.25-14 eV. The collisional-radiative model used energy levels upto n = 25 with separated sublevels upto n = 8. He assumed that for the levels with n > 26 Saha equilibrium is valid. Johnson and Hinnov[35] measured electron densities and population densities of excited states of neutral helium as a function of time in afterglows in the C Stellarator in the electron density range 10^{11}-3×10^{13} cm^{-3} and electron temperature range 0.04-1 eV. They also carried out calculations on population densities and derived semiempirical cross section formulas for transitions among excited levels by comparing experimental and theoretical population densities.

Ikee and Takeyama[36] determined n_e and T_e from measurements of spectral intensities of the continuum spectrum following the

series 2^3S-n^3P in a brush cathode plasma in a magnetic field of 1.3×10^3 Oe and showed that for brush cathode discharge, in a magnetic field, n_e increases as the current density of the plasma increases. Ikee and Takeyama[37] also determined population densities of various helium levels by measuring spectral line intensities emitted by a brush cathode helium discharge in a magnetic field. They also calculated excited state population densities for their experimental conditions by interpolating the results of Drawin et al[30] and compared the calculated and experimental population densities.

Otsuka, Ikee and Ishee[38] have made studies on helium plasma using their TPD (Test Plasma by Direct Current Discharge) machine. They measured HeI and HeII line intensities at various points of the magnetised plasma column and also estimated plasma parameters at the points of emission intensity measurements. The T_e range of their experiment was $\sim 0.2-8$ eV, $n_e \sim 10^{14}$ cm^{-3} and the gas pressure $\sim 10^{-3}$ torr. The estimated values of n^+ and n^{++} densities were of the order of $\sim 10^{14}$ cm^{-3} and $\sim 10^{11}-10^{12}$ cm^{-3} respectively. From emission intensities, absolute population densities of HeI and HeII ($i = 4$) levels were determined. The estimates of T_e, n_e, n^+ and n^{++} were applied to predict, using a collisional-radiative model, the expected population densities for $i = 4$ state of HeII. They also proposed a mechanism for the observed phenomena in TPD machine, according to which He^{++} recombination is the major process upstream in the plasma column causing HeII excited states to be populated by cascading of higher states. At down stream conditions, with lower electron temperatures, recombination of He$^+$

ion constitutes the major process causing higher levels of neutral helium to increase in population density which results in enhanced emission from such states. Because of the reduced recombination entire plasma column was found to be in quasi-steady state with respect to atomic processes.

Hegde and Ghosh[11] carried out experiments and also made calculations on electron beam excited helium plasmas. They measured emission intensity enhancements of HeI and HeII lines from a helium plasma column in a longitudinal magnetic field in the range 0-700 Oe at a neutral particle density of 10^{14} cm^{-3}. The measured HeI lines were n^3D-2^3P (n = 3-5), n^3S-2^3P (n = 3-5), n^3P-2^3S (n = 3, 4), n^1D-2^1P (n = 3-6), n^1P-2^1S (n = 3, 4), n^1P-2^1P (n = 4, 5) and that of HeII was i = 4 to i = 3. They also measured electron density and electron temperature as a function of magnetic field and found that on increasing the field from 0 to 700 Oe, the axial electron density increases from 10^{10} cm^{-3} to 10^{12} cm^{-3} and the electron temperature falls from 11 eV to 6 eV. The experimental emission enhancement profiles were compared with those calculated on the basis of a collisional-radiative model.

Several laser induced selective excitation studies have also been made in helium plasmas. Catherinot et al[39] optically pumped 2^1S-3^1P and 2^1P-4^1D transitions of HeI with a tunable dye laser of power 500 W/pulse at 5000 Å with a pulse width 5 ns and spectral width 0.1 Å in a helium glow discharge. The measurement of temporal decay of the fluorescence revealed a large excitation transfer between the n^1D and n^3D levels. They estimated a cross

section $\sigma = 5 \times 10^{-14}$ cm^2 for the reaction He (4^1D) + He (1^1S) $\rightarrow$ He (4^3D) + He (1^1S).

Dubreuil and Catherinot[40] used a two laser absorption-perturbation technique to study the population relaxation of 2^3P level in a helium glow discharge. They pumped the transition 4^3D–2^3P, and studied the population relaxation of 2^3P by a probe laser beam tuned to 3^3D–2^3P transition. Using the laser pertur-bation method, Dubreuil and Catherinot[41] determined the optical escape factor for 3^1P–1^1S transition. They pumped the 2^1S–3^1P transition with a tunable dye laser and analysed the 3^1P level population relaxation for different experimental conditions in a helium capillary glow discharge. The optical escape factor for 3^1P–1^1S transition at 350°K and 0.4 torr pressure was estimated to be 0.014.

Yasumaru et al[42] optically pumped 2^1S–3^1P transition of HeI with a tunable dye laser, FWHM 5 ns, spectral width 0.1 Å and monitored the population densities of 3^1P and 3^1D levels at two pressures 0.4 torr and 5 torr, and estimated cross sections for the excitation transfer processes.

Thoma[43] measured the absolute helium emission coeffi-cients in the range λ = 109–540 nm from the radiations originating from axis of a cylindrical helium arc at 1 atmospheric pressure with T_e in the range 2.5 × 10^4 °K–2.65 × 10^4 °K and n_e in the range 3 × 10^{16}–4 × 10^{16} cm^{-3}. This measurement was claimed to be helpful in the use of helium continuum radiation for calibration purposes.

The above examples provide an idea of the experiments done in helium plasmas. Besides the theoretical calculations

described in some of the above studies, there has been considerable work solely on collisional-radiative models. We describe here some representative ones.

Bates and Kingston[44] calculated radiative recombination coefficients, quasi-equilibrium electron temperature and ion temperature using an approximate expression for ion-electron elastic scattering cross section. Bates, Bell and Kingston[45] studied theoretically the decaying properties of an optically thick helium plasma in the electron temperature range 0.09-1.4 eV and electron density range 10^8-10^{16} cm^{-3}. Considering Penning ionization, they found that the collisional-radiative recombination is a significant process   in populating the first excited state.

Drawin and co-workers, using their collisional-radiative model, carried out extensive calculations on helium plasmas and presented numerical values of population coefficients in a wide range of plasma parameters. In their collisional-radiative model[30,46] they separated the level system of helium into two parts, the singlet system termed as the X system and the triplet system termed as the Y system and the two systems were separately taken into account. The separated sublevels were used only up to the principal quantum number n = 2, and for levels n $\geq$ 3 the singlet and triplet sublevels of a particular principal quantum number were grouped separately. The highest level taken into account was that of principal quantum number n = 25. Thus a total of 51 levels were used in the collisional-radiative model. In an earlier work[47], Drawin included the atom-atom exchange collisions between the singlet and triplet levels but later on[30],

heavy particle collisions were dropped in order to get a linear system of equations. To compensate the error, they incorporated electron atom exchange collisions between all levels of triplet and singlet systems. The rate coefficients were calculated using a Maxwellian velocity distribution. The 51 linear simultaneous equations thus obtained were solved numerically both for homogeneous stationary state and inhomogeneous transient state solutions. The numerical values of collisional-radiative volume recombination and ionization coefficients for quasi-stationary helium plasmas in n_e range 10^4-10^{19} cm^{-3} and T_e range 0.25 x 10^3 °K-2.56 x 10^5 °K were presented.[46] They[30] also calculated Saha decrements of ground state population densities in the n_e range 10^{10}-10^{20} cm^{-3} and T_e range 8.0 x 10^3-1.28 x 10^5 °K for optically thin, slightly optically thick and strongly absorbing plasmas.

Drawin and Emard[48] listed extensive tables of reduced population coefficients for various levels of HeI in a wide range of plasma parameters using six sets of optical escape factors. For hydrogen like ions also, they[22,49] calculated the values of population coefficients for optically thin and partially optically thick conditions in reduced electron density ($n_z = n_e/z^7$) range 10^4-10^{18} cm^{-3} and reduced electron temperature ($\Theta_z = T_e/z^2$) range 1 x 10^3-2.56 x 10^5 °K. In all the above calculations, however, the separated sublevels are used only up to n = 2 and the HeI and HeII levels are treated separately. Mostly empirical or semiempirical cross sections were used. The term system of energy levels is largely simplified and applies to plasmas of sufficiently high electron density. Moreover the

model does not take into account the processes like ionization due to collisions of two metastable states.

Hegde and Ghosh[11,50] developed a collisional-radiative model which considers both HeI and HeII levels simultaneously. They used completely separated sublevels up to n = 5, with sublevels of principal quantum numbers 6-12 grouped together. In addition to these levels,13 levels of HeII were also included. They interpreted the results of their emission enhancement experiments on the basis of this model. They also calculated relaxation times for establishing steady state population in optically thin helium plasmas. However mostly semiempirical analytic forms of cross sections were used in this work.

Hess and Burrell[51] in their collisional-radiative model considered completely separated sublevels up to n = 4 and included the effect of optical pumping. They presented results for both steady state and quasi-steady state solutions. The enhancement of populations on pumping with a laser of power 10^4 W/cm^2-$\overset{\circ}{\text{A}}$ having various rise times, were also presented. The enhancement was found to be larger at low electron densities. In their model, Hess and Burrell did not include HeII levels. Neutral-neutral collisions and dielectronic recombinations were also not included.

Fujimoto[52] applied his collisional-radiative model to a discharge plasma. This model takes into account completely separated sublevels up to n = 7 with an upper limit of n = 26 and deals with time-independent solutions. Two types of formulations were emphasized in this work. In the first case, the population densities of the levels located above a sufficiently high lying

level v were assumed to be given by Saha-Boltzmann equilibrium.
Further, the rate equations of the levels $p \leq v$, except for
ground state and two metastable states were set equal to zero.
The rate equations for the ground state 1^1S, and the two meta-
stable states 2^1S and 2^3S were solved independently. In the
second case, when the change in population densities is slow
enough as compared to the relaxation times, the rate equations
of all the level $p \leq v$, except that of the ground state, were
made equal to zero and population densities of the excited states
were calculated in terms of ground state population density. The
results were presented at $T_e = 1.6 \times 10^4$ °K and in the n_e range
10^6-10^{18} cm^{-3}. The population density distribution among excited
levels was also interpreted in terms of excitation-ionization
mechanism in the plasma. This model used mostly semiempirical
cross sections and did not include HeII levels along with the
HeI levels. Fujimoto[53] also discussed the kinetics of ionization-
recombination of a plasma. He showed that the population density
of ions in a low density plasma could be described by corona
equilibrium or by the capture cascade scheme. In case of a
optically thin, high temperature plasma for hydrogen like ions
the population density per unit statistical weight of a given
level was found to be proportional to inverse of the square root
of the principal quantum number of that level.

Dubreuil and Catherinot[14] studied quenching and excitation
transfer of n = 3 helium sublevels in a low pressure glow
discharge by means of a laser perturbation method. They calcu-
lated the perturbations in population densities induced by a
laser by solving the coupled rate equations as a function of time.

By comparing the theoretical results with the experimental ones, they deduced radiative coefficients and collisional cross sections. At a pressure p < 10 torr and discharge current i < 50 mA, they found that only radiative and atom-atom collision processes contribute to quenching and excitation transfer in the n = 3 levels of HeI. Also, by using this technique, they[54] estimated a set of thermally averaged cross sections for quenching and excitation transfer processes for n = 4 level of HeI.

Dothan and Kagan[55] proposed a scheme for calculating populations of excited levels and intensities of spectral lines in the positive column of helium discharges at intermediate pressure (p > 5 torr). They used a non-Maxwellian electron distribution (for E_e > 19.8 eV) and found the excitation from 2^1S level to be very important for populating higher singlet levels.

The collisional-radiative models mentioned above differ in the number of energy levels used, choice of the processes included, and the nature of atomic parameters employed. All the collisional-radiative models cited here, except that of Ref. 11, do not consider HeI and HeII levels simultaneously. Whereas in isolated ranges several of these models do predict population densities satisfactorily, due to their peculiar choice of atomic processes and parameters, none is applicable over a wide range of electron density and electron temperature. Also there has been no concerted effort on inclusion of experimental cross sections, and this could be one reason why agreement between theoretical and experimental population densities is unsatisfactory in several cases. Further, in the above studies, there has been no attempt to explore the quantitative role of a particular rate process in

populating a given level. There seems to be thus a need for an improved model which eliminates some of the above deficiencies.

The purpose of the present work is to evolve an improved collisional-radiative model of helium plasmas. This is carried out by (a) first incorporating in the model,[56] as many as possible experimentally obtained excitation cross sections and then examining predictions from the model against population densities observed in steady-state experiments (a detailed examination of the role of direct ionization-excitation process is also made[57]), (b) quantitatively examining the role of a given process in populating a particular level and thus evolving a detailed population mechanism,[58] and (c) critically examining the results of a number of recent laser induced selective excitation experiments. On the basis of theoretical results, a brief examination is also made of the line intensity ratio method for estimating electron temperatures.

We first present methods of calculations and choice of atomic parameters. This is followed by results of the collisional-radiative model calculations, and then finally a discussion of all the results.

THE MODEL, ATOMIC PARAMETERS AND METHOD OF CALCULATION

In this chapter, we first present the collisional-radiative model used in the present work, then details about the cross sections employed, and finally present the procedure adopted in the calculations.

2.1. THE COLLISIONAL-RADIATIVE MODEL

The various collisional-radiative models suggested for the helium system differ in the number of atomic levels used, mode of grouping of sublevels, choice of atomic parameters and methods of solving the linear simultaneous equations. The collisional-radiative model[56] used in this work consists of completely separated HeI sublevels up to principal quantum number n = 5. The sublevels of principal quantum numbers n = 6-12 are grouped together and are treated as single levels. This makes a total of 32 sublevels for HeI. Besides these levels, 15 levels of HeII have been included, thus making a total of 47 levels. The energies (in cm^{-1}) and the weight factors[59] for these levels are given in Table 2.1. In this section the levels of HeI are represented by p and q while the levels of HeII are represented by i and j.

The following processes are included in the model. Here K's represent electron impact excitation and deexcitation rate coefficients, A's represent spontaneous transition probabilities and β's represent radiative recombination rate coefficients.

Table 2.1.   Energy levels of HeI and HeII used in the model

Level No. (p)	State	Energy (cm^{-1}) E_p	g_p	Level No. (p)	State	Energy (cm^{-1}) E_p	g_p
1	1^1S	0	1	17	$4^3F, 4^1F$	191452	28
2	2^3S	159856	3	18	4^1P	191493	3
3	2^1S	166278	1	19	5^3S	193347	3
4	2^3P	169078	9	20	5^1S	193663	1
5	2^1P	171135	3	21	5^3P	193801	9
6	3^3S	183237	3	22	5^3D	193917	15
7	3^1S	184865	1	23	5^1D	193919	5
8	3^3P	185565	9	24	$5^3F, 5^1F,$ $5^3G, 5^1G$	193921	64
9	3^3D	186102	15	25	5^1P	193943	3
10	3^1D	186105	5	26	6(n)	195251	144
11	3^1P	186210	3	27	7	196070	196
12	4^3S	190298	3	28	8	196595	256
13	4^1S	190940	1	29	9	196954	324
14	4^3P	191217	9	30	10	197213	400
15	4^3D	191445	15	31	11	197398	484
16	4^1D	191447	5	32	12	197543	576
					$n = \infty$	198311	-

The energy levels of HeII used in the model for i = 1 to 15 were calculated from the expression

$$E_i = 109677 \times 4 \left(1 - \frac{1}{i^2}\right) + 198311 \ cm^{-1}, \quad g_i = 2i^2.$$

(i)   Electron impact excitation and deexcitation:

$$He(p) + e \xrightarrow{\frac{K(p,q)}{K(q,p)}} He(q) + e \tag{2.1}$$
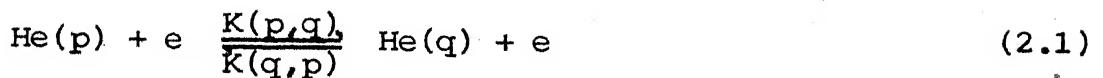
(ii)   Electron impact ionization:

$$He(p) + e \xrightarrow{K(p,i)} He^{+}(i) + e + e \tag{2.2}$$
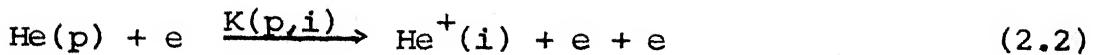
This process represents the direct ionization-excitation of HeI levels (p = 1-32) to excited HeII levels (i = 1-15).

(iii) Three-body recombination:

$$He^{+}(1) + e + e \xrightarrow{K(i,p)i=1} He(p) + e \tag{2.3}$$
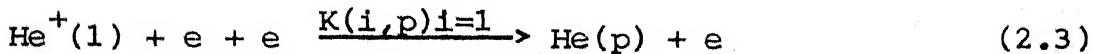
Since recombination of higher excited states of HeII is not important in populating HeI levels, only the recombination from the ground state of HeII has been taken into account; K(i,p) represents the rate coefficient for this process.

(iv)   Spontaneous radiative transitions:

$$He(p) \xrightarrow{A(p,q)p>q} He(q) + h\nu \tag{2.4}$$

(v)   Radiative recombination:

$$He^{+}(1) + e \xrightarrow{\beta(p)} He(p) + h\nu \tag{2.5}$$
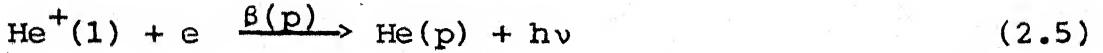
(vi)   Heavy particle collisions involving excitation, deexcitation, ionization and recombination:

$$He(p) + He(1) \xrightarrow{\frac{KN(p,q)}{KN(q,p)}} He(q) + He(1) \tag{2.6}$$

$$He(p) + He(1) \xrightarrow{\frac{KN(p,i)i=1}{KN(i,p)i=1}} He^{+}(1) + He(1) + e \tag{2.7}$$
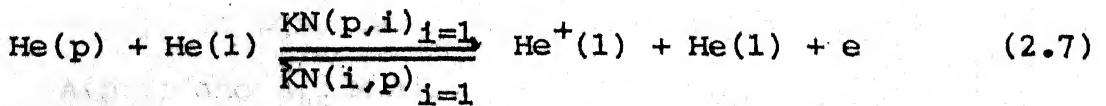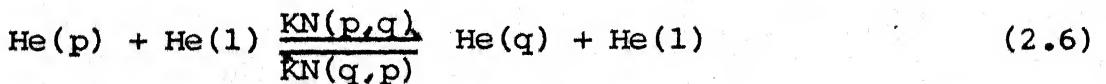
At high gas pressures (≥ 1 torr) the neutral-neutral collisions become significant.

(vii) For HeII, the processes similar to processes (2.1), (2.2), (2.3), (2.4) and (2.5) for HeI, are included. They are represented by the following equations:

$$He^+(i) + e \xrightarrow{\frac{K(i,j)}{K(j,i)}} He^+(j) + e \qquad (2.8)$$

$$He^+(i) + e \xrightarrow{K(i,c)} He^{++} + e + e \qquad (2.9)$$

$$He^{++} + e + e \xrightarrow{K(c,i)} He^+(i) + e \qquad (2.10)$$

$$He^+(i) \xrightarrow{A(i,j)i>j} He^+(j) + h\nu \qquad (2.11)$$

$$He^{++} + e \xrightarrow{\beta(i)} He^+(i) + h\nu \qquad (2.12)$$
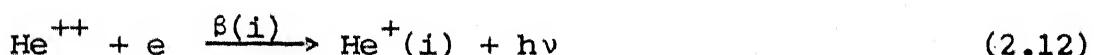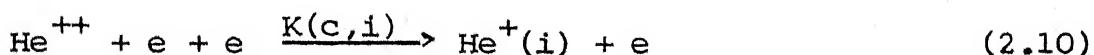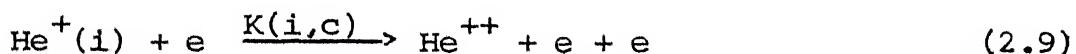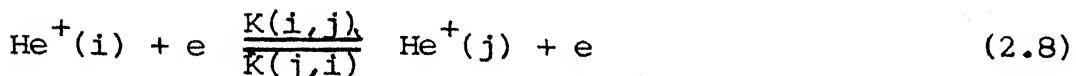
In the above equations, $K(i,j)$ represents the rate coefficient for the electron impact excitation from ith level to jth level and $K(j,i)$ is the rate coefficient for the reverse process. $K(i,c)$ denotes the rate coefficient for the electron impact ionization from ith level of HeII to the continuum. c represents the continuum of free electrons. $K(c,i)$ is the rate coefficient for the three-body recombination. $A(i,j)$ and $\beta(i)$ respectively represent the spontaneous transition probability and radiative recombination coefficient for HeII.

In partially optically thick plasmas, the reabsorption of radiation is taken into account through optical escape factors Λ_{pq} and Λ_{ij}.[83] In such a situation $A(p,q)$ and $A(i,j)$ in Eqs. (2.4) and (2.11) are replaced by $\Lambda_{pq} \times A(p,q)$ and $\Lambda_{ij} \times A(i,j)$ respectively, where Λ_{pq} and Λ_{ij}

are optical escape factors for the corresponding transi-
tions of HeI and HeII.

(viii)   Optical pumping: If a laser beam of radiation density
$\rho(\nu)$ (energy per unit volume per unit frequency interval)
is tuned to a particular transition $p \to q$, the population
of upper level q could be significantly enhanced. This
laser induced selective excitation may be described as
follows:

$$\text{He}(p) + h\nu \ \frac{W(p,q)}{W(q,p)} \ \text{He}(q) \tag{2.13}$$

where $W(p,q)$ and $W(q,p)$ are the rates of induced absorption
and emission given by $W(p,q) = \rho(\nu) \times B(p,q)$ and $W(q,p) =$
$\rho(\nu) \ B(q,p)$ where $B(p,q)$ and $B(q,p)$ denote the Einstein
coefficients defined by the following equations (see,
however Section 2.3.5)

$$B(q,p) \ = \ \frac{c^3}{8\pi h \nu^3} \cdot A(q,p) \tag{2.14}$$

$$B(p,q) \ = \ \frac{g_p}{g_q} \cdot B(q,p) \tag{2.15}$$

where c is the velocity of light and h is the Planck's
constant. ν represents the frequency of the transition
$p \to q$ and g_p and q_q represent the weight factors of levels
p and q respectively.

In the model, autoionization processes are not taken into
account and the losses' due to diffusion to the walls for
all the excited states of HeI and HeII are also assumed
to be negligible.

2.2. ATOMIC DATA

2.2.1. Cross Sections

While choosing cross section data, emphasis has been given on the use of experimental cross sections. When more than one experimental cross section is available, the one which is more recent has been used. Theoretical cross sections have been used only when experimental cross sections are not available. For a given transition, if more than one theoretical cross section are available in the literature, the one which leads to calculated population densities closer to experimental results is used.

(a) Optically allowed transitions: Among the optically allowed transitions, the experimental cross sections of Westerveld et al [60] have been used for the cases 1^1S-2^1P and 1^1S-3^1P. For 1^1S-4^1P, the data have been taken from the experimental work of Donaldson et al.[61] The cross sections used for the transition 1^1S-5^1P are from Scott and McDowell.[62] Theoretical values of the cross section of Flannery and McCann[63] have been used for the transition 2^1S-3^1P. For the transitions 2^3S-2^3P, 2^3S-3^3P, 2^3S-4^3P, and 2^3S-5^3P, the data have been taken from the theoretical calculations of Ton-That et al.[64] The cross sections for the remaining optically allowed transitions have been taken from Drawin.[65] Following is the expression used by Drawin for electron impact excitation cross section $q_{p,q}(E_e)$

$$q_{p,q}(E_e) = 4 \pi a_o^2 \left(\frac{E_1^H}{E_{p,q}}\right)^2 f(p,q) \, g(U_{p,q}) \qquad (2.16)$$

where E_e represents the electron kinetic energy, a_o is the Bohr radius, E_1^H is the ionization potential of hydrogen equal to

13.59 eV, $E_{p,q}$ is the difference in the energies of levels q and p. f(p,q) is the absorption oscillator strength, $g(U_{p,q})$ is given by

$$g(U_{p,q}) = \alpha_{pq} \left(\frac{U_{p,q} - 1}{U_{p,q}^2}\right) \ln(1.25\, \beta_{p,q}\, U_{p,q}) \qquad (2.17)$$

Here $U_{p,q} = \dfrac{E_e}{E_{p,q}}$; $\alpha_{p,q}$ and $\beta_{p,q}$ are constants for a given transition. In general $\alpha_{p,q}$ is about 1 and $\beta_{p,q}$ lies between the values 1 and 3. The oscillator strength values have been taken from the tables of Wiese, Smith and Glennon.[66] Rate coefficients are obtained by integrating the cross section expression over Maxwellian electron energy distribution using Eq. (1.4).

(b) Optically forbidden transitions without change in multiplicity: The cross sections for the transitions 1^1S-2^1S, 1^1S-4^1S and 1^1S-5^1S are taken from the experimental results of Rice et al [67], Raan et al [68] and Pochat et al [69], respectively. The cross sections for the transitions 1^1S-3^1D and 1^1S-4^1D have been taken, respectively, from the experimental results of St. John et al [70] and Moussa et al.[71] The theoretical values of Flannery and McCann[63] have been used for the transitions 2^1S-3^1S and 2^1S-3^1D. Theoretical cross sections of Khayrallah et al [72] have been taken for the transition 2^3S-3^3S. For the transitions 2^3S-3^3D, 2^3S-4^3S, 2^3S-4^3D, 2^3S-4^3F, 2^3S-5^3S, 2^3S-5^3D, 2^3S-5^3F, and 2^3S-5^3G, the theoretical cross sections of Ton-That et al [64] have been used. For the cross sections of other optically forbidden transitions, without change in multiplicity, that are not available in recent literature, following expression due to Drawin[65] has been used.

$$q_{p,q}(E_e) = 4\pi a_o^2 Q_{p,q} U_{p,q}^{-1} (1 - U_{p,q}^{-1}) \tag{2.18}$$

where $U_{p,q}$ has the same meaning as in Eq. (2.17). $Q_{p,q}$ is a constant for a given transition and its values for various transitions in helium are tabulated by Drawin.[65]

(c) Optically forbidden transitions with change in multiplicity: Among these transitions, the experimental cross sections of Jobe and St. John[73] have been used for the transition 1^1S-2^3P. For the transition 1^1S-2^3S, the theoretical cross sections of Lins de Barros and Brandi[74] have been used. For other such transitions, empirical cross sections from Drawin[65] have been taken. For such transitions which involve the ground state, Drawin[65] has used the following expression

$$q_{p,q}(E_e) = 4\pi a_o^2 Q_{p,q} \frac{U_{p,q}^2 - 1}{U_{p,q}^n} \tag{2.19}$$

where $n = 5$ and the other symbols retain their meanings mentioned earlier. For transitions between excited states i.e. not involving the ground state (e.g. 2^3S-2^1S, 2^3S-3^1S etc.), Drawin[65] suggested the following expression for the cross sections

$$q_{p,q}(E_e) = 4\pi a_o^2 Q_{p,q} U_{p,q}^{-1} \tag{2.20}$$

The values of $Q_{p,q}$ are given by Drawin.[65] The cross sections for the optically forbidden transitions with change in multiplicity not given by Drawin[65] are taken from Moisewitsch and Smith.[75]

(d) Electron impact ionization: For the cross sections of electron impact ionization processes involving the excited

states of neutral helium and ground state of helium ion, following expression due to Gryzinski[76] is used.

$$\text{He}_e \, Q^{\text{He}^+}(E_e/E_p') = \frac{2\pi e^4}{E_p'^2} \, g_p(E_e/E_p) \tag{2.21}$$

where E_p' is the ionization potential of the pth level and E_e is the electron kinetic energy. Putting $E_e/E_p' = x$, $g_p(x)$ is given by

$$g_p(x) = \frac{1}{x} \frac{(x-1)^{3/2}}{(x+1)} \left[1 + \frac{2}{3}(1 - \frac{1}{2x}) \ln(2.7 + (x-1)^{1/2} \right] \tag{2.22}$$

(e) Direct ionization-excitation: For the direct ionization-excitation from the ground and excited states of HeI to the excited states of HeII, following empirical formula for the cross section[57] has been used:

$$q_{pi}(x) = 46 \times 10^{-4} \, \pi a_o^2 \left[\frac{E_1^H}{E_{pi}} \right]^2 \frac{x-1}{x^2} \ln(10 \, x) \tag{2.23}$$

where $E_1^H = 13.59$ eV, $x = \frac{E_e}{E_{pi}}$, $E_{pi} = E_i - E_p$ and E_i and E_p respectively, are the energies of ith level of HeII and pth level of HeI. The cross sections given by this empirical formula agree well with the experimental cross sections of Weaver and Hughes[77] and Sutton and Kay[78] for level i = 4 of HeII. A comparison between the empirical and experimental cross sections is given in Figure 2.1.

(f) Heavy particle collisions: For neutral-neutral excitation, deexcitation, ionization and recombination processes the expressions for rate coefficients given by Drawin and Emard[79] have been used. For neutral-neutral excitation, the rate coefficient $KN(p,q)$ is given by
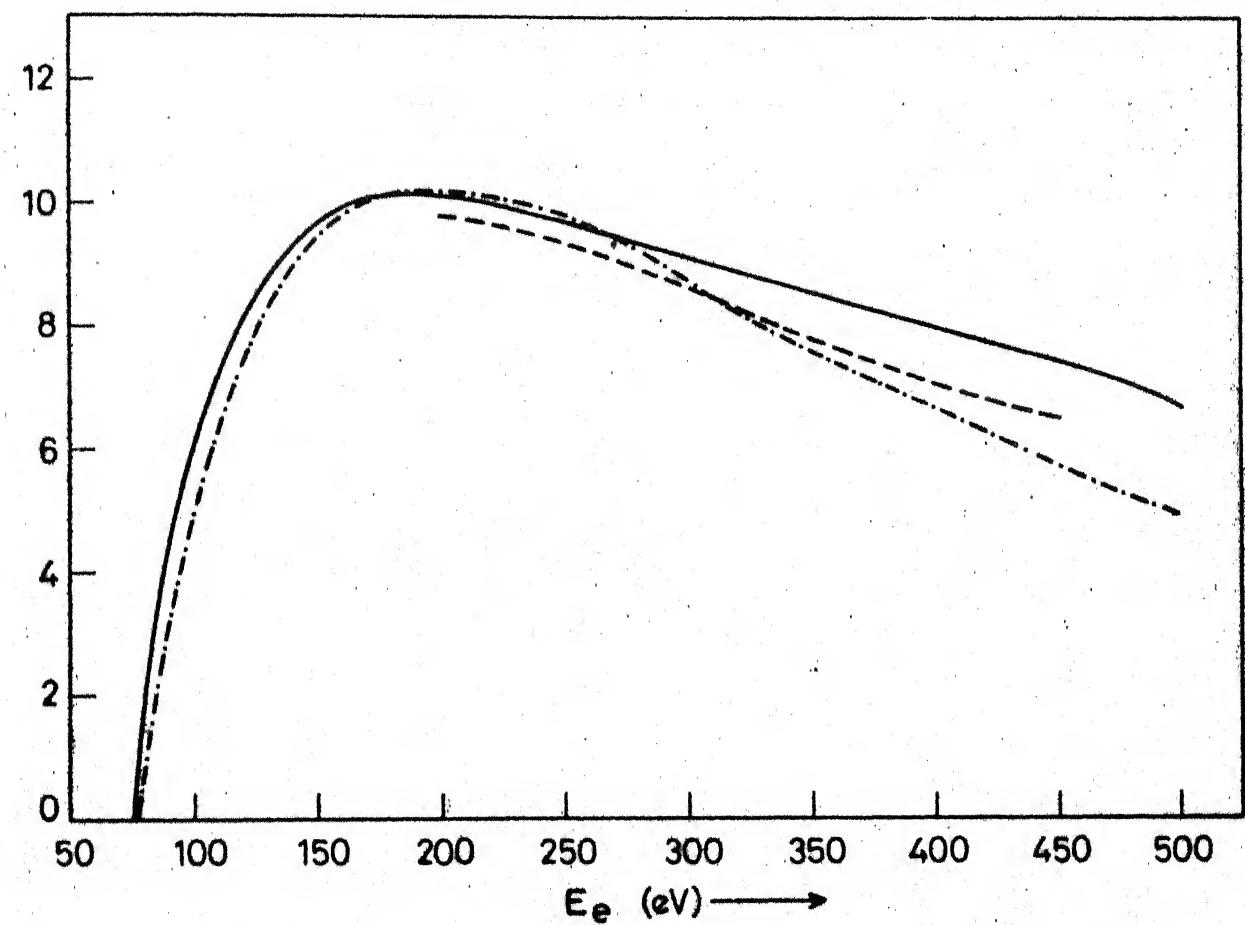
Figure 2.1: The direct ionization-excitation cross section for level i = 4 of HeII; ———, Eq. (2.23); -.-.-, Weaver and Hughes[77]; -----, Sutton and Kay[78].

$$KN(p,q) = 128 \pi a_o^2 \left(\frac{E_1^H}{E_{p,q}}\right)^2 f(p,q) \left(\frac{kT_g}{\pi m_{He}}\right)^{1/2} \frac{m_e \cdot m_{He}}{m_H(m_{He} + m_e)} \cdot$$

$$\Psi_{m_{He}}(W_{p,q}) \qquad (2.24)$$

where a_o, E_1^H, $E_{p,q}$ and $f(p,q)$ retain the same meaning as in Eq. (2.16). T_g represents the gas temperature. m_{He} and m_e, respectively stand for the mass of helium atom and mass of hydrogen atom. $W_{p,q}$ represents the excitation energy in units of kT_a and is given by $W_{p,q} = \frac{E_{p,q}}{kT_g}$. $\Psi_{m_{He}}(W_{p,q})$ is defined as

$$\Psi_{m_{He}}(W_{p,q}) = \frac{1 + \frac{2}{W_{p,q}}}{1 + \left(\frac{2m_e}{(m_{He} + m_e)W_{p,q}}\right)^2} \exp(-W_{p,q}) \qquad (2.25)$$

The recombination rate coefficient $KN(q,p)$ is given by

$$KN(q,p) = \frac{g_q}{g_p} \cdot KN(p,q) \exp(W_{p,q})$$

where g_p and g_q are the weight factors for levels p and q respectively.

The rate coefficient $KN(p,i)$ for neutral-neutral ionization is given by

$$KN(p,i) = 128 \pi a_o^2 \left(\frac{E_1^H}{E_p'}\right) \xi_p \left(\frac{kT_g}{\pi m_{He}}\right)^{1/2} \cdot \frac{m_e \cdot m_{He}}{m_H(m_{He} + m_e)} \cdot \Psi_{He}(W_p') \qquad (2.26)$$

where W_p' is the ionization energy of level p in units of kT_a and is given by $W_p' = \frac{E_p'}{kT_g}$. ξ_p is the number of equivalent electrons in shell p. Ψ_{He} is given by Eq. (2.25) with $W_{p,q}$ replaced by W_p'. The rate coefficient $KN(i,p)$ for the reverse process is given by

$$KN(i,p) = \frac{g_p}{2g_{He^+}} \left(\frac{m_{He} + m_e}{m_{He} \cdot m_e}\right)^{1/2} \frac{h^3}{(2\pi k)^{3/2}} \cdot \frac{1}{T_g^{1/2} \cdot T_e} \cdot$$

$$KN(p,i) \exp(-U_p + 2(U_p \cdot W_p')^{1/2}) \qquad (2.27)$$

where $U_p = \dfrac{E_p'}{kT_e}$.

(g) HeII transitions: Rate coefficients for electron impact excitation and ionization for HeII are calculated by using the expressions given by Bates et al.[16] For electron impact excitation, the rate coefficient $K(i,j)$ is given by

$$K(i,j) = 4.75 \times 10^{-5} \frac{i^2 \cdot j^2}{j^2 - i^2} \cdot \frac{f(i,j)}{z^2 \, T_e^{1/2}} \exp\left(-\frac{E_{i,j}}{kT_e}\right)$$

$$(2.28)$$

where z is the nuclear charge and $E_{i,j}$ is the excitation energy i.e. $E_{i,j} = E_j - E_i$. The rate coefficient for electron impact ionization $K(i,c)$ is given by

$$K(i,c) = \frac{1.4 \times 10^{-5} \cdot i^2}{z^2 \, T_e^{1/2}} \exp\left(-\frac{E_i'}{kT_e}\right) \qquad (2.29)$$

where E_i' is the ionization energy of level i.

2.2.2. Other Data

Spontaneous transition probabilities for HeI are taken from Wiese et al [66] and those for HeII from Green et al.[80] Radiative recombination coefficients $\beta(p)$ for HeI are obtained by integrating the following expression due to Kramers[81]

$$q(\nu) = \frac{128}{3\sqrt{3}} \frac{\pi^4 \, z^4 \, e^{10}}{c^3 \, h^4 \, m_e \, \nu^2 \, n^3} g(\nu) \qquad (2.30)$$

where v is given by $h\nu = h\nu_o + \frac{1}{2} m_e v^2$, ν is the frequency of radiation, ν_o the threshold frequency and $g(\nu)$ is the free-bound Gaunt factor, z is the nuclear charge.

$\beta(i)$ for HeII are calculated from the following Seaton's[82] formula for hydrogenic ions

$$\beta(i) = 5.197 \times 10^{-14} \, z \, x_i^{3/2} \, S_n(D) \tag{2.31}$$

where $D = 157890 \, z^2/T_e$ and $x_i = \frac{D}{i^2}$. $S_n(D)$ values are obtained by interpolating Seaton's values.

2.2.3. Optical Escape Factors

Optical escape factors have been calculated using the treatment of Drawin and Emard.[83] They considered stark broadening and used a Voigt profile to calculate the optical escape factors. The expression for the escape factor for HeI and HeII is as follows:

$$\Lambda_{i,j}^v = \frac{1 + \dfrac{\hat{\tau}_{ij}}{2 + \hat{\tau}_{ij}^2}}{1 + \hat{\tau}_{ij} \left[\pi \ln(1 + \hat{\tau}_{ij}) \right]^{1/2}} + \left[\pi U_{ij}(0, \, \alpha_{ij}) \right]^{1/2}$$

$$\times \frac{\alpha_{ij} \, \beta\hat{\tau}_{ij}}{1 + \beta (\alpha_{ij}^{1/2} \, \hat{\tau}_{ij} + \alpha_{ij} \, \hat{\tau}_{ij}^{1/2})} + \frac{1 + \dfrac{\hat{\tau}_{ij}}{2 + \hat{\tau}_{ij}^2}}{1 + (\pi\hat{\tau}_{ij})^{1/2}} \tag{2.32}$$

where

$$U_{ij}(0, \, \alpha_{ij}) = \frac{1}{\pi^{1/2}(1 + \pi\alpha_{ij}^2)^{1/2}} \left[1 - \frac{\alpha_{ij}}{\pi^{1/2}(1 + \pi\alpha_{ij}^2)} \right]$$

$$\hat{\tau}_{ij} = 4.11 \times 10^{-6} \frac{n(1) \, l \, f(i,j)}{T_g^{1/2}} \lambda_{ij} \, x$$

$$\left[\frac{1}{\pi^{1/2}(1 + \pi \alpha_{ij}^2)} \cdot \left(1 - \frac{\alpha_{ij}}{\pi^{1/2}(1 + \pi \alpha_{ij}^2)}\right) \right]$$

and

$$\alpha_{ij} = \frac{3.72 \times 10^{-22} \, n_e \, j^3 (j-1)}{\lambda_{ij} \, T_g^{1/2}}$$

In the above expressions, $\beta = 100$, $n(1)$ is the ground state population density, l is the diameter of the plasma tube, $f(i,j)$ represents the oscillator strength, λ_{ij} the wavelength and T_g denotes the gas temperature (or the ion temperature in case of HeII).

2.3. METHOD OF CALCULATION

2.3.1. Rate Coefficients

As mentioned above, rate coefficients are obtained by integrating the cross section over Maxwellian velocity distribution of electrons. Two cases may arise — cross section is given either in the form of an algebraic expression or in the form of data (as in the experimental cross section case). Methods of calculations in both the cases are described below.

(a) When an empirical formula for cross section is given: For example, in case of optically allowed transitions, the empirical expression given by Drawin[65] is as follows

$$q_{p,q}(E_e) = 4 \pi a_o^2 \left(\frac{E_1^H}{E_{p,q}}\right)^2 f(p,q) \, g(U_{p,q})$$

where $g(U_{p,q}) = \alpha_{p,q} \dfrac{U_{pq} - 1}{U_{pq}^2} \ln(1.25\, \beta_{p,q}\, U_{p,q})$

On integrating the above expression over Maxwellian electron energy distribution, in the range of velocity v^* to ∞, where v^* is the threshold velocity, we get the rate coefficient $K(p,q)$ as follows:

$$K(p,q) = \int_{v^*}^{\infty} 4\pi a_o^2 \left(\frac{E_1^H}{E_{p,q}}\right)^2 f(p,q)\, g(U_{p,q})\, f(v) \cdot v \cdot dv$$

(2.33)

where $f(v) = \left(\dfrac{2}{\pi}\right)^{1/2} \left(\dfrac{m}{kT_e}\right)^{3/2} e^{-1/2\, mv^2/kT_e}\, v^2$,

and $v^* = \left(\dfrac{2E_{p,q}}{m}\right)^{1/2}$. k is the Boltzmann constant and T_e is the electron temperature, m and v respectively are the mass and velocity of the electron. $E_{p,q}$ is the difference in the energies of levels q and p.

Putting $\frac{1}{2} mv^2 = E_e$, which gives $v^3\, dv = \dfrac{2E_e\, dE_e}{m^2}$, Eq. (2.33) can be rewritten as

$$K(p,q) = 4\pi a_o^2 (E_1^H)^2 \left(\frac{2}{\pi}\right)^{1/2} \left(\frac{m}{kT_e}\right)^{3/2} \frac{2}{m^2} \int_{E_{p,q}}^{\infty} \frac{1}{E_{p,q}^2} f(p,q)\, g(U_{p,q})$$

$$e^{-E_e/kT_e}\, E_e\, dE_e$$

(2.34)

Substituting $\dfrac{E_e}{E_{p,q}} = U_{p,q}$ and putting the value of $g(U_{p,q})$, one gets

$$K(p,q) = C'' \alpha_{p,q} \int_1^{\infty} \frac{U_{p,q} - 1}{U_{p,q}} \ln(1.25\, \beta_{p,q} \cdot U_{p,q}) \cdot f(p,q)$$

$$e^{-U_{p,q} \cdot E_{p,q}/kT_e}\, dU_{p,q}$$

(2.35)

where $C' = 4 \pi a_o^2 (E_1^H)^2 (\frac{2}{\pi})^{1/2} (\frac{m}{kT_e})^{3/2} \cdot \frac{2}{m^2}$

Substituting $U_{p,q} - 1 = Y$, and $\frac{E_{p,q}}{kT_e} = \alpha$, Eq. (2.35) reduces to

$$K(p,q) = C' \cdot \alpha_{p,q} \, f(p,q) e^{-\alpha} \int_0^\infty \frac{Y}{Y+1} \ln \{1.25 \, \beta_{p,q} (1+Y)\} \, e^{-\alpha Y} \, dY$$

(2.36)

further substituting $\alpha Y = Z$, one gets

$$K(p,q) = C' \, \alpha_{p,q} \, f(p,q) \, \frac{e^{-\alpha}}{\alpha} \int_0^\infty \frac{Z}{\alpha + Z} \ln \{1.25 \, \beta_{p,q} (1 + \frac{Z}{\alpha})\} e^{-Z} \, dZ$$

(2.37)

Substituting the numerical value of C', Eq. (2.37) is reduced to

$$K(p,q) = 5.436272598 \, \frac{\alpha_{p,q} \, f(p,q) \, e^{-\alpha}}{\alpha \cdot T_e^{3/2}} \int_0^\infty f(Z) \, e^{-Z} \, dZ \qquad (2.38)$$

This equation can be integrated numerically using Gaussian quadrature method involving Laguerre polynomials

$$\int_0^\infty f(Z) \, e^{-Z} \, dZ = \sum_{i=1}^n H_i \, f(a_i) \qquad (2.39)$$

where H_i's and a_i's are respectively the weight factors and zeros of nth order Laguerre polynomial.[84] The accuracy of the results depends upon the proper choice of the order n of the polynomial.

(b) In case of experimental cross sections, when the numerical values of cross section are available at discrete values of E_e, following procedure for integration is adopted.

If $Q(E_e)$ is the cross section as a function of E_e, $K(p,q)$ is given by

$$K(p,q) \quad = \quad \int_{v_*}^{\infty} \quad Q(E_e) \; f(v) \; v \cdot dv \tag{2.40}$$

where $f(v)$ and v retain their old meaning. Substituting for $f(v)$ and putting $\frac{1}{2} mv^2 = E_e$, the above equation reduces to

$$K(p,q) \quad = \quad (\tfrac{2}{\pi})^{1/2} \; (\tfrac{m}{kT_e})^{3/2} \cdot \frac{2}{m^2} \int_{E_p}^{\infty} Q(E_e) \; e^{-E_e/kT_e} \; E_e \; dE_e \tag{2.41}$$

where E_p is the threshold energy.

This equation is integrated numerically using either trapezoidal method or Simpson's rule of integration. Results obtained with Simpson's rule are more accurate.

2.3.2. Population Densities

Applying the principle of detailed balancing in the processes used in the model and putting $\dfrac{n_e}{n^+(1)} = \overline{X}$, and $\dfrac{n_e}{n^{++}} = \overline{Y}$; where $n^+(1)$ and n^{++}, respectively, are the population densities of the ground state of HeII and that of doubly charged helium ion, the following equilibrium relations are obtained.

$$K(p,q) \; n_E(p) \quad = \quad K(q,p) \; n_E(q) \tag{2.42}$$

$$\frac{n_e}{\overline{X}} \; K(i,p)_{i=1} \quad = \quad K(p,i)_{i=1} \; n_E(p) \tag{2.43}$$

$$K(i,j) \; n_E^+(i) \quad = \quad K(j,i) \; n_E^+(j) \tag{2.44}$$

$$\frac{n_e}{\overline{Y}} \; K(c,i) \quad = \quad K(i,c) \; n_E^+(i) \tag{2.45}$$

Here $n_E(p)$ and $n_E(q)$ are, respectively, the Saha equilibrium population densities of the pth and qth levels of HeI; $n_E^+(i)$ and $n_E^+(j)$ are the Saha equilibrium population densities of the ith and jth levels of HeII.

For the processes described by Eqs. (2.1-2.12), the time derivatives of the HeI and HeII levels, after incorporating the Saha equilibrium population densities, may be written as follows:

$$\frac{\dot{n}(p)}{n_E(p)} = -\rho(p)\left\{ n_e\left[\sum_{i=1}^{15} K(p,i) + \sum_{q \neq p}^{32} K(p,q) \right] \right.$$

$$+ n(1) \sum_{q \neq p}^{32} KN(p,q) + \sum_{p>q} A(p,q) + n(1) \left. KN(p,i)_{i=1} \right\}$$

$$+ \sum_{p \neq q}^{32} \rho(q) KN(q,p) n(1) \frac{n_E(q)}{n_E(p)} + \sum_{p \neq q}^{32} \rho(q) K(p,q) n_e$$

$$+ \sum_{q>p} \rho(q) A(q,p) \frac{n_E(q)}{n_E(p)} + n_e K(p,i)_{i=1} + \frac{n_e^2}{X\, n_E(p)} \beta(p)$$

$$\tag{2.46}$$

and

$$\frac{\dot{n}^+(i)}{n_E^+(i)} = -\rho^+(i)\left\{ n_e\left[K(i,c) + \sum_{i \neq j}^{15} K(i,j) \right] + \sum_{i>j} A(i,j) \right\}$$

$$+ \sum_{i \neq j}^{15} \rho^+(j) K(i,j) n_e + \sum_{j>i} \rho^+(j) \frac{n_E^+(j)}{n_E^+(i)} A(j,i)$$

$$+ \sum_{p=1}^{32} \rho(p) n_e \frac{n_E(p)}{n_E^+(i)} K(p,i) + n_e K(i,c) + \frac{n_e^2}{Y} \frac{\beta(i)}{n_E^+(i)}$$

$$\tag{2.47}$$

where

$$\rho(p) = \frac{n(p)}{n_E(p)} \quad \text{and} \quad \rho^+(i) = \frac{n^+(i)}{n_E^+(i)} \,; \tag{2.48}$$

$n(p)$ and $n^+(i)$ represent the population densities of pth level of HeI and ith level of HeII respectively. In the form of matrix,

the rate equations (2.46) and (2.47) can be represented (Figure 2.2) as

$$\frac{\dot{n}(p)}{n_E(p)} = A\,\rho(p) + B + C \qquad (2.49)$$

where $\frac{\dot{n}(p)}{n_E(p)}$ is a column matrix containing 47 elements. The values of p from 1 to 32 refer to HeI levels and from 33 to 47 refer to HeII levels. p = 33 represents the ground level (i = 1) of HeII while p = 47 indicates i = 15 level of HeII. A is a 47 x 47 matrix containing the coefficients of ρ's. B and C are column matrices, each containing 47 elements which are independent of ρ's.

Under the quasi-steady state conditions, it may be assumed that the time derivatives $\dot{n}(p)$ for the excited states are negligible compared to those for the ground states of HeI and HeII. Hence an inhomogeneous stationary state solution can be obtained by equating the right hand sides of Eq. (2.46) for $p \neq 1$ and Eq. (2.47) for $i \neq 1$ to zero. Thus equation (2.49) reduces to

$$A\,\rho(p) = -B - C \qquad (2.50)$$

where A now is a 45 x 47 matrix, the elements of which correspond to p = 2 to p = 32 and p = 34 to p = 47. It may be mentioned here that A is obtained by droping the first and thirty third rows of the old matrix. Similarly B and C, now contain only 45 elements each.

On transferring the first and thirty third columns of A to right hand side and multiplying both sides by -1, one gets (Figure 2.3)

$$-A\,\rho(p) = B + C + D\,\rho(1) + E\,\rho(33) \qquad (2.51)$$

$$\begin{matrix} \dfrac{\dot{n}(p)}{n_E(p)} \\ \\ \dfrac{\dot{n}(i)}{n_E^+(i)} \end{matrix} = \text{(matrix A)} \times P(p), P^+(i) \; + \; B \; + \; C$$

Matrix labels (regions):

FIRST ROW

$n_e K(p,q) + A(q,p) \cdot \dfrac{n_E(q)}{n_E(p)}$

$n_e K(p,q)$

ZEROS

2

1

33 — THIRTY THIRD ROW

47

$n_e K(p,i) \cdot \dfrac{n_E(p)}{n_E^+(i)}$

(DIRECT IONIZATION - EXCITATION)

$n_e K(i,j) + A(j,i) \cdot \dfrac{n_E^+(j)}{n_E^+(i)}$

$n_e K(i,j)$

Columns: $P(p)$, $P^+(i)$; B ; C

Legend:
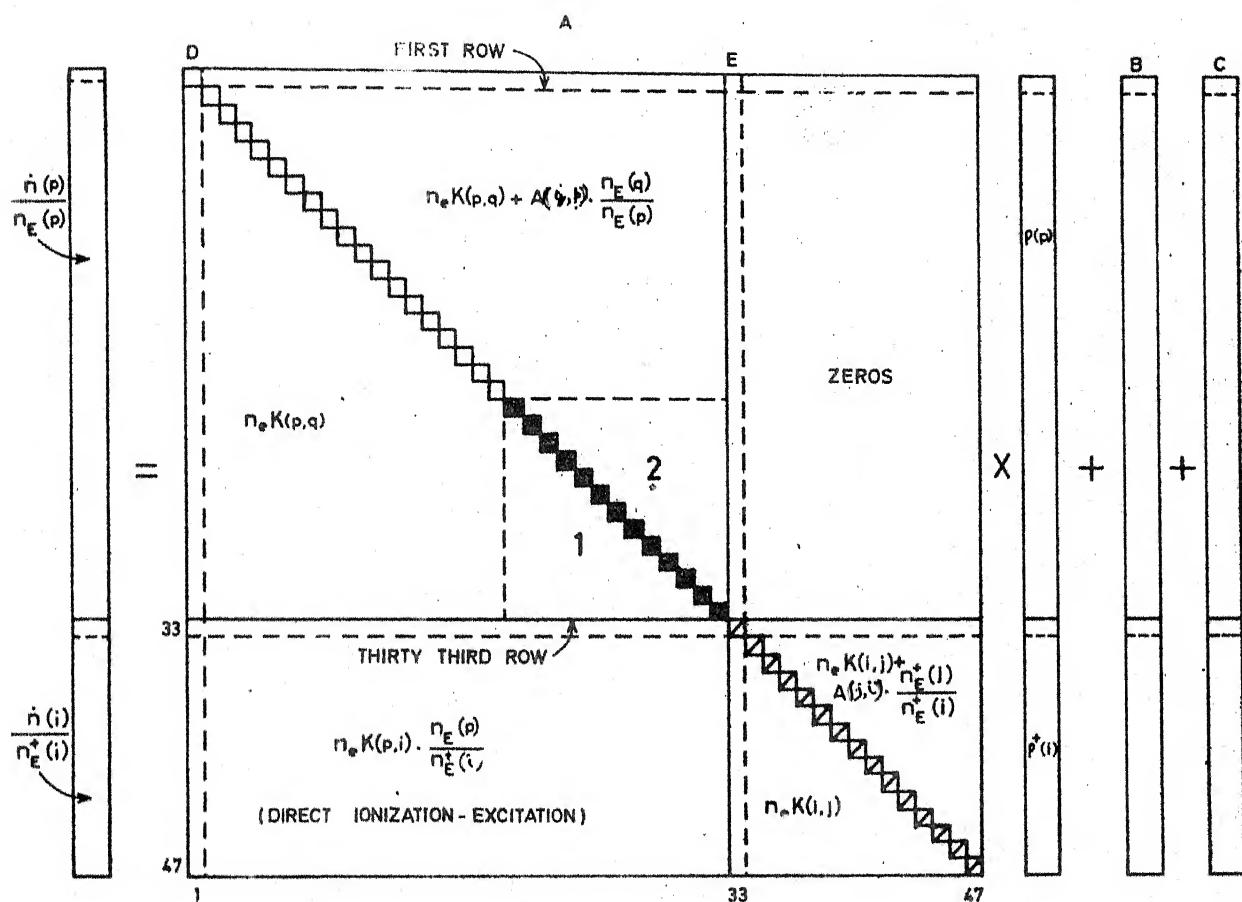
$\square \longrightarrow -n_e\left\{\displaystyle\sum_{i=1}^{15} K(p,i) + \sum_{p \neq q}^{32} K(p,q)\right\} - \sum_{p>q} A(p,q) \qquad p=1\text{-}19$

$\blacksquare \longrightarrow -n_e\left\{\displaystyle\sum_{i=1}^{15} K(p,i) + \sum_{p \neq q}^{32} K(p,q)\right\} - \sum_{p>q} A(p,q) - n(1)\left\{KN(p,i) + \sum_{p \neq q}^{32} KN(p,q)\right\} \qquad p=20\text{-}32$

$\boxtimes \longrightarrow -n_e\left\{K(i,c) + \displaystyle\sum_{i \neq j}^{15} K(i,j)\right\} - \sum_{i>j} A(i,j) \qquad i=1\text{-}15 \ (\text{He II})$

$1 \longrightarrow n_e K(p,q) + n(1) \cdot \dfrac{n_E(q)}{n_E(p)} \cdot KN(q,p) \qquad p=20\text{-}32$

$2 \longrightarrow n_e K(p,q) + A(q,p) \cdot \dfrac{n_E(q)}{n_E(p)} + n_E(q) \cdot KN(p,q) \cdot \dfrac{n(1)}{n_E(p)} \qquad p=20\text{-}32$

$B \longrightarrow n_e K(p,i)_{i=1} \quad \text{and} \quad n_e K(i,c) \qquad p=1\text{-}32, \ i=1\text{-}15$

$C \longrightarrow \dfrac{\beta(p) \, n(1) \, n_e}{n_E(p)} \quad \text{and} \quad \dfrac{\beta(i) \, n^{++} n_e}{n_E^+(i)} \qquad p=1\text{-}32, \ i=1\text{-}15$

Figure 2.2. Matrix representation of collisional-radiative rate processes.

$$O = \begin{bmatrix} 45 \times 45 \end{bmatrix}\begin{bmatrix} \rho \end{bmatrix} + \begin{bmatrix} \\ \end{bmatrix} + \begin{bmatrix} \\ \end{bmatrix} + \begin{bmatrix} \\ \end{bmatrix}^{\rho(1)} + \begin{bmatrix} \\ \end{bmatrix}^{\rho(33)}$$

A   B   C   D   E

$$- \begin{bmatrix} \\ \end{bmatrix}\begin{bmatrix} \rho \end{bmatrix} = \begin{bmatrix} \\ \end{bmatrix} + \begin{bmatrix} \\ \end{bmatrix} + \begin{bmatrix} \\ \end{bmatrix}^{\rho(1)} + \begin{bmatrix} \\ \end{bmatrix}^{\rho(33)}$$

A   B   C   D   E

$$\begin{bmatrix} \rho \end{bmatrix} = \begin{bmatrix} \\ \end{bmatrix}^{-1} \times \left(\begin{bmatrix} \\ \end{bmatrix} + \begin{bmatrix} \\ \end{bmatrix} + \begin{bmatrix} \\ \end{bmatrix}^{\rho(1)} + \begin{bmatrix} \\ \end{bmatrix}^{\rho(33)} \right)$$

A   F

$$\begin{bmatrix} n \end{bmatrix} = \sum_{k=1}^{4} \sum_{j=1}^{45}$$

G

Figure 2.3. Diagrammatic representation of the procedure of calculating population densities of HeI and HeII levels.

The elements of A (a 45 x 45 matrix) correspond to levels $p = 2$ to $p = 32$ and $p = 34$ ($i = 2$) to $p = 47$ ($i = 15$). The column vector $\rho(p)$ contains ρ's corresponding to $p = 2$ to $p = 32$ and $p = 34$ to $p = 47$. $\rho(1)$ is given by $n(1)/n_E(1)$ and $\rho(33)$ by $n^+(1)/n_E^+(1)$ where $n(1)$ and $n^+(1)$ represent the population densities of HeI and HeII ground states. $n_E(1)$ and $n_E^+(1)$ are corresponding Saha equilibrium population densities. D is a column matrix whose elements are those which are transferred from the first column of A and E contains the elements of the thirty third column of A. Eq. (2.51) can be rewritten as

$$\rho(p) \;=\; A^{-1} \left[B + C + D \, \rho(1) + E \, \rho(33) \right] \tag{2.52}$$

or $\qquad \rho(p) \;=\; r_0(p) + r_1(p) \, \rho(1) + r_2(p) \, \rho(33) \tag{2.53}$

where $\quad r_0 = A^{-1}(B + C), \quad r_1 = A^{-1}D \quad$ and $\quad r_2 = A^{-1}E.$

where $\quad A^{-1}$ represents the inverse of matrix $(-A)$.

Eq. (2.53) represents the solution of Eqs. (2.46) and (2.47) in terms of local ground state population densities of HeI and HeII. Eq. (2.53) can be written separately for HeI and HeII levels in the following form

$$\rho(p) \;=\; r_0(p) + r_1(p) \, \rho(1) \tag{2.54}$$

$$\rho^+(i) \;=\; r_0^+(i) + r_1^+(i) \, \rho(1) + r_2^+(i) \, \rho^+(1) \tag{2.55}$$

Diagramatically this is shown in Figure 2.3. Eq. (2.54) gives the reduced population coefficients for HeI levels. It may be mentioned that this equation contains no term involving r_2 because first 31 elements of E are zeros. $r_0(p)$, $r_1(p)$ and r_2 are termed

as the population coefficients. $r_0(p)$ represents the contribution from the first continuum towards $\rho(p)$ and $r_1(p)$ $\rho(1)$ is the contribution from the ground state of HeI. Eq. (2.55) gives the reduced population coefficients of HeII excited states. $\rho^+(i)$ stands for the values of ρ for He$^+$ levels. r_0^+, r_1^+ and r_2^+ correspond to r_0, r_1 and r_2 values of Eq. (2.53) for He$^+$ levels and $\rho^+(1)$ corresponds to $\rho(33)$. $r_0^+(i)$ is the contribution from the second continuum towards $\rho^+(i)$; $r_1^+(i)$ $\rho(1)$ is the contribution from the ground state of HeI i.e. the contribution from the direct-ionization-excitation process and $r_2^+(i)$ $\rho^+(1)$ is the contribution from the ground state of HeII towards $\rho^+(i)$. It is to be noted that

$$\frac{n_E(p)}{n_E^+(i)} = \frac{g_p}{2g_i} \frac{n^+(1)}{n^{++}} \exp\left(\frac{E_p - E_i}{kT_e}\right) \qquad (2.56)$$

Here g_p and g_i are, respectively, the weight factors of the pth state of HeI and of the ith state of HeII. From Eq. (2.56) it is clear that the value of the ratio $\frac{n^+(1)}{n^{++}}$ must be known in order to obtain the final solution. The final solution for $\rho(p)$, $\rho^+(i)$ and population densities of excited levels of HeI and HeII are thus obtained in terms of n_e, T_e, gas temperature, $n(1)$, $n^+(1)$ and $\frac{n^+(1)}{n^{++}}$ (for computer programme see Appendix IV).

2.3.3. Role of Direct Ionization-Excitation

The rate coefficients for direct ionization-excitation process (Eq. 2.2) are obtained by integrating the cross section expression (Eq. 2.23) over a Maxwellian velocity distribution of electrons in the following way:

$$K(p,i) = \int_{v^*}^{\infty} 46 \times 10^{-4} \; \pi a_o^2 \left(\frac{E_1^H}{E_{pi}}\right)^2 \frac{x-1}{x^2} \ln(10 \; x) \left(\frac{2}{\pi}\right)^{1/2} \left(\frac{m}{kT_e}\right)^{3/2}$$

$$e^{-1/2 \; mv^2/kT_e} \cdot v^2 . v dv \qquad (2.57)$$

Here the terms involved have the same meaning as described in Eqs. (2.23) and (2.33). Following the procedure described in Eqs. (2.33-2.37), one obtains the following expression for $K(p,i)$

$$K(p,i) = 6.25 \times 10^{-3} \frac{1}{T_e^{3/2}} e^{-\alpha} \cdot \frac{1}{\alpha} \int_o^{\infty} \frac{\frac{Z}{\alpha}}{\frac{Z}{\alpha}+1} \ln \left\{10.0\left(1 + \frac{Z}{\alpha}\right)\right\}$$

$$e^{-Z} dZ \qquad (2.58)$$

where $\alpha = \dfrac{E_{pi}}{kT_e}$ and $Z = \alpha(x-1)$

Eq. (2.58) is solved numerically by using the Gaussian Quadrature method involving Laguerre integration.[84]

In Eq. (2.46), the term $-\rho(p) \; n_e \displaystyle\sum_{i=1}^{15} K(p,i)$ represents direct ionization-excitation and depopulates the excited states of HeI. In Eq. (2.47) the direct ionization-excitation process populates the excited states of HeII through the term
$\displaystyle\sum_{i=1}^{32} \rho(p) \; n_e \frac{n_E(p)}{n_E^+(i)} K(p,i)$. On dropping these terms from Eqs. (2.46) and (2.47) and solving the equations simultaneously, the role of this process can be explored.

2.3.4. Mechanism of Population of Excited States

Quantitative calculations based on the collisional-radiative models use cross sections of various processes involved. Due to a paucity of experimentally determined cross-sections, collisional radiative models often lean heavily on cross section data which are either theoretical or empirical. Whereas, some

times there are no alternatives, it is clear that use of these must be kept to a minimum; because, not infrequently, theoretical population densities wherever they can be compared with experimental results are off by as much as 100% and little is achieved by including processes which are not of outstanding importance and whose experimental cross sections are unknown.

As mentioned earlier, the various collisional radiative models, employ a very large number of processes. Therefore, it is worthwhile to neglect the processes whose role is insignificant in populating the excited states. On this basis a simplified model can be evolved. It will be shown in the next chapter that (adopting the procedure outlined below) even more than 70% of the atomic processes used in some of the recent models can be neglected and yet obtaining theoretical population densities substantially close to the values predicted from the models which include all the processes. The following method also permits an insight into the mechanism of the population of a particular level.

For a quasi-steady state solution with population densities of the excited states derived using the population densities of ground levels of HeI and HeII as parameters, the first and the thirty third rows in matrices of Figure 2.2 are removed, and then the left hand side vector is made equal to zero. This results in 45 linear simultaneous equations. The first and the thirty third columns, which respectively involve transitions from the ground states of HeI and HeII, are then transposed (Eq. 2.51).

To identify the important elementary processes and thus to evolve the population mechanism, we proceed with the matrix Eq. (2.52). On the left hand side we have matrix A of dimension

45 x 45 and on the right hand side we have four column matrices B, C, D, and E, each of dimension 45 x 1, which for convenience may be represented by a single matrix F of dimension 45 x 4 (Figure 2.3). The first column of this matrix F contains the three-body recombination coefficients, the second column contains the radiative recombination coefficients. The third and the fourth columns are those transferred from the left side; these contain transitions from the ground levels of HeI and HeII. A three dimensional matrix G of dimension 45 x 45 x 4 is then formed in the following manner:

$$G(i,j,1) = A^{-1}(i,j).F(j,1).n_E(i+1) \qquad (2.59)$$

$$G(i,j,2) = A^{-1}(i,j).F(j,2).n_E(i+1) \qquad (2.60)$$

$$G(i,j,3) = A^{-1}(i,j).F(j,3).n(1).n_E(i+1)/n_E(1) \qquad (2.61)$$

$$G(i,j,4) = A^{-1}(i,j).F(j,4).n_e.n_E(i+1)/n_E(33) \qquad (2.62)$$

where both i and j vary from 1 to 45 and represent both HeI and HeII levels. A^{-1} represents the inverse of matrix $(-A)$, and $n(1)$ and $n(33)$ respectively represent the population densities of ground states of HeI and HeII. For population densities of HeII levels (i.e. $34 \leq i \leq 47$) the factor $(i+1)$ in Eqs. (2.59-2.62) is to be replaced by $(i+2)$. Diagramatically, this is represented in the last equation of Figure 2.3.

The sum of the elements of the ith row of all the four planes of G constitutes the population density of the ith level. The elements on the first plane of G represent contributions from three body recombination and those on the second plane represent

contributions from radiative recombination. The elements of the third and fourth planes represent contributions from the ground states of HeI and HeII respectively. In order to identify the dominant terms, say for level i population density, we start scanning from the ith row of the first plane of G and scan all the elements of the corresponding rows on the four planes. We set all those elements equal to zero whose contributions to population density is less than 5%. This sorts out those terms of F and those of the inverted matrix A^{-1} which are important and also provides relative contributions of the four segments to population density of a particular level. The insignificant elements of F (corresponding to small $A^{-1}.F$ values) are then set equal to zero. This is done for all the levels and this process identifies the important elements of F.

For sorting out those rate coefficients which make dominant contribution to a particular element of the original matrix A, the following procedure is adopted. The diagonal element of the original matrix contain those collisional rate coefficients which contribute to depopulating a level. We scan all the rate coefficients contained in a diagonal element and retain only those rate coefficients which contribute significantly. For non-diagonal elements of the original matrix, we start elementwise from the first row of A. A chosen non-diagonal element is then set equal to zero, matrix A is again inverted and a corresponding matrix G1 of dimension 45 x 45 x 4 is formed after Eqs. (2.59-2.62). A comparison of the non zero elements of G with the corresponding elements of G1 brings out the quantitative role of the element which is set equal to zero in the original matrix.

If any element of G1 differs from the corresponding element of G by more than 15% (an arbitrary limit), it is assumed that the element of A which was made equal to zero is important and is reinstated for all further operations, otherwise it is left as zero. This process is repeated over all the elements of A. The individual rate coefficients and transition probabilities contained in the remaining non-diagonal elements are further scanned and only those which contribute significantly are retained. A is then left with only important rate coefficients and transition probabilities in diagonal and non-diagonal elements. In order to identify the processes which are important in determining the population densities of individual levels, we proceed as follows. In matrix A (now containing only the important terms), one particular rate coefficient is set equal to zero and the resulting matrix A_o' is inverted $(A_o'^{-1})$. Those elements of the inverted matrix $A_o'^{-1}$ which are important for population of a particular level are compared with the corresponding elements of the inverted matrix A^{-1} (with no rate coefficient equal to zero). If the inverted matrix elements of A_o^{-1} show significant departure (say more than 10%), we assume that the particular rate coefficient, which was set to zero, to be important for all those levels whose corresponding matrix elements show considerable departures. This is repeated with all rate coefficients and transition probabilities and this yields the mechanism of population.

2.3.5. Laser Induced Selective Excitation

If the plasma is subjected to a tunable laser radiation resonant between a lower state p and an upper state q of HeI, the radiative processes induced can be written as

$$He(p) + h\nu \quad \frac{W(p,q)}{W(q,p)} \quad He(q) \qquad (2.63)$$

where $W(p,q)$ is the rate of induced absorption and $W(q,p)$ represents the rate of induced emission. The induced transition rate may be obtained by multiplying the radiation density per unit frequency interval $\rho(\nu)$ with the Einstein absorption coefficients corresponding to the transition and integrating the product over the line shape functions of the transition as well as that of the laser pulse. We must mention here that due to non equilibrium situation, the commonly used A, B (Einstein coefficients) relationship is not strictly applicable, though it has been used in recent literature.[51] In a later section we shall discuss the possible nature of the departures.

(a) Laser power and radiation density: Radiation density $\rho(\nu)$ is defined in terms of the energy per unit volume per unit frequency interval. Let I be the intensity (in watt/cm^2) of the laser pulse. This means that I amount of energy is passing through 1 sq. cm. area in 1 sec. Therefore in 1 sec, I energy will b contained in volume c cm^{-3} (1 sq. cm x c), where c is the velocity of light. Therefore density is given by

$$\rho = \frac{I}{c} \qquad (2.64)$$

Further if the full width at half maximum of the laser pulse $\Delta\nu'$ is larger than the width of the transition $\Delta\nu$, the energy density per unit volume per unit frequency interval may be given by

$$\rho(\nu) = \frac{I/\Delta\nu'}{c} \qquad (2.65)$$

(b)   Rate of induced transitions: The Einstein coeffi-
cients for induced absorption $B(p,q)$ and for induced emission
$B(q,p)$ are given by

$$B(q,p) \;=\; \frac{c^3}{8\pi h\, \nu^3} \cdot A(q,p)_{q>p} \tag{2.66}$$

and $$B(p,q) \;=\; \frac{g_q}{g_p} \cdot B(q,p) \tag{2.67}$$

where ν is the frequency of the transition $q \to p$ and g_p and g_q
are the weight factors of levels p and q respectively.

The induced transition rate $W'(q,p)$ due to interaction
with the field is given by[85]

$$W'(q,p) \;=\; B(q,p)\,\rho(\nu)$$

$$\;=\; \frac{c^3}{8\pi h\, \nu^3} \cdot A(q,p) \cdot \rho(\nu) \tag{2.68}$$

To derive the induced transition rate $W(q,p)$ due to a single
frequency field, it is postulated that the transition rates due
to different frequencies in a multifrequency radiation field are
additive so that Eq. (2.68) is a special case of a more general
form given by

$$W'(q,p) \;=\; \int_{-\infty}^{\infty} \frac{c^3\, A(q,p)}{8\pi h\, \nu^3}\, \rho(\nu')\, g(\nu' - \nu_0)\, d\nu' \tag{2.69}$$

where $g(\nu' - \nu_0)$ is the normalized line shape function (centred
at ν_0) for the transition. ν_0 is the frequency corresponding to
the peak of the radiation field.

In a monochromatic radiation field of frequency ν and
radiation density ρ_ν the energy density per unit frequency $\rho(\nu')$ is

$$\rho (\nu') = \rho_\nu \, \delta (\nu' - \nu) \tag{2.70}$$

where $\delta (\nu' - \nu)$ is a Dirac delta function. Eq. (2.70) when used in Eq. (2.69) gives

$$W(q,p) = \frac{c^3}{8 \pi h \, \nu^3} A(q,p) \, \rho_\nu \qquad g(\nu - \nu_o) \tag{2.71}$$

The rate of induced absorption similarly is given by

$$W(p,q) = (\frac{g_q}{g_p}) \frac{c^3}{8 \pi h \, \nu^3} \cdot A(q,p) \cdot \rho_\nu \qquad g(\nu - \nu_o) \tag{2.72}$$

It is assumed that the laser pulse is of Gaussian shape. The Gaussian line shape results most often in absorption or emission from gaseous particles. The resulting radiation is Doppler shifted owing to the velocity spread of the emitting particles. For a gas in thermal equilibrium, the velocity distribution function is Maxwellian and the resulting frequency distribution function $g(\nu - \nu_o)$ is a Gaussian. The normalized Gaussian[85] can be written as

$$g(\nu - \nu_o) = \frac{2(\ln 2)^{1/2}}{\pi^{1/2} \, \Delta\nu} \, e^{-4(\ln 2)(\frac{\nu - \nu_o}{\Delta\nu})^2} \tag{2.73}$$

where $\Delta\nu$ is the full width at half maximum (FWHM) and is given by

$$\Delta\nu = \Delta\nu_{Doppler} = 2\nu_o \sqrt{\frac{2k \, T_g}{m_{He} c^2} \ln 2}$$

where T_g is the gas temperature and m_{He} the mass of helium atom.

(c) Enhancement in population densities: When a laser pulse is tuned to a particular transition (say $p' \to q'$), the population densities of most of the other levels do not change

much. Only the population densities of the upper level q' and few other levels are enhanced. The time derivatives of the excited states other than p' and q' can still be described by Eqs. (2.46) and (2.47). The time derivative of the lower level p' is given by the following equation:

$$
\frac{\dot{n}(p')}{n_E(p')} = -\rho(p')\left\{n_e\left[\sum_{i=1}^{15} K(p',i) + \sum_{q\neq p'}^{32} K(p',q)\right]\right.
$$

$$
+ n(1) \sum_{q\neq p'}^{32} KN(p',q) + \sum_{p'>q} A(p',q) + n(1)\, KN(p',i)_{i=1}
$$

$$
+ W(p',q')\, L(t)\right\} + \rho(q')\, W(q',\mathbf{p'}) \frac{n_E(q')}{n_E(p')} L(t) + \sum_{p'\neq q}^{32} \rho(q)\cdot
$$

$$
KN(q,p')\, n(1) \frac{n_E(q)}{n_E(p')} + \sum_{p'\neq q}^{32} \rho(q)\, K(q,p')n_e
$$

$$
+ \sum_{q>p'} \rho(q)\, A(q,p') \frac{n_E(q)}{n_E(p')} + n_e\, K(p',i)_{i=1}
$$

$$
+ \frac{n_e^2}{\bar{x}\, n_E(p')}\, \beta(p') \tag{2.74}
$$

where L(t) is the shape function of the laser pulse. Similarly, the time derivative of the upper level q' can be obtained by replacing p' by q' and q' by p' in Eq. (2.74).

Eq. (2.46) (for p ≠ p' and q'), Eq. (2.47) and Eq. (2.74) (for p' and q') form a set of 47 linear first order differential equations. On multiplying these equations with the corresponding $n_E(p)$ values, one gets the following equation in the matrix form

$$
\frac{d}{dt}\, n(p) = A \cdot n(p) + B \tag{2.75}
$$

where n(p) is a vector of population densities containing 47 elements. A is a 47 x 47 matrix, which is a function of time and

B is a column matrix containing 47 elements and is independent of time.

Assuming that the electron density does not change with time, the population densities as a function of time can be obtained by solving the system of equations described by Eq. (2.75). In this work, the system of 47 coupled linear first order differential equations is solved numerically by using Hamming's modified predictor-corrector method.[86] It is a stable fourth order integration procedure and obtains a fairly accurate solution of the system of coupled differential equations with given initial values. The initial population densities of all excited states are taken as the quasi-steady state population densities. Hamming's predictor-corrector method is not self starting i.e. the functional values at a single previous point are not enough to obtain the functional values ahead. Therefore, to get the starting values, a special Runge Kutta procedure[87] followed by one iteration step is added to the predictor-corrector method. The solution of Eq. (2.75) gives the population densities of all excited states (including those optically pumped) as a function of time. The enhancement of the population density $n_{p'}$ of level p' is defined as follows:

$$E_{p'}(t) = \frac{n_{p'}(t) - n_{p'}(t = 0)}{n_{p'}(t = 0)} \tag{2.76}$$

where $n_{p'}(t = 0)$ is the population of level p' before the laser pulse is injected. This initial state is assumed to be a quasi-steady state solution of Eqs.(2.46) and (2.47).

In the time dependent solution of Eq. (2.75), only the laser flux is assumed to be a time dependent quantity. The shape of the laser pulse L(t) is given by

$$L(t) = \frac{t}{\tau} \qquad \text{for} \quad 0 < t < \tau \qquad (2.77)$$

$$L(t) = \frac{2\tau - t}{\tau} \qquad \tau < t \qquad (2.78)$$

where τ is the FWHM (nsec) of the laser pulse. The subroutine used to solve the linear system of first-order coupled differential equations is given in Appendix V.

CHAPTER 3

RESULTS OF CALCULATIONS

3.1. RATE COEFFICIENTS

Typical values of rate coefficients for various types of transitions of HeI and HeII calculated on the basis of procedure described in Chapter 2 for a wide range of kT_e are presented in Tables 3.1-3.4. Electron impact excitation rate coefficients for optically allowed and optically forbidden transitions of HeI are presented in Table 3.1 in the kT_e range 1-20 eV. Table 3.2 presents electron impact ionization, direct ionization-excitation and radiative recombination rate coefficients for HeI. The rate coefficients for heavy particle excitation, deexcitation, ionization and recombination are listed in Table 3.3. Table 3.4 presents rate coefficients for electron impact excitation, ionization and radiative recombination for HeII in the kT_e range of 1-20 eV.

3.2. OPTICAL ESCAPE FACTORS

Values of optical escape factors for the resonance transitions of HeI and HeII calculated using Eq. (2.32) are presented in Table 3.5. The values correspond to $T_g = 300°K$, $n(1) = 2.0 \times 10^{14}$ cm^{-3}, $1 = 0.84$ cm and $n_e = 10^{10}$, 10^{12} and 10^{14} cm^{-3}. The corresponding values of α_{pq} and $\hat{\tau}_{pq}$ are also given in Table 3.5.

3.3. POPULATION DENSITIES

The computed values of reduced population coefficients (results partially presented in Ref. 56) r_o and r_1 for HeI are

Table 3.1. Electron impact excitation rate coefficients for HeI (cm^3 sec^{-1})

Type of Transition	Transition	kT_e =1 eV	3 eV	5 eV	8 eV	10 eV	12 eV	15 eV	18 eV
Optically allowed	1^1S-2^1P	7.4-18*	2.9-12	4.8-11	2.6-10	4.6-10	6.9-10	1.1-09	1.4-09
	1^1S-3^1P	7.3-19	4.5-13	8.2-12	4.8-11	8.9-11	1.4-10	2.2-10	3.0-10
	1^1S-4^1P	2.9-19	1.1-13	2.5-12	1.7-11	3.3-11	5.2-11	8.7-11	1.2-10
	1^1S-5^1P	4.6-19	9.3-14	1.5-12	8.7-12	1.6-11	2.6-11	4.3-11	6.1-11
	2^1P-3^1D	5.9-08	3.3-07	4.8-07	5.8-07	6.2-07	6.5-07	6.7-07	6.8-07
Optically forbidden (with change in multiplicity)	1^1S-2^3S	4.5-17	4.8-12	4.5-11	1.5-10	2.1-10	2.5-10	2.9-10	3.2-10
	1^1S-3^3S	6.5-20	2.8-12	5.5-12	2.7-11	4.3-11	5.7-11	7.4-11	8.5-11
	1^1S-2^3P	4.3-18	4.1-13	3.7-12	1.2-11	1.7-11	2.1-11	2.6-11	2.8-11
	2^3S-2^1S	2.5-07	2.5-07	2.1-07	1.8-07	1.6-07	1.5-07	1.4-07	1.3-07
	2^3S-3^1D	2.0-09	9.4-09	9.3-09	7.3-09	6.2-09	5.3-09	4.3-09	3.6-09
Optically forbidden (without change in multiplicity)	1^1S-2^1S	3.2-18	8.2-13	1.0-11	4.5-11	7.4-11	1.0-10	1.5-10	1.8-10
	1^1S-3^1S	1.3-20	8.7-14	2.1-12	1.3-11	2.4-11	3.6-11	5.4-11	7.0-11
	1^1S-4^1S	4.4-19	9.1-14	1.4-12	7.0-12	1.2-11	1.6-11	2.3-11	2.9-11
	1^1S-5^1S	2.1-22	2.0-14	5.6-13	3.2-12	5.4-12	7.8-12	1.1-11	1.4-11
	2^1S-3^1S	1.4-08	5.3-08	6.2-08	6.4-08	6.3-08	6.2-08	5.9-08	5.7-08

* Read 7.4-18 as 7.4×10^{-18}.

Table 3.2. Electron impact ionization, direct ionization-excitation and radiative coefficients for HeI (cm^3 sec^{-1})

Type of Transition	Transition	kT_e=1 eV	3 eV	5 eV	8 eV	10 eV	12 eV	15 eV	18 eV
Electron impact ionization	1^1S–i=1	3.7–20*	1.4–12	5.6–11	5.0–10	1.1–09	1.8–09	3.2–09	4.6–09
	2^3S–i=1	7.7–10	4.0–08	9.7–08	1.6–07	2.0–07	2.2–07	2.5–07	2.6–07
	2^1S–i=1	2.6–09	7.5–08	1.6–07	2.5–07	2.9–07	3.2–07	3.5–07	3.7–07
	3^1P–i=1	2.5–07	1.1–06	1.4–06	1.7–06	1.7–06	1.7–06	1.8–06	1.8–06
	n=6–i=1	1.0–05	1.4–05	1.4–05	1.3–05	1.3–05	1.2–05	1.1–05	1.1–05
Direct ionization- excitation	1^1S–i=4	< 10^{-38}	3.8–23	1.1–18	4.0–16	2.9–15	1.1–14	4.2–14	1.0–13
	2^3S–i=4	2.2–36	5.1–20	1.1–16	8.6–15	3.7–14	1.0–13	2.8–13	5.4–13
	2^1S–i=4	5.0–36	6.9–20	1.3–16	9.7–15	4.2–14	1.1–13	3.0–13	5.8–13
	2^1P–i=4	9.3–36	8.6–20	1.5–16	1.1–14	4.5–14	1.2–13	3.2–13	6.1–13
	3^1P–i=10	3.3–36	6.0–20	1.2–16	9.1–15	3.9–14	1.1–13	2.9–13	5.6–13
Radiative recombin- ation	i=1–1^1S	3.6–02	2.1–02	1.6–02	1.3–02	1.1–02	1.0–02	9.3–03	8.5–03
	–2^3S	3.5–03	2.0–03	1.5–03	1.2–03	1.1–03	9.9–04	8.9–04	8.2–04
	–2^1S	2.5–03	1.4–03	1.1–03	8.9–04	7.9–04	7.2–04	6.5–04	5.9–04
	–3^1P	5.0–04	2.9–04	2.3–04	1.8–04	1.6–04	1.5–04	1.3–04	1.2–04
	–4^1D	2.1–04	1.2–04	9.3–05	7.4–05	6.6–05	6.0–05	5.4–05	4.9–05

* Read 3.7–20 as 3.7 x 10^{-20}.

Table 3.3.   Heavy particle collisional excitation, deexcitation
              ionization and recombination rate coefficients
              $(cm^3 \ sec^{-1})$

              $(kT_e = 10 \ eV, \quad T_g = 300°K \quad and \quad 1000°K)$

Type of Transition	Transition	$T_g = 300°K$	$T_g = 1000°K$
Neutral-neutral excitation KN(p,q)	3^1D-3^1P	$2.23-10^*$	$1.66-09$
	3^3D-3^1P	$1.09-10$	$8.12-10$
	3^1S-3^1P	$4.24-14$	$1.09-11$
Neutral-neutral deexcitation KN(q,p)	3^1P-3^1D	$6.15-10$	$3.22-09$
	3^1P-3^3D	$9.10-10$	$4.74-09$
	3^1P-3^1S	$8.94-12$	$2.53-11$
Neutral-neutral ionization $KN(p,i)_{i=1}$	n=6 i=1	$2.34-16$	$2.02-11$
	n=8 i=1	$9.38-13$	$1.15-09$
	n=10 i=1	$4.47-11$	$8.78-09$
Recombination $KN(i,p)_{i=1}$	i=1 n=6	$7.44-36$	$1.79-31$
	i=1 n=8	$5.59-32$	$2.58-29$
	i=1 n=10	$3.11-30$	$2.62-28$

* Read 2.23-10 as 2.23×10^{-10}.

Table 3.4. Rate coefficients for HeII (cm^3 sec^{-1})

Type of Transition	Transition	kT_e=1 eV	3 eV	5 eV	8 eV	10 eV	12 eV	15 eV	18 eV
Electron impact excitation	i=1-i=2	1.2-25*	4.5-14	8.1-12	1.4-10	3.4-10	6.1-10	1.1-09	1.5-09
	1-i=3	1.0-29	5.9-16	2.9-13	8.5-12	2.6-11	5.2-11	1.0-10	1.6-10
	1-i=4	2.5-31	8.4-17	5.9-14	2.1-12	6.8-12	1.5-11	3.0-11	4.9-11
	2-i=4	2.6-12	1.4-09	4.1-09	7.0-09	8.1-09	8.8-09	9.3-09	9.5-09
	3-i=4	1.4-07	4.6-07	5.1-07	4.9-07	4.7-07	4.5-07	4.2-07	3.9-07
Electron impact ionization	i=1-c	1.5-31	5.0-16	5.5-13	2.6-11	8.9-11	2.0-10	4.5-10	7.5-10
	2-c	3.2-13	1.6-09	7.7-09	1.7-08	2.1-08	2.4-08	2.7-08	2.9-08
	4-c	3.5-08	1.9-07	2.4-07	2.4-07	2.3-07	2.3-07	2.1-07	2.0-07
	10-c	3.8-06	3.1-06	2.6-06	2.1-06	1.9-06	1.8-06	1.6-06	1.5-06
	15-c	1.1-05	7.8-06	6.2-06	5.0-06	4.5-06	4.1-06	3.7-06	3.4-06
Radiative recombination	He^{++} -i=1	3.2-01	6.0-02	2.8-02	1.3-02	9.3-03	6.9-03	4.8-03	3.6-03
	-i=2	4.3-02	7.6-03	3.3-03	1.5-03	1.0-03	7.3-04	4.9-04	3.5-04
	-i=4	4.9-03	7.5-04	3.0-04	1.2-04	7.9-05	5.6-05	3.6-05	2.5-05
	-i=5	2.4-03	3.4-04	1.3-04	5.1-05	3.3-05	2.3-05	1.4-05	9.8-06
	-i=10	2.0-04	2.3-05	7.8-06	2.8-06	1.7-06	1.1-06	6.7-07	4.4-07

* Read 1.2-25 as 1.2×10^{-25}.

Table 3.5. Optical escape factors for resonance transitions of HeI and HeII

$$ (n(1) = 2.0+14 \text{ cm}^{-3}, \quad T_g = T_i = 300°K, \quad l = 0.84 \text{ cm}) $$

Transition (p,q)	$n_e = 10^{10} \text{ cm}^{-3}$			$n_e = 10^{12} \text{ cm}^{-3}$			$n_e = 10^{14} \text{ cm}^{-3}$	
	α_{pq}	$\hat{\tau}_{pq}$	Λ_{pq}	α_{pq}	$\hat{\tau}_{pq}$	Λ_{pq}	α_{pq}	$\hat{\tau}_{pq}$
HeI								
$2^1P \rightarrow 1^1S$	2.94−07*	3.63+01	8.37−03	2.94−05	3.63+01	8.93−03	2.94−03	3.62+01
$3^1P \rightarrow 1^1S$	2.16−06	8.86+00	4.50−02	2.16−04	8.86+00	4.80−02	2.16−02	8.74+00
$4^1P \rightarrow 1^1S$	7.89−06	3.54+00	1.43−01	7.89−04	3.54+00	1.52−01	7.89−02	3.32+00
$5^1P \rightarrow 1^1S$	2.08−05	1.77+00	3.23−01	2.08−03	1.77+00	3.43−01	2.08−01	1.39+00
$6^1P \rightarrow 1^1S$	4.53−05	9.76−01	5.49−01	4.53−03	9.73−01	5.84−01	4.53−01	5.01−01
HeII								
$2^2P \rightarrow 1^2S$	5.66−07	1.42−03	1.0	5.66−05	1.42−01	9.81−01	5.66−03	1.42+01
$3^2P \rightarrow 1^2S$	4.52−06	2.28−04	1.0	4.52−04	2.28−02	1.0	4.52−02	2.20+01
$4^2P \rightarrow 1^2S$	1.69−05	7.92−05	1.0	1.69−03	7.91−03	1.0	1.69−01	6.62−01
$5^2P \rightarrow 1^2S$	4.52−05	3.72−05	1.0	4.52−03	3.71−03	1.0	4.52−01	1.91−01
$6^2P \rightarrow 1^2S$	9.89−05	2.05−05	1.0	9.89−03	2.04−03	1.0	9.89−01	4.34−01

* Read 2.94−07 as 2.94×10^{-7}.

presented in Figures 3.1-3.8 and the values of r_o^+, r_1^+ and r_2^+ are presented in Figures 3.9-3.14. The data presented in these figures refer to kT_e = 1.38 eV (1.6 x 10^4 °K) or kT_e = 10 eV, T_g = 1000°K, (n^+/n^{++}) = 1000, $n(1)$ = 1.0 x 10^{14} cm^{-3}, and $n^+ \approx n_e$. The electron temperature kT_e = 1.38 eV and 10 eV were chosen to allow a comparison of calculated results with the results of Refs. 51 and 52. In Ref. 51, the results are presented at kT_e = 10 eV while in Ref. 52 the results are given at kT_e = 1.38 eV.

Figure 3.1 shows a plot of log r_o vs electron density at kT_e = 1.38 eV for optically thin conditions. The dotted lines represent the results of Fujimoto.[52]. Figure 3.2 presents a plot of log r_o against electron density at kT_e = 10 eV under optically thin condition. The r_o values for the 3^1S, 3^1P and 4^1F levels are compared with the values of Hess and Burrell.[51] Using partially optically thick conditions, the values of r_o increase considerably. This is evident from Figures 3.3 and 3.4 where log r_o values have been plotted against n_e at kT_e = 1.38 eV and kT_e = 10 eV, respectively. Figure 3.5 presents log r_1 values plotted against n_e at kT_e = 1.38 eV for optically thin conditions. At kT_e = 10 eV, log r_1 values are plotted against n_e for the optically thin case in Figure 3.6. The dotted lines correspond to the r_1 values of 3^1D from Hess and Burrell.[51] Figures 3.7 and 3.8 are plots of log r_1 vs n_e for the partially optically thick case at kT_e = 1.38 and 10 eV, respectively. The values of r_1 also increase in the transition from the optically thin case to the partially optically thick case.

Figures 3.9-3.11 present reduced population coefficients of HeII levels at kT_e = 1.38 eV under optically thin conditions.
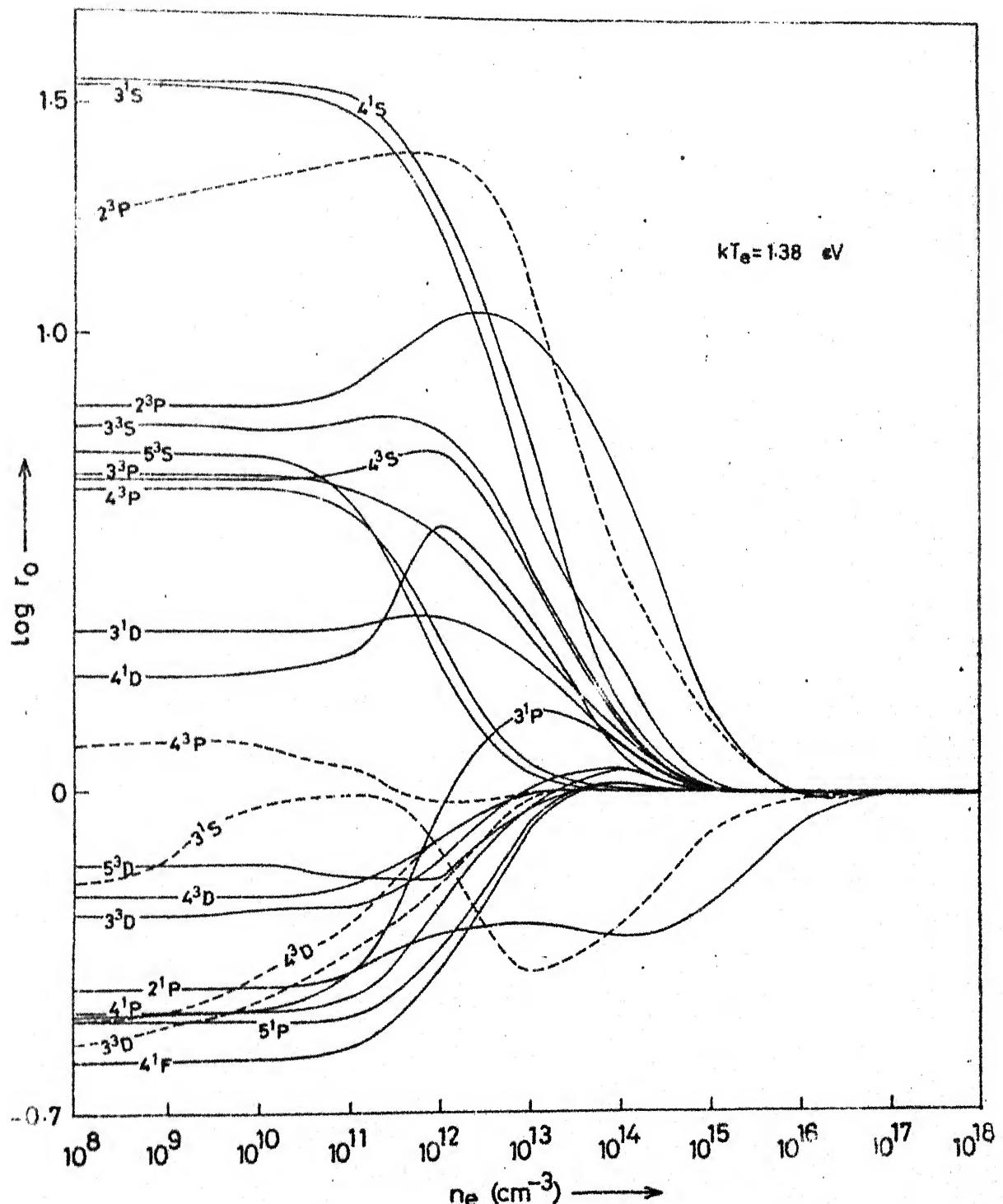
Figure 3.1. Plot of log r_o for HeI as a function of electron density at $kT_e = 1.38$ eV for the optically thin case; ———, present work; ------, Ref. 52.
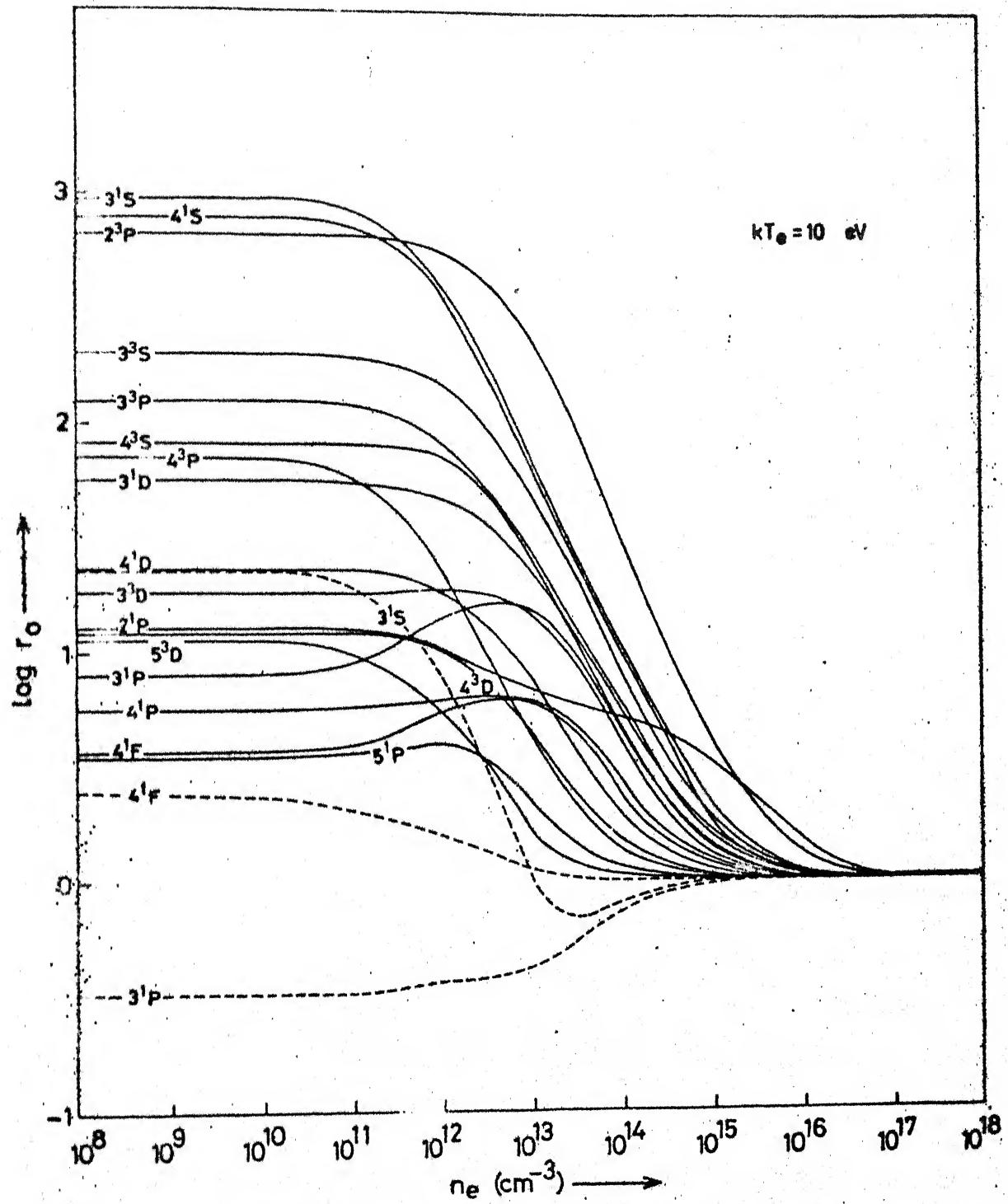
Figure 3.2. Plot of log r_o for HeI vs electron density at $kT_e = 10$ eV for the optically thin case; ———, present work; —————, Ref. 51.
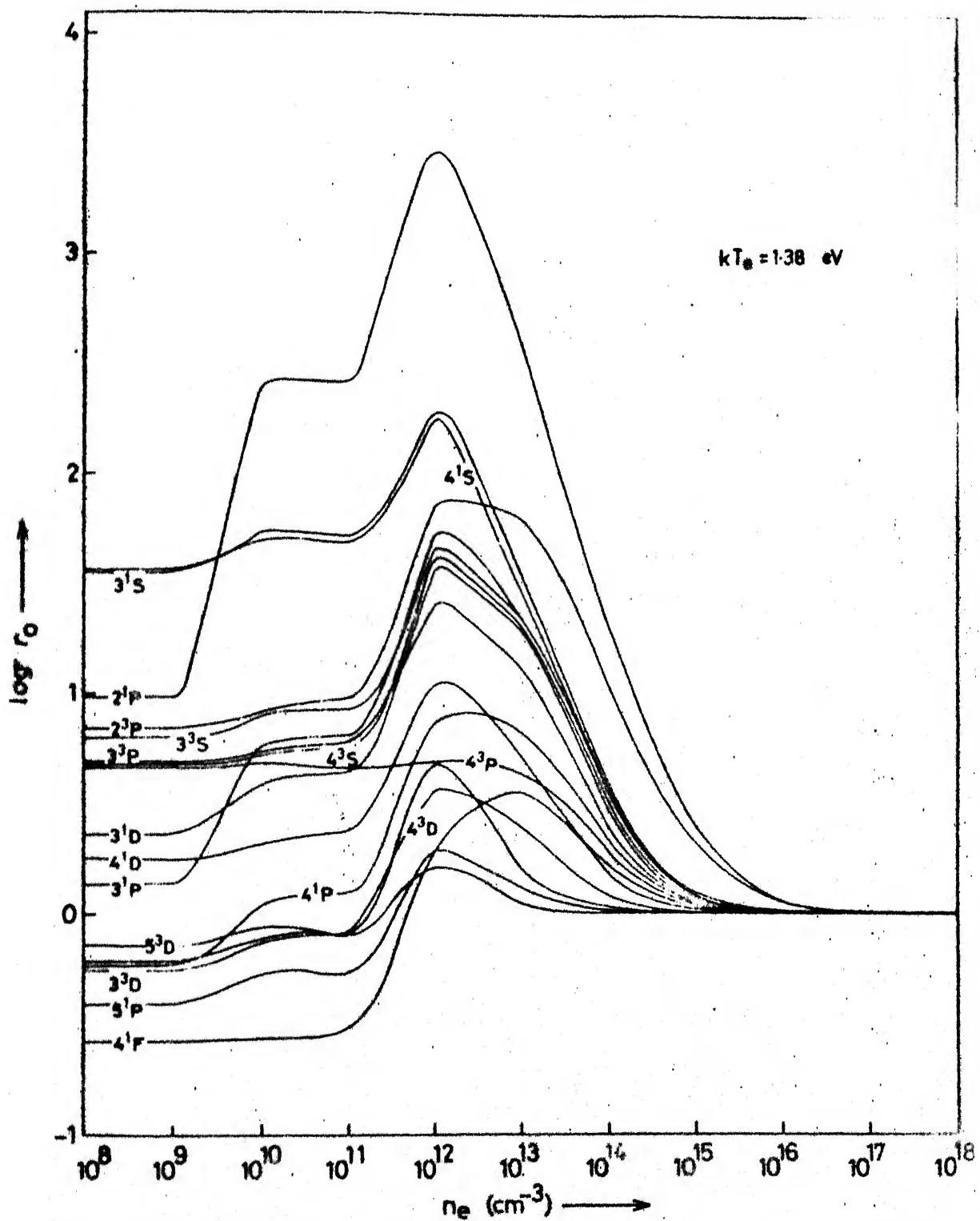
Figure 3.3. Plot of log r_0 for HeI vs electron density at $kT_e = 1.38$ eV for the partially optically thick case.
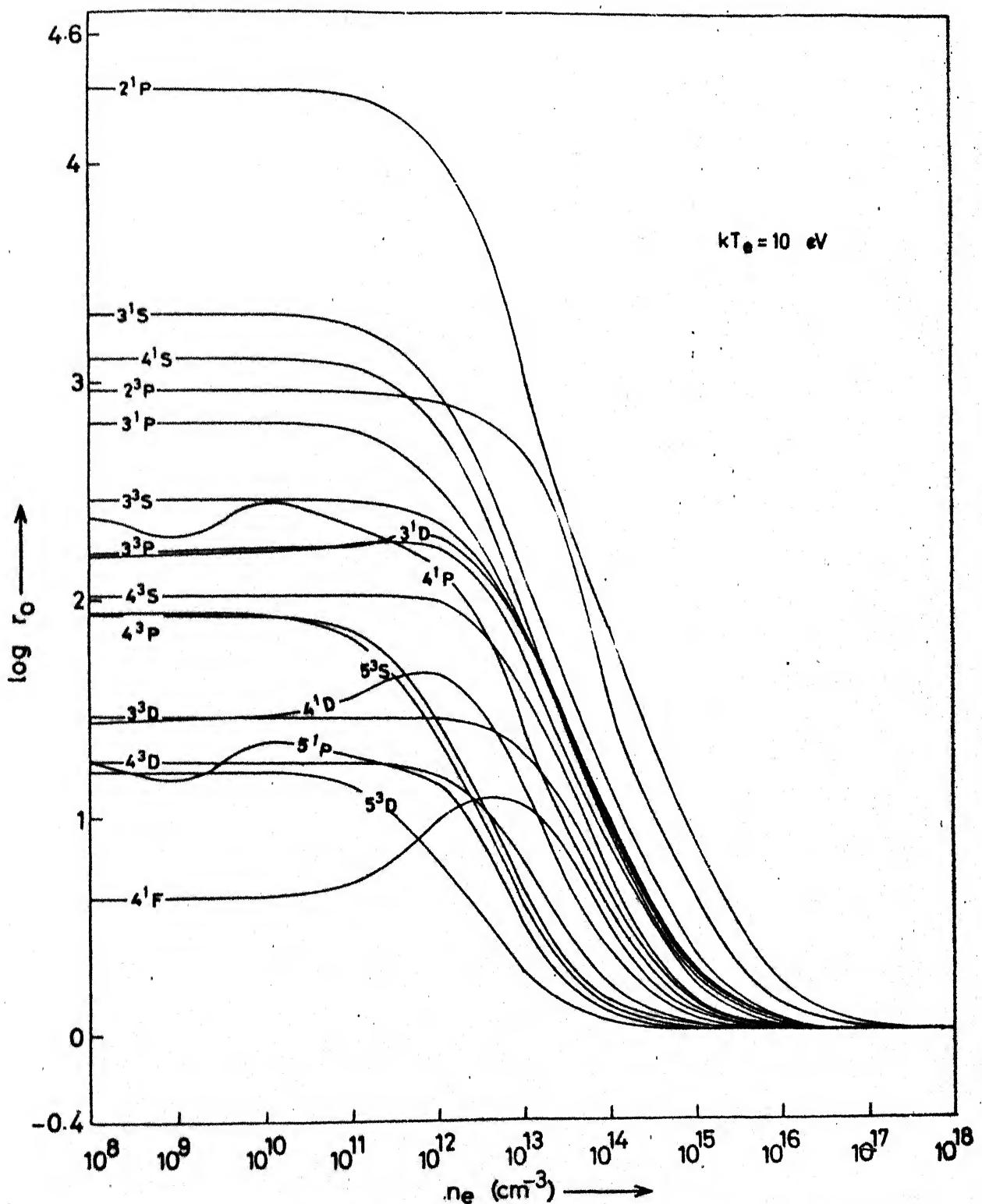
Figure 3.4. Plot of log r_o for HeI vs electron density at $kT_e = 10$ eV for the partially optically thick case.
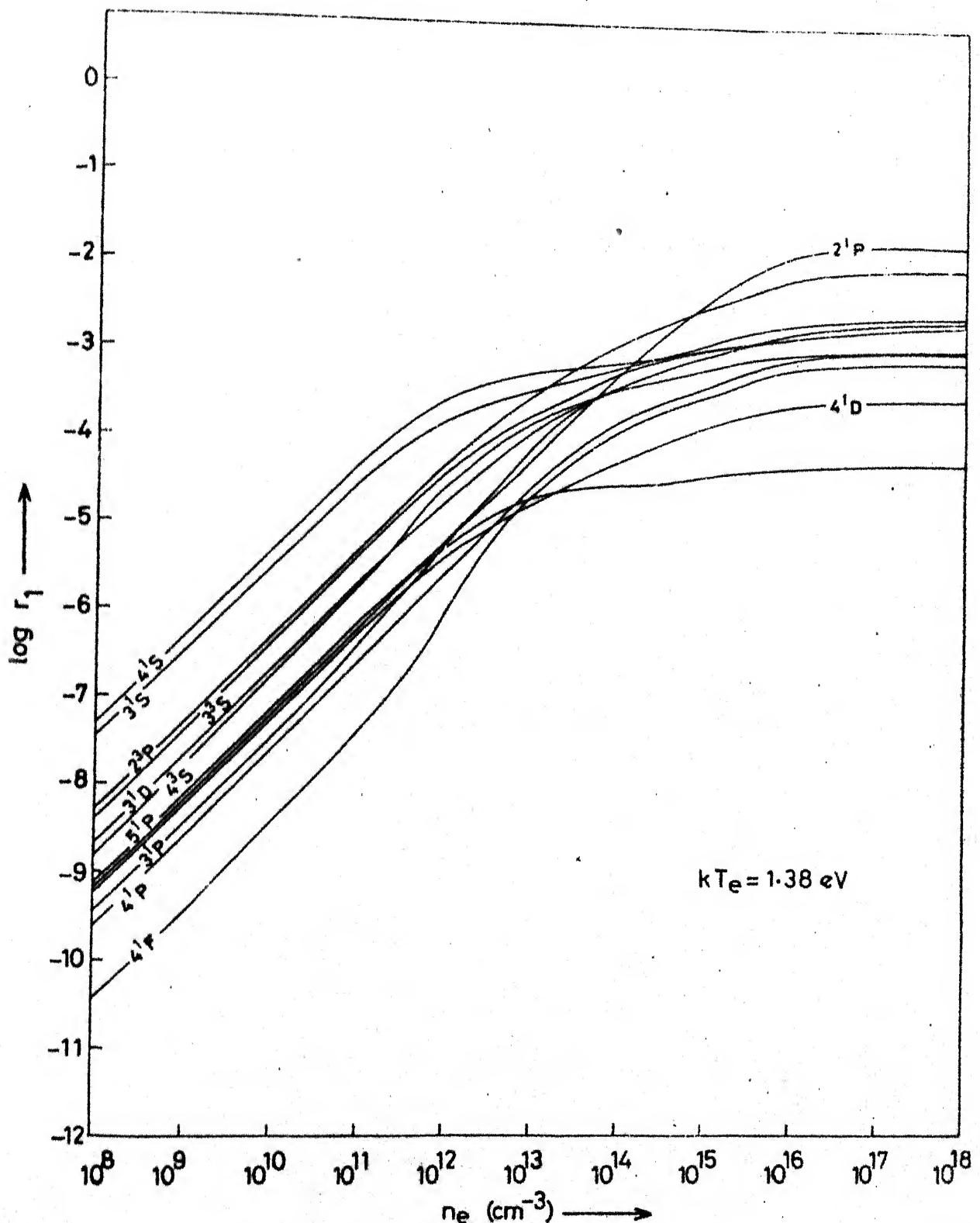
Figure 3.5. Plot of log r_1 for HeI vs electron density at $kT_e = 1.38$ eV for the optically thin case.
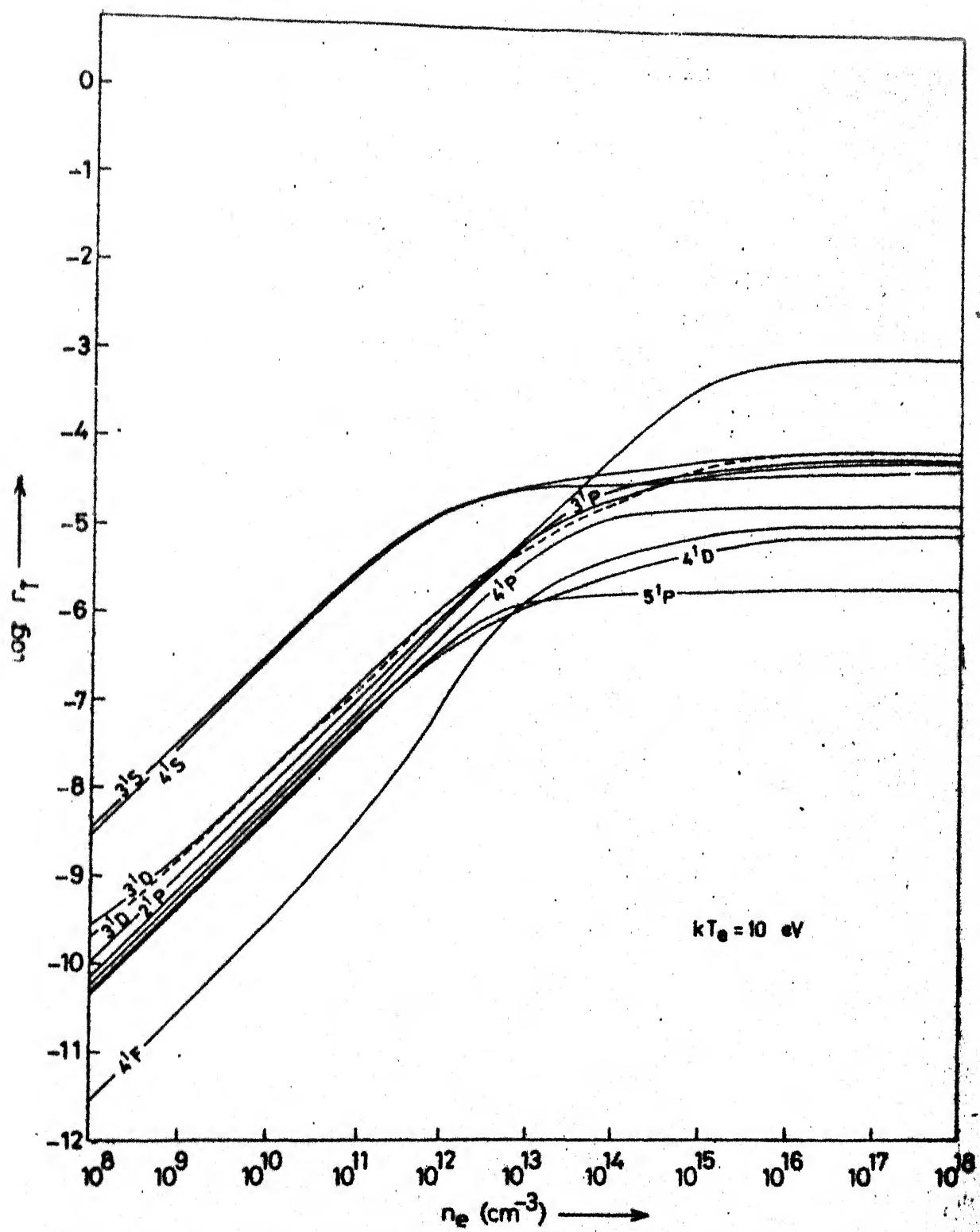
Figure 3.6.   Plot of log r_1 for HeI vs the electron density at kT_e = 10 eV for the optically thin case; ———, present work; -----, Ref. 51.
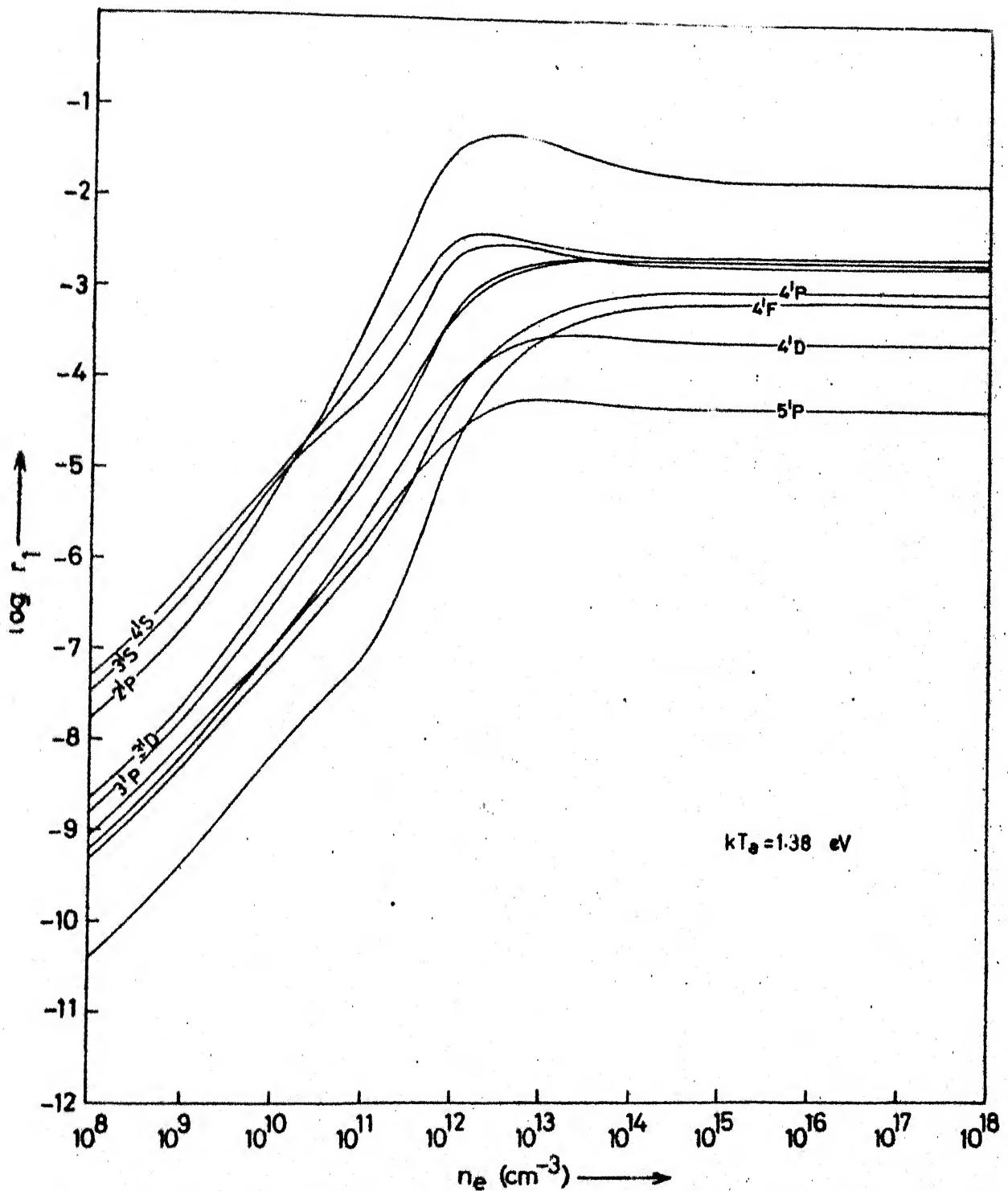
Figure 3.7. Plot of log r_1 for HeI vs electron density at $kT_e = 1.38$ eV for the partially optically thick case.
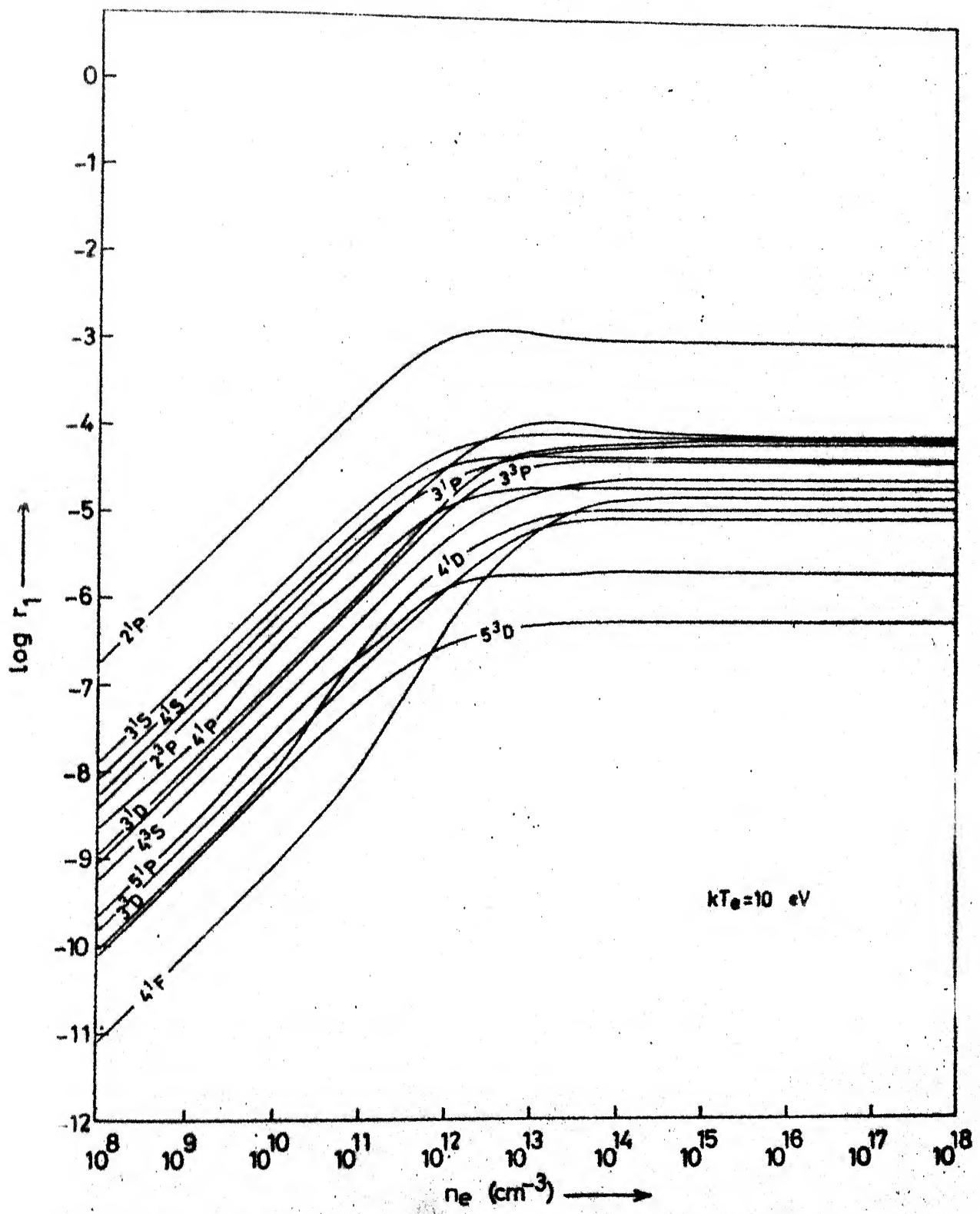
Figure 3.8. Plot of log r_1 for HeI vs electron density at $kT_e = 10$ eV for the partially optically thick case.
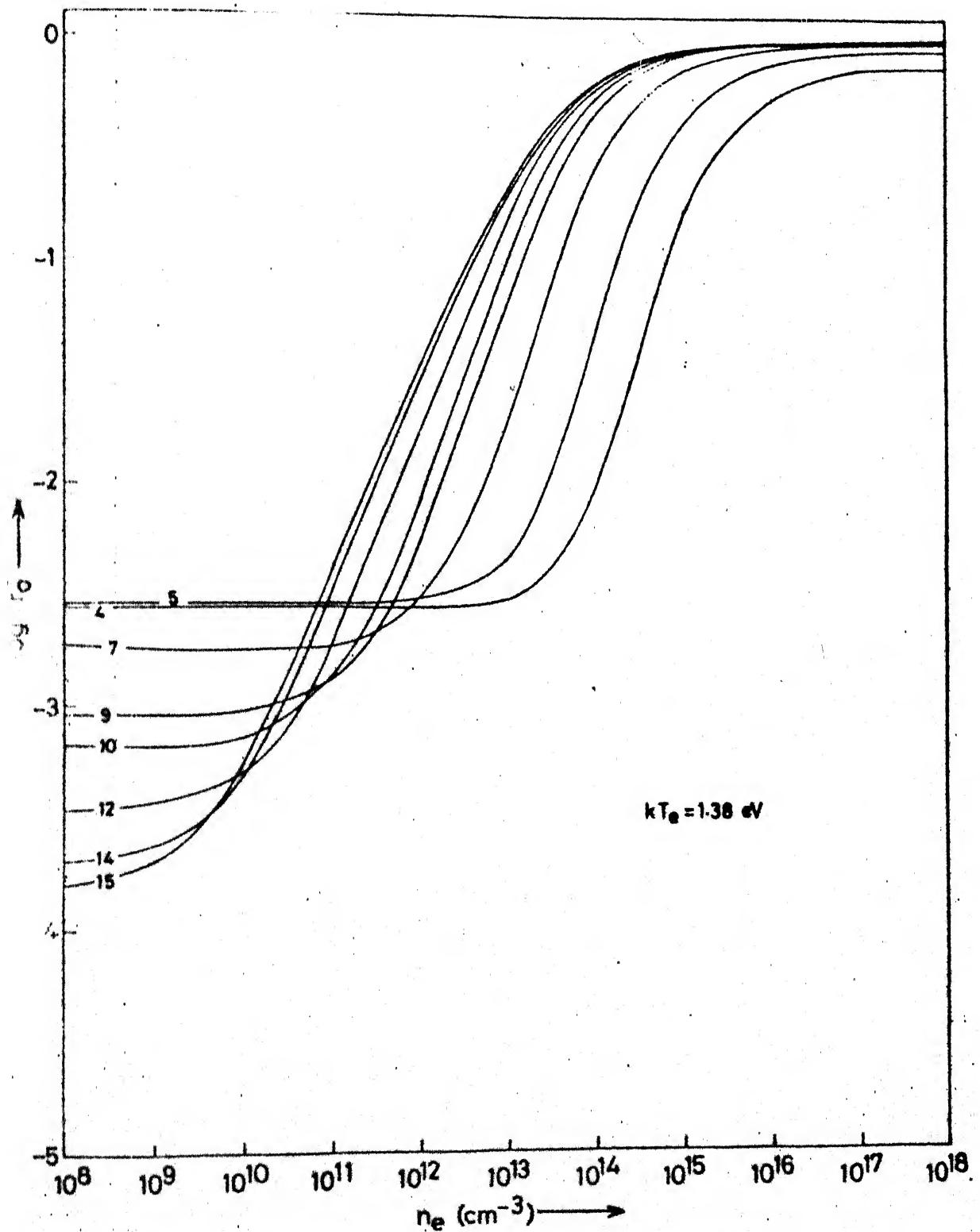
Figure 3.9.   Plot of $\log r_o^+$ for HeII vs electron density at
$kT_e = 1.38$ eV for the optically thin case.
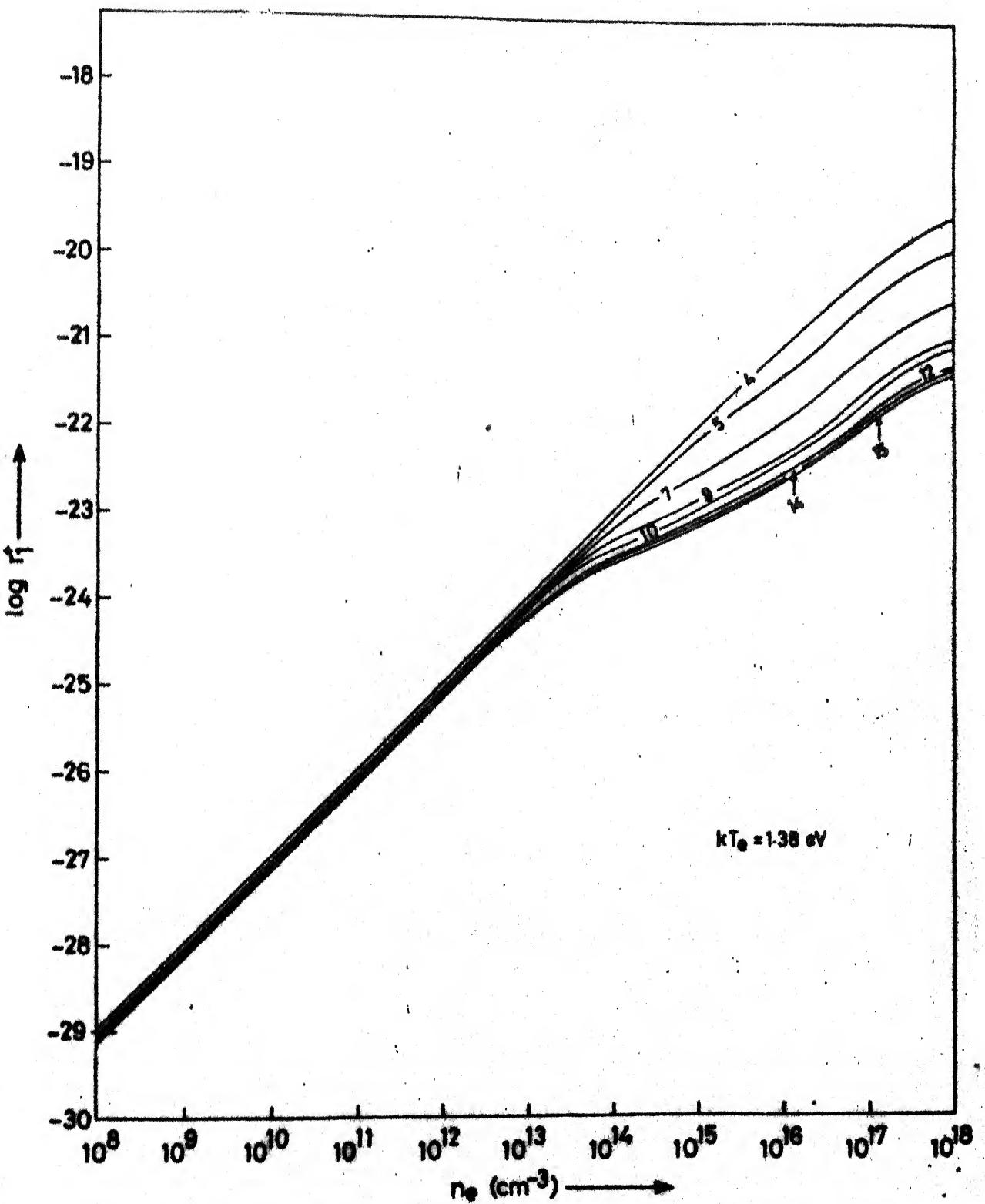
Figure 3.10. Plot of log r_1^+ for HeII vs electron density at $kT_e = 1.38$ eV for the optically thin case.

Figure 3.11. Plot of log r_2^+ for HeII vs electron density at $kT_e = 1.38$ eV for the optically thin case.

Figure 3.12. Plot of $\log r_o^+$ for HeII vs electron density at $kT_e = 1.38$ eV for partially optically thick case.
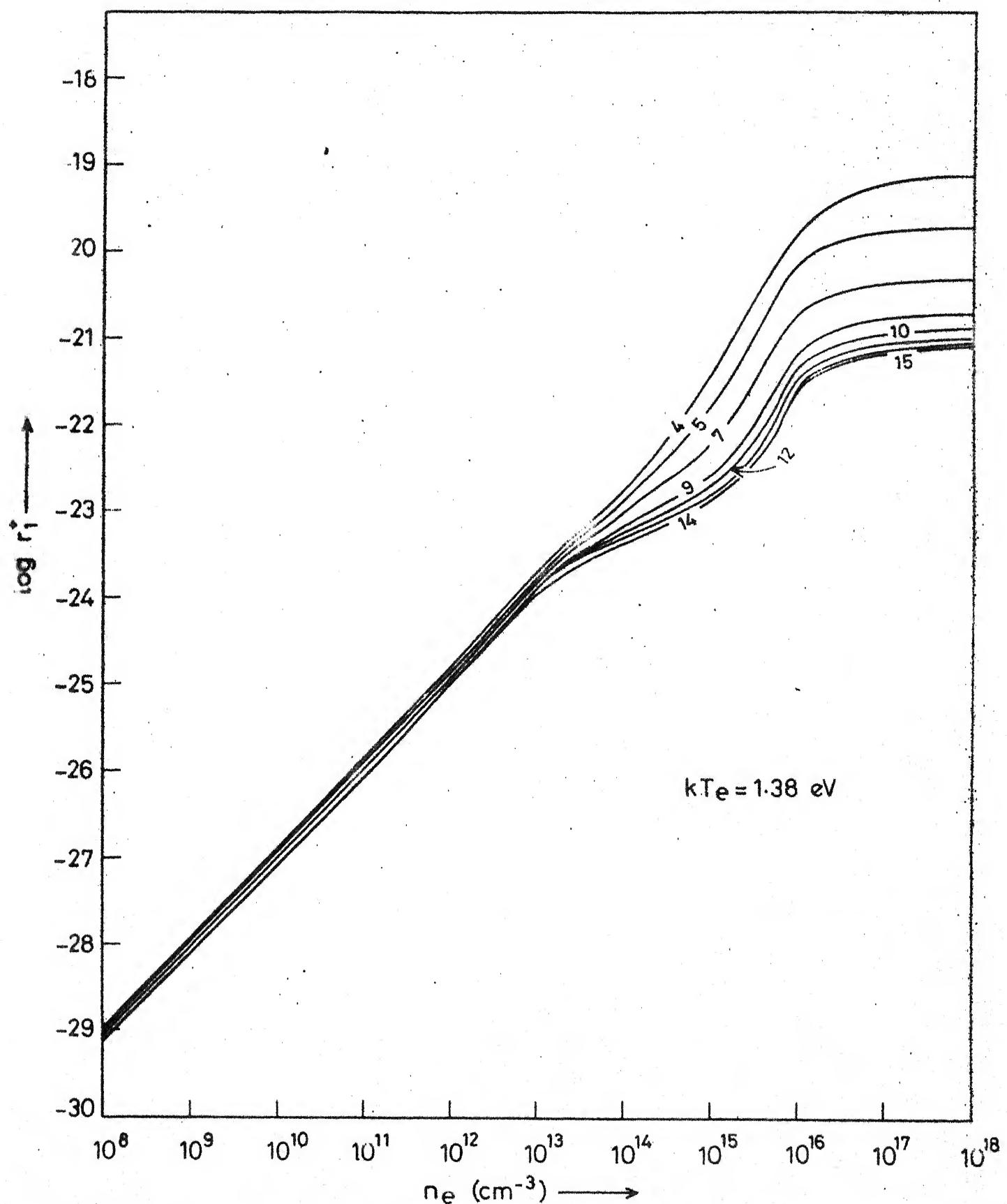
Figure 3.13. Plot of log r_1^+ for HeII vs electron density at kT_e = 1.38 eV for partially optically thick case.
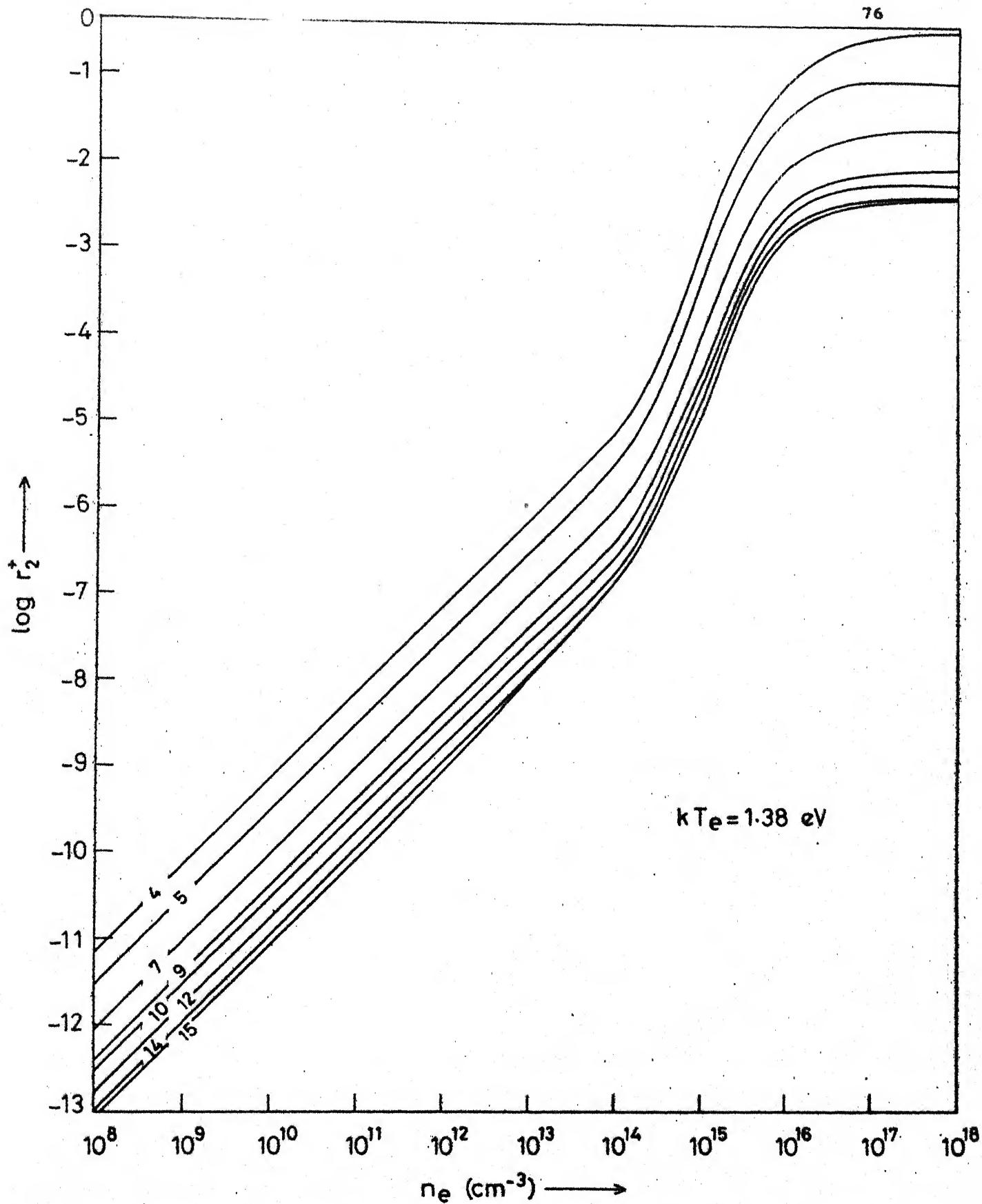
Figure 3.14. Plot of $\log r_2^+$ for HeII vs electron density at $kT_e = 1.38$ eV for partially optically thick case.

Figure 3.9 presents values of r_o^+ for the HeII levels i = 4-15, the r_1^+ values are shown in Figure 3.10 and r_2^+ is plotted in Figure 3.11. For partially optically thick conditions, the values of r_o^+, r_1^+ and r_2^+ for HeII levels at kT_e = 1.38 eV are plotted in Figures 3.12-3.14.

3.4. ROLE OF DIRECT-IONIZATION EXCITATION

In Ref. 11, possible importance of the direct ionization excitation process in populating the HeII levels was indicated. Here we make a detailed calculation on the role of this process. In Eq. (2.55), at low gas pressures (< 1 torr), the first term $r_o^+(i)$ is essentially the contribution from the second continuum towards $\rho^+(i)$, the second term, $r_1^+(i)$ $\rho(1)$, is the contribution from the ground state of HeI, i.e. the contribution from the direct ionization-excitation process. The third term, $r_2^+(i)$ $\rho^+(1)$ represents the contribution from the ground state of HeII. Rewriting Eq. (2.55), one gets[57]

$$n^+(i) = r_o^+(i) n_E^+(i) + r_1^+(i) \frac{n(1)}{n_E(1)} \cdot n_E^+(i) + r_2^+(i) n^+(1) \frac{n_E^+(i)}{n_E^+(1)}$$

$$(3.1)$$

where $n^+(1)$ is the population density of the ground level of HeII which is approximately taken equal to the electron density n_e.

In the results presented in Figures 3.15-3.19 the plasma parameters used are n_e = 10^8-10^{14} cm^{-3}, kT_e = 0.1-18 eV, n(1) = 1.0 x 10^{12}-2.25 x 10^{14} cm^{-3} and $\frac{n^+(1)}{n^{++}}$ = 1-10^4. Figure 3.15 shows the individual contributions of the first, second and third terms of Eq. (3.1) for i = 4 at n_e = 10^8, 10^{10}, 10^{11} and 10^{12} cm^{-3}. At n_e = 10^8 cm^{-3} and kT_e < 3.0 eV the contribution of the third
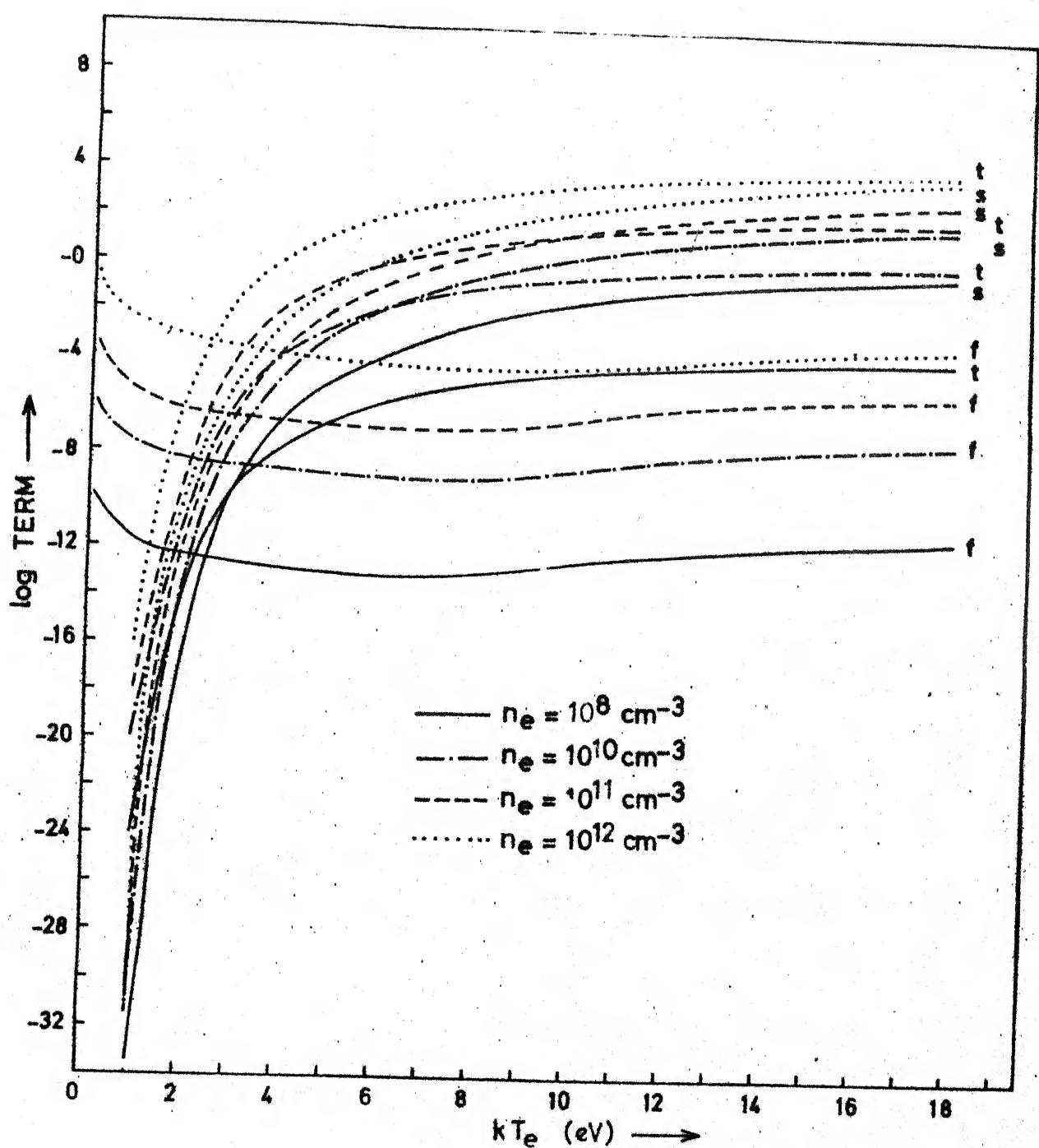
Figure 3.15. Plot of contributions from the first, second and third terms of Eq. (3.1) for i = 4 as a function of electron temperature, at electron densities $n_e = 10^8$, 10^{10}, 10^{11} and 10^{12} cm^{-3}; f = first term; s = second term and t = third term.
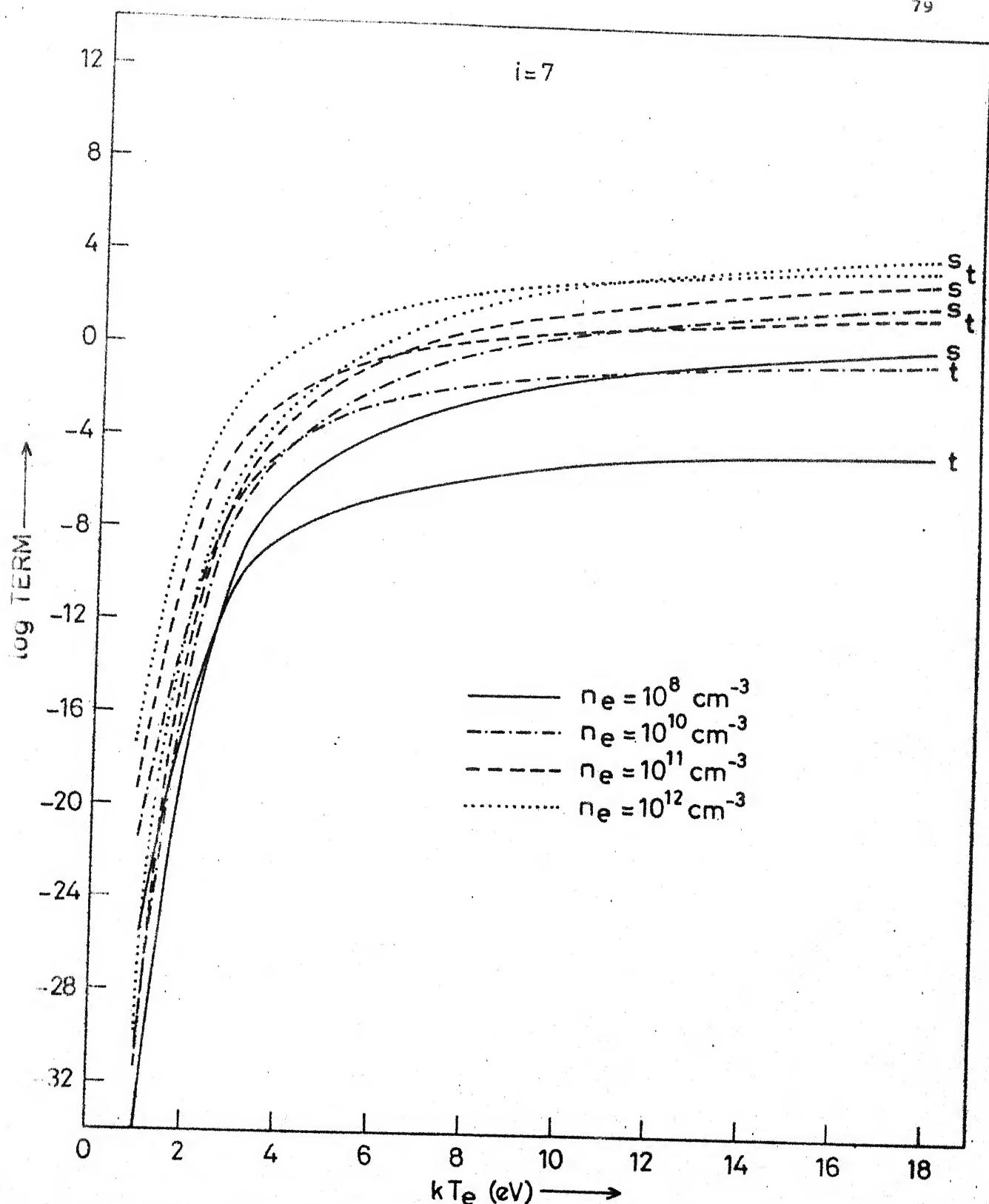
Figure 3.16. Plot of contributions from the second and third terms of Eq. (3.1) for i = 7 as a function of electron temperature at $n_e = 10^8$, 10^{10}, 10^{11} and 10^{12} cm^{-3}; s = second term, t = third term.
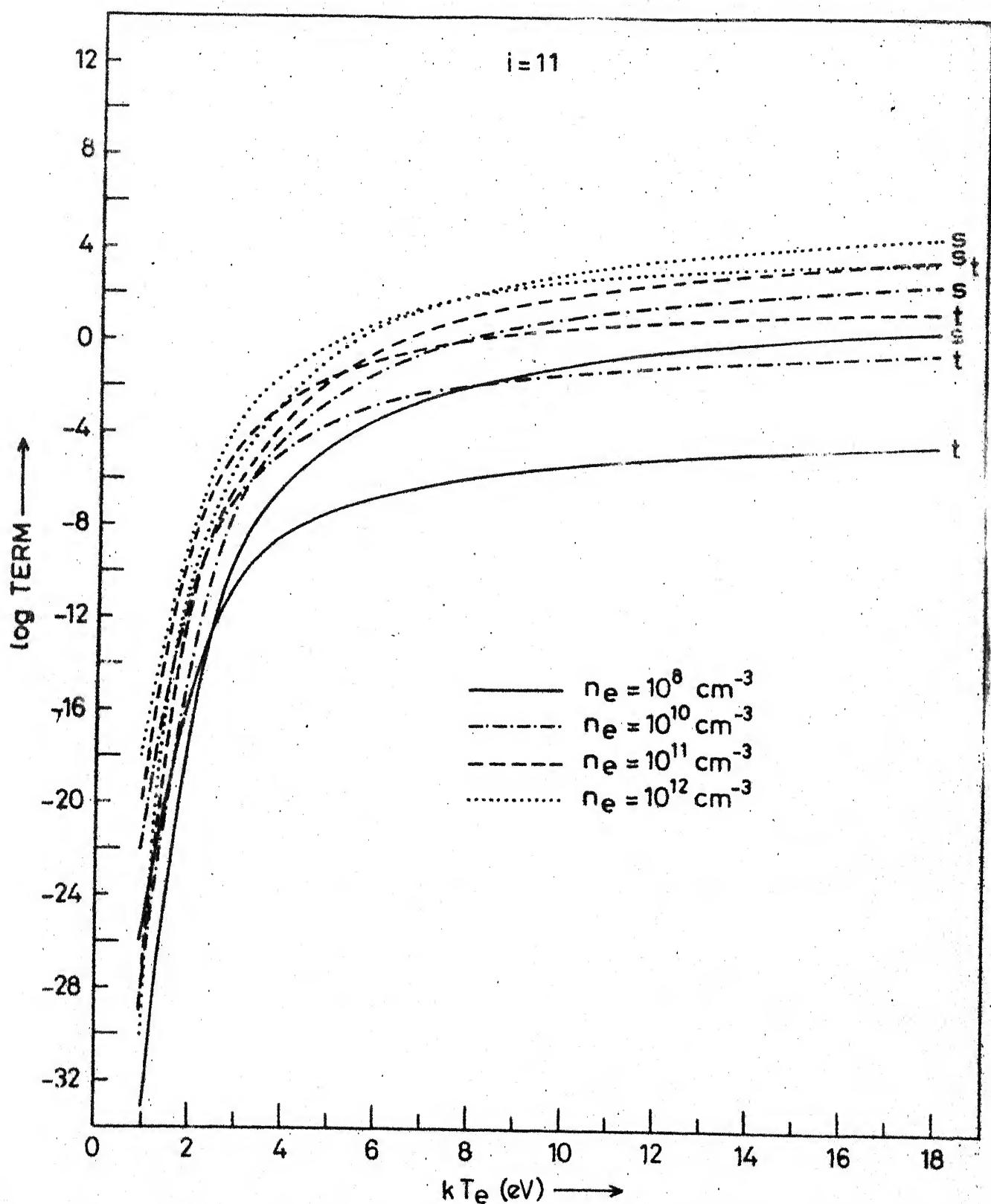
Figure 3.17. Plot of contributions from the second and third terms of Eq. (3.1) for $i = 11$ as a function of electron temperature at $n_e = 10^8$, 10^{10}, 10^{11} and 10^{12} cm^{-3}; s = second term, t = third term.
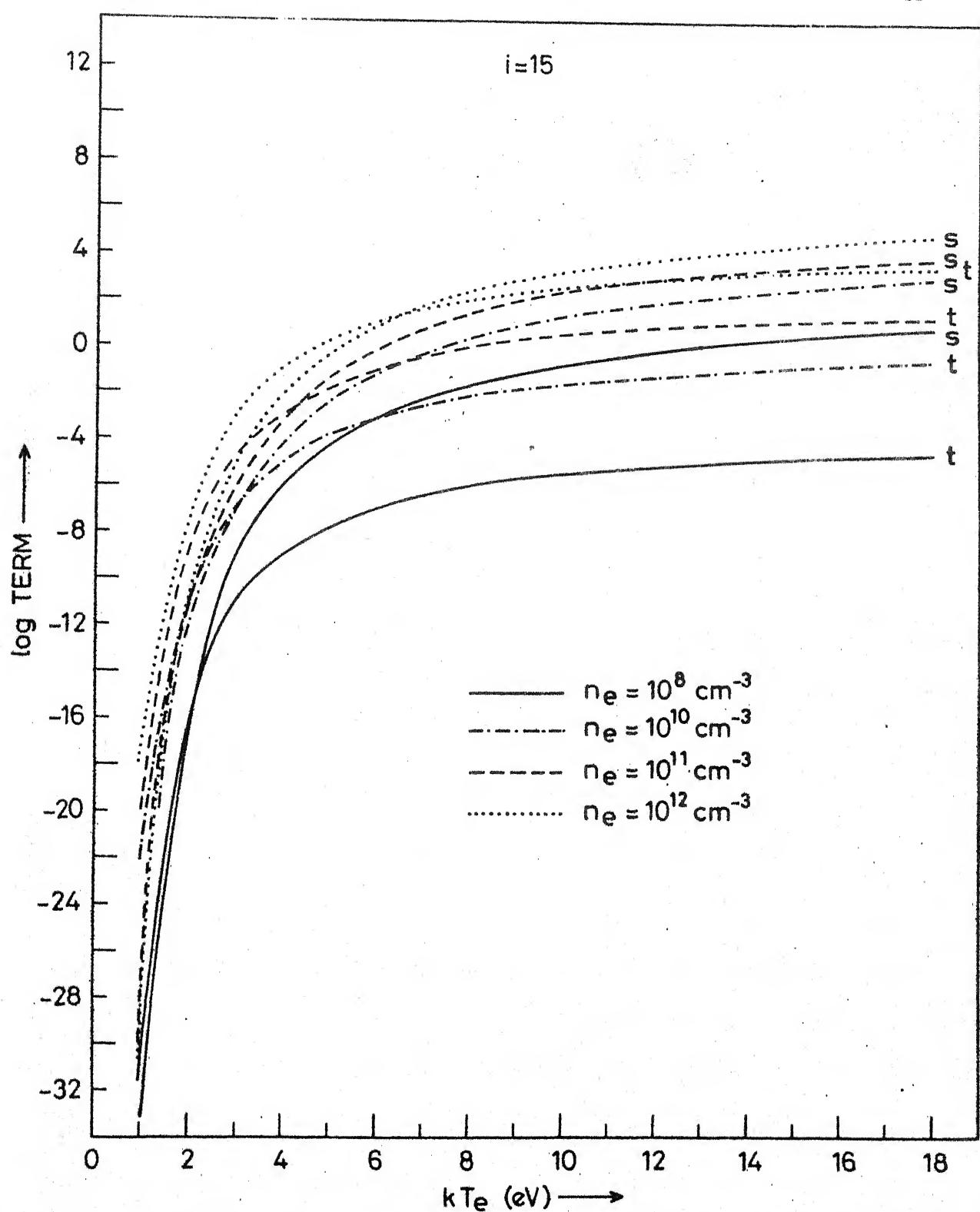
Figure 3.18. Plot of contributions from the second and third terms of Eq. (3.1) for i = 15 as a function of electron temperature at n_e = 10^8, 10^{10}, 10^{11} and 10^{12} cm^{-3}; s = second term, t = third term.

term is larger than the contribution of the second term. For $kT_e > 3$ eV, the reverse is true. At $kT_e = 5$ eV, the second term is about two orders of magnitude and at $kT_e = 15$ eV it is about three to four orders of magnitude larger than the third term. At $n_e = 10^{10}$ cm^{-3}, the direct ionization-excitation is important only above $kT_e = 6.3$ eV. At this higher electron density, the direct ionization-excitation becomes relatively less important compared to the case at $n_e = 10^8$ cm^{-3}. This is evident from the fact that at $kT_e = 15$ eV, the second term is only about one to two orders of magnitude larger than the third term. At $n_e = 10^{11}$ cm^{-3}, ionization-excitation process is important above $kT_e = 10$ eV. At $kT_e = 15$ eV, the second term is about one order of magnitude larger than the third term. At $n_e = 10^{12}$ cm^{-3}, the third term dominates over the second term up to 18 eV, the upper limit of kT_e used in the computation. Thus at $n_e = 10^{12}$ cm^{-3}, the i = 4 level of HeII is populated mainly from the ground state of HeII and not from the ground level of HeI. At low electron temperatures (< 2 eV), the first term of Eq. (3.1) dominates over the second and third terms, which means that the contribution from the second continuum is the main factor in populating HeII excited levels at low electron temperatures.

Figures 3.16-3.18 present similar plots for HeII levels i = 7, 11, and 15. log of second and third terms of Eq. (3.1) for HeII level i = 7 are plotted against kT_e in Figure 3.16, for level i = 11 in Figure 3.17 and for level i =15 in Figure 3.18.

From Figures 3.15-3.18, it is evident that for a particular HeII excited state a range of electron density exists where the role of ionization-excitation is considerable and above a

particular electron temperature this process plays a dominant role. These findings have been summarized in Figure 3.19. This figure shows, for i = 2 to i = 15 and in the electron density range 10^8-10^{13} cm^{-3}, the electron temperature above which the direct ionization-excitation dominates. At low electron densities (10^8-10^9 cm^{-3}) and at low electron temperatures, the direct ionization-excitation becomes important. At higher electron density (10^{10} cm^{-3}), the ionization-excitation is important at relatively higher electron temperature. Up to $n_e = 10^{10}$ cm^{-3}, the direct ionization-excitation is the main process for populating all HeII excited states from i = 2 to i = 15. The electron temperature above which the direct ionization-excitation is important is lower for higher excitation. At $n_e = 10^{11}$ cm^{-3} and for the level i = 2, the ionization-excitation process is not the major population mechanism up to kT_e = 18 eV, the highest value for which the computations were carried out. At still higher electron densities and kT_e < 18 eV, the direct ionization-excitation is important only for higher HeII levels. It is to be noted that at all electron densities, the most of dominance of the ionization-excitation process occurs for the higher levels at relatively low electron temperatures.

Table 3.6 presents the population densities of i = 4 level at $n_e = 10^8$, 10^{10}, 10^{11}, 10^{12} and 10^{13} cm^{-3}, calculated both with and without direct ionization-excitation process at various electron temperatures. The data given in this table correspond to n(1) = 2.25 x 10^{14} cm^{-3} and $\frac{n^+(1)}{n^{++}}$ = 1000. From this table it is clear that the population densities increase considerably (one to three orders of magnitude) on adding the direct ionization-excitation processes.
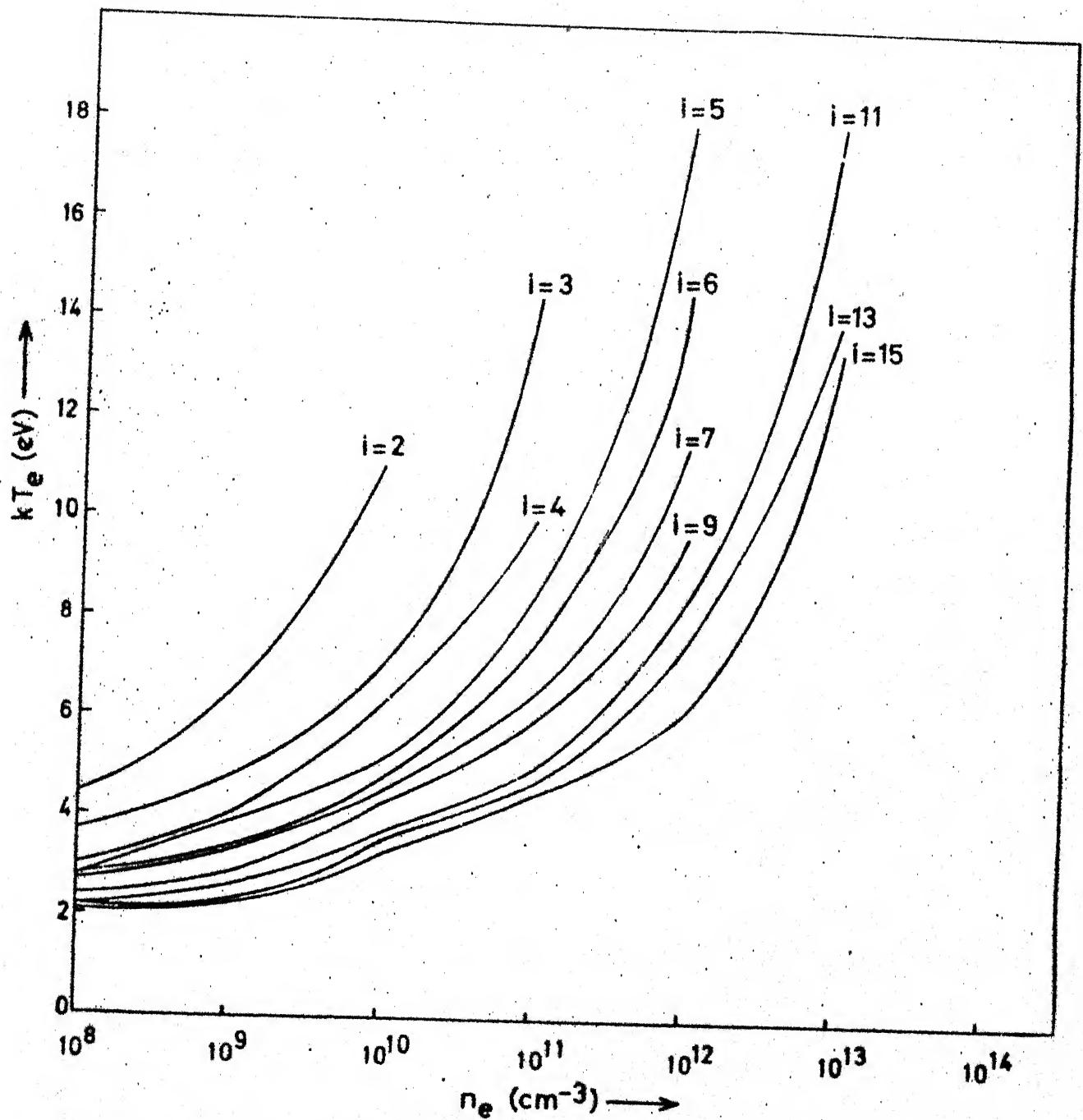
Figure 3.19. Plot of the electron temperatures above which the direct ionization-excitation process is dominant, for various HeII levels, as a function of electron density.

Table 3.6. Population densities (cm^{-3}) for i = 4 level of HeII

kT_e (eV)	$n_e = 10^8$ cm^{-3}		$n_e = 10^{10}$ cm^{-3}		$n_e = 10^{11}$ cm^{-3}		$n_e = 10^{12}$ cm^{-3}		$n_e = 10^{13}$ cm^{-3}	
	W/o	W	W/o	W	W/o	W	W/o	W	W/o	W
5	2.13-07*	9.79-06	2.13-03	3.09-03	2.13-01	2.23-01	2.13+01	2.14+01	2.13+03	2.13+03
8	7.73-06	3.41-03	7.73-02	4.18-01	7.73+00	1.11+01	7.73+02	8.07+02	7.72+04	7.75+04
10	2.47-05	2.47-02	2.47-01	2.71+00	2.47+01	4.94+01	2.47+03	2.72+03	2.47+05	2.49+05
13	7.04-05	1.56-01	7.04-01	1.63+01	7.04+01	2.26+02	7.04+03	8.59+03	7.03+05	7.19+05
15	1.11-04	3.57-01	1.11+00	3.68+01	1.11+02	4.67+02	1.11+04	1.46+04	1.10+06	1.14+06
18	1.78-04	8.80-01	1.78+00	8.98+01	1.78+02	1.06+03	1.78+04	2.65+04	1.78+06	1.86+06

* Read 2.13-07 as 2.13 x 10^{-7}; W/o represents without inclusion of the direct ionization-excitation process and W represents with inclusion of the direct ionization-excitation process.

3.5. MECHANISM OF POPULATION

Using the procedure outlined in Chapter 2, the collisional-radiative model is optimized at $kT_e = 12$ eV, $n_e = 10^{12}$ cm^{-3}, $n(1) = 2.0 \times 10^{14}$ cm^{-3} and $T_g = 1000\,°K$. On optimization, it is found that only 30% of the atomic processes of the elaborate model[56] are sufficient (results partially presented in Ref. 58) to yield population densities within 15% of the results of Ref. 56.

For most of the levels, the major contribution to population densities is found to originate from the HeI ground state through electron impact excitation process.

Individual rate coefficients and transition probabilities of the processes affect the elements of inverted matrix A^{-1} (Eqs. 2.59-2.62) considerably. Table 3.7 shows the quantitative effect of a few rate coefficients on the elements of the inverted matrix. On using the important rate coefficients and transition probabilities (obtained by the procedure outlined in Chapter 2) the calculated population densities obtained are compared with the population densities obtained from the elaborate model in Table 3.8. To test the validity of this simplified model (having only 30% of the total processes) in a range of plasma parameters, the population densities were calculated using the simplified model in the electron temperature range 4-20 eV, electron density range 10^6-10^{12} cm^{-3} and pressure range 0.01-1 torr. The percent change in population densities compared to those of the elaborate model[56] is presented in Table 3.9. From this table it is evident that the simplified model containing only 30% of the total terms can predict the population densities within 20% of those obtained from elaborate model[56] in a wide range of electron density and electron temperature.

Table 3.7. Effect of dropping some electron impact rate coefficients on elements of inverted matrix

Rate Coefficient	Elements of Inverted Matrix Affected
K(2,3)	2,2(21)*; 2,3(-98); 2,4(21); 2,6(21); 2,8(21); 2,9(21); 3,2(21); 3,4(21); 3,6(21); 3,8(20); 4,2(21); 4,3(-93); 5,2(21); 6,2(21); 6,3(-91); 7,2(21); 7,3(-40); 7,6(17); 7,8(19); 8,2(21); 8,3(-89); 9,2(21); 9,3(-91); 9,4(16); 9,6(17); 9,8(19); 9,12(17); 10,2(21); 10,3(-16); 10,4(21); 10,6(20); 10,8(18); 11,2(21); 11,3(-33); 12,2(21); 13,2(21); 13,3(-98); 13,4(21); 13,6(20); 13,8(20); 14,2(21); 15,2(21); 15,3(-96); 15,4(18); 15,9(18); 16,2(21); 16,3(-82); 16,6(17); 17,2(21); 17,3(-42); 17,4(18); 17,6(19); 17,8(19); 17,12(19); 18,2(21); 18,3(-20); 19,2(21); 19,6(16); 21,2(21); 22,2(21); 22,3(-96); 22,4(19); 23,2(21); 24,2(21); 24,3(-83); 24,4(19); 25,2(21); 26,2(21); 26,3(-85); 27,2(21); 27,3(-75); 27,4(19); 28,2(21); 28,3(-75); 28,4(19); 28,9(16); 29,2(21); 29,3(-74); 29,4(19); 29,9(16); 30,2(21); 30,3(-73); 30,4(-19); 30,9(16); 31,2(21); 31,3(-73); 31,4(19); 31,9(16); 32,2(21); 32,3(-73); 32,4(19); 32,9(16)
K(4,2)	4,2(-27); 4,3(-25)
K(5,2)	5,2(-55)
K(6,2)	4,2(-25); 4,3(-23); 6,2(-84); 6,3(-77); 6,8(-17); 8,2(-39); 8,3(-35)
K(10,3)	5,2(-16); 10,2(-72); 10,3(-95); 10,4(-71); 10,6(-69); 10,8(-64); 10,9(-50); 10,11(-16); 17,2(-19); 17,3(-65); 17,4(-16); 17,6(-17); 17,8(-18); 17,12(-17)

* 2,2(21) means that the value of the element 2,2 of the inverted matrix is increased by 21%.

Table 3.8.   Population densities of HeI and HeII levels obtained from elaborate[56] and simplified models

$$(kT_e = 12 \text{ eV}, \quad n_e = 1.0+12 \text{ cm}^{-3}, \quad n(1) = 2.0+14 \text{ cm}^{-3})$$

Level	Population Densities (cm^{-3}) from Elaborate Model	Population Densities (cm^{-3}) from Simplified Model	Percent Change in Population Densities
2^3S	1.854+11	1.674+11*	-9.7
2^1S	4.591+10	4.182+10	-8.9
2^1P	9.721+07	8.392+07	-13.6
3^1S	4.183+08	3.897+08	-6.8
3^3P	9.300+08	7.926+08	-14.8
3^3D	2.104+08	1.913+08	-9.1
3^1D	1.658+08	1.397+08	-15.7
3^1P	7.732+07	6.811+07	-11.9
4^3S	2.345+08	2.224+08	-5.2
4^1S	3.917+08	3.573+08	-8.8
4^3P	2.759+08	2.695+08	-2.3
4^3D	1.159+08	1.027+08	-11.4
$4^3F, 4^1F$	6.092+07	5.380+07	-11.7
5^1D	2.359+07	2.351+07	-0.3
5^1P	3.396+07	3.366+07	-0.9
n=6	5.751+07	5.708+07	-0.7
n=10	2.503+07	2.868+07	14.6
n=12	3.121+07	3.712+07	18.9
HeII i=2	8.512+04	8.417+04	-1.1
i=5	4.302+03	4.292+03	-0.2
i=10	4.161+03	3.918+03	-5.8
i=15	7.071+03	6.809+03	-3.7

* Read 1.674+11 as 1.674×10^{11}.

Table 3.9. Percent change in population densities on using the simplified model ($n(1) = 2.0+14$ cm^{-3})

Levels	kT_e = 4 eV			10 eV			15 eV			20 eV		
	$n_e=10^6$ cm^{-3}	10^9 cm^{-3}	10^{12} cm^{-3}	10^6 cm^{-3}	10^9 cm^{-3}	10^{12} cm^{-3}	10^6 cm^{-3}	10^9 cm^{-3}	10^{12} cm^{-3}	10^6 cm^{-3}	10^9 cm^{-3}	10^{12} cm^{-3}
2^3S	-6	-6	-6	-6	-6	-6	-6	-6	-5	-6	-6	-6
2^1S	-5	-5	-4	-3	-3	-3	-3	-3	-2	-2	-2	-2
2^3P	-17	-17	-21	-14	-14	-17	-13	-13	-16	-13	-13	-15
2^1P	-5	-5	-4	-2	-2	-1	-1	-1	-1	0	0	0
3^3S	-4	-4	-6	-3	-3	-4	-2	-2	-3	-2	-2	-2
3^3D	-5	-5	-6	-5	-5	-6	-5	-5	-5	-5	-5	-5
3^1P	-21	-21	-19	-11	-11	-11	-8	-8	-8	-6	-6	-6
4^3D	-5	-5	-9	-4	-4	-7	-4	-4	-7	-4	-4	-8
4^1P	-1	-1	-2	0	0	0	0	0	0	0	0	0
5^3P	-1	-1	-1	-1	-1	-1	-1	-1	0	-1	-1	0
5^1P	0	0	-1	0	0	0	0	0	0	0	0	0
$n=6$	-2	-2	-2	0	0	0	0	0	0	0	0	0
$n=9$	-1	-1	1	0	0	4	0	0	4	0	0	4
$n=12$	-1	-1	3	0	0	6	0	0	7	0	0	7
HeII $i=2$	-2	0	0	-1	-1	0	-1	-1	0	-1	-1	0
$i=4$	-2	-1	0	-1	-1	0	-1	-1	0	-1	0	0
$i=10$	-2	-2	-19	-1	-1	-6	-1	-1	-5	0	0	-4

The population densities of 18 lowest levels of HeI were also calculated by truncating the elaborate model[56] to contain only 18 levels of HeI besides the ionic ground state. The mechanism of population, i.e., the processes which contribute significantly to the population of a particular level, evolved from this further simplification is presented in Table 3.10. Absolute population densities and percent change in population densities compared to those of the elaborate model are also given in Table 3.10. The population densities of most of the levels are again within 20% of those predicted by the elaborate model. It may be added here that 18 levels of HeI would still provide a range of lines for spectroscopic measurements. This model, containing only 18 levels, consists of only 6% of the total number of processes of the elaborate model.[56] The size of the model can further be reduced, without sacrificing much the accuracy in calculation of population densities, by taking into account only 10 levels. The results are shown in the enclosure in Table 3.10. This latter model consists only 2.4% of the total terms of the elaborate model and yet predicts the populations of first ten levels quite closely.

3.6. LASER INDUCED SELECTIVE EXCITATION

As discussed in Chapter 2, the process of optical pumping by a laser pulse is included in the collisional-radiative model and absolute population densities as a function of time are calculated. A typical plot of the enhancement and decay of absolute population densities against time for the pumping of 2^3P-4^3D level by a laser pulse of power 10^3-10^4 W/cm^2, FWHM = 5 nsec, spectral width 0.1 Å is shown in Figure 3.20. The data

Table 3.10. Mechanism of population

Level No.	Level	Absolute population densities	Per cent change in population densities	Mechanism of population[a] (Electron impact processes and optical transitions for populating individual levels)
2	2^3S	1.85+11[b]	-4[c] 1[d]	1-2,-3,-4,-6,-8,-9;2-3,-4,-5,-6,-7,-8,-9,-10; 3-2,-10; (4-2;5-1;6-4;8-2;9-4) 2-11,-12,-13,-14,-15,-16,-17;7-11;8-11;10-17; 11-8;13-12 (11-1)
3	2^1S	4.59+10	-3 4	1-2,-3,-4,-6,-8;2-3,-5;3-2,-7,-10; (4-2;5-1;6-4;8-2) 3-11,-18;7-11;8-11;10-11,-17;11-8;13-12; (11-1)
4	2^3P	4.16+09	-17 -27	1-3,-4,-6,-8,-9;2-3,-5,-6,-9;3-2,-10;4-2;-5, -6,-9;6-8;5-6; (4-2;5-1;6-4;8-2;9-4;10-5) 1-12,-14,-15;4-11,-12,-15,-19;7-11;9-11;11-8; 10-17;13-12; (11-1;12-4;12-9;15-4)
5	2^1P	9.72+07	-2 1	1-2,-5;2-5;3-2,-10; (5-1;10-5) 7-11;8-11;10-11;11-7,-10;13-12; (11-1)
6	3^3S	5.69+08	-8 -4	1-2,-3,-6,-8;2-3,-5,-6;3-2,-10;6-4,-7,-8;8-6; (5-1;6-4;8-2) 6-13;7-11;8-11;10-11,-17;11-8;12-8; (11-1)
7	3^1S	4.18+08	-4 81	1-2,-3,-6,-7,-8;2-5,-7;3-7,-10;7-6; (4-2;5-1;7-5;8-2) 1-11;7-11,-18;8-11;10-11,-17;11-7;13-12; (11-1)
8	3^3P	9.30+08	-12 2	1-2,-3,-6,-8;2-5,-6;3-2,-10;6-8;8-6; (5-1;6-4;8-2) 1-11,-12;2-12,-15;7-11;8-11,-15;10-11,-17; 11-8;12-8;13-12;15-8; (11-1;12-4;12-9;)
9	3^3D	2.10+08	-5 -3	1-2,-3,-4,-6,-8,-9;2-3,-5,-9;3-2,-9;6-8;8-6; 9-4; (4-2;5-1;6-4;8-2;10-5) 1-12;7-11;8-11;9-14,-17;10-11,-17;11-8,-10; 13-12;14-9; (11-1;12-4)
10	3^1D	1.66+08	-11 -5	1-8,-9,-10;2-3,-5;3-2,-10;10-5; (4-2;5-1;6-4;8-2;9-4;10-5) 1-11;7-11;9-17;10-11,-17;11-10;13-11,-12; (11-1;17-9,-10)
11	3^1P	7.73+07	-9	1-2,-3,-6,-7,-8,-11;2-5,-7,-13;3-7,-10;6-8;7-11;8-6,-11;10-11;11-4,-7,-8,-10, -16;12-8;13-11; (5-1;6-4;7-5;8-2;10-5;11-1)
12	4^3S	2.35+08	3	1-2,-6,-8,-12;2-13;2-3,-5,-12,-13;3-2,-10;6-8;7-11;8-6,-11;8-6,-11,-12;10-11,-17;11-8; 12-8,-13;13-12; (4-2;6-4;8-2;12-4,-8;13-5,-11)
13	4^1S	3.92+08	7	1-2,-3,-4,-6,-8,-12,-13;2-3,-5;3-5;3-2,-10;7-11;8-11;10-17;11-8;13-2,-6,-11,-12; (4-2;5-1;6-4;8-2;11-1;13-5,-11)
14	4^3P	2.76+08	67	1-2,-14;14-5,-14;5-2,-10;7-11;8-11;10-17;11-8;13-12;14-9; (14-2)
15	4^3D	1.16+08	25	1-2,-3,-4,-6,-8,-9,-12;2-15;2-3,-5,-15;3-2,-10;4-15;6-8;7-11;8-6,-11,-15;10-17; 11-8;12-8;13-12;15-8; (4-2;5-1;6-4;8-2;9-4;11-1;12-4,-8;15-4)
16	4^1D	5.08+07	-9	1-2,-3,-6,-8;2-11,-14,-16;2-3,-5,-16;3-2,-10;7-11;8-11;15-10-11,-17;11-16;16-11; (4-2;5-1;10-5;11-1;14-2;16-4;16-5,-11)
17	$4^{3,1}P$	6.09+07	-6	1-2,-3,-4,-6,-8,-9;2-5,-10,-11,-12;2-5,-17;3-10;4-9;6-8;7-11;8-11;9-17;10-11,-17; 13-12;17-9,-10; (4-2;5-1;6-4;8-2;9-4;10-5;11-1,-3;12-4;17-9,-10)
18	4^1P	4.78+07	-3	1-2,-3,-18;2-3,-5,-18;3-2,-10,-18;4-18;6-8;7-11,-18;9-6,-11;10-17;11-7,-8;13-12; 18-4,-7,-10; (4-2;5-1;18-1)

a.
The numbers represent the level numbers; e.g.,1-2 stands for the electron impact excitation process $1^1S \rightarrow 2^3S$.
The numbers in parentheses denote spontaneous transition probabilities.

b. Read 1.85+11 as 1.85×10^{11}.

c. Per cent change in population densities when only 19 levels of He I besides the ionic ground state are considered.

d. Per cent change in population densities when only 10 levels of He I besides the ionic ground state are considered.

presented in Figure 3.20 correspond to T_e = 10 eV, n_e = 10^{12} cm^{-3}, T_g = 300°K and optically thin conditions. Continuous curves correspond to calculations involving laser power = 10^3 W/cm^2 and n(1) = 1.0 x 10^{14} cm^{-3}. Dotted line curves are obtained by using laser power = 10^4 W/cm^2 and n(1) = 1.0 x 10^{14} cm^{-3} while the dashed and dotted line curves correspond to data obtained by using laser power = 10^4 W/cm^2 and n(1) = 1.0 x 10^{16} cm^{-3}. On pumping 2^3P-4^3D transition, the population densities of levels 4^3F, 5^3P and 4^1D also change considerably. An increase in the laser power shifts the enhancement curves towards left on the time axis. From the figure, it is evident that the excitation transfer between 4^3D and 4^1D level is more pronounced at higher gas pressure.

CHAPTER 4

DISCUSSION

The procedure of calculations and the results of calculations have already been presented in Chapters 2 and 3 respectively. In this chapter we critically examine the results obtained in the present work in the perspective of results of other workers, and derive conclusions. The order of presentation is the same as the order of results presented in Chapter 3. First a discussion of cross sections and rate coefficients and their effect on calculated population densities is presented (Section 4.1); and this is followed by a discussion of the optical escape factors in the light of calculations of other workers (Section 4.2). Then the calculated reduced population coefficients and population densities are compared with the calculated and experimental results of other workers (Section 4.3). Section 4.4 examines various factors which affect the role of direct ionization excitation process. In Section 4.5, a discussion on the simplified model is presented. This is followed by (Section 4.6) an examination of results of the laser induced selective excitation experiments and finally (Section 4.7) a discussion on the line ratio method of determination of electron temperature.

4.1. CROSS SECTIONS AND RATE COEFFICIENTS

In the present work, while choosing the cross sections, emphasis has been given on use of experimental cross sections; the theoretical cross sections are used only when the experimental cross sections are not available. Sometimes there is considerable

difference between cross sections obtained by various workers.

Figures 4.1-4.3 present a comparison of cross sections for electron impact excitation of levels 2^1P, 3^1P and 4^1S from the ground state. In Figure 4.1 the electron impact cross sections for the transition 1^1S-2^1P of Drawin[65], Scott and McDowell[62], Donaldson et al[61], Moustaffa Moussa et al[71] and Westerveld et al[60] are compared. The peak value of the theoretical cross section of Scott and McDowell[62] is larger than the experimental cross section of Donaldson et al[61] and Moustaffa Moussa et al[71], but is smaller than the experimental cross section of Westerveld et al[60]. The empirical formula of Drawin[65] for the cross section of optically allowed transitions gives the largest peak value. The experimental cross section of Westerveld et al[60], being the latest one, has been used in this work. Figure 4.2 compares the cross sections of various workers for the transition 1^1S-3^1P and Figure 4.3 presents a comparison for the optically forbidden transition 1^1S-4^1S. In Figure 4.3, the peak of the theoretical cross section of Scott and McDowell[62] appears at about 30 eV impact energy, whereas in the experimental curve of St. John et al[70] it appears at about 45 eV. However, the magnitude of the cross section at peak is not much different. The peak of the experimental cross section of Van Raan et al[68] (used in the present work) is in between the above two cross sections. This cross section yields a better value of the population density of level 4^1S.

The choice of cross sections determines the value of rate coefficients and population densities of levels involved. Table 4.1 compares rate coefficients and population densities for some electron impact processes obtained on using different cross
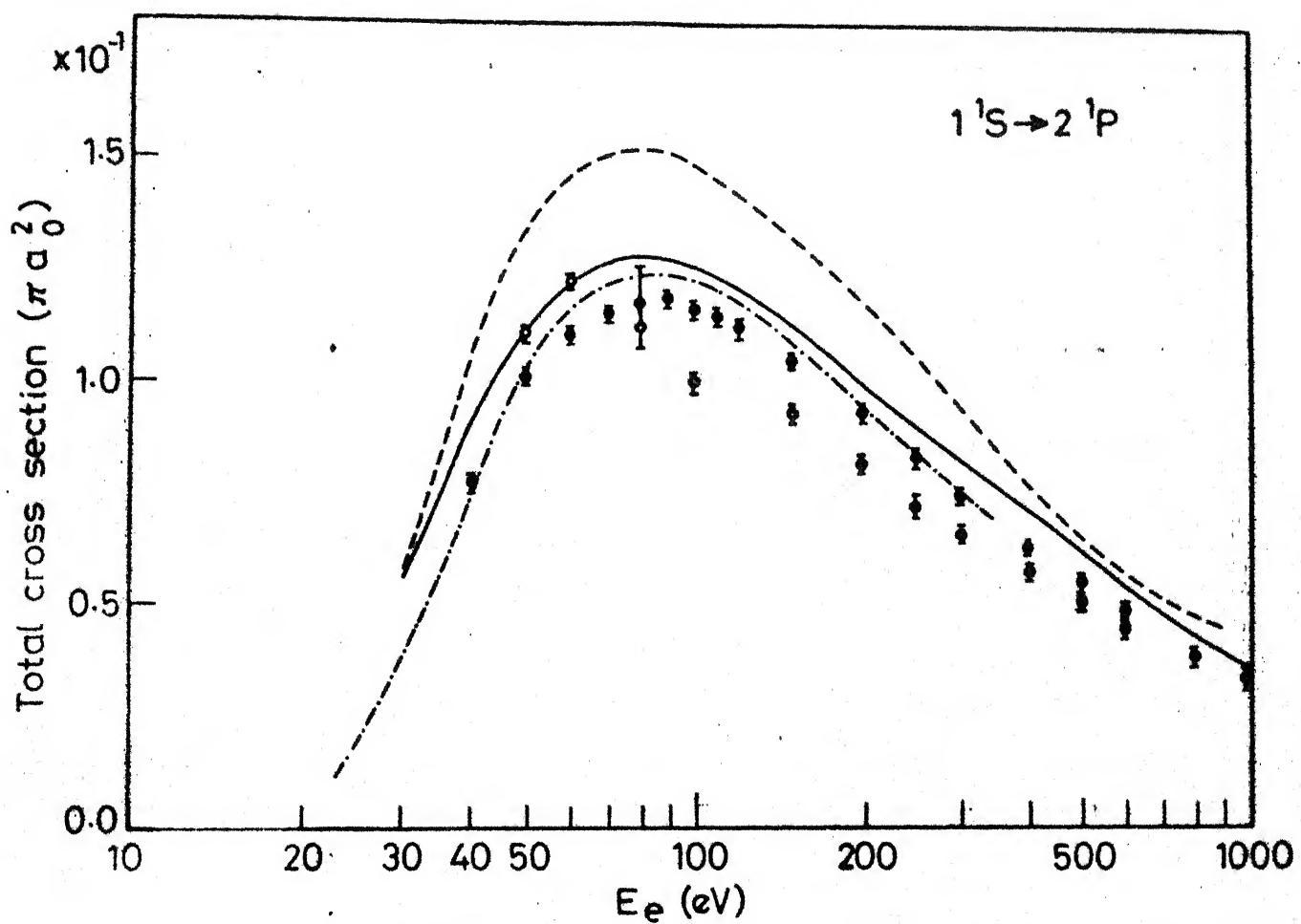
Figure 4.1. Total cross sections for the electron impact excitation process 1^1S-2^1P in units of a_o^2; ------, Drawin[65]; -.-.-, Scott and McDowell[62]; _____, Westerveld et al[60]; ☐, Donaldson et al[61]; ○, Moustaffa Moussa et al[71].
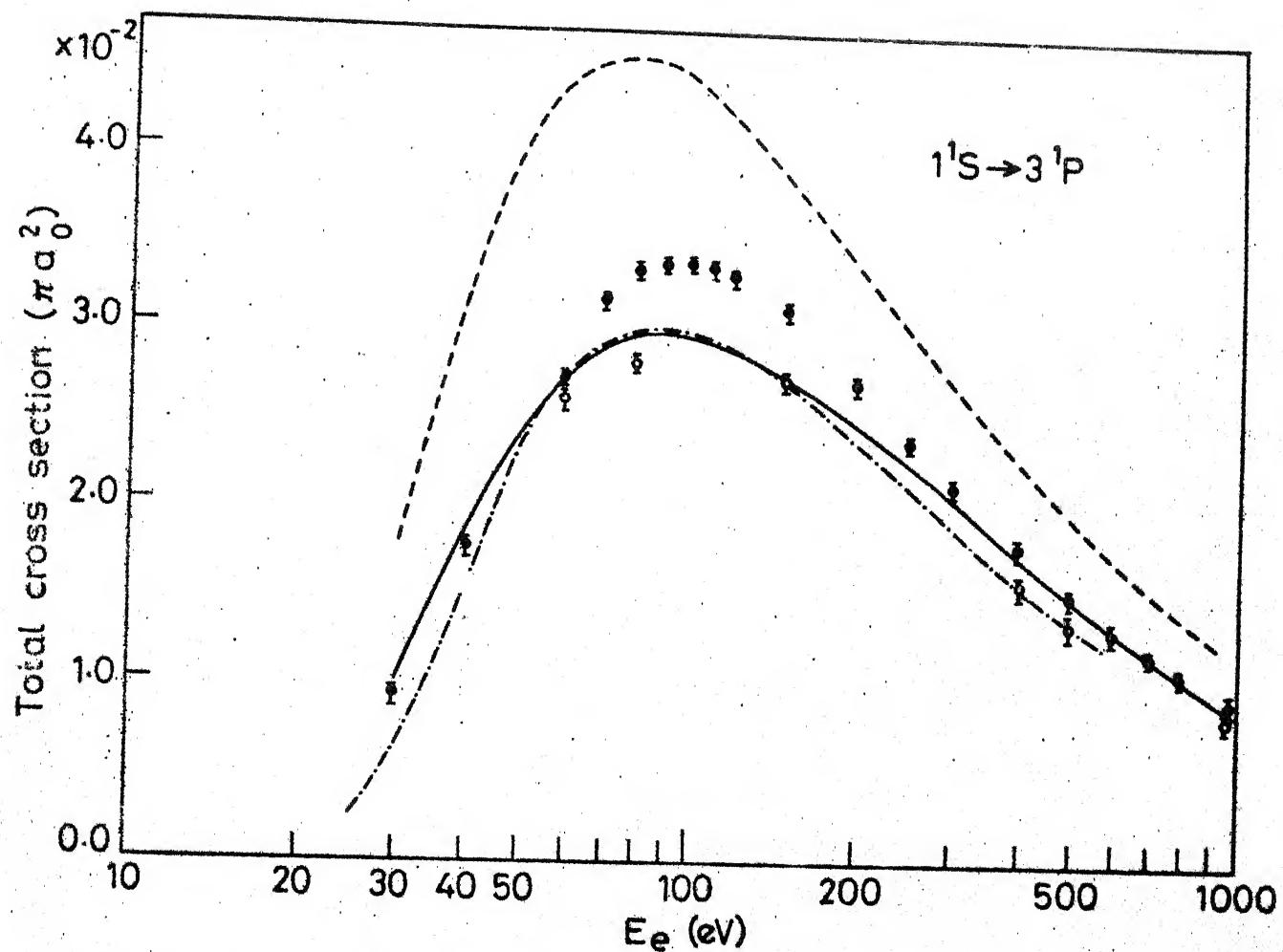
Figure 4.2. Total cross sections for the electron impact excitation process 1^1S-3^1P in units of a_o^2; ————, Drawin[65], –.–.–, Scott and McDowell[62], ————, Westerveld et al[60], Ⅰ, Donaldson et al[61], ȹ, Moustaffa Moussa et al[71].
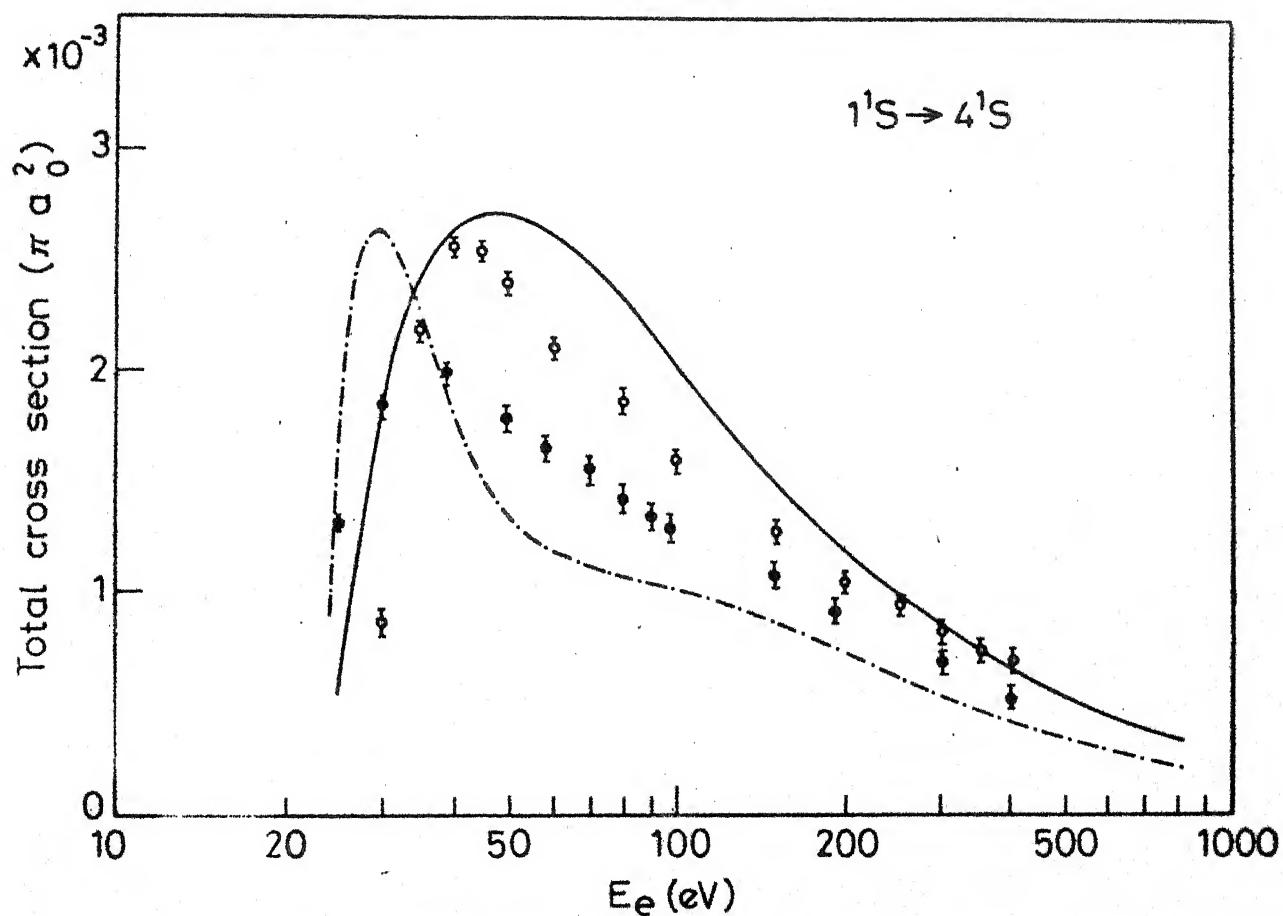
Figure 4.3. Total cross sections for the electron impact excitation process 1^1S-4^1S; ——, Drawin[65]; –.–.–, Scott and McDowell[62]; Van Raan et al[68]; St. John et al[70].

sections. All rate coefficients listed in Table 4.1 have been obtained by integrating cross sections over Maxwellian electron energy distribution. For a given transition, with a larger area under the cross sectional curve, the rate coefficient obtained is higher and consequently the population density of the upper level involved in the transition is also high. The population densities given in Table 4.1 have been calculated at $kT_e = 10$ eV, $n_e = 10^{12}$ cm^{-3} and $n(1) = 2.25 \times 10^{14}$ cm^{-3}. This table examines various cross sections and their effects on rate coefficients and population densities. For optically allowed excitations from the ground state and for optically forbidden transitions without change in multiplicity, various cross sections are available in the literature and one can choose the most suitable cross section by comparing them critically. However, for electron impact transitions between excited states and also for optically forbidden transitions with change in multiplicity, the choice is very limited and often one has to depend on empirical or semiempirical cross sections. Similarly, for electron impact ionization, radiative recombination and heavy particle collisions, one has to depend on empirical, semiempirical, or theoretical cross sections.

4.2. OPTICAL ESCAPE FACTORS

The optical escape factors calculated from Holstein's[8] expression are small as pointed out by Otsuka et al[10]. In the present work the expression given by Drawin and Emard[83] has been used for the calculation of optical escape factors. This expression considers Stark broadening and uses a Voigt profile to calculate the optical escape factors. The optical escape factors

Table 4.1. Rate coefficients and population densities (of the upper level, cm^{-3}) obtained on using different cross sections

$$(kT_e = 10 \text{ eV}, \quad n(1) = 2.25+14 \text{ cm}^{-3}, \quad n_e = 1.0+12 \text{ (cm}^{-3}))$$

Transition (p,q)	1			2			3			4		
	C.S. (Ref.)	K(p,q) cm^3 sec^{-1}	n(q) cm^{-3}	C.S. (Ref.)	K(p,q) cm^3 sec^{-1}	n(q) cm^{-3}	C.S. (Ref.)	K(p,q) cm^3 sec^{-1}	n(q) cm^{-3}	C.S. (Ref.)	K(p,q) cm^3 sec^{-1}	n(q) cm^{-3}
1^1S-2^1P	65	4.7-10*	7.9+07	62	4.2-10	7.3+07	61	3.6-10	6.6+07	60	4.6-10	7.9+07
1^1S-3^1P	65	9.5-11	7.5+07	62	7.9-11	6.9+07	61	8.4-11	7.1+07	60	9.0-11	7.3+07
1^1S-4^1P	65	4.0-11	4.8+07	62	4.2-11	5.0+07	61	3.3-11	4.2+07			
1^1S-5^1P	65	1.8-11	2.9+07	62	1.7-11	2.7+07						
2^1S-3^1P	65	7.1-08	7.5+07	63	3.5-08	7.1+07	63	4.8-08	7.3+07			
2^3S-2^3P	65	5.9-07	1.8+10	64	3.8-08	6.8+09						
2^3S-3^3P	65	2.1-08	1.1+09	64	1.6-08	1.0+09						
2^3S-4^3P	65	4.5-09	3.1+08	64	4.3-09	3.0+08						
2^3S-5^3P	65	2.1-09	4.9+07	64	1.9-09	4.9+07						
1^1S-2^1S	65	9.7-11	8.4+10	74	4.2-11	6.1+10	94	4.9-11	6.4+10	67	7.5-11	7.4+10
1^1S-4^1S	65	1.1-11	4.6+08	62	4.6-12	3.8+08	68	1.2-11	4.6+08	70	8.4-12	4.3+08

Table 4.1 (continued)

Transition (p,q)	1			2			3			4		
	C.S. (Ref.)	K(p,q) cm³ sec⁻¹	n(q) cm⁻³	C.S. (Ref.)	K(p,q) cm³ sec⁻¹	n(q) cm⁻³	C.S. (Ref.)	K(p,q) cm³ sec⁻¹	n(q) cm⁻³	C.S. (Ref.)	K(p,q) cm³ sec⁻¹	n(q) cm⁻³
1^1S-5^1S	65	4.1-12	2.8+07	62	6.7-12	4.0+07	68	5.1-12	3.3+07	69	5.5-12	3.4+07
1^1S-3^1D	65	1.7-11	9.7+07	95	1.9-12	5.2+07	95	2.0-12	5.2+07	70	6.5-12	6.5+07
1^1S-4^1D	65	7.0-12	7.0+07	62	1.1-12	4.0+07	95	1.4-12	4.2+07	71	2.7-12	4.9+07
2^3S-3^3S	65	4.3-08	6.5+08	72	3.6-08	6.1+08	72	1.1-08	4.7+08			
2^3S-4^3S	65	7.8-09	2.8+08	64	7.3-09	2.7+08						
2^3S-5^3S	65	2.8-09	6.5+07	64	2.7-09	6.4+07						
2^3S-3^3D	65	8.2-08	1.1+09	64	7.3-08	3.7+08						
2^3S-4^3D	65	6.7-10	1.8+08	64	1.8-08	1.7+08						
2^3S-4^3F	65	3.3-10	7.1+07	64	2.9-09	8.9+07						
$2^3S-5^3F,5^3G$	65	1.9-10	9.3+07	64	1.7-09	1.0+08						
1^1S-2^3S	65	9.5-11	2.3+11	74	1.6-10	2.7+11	74	2.1-10	3.1+11			
1^1S-2^3P	65	6.3-11	1.8+10	74	1.3-11	1.5+10	74	1.5-11	1.5+10	73	1.7-11	1.5+10

* Read 4.7-10 as 4.7×10^{-10}. The values in the first set of columns refer to calculations using cross sections from Ref. 65. In the remaining sets, cross sections of referred transitions were changed one at a time, keeping the rest from Ref. 65, and the change in population densities noted.

calculated by this method agree well with the values obtained by Otsuka et al[10] both for HeI and HeII transitions under various experimental conditions. In Ref. 10 optical escape factors have been calculated by numerical integration of the expression for an infinite cylindrical geometry and the Doppler profile. The particle distribution is assumed to have "a bell-shaped form" proportional to that of electrons. For a cylindrical geometry, Otsuka et al[10] give the following expression.

$$\Lambda_{ik}(r_o) = \frac{2}{\sqrt{\pi}} \int_0^\infty dx \int_0^t dt \exp[- \frac{x^2}{1} - \frac{\hat{\tau}}{\sqrt{1 - \hat{\tau}^2}} \exp(- x^2)]$$

(4.1)

For larger $\hat{\tau}$ this expression approximately behaves as

$$\Lambda_{ik} = \frac{0.746}{\hat{\tau} (\pi \log \hat{\tau})^{1/2}}$$

where $\hat{\tau}$ is the optical depth.

A comparison of Drawin and Emard's[83] and Otsuka et al's[10] values of OEF for cylindrical geometry and for given values of $\hat{\tau}$ is given in Table 4.2. Otsuka et al's[10] values of optical escape factors are lower bounds, and an use of additional broadening (e.g. Stark broadening) causes an increase in the escape factors. Following Drawin and Emard[83], the Voigt profile was used in this work and optical escape factors were calculated for the various conditions of TPD plasma machine experiment.[38] These values are compared with those of Otsuka et al[10] in Table 4.3. Although the present values are somewhat higher (due to inclusion of additional broadening) than the corresponding values of Otsuka et al[10], yet the overall agreement may be considered to be reasonably good.

Table 4.2.   Comparison of Drawin and Emard's[83] and Otsuka et al[10] values of optical escape factors for a cylindrical geometry and Doppler profile

$\overset{\leftrightarrow}{\tau}$	O.E.F. from Drawin and Emard[83]	O.E.F. from Otsuka et al[10]
1.0-01	9.320-01*	9.007-01
1.5-01	9.000-01	8.573-01
1.0+00	5.138-01	4.211-01
2.0+00	2.894-01	2.197-01
1.0+02	2.531-03	1.951-03
1.0+03	2.083-04	1.615-04

* Read 9.320-01 as 9.320×10^{-1}.

Table 4.3. Optical escape factors for HeI and HeII transitions for the TPD plasma experiment conditions, calculated by using Eq. (2.32)

HeI ($\Gamma_g = 300°K$)

Transition	Present work	Ref. 10
$2^1P \to 1^1S$	7.35-3*	8.34-3
$3^1F \to 1^1S$	3.91-2	4.52-2
$4^1P \to 1^1S$	1.24-1	1.55-1
$5^1P \to 1^1S$	2.86-1	3.33-1
$6^1P \to 1^1S$	5.05-1	5.16-1

HeII

Transition	Window 3				Window 4				Window 5			
	$T_i = 300°K$		$T_i = 3.68+4°K$		$T_i = 300°K$		$T_i = 1.20+4°K$		$T_i = 300°K$		$T_i = 3.95+3°K$	
	Present	Ref.10	Present	Ref.10	Present	Ref.10	Present	Ref.10	Present	Ref.10	Present	Ref.10
$2^2P \to 1^2S$	7.98-3	9.05-3	1.48-1	1.87-1	1.24-2	1.46-2	1.06-1	1.40-1	2.36-2	2.68-2	1.17-1	1.47-1
$3^2P \to 1^2S$	7.21-2	8.73-2	7.52-1	7.00-1	1.17-1	1.53-1	6.65-1	6.45-1	2.28-1	2.78-1	6.90-1	6.55-1
$4^2P \to 1^2S$	2.66-1	3.14-1	9.58-1	8.76-1	3.96-1	4.42-1	9.28-1	8.49-1	6.08-1	5.94-1	9.37-1	8.53-1
$5^2P \to 1^2S$	5.43-1	5.45-1	9.98-1	9.38-1	6.86-1	6.58-1	9.90-1	9.23-1	8.45-1	7.70-1	9.93-1	9.26-1
$6^2P \to 1^2S$	7.58-1	7.01-1	1.0	9.65-1	8.58-1	7.85-1	1.0	9.56-1	9.48-1	8.61-1	1.0	9.58-1

* Read 7.35-3 as 7.35×10^{-3}.

4.3. POPULATION DENSITIES

The values of reduced population coefficients r_0 plotted against electron density at $kT_e = 1.38$ eV and $kT_e = 10$ eV under optically thin conditions are compared with the corresponding values of Fujimoto[52] and Hess and Burrell[51] (shown by dotted lines in Figures 3.1 and 3.2 respectively). In general, the values are about 1-2 orders of magnitude higher than the corresponding values of Hess and Burrell[51]. The r_0 values for 4^1F are 10% larger than those of Ref. 51 at $n_e = 10^8$ cm^{-3}. The differences between the r_0 results at low electron densities of Refs. 51 and 52 and those of the present work may be traced to the choice of radiative recombination coefficients $\beta(p)$ used in the calculations. Whereas authors of Refs. 51 and 52 use empirical and semiempirical cross sections, the present work uses theoretical cross sections from Kramers[81]. Experimental results on helium plasmas that are available at present refer to sufficiently high ground state densities and electron temperatures that the contribution from the second term of Eq. 2.54 dominates. Experimental values of HeI population densities from plasmas at very low ground state densities e.g. $< 10^9$ cm^{-3} or at extremely low electron temperatures (where the first term of Eq. 2.54 dominates) can help settle the question of r_0 values at low electron densities. The comparison of r_1 values of the present work and those of Ref. 51 presented in Figures 3.6 show that the r_1 values of the present work agree well with those of Hess and Burrell[51].

The values of r_0^+, r_1^+ and r_2^+ for HeII levels were shown in Figures 3.9-3.14. For lower levels of HeII, the values of r_0^+ (Figure 3.9) remain constant up to $n_e = 10^{12}$ cm^{-3} and then rise

sharply. In going from lower levels to higher levels the electron density at which this sharp rise takes place decreases. The r_1^+ values (Figure 3.10) remain almost the same for all the levels of HeII up to $n_e = 10^{13}$ cm^{-3}, beyond which the values are lower for higher levels. Similarly r_2^+ values (Figure 3.11) are lower for higher levels at all electron densities. In contrast to r_1^+ and r_2^+ values, the values of r_0^+ (Figure 3.9) are higher for higher levels at high electron densities. Thus it can be concluded that at higher electron densities, the contribution from the second continuum (through r_0^+) dominates over the contribution from the ground state of HeI (through r_1^+) and from the ground state of HeII (through r_2^+).

It may be pointed out here that, strictly speaking, r_0 values for HeI levels such as those presented in Figures 3.1-3.4, are functions of n(1), the HeI ground state population density, as the heavy particle collisions have been taken into account in the model. Contributions to r_0 are thus not exclusively from the first continuum. The contribution from the ground state of HeI is through both r_0 and r_1 terms, but the dominant contribution is through r_1. The dominant contribution to $r_0(p)$ is thus from the first continuum. The values of r_0 presented in Figures 3.1-3.4 have been computed at low He pressure corresponding to a ground state population density n(1) = 2.25 x 10^{14} cm^{-3}. At this low pressure, the heavy particle collisions are not very effective and do not contribute significantly to r_0 values. Hence r_0 values given in Figures 3.1-3.4 may be taken to be independent of the gas pressure.

Perhaps the best way of testing a collisional-radiative model is to apply it to an experiment and to compare the calculated and experimentally observed population densities. The present collisional radiative model explains quite well the experimental results of Johnson[34], Johnson and Hinnov[35], Otsuka et al[38], and Hegde and Ghosh[11].

We have made comparisons of our calculated population densities with the experimental values of Johnson[34] for eight sets of conditions. Results for two sets of conditions, which show the best and the worst agreements are shown in Table 4.4. In the first set the plasma parameters are $kT_e = 7.9$ eV, $n_e = 3.3 \times 10^{13}$ cm^{-3} and $n(1) = 1.8 \times 10^{13}$ cm^{-3}. In the second set, the values of plasma parameters are $kT_e = 14.4$ eV, $n_e = 5.1 \times 10^{12}$ cm^{-3} and $n(1) = 4.1 \times 10^{11}$ cm^{-3}. The agreement is better at low electron temperatures. In the worst case the population densities agree within one order of magnitude.

Figure 4.4 presents the population densities of HeI excited states from the experiments of Johnson and Hinnov[35] along with the values calculated by Hess and Burrell[51] and also those obtained from the present calculations. The plasma parameters are $kT_e = 1.1$ eV, $n_e = 2.4 \times 10^{13}$ cm^{-3}, and $n(1) = 5.75 \times 10^{13}$ cm^{-3}. Major discrepancies (by about a factor of 2) between the experimental values and those calculated in this work are observed for 3^1P and 3^1D. The population densities of the remaining states are in fair agreement with experimental values, including the states $5^1S, 5^1P, 5^1D$, 5^3S, 5^3P, and 5^3D for which results are not available from Hess and Burrell[51], as they consider separated sublevels only up to $n = 4$.

Table 4.4.   Comparison of Johnson's[34] experimentally observed values of HeI population densities $n(p)/g_p$ with present calculations

States	$kT_e = 7.9$ eV $n_e = 3.3{+}13^*$ cm^{-3} $n(1) = 1.8{+}13$ cm^{-3} $n(p)/g_p$ (cm^{-3})		$kT_e = 14.4$ eV $n_e = 5.1{+}12$ cm^{-3} $n(1) = 4.1{+}11$ cm^{-3} $n(p)/g_p$ (cm^{-3})	
	Expt. (Ref. 34)	Present Calculations	Expt. (Ref. 34)	Present Calculations
4^1S	4.80+6	3.27+7	9.30+5	1.64+6
5^1S	1.18+6	3.33+6	4.10+5	1.60+5
3^1P	1.91+7	2.23+7	1.11+6	3.73+5
4^1P	4.10+6	8.17+6	5.90+5	2.21+5
5^1P	1.09+6	1.43+6	3.20+5	9.40+4
3^1D	1.00+7	1.95+7	4.80+5	3.34+5
4^1D	3.00+6	2.62+6	4.10+5	7.28+4
5^1D	7.40+5	4.12+5	1.85+5	2.04+4
3^3S	2.60+7	3.53+7	2.30+6	1.22+6
4^3S	4.40+6	1.58+7	7.00+5	5.60+5
5^3S	9.70+5	1.11+6	1.76+5	6.76+4
3^3P	1.89+7	2.29+7	2.20+6	6.86+5
4^3P	3.40+6	1.82+6	5.00+5	1.10+5
5^3P	1.04+6	3.28+5	2.10+5	1.81+4
3^3D	1.47+7	7.60+6	1.11+6	1.46+5
4^3D	2.90+6	1.83+6	3.60+5	5.85+4
5^3D	7.50+5	3.53+5	1.22+5	1.75+4

* Read 3.3+13 as 3.3×10^{13}.
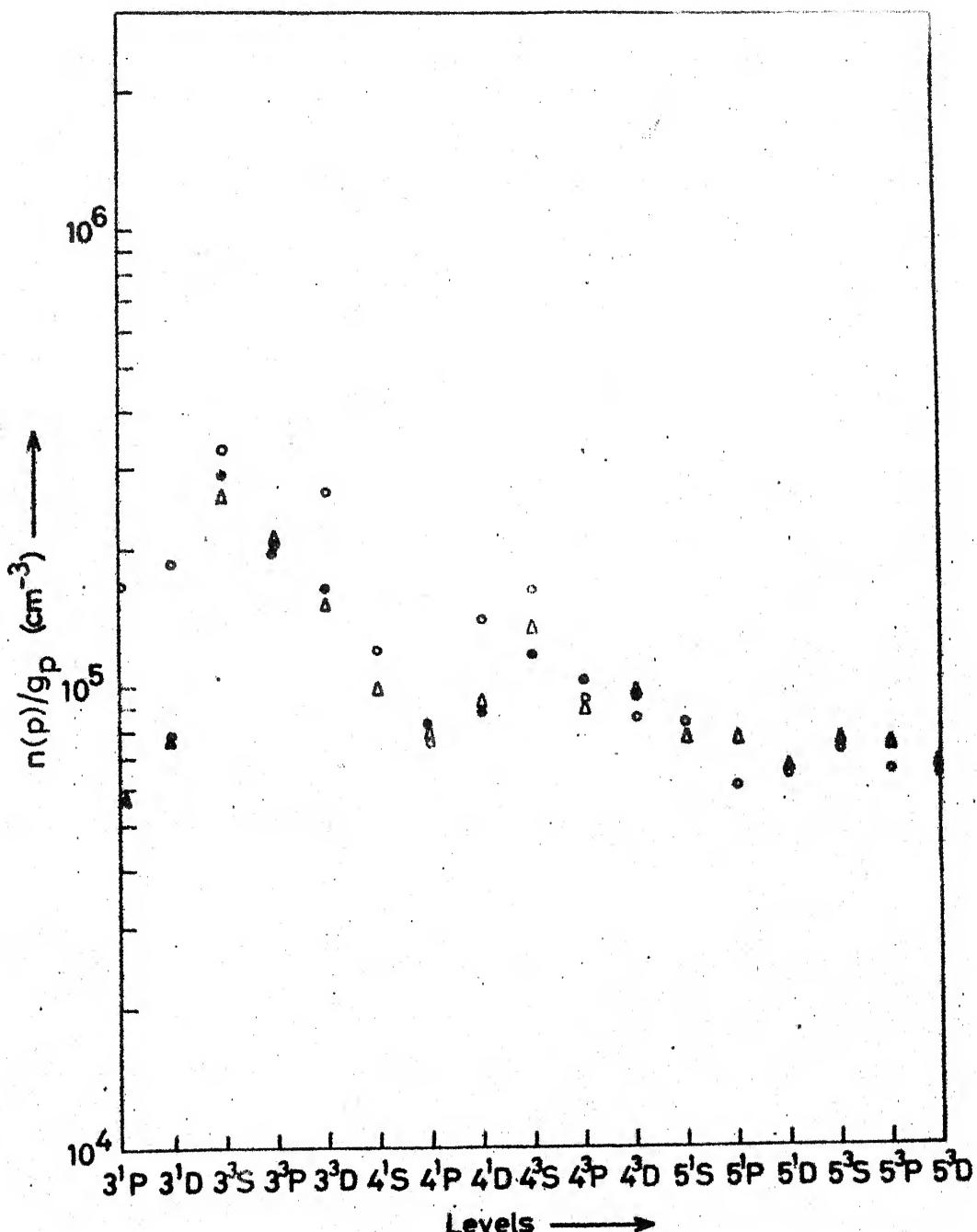
Figure 4.4. Comparison of calculated and experimental population densities of HeI levels; △ experimental results[35]; ●, calculated values[51]; ○, present calculated values.

The experimentally observed population densities for levels 3^3D and 4^1D of HeI of Otsuka et al[38] and those calculated for their experimental conditions using the present model are shown in Table 4.5. The calculated population densities of Ref. 88 are also presented in this table. In this experiment, $n(1) = 2.25 \times 10^{14} cm^{-3}$, the values of electron temperatures at three windows are respectively 3.17, 0.88 and 0.34 eV, and those of electron densities are 2.68×10^{14}, 1.83×10^{14} and 1.06×10^{14} cm^{-3} respectively. For window 3, the results of present calculation are worse than those reported in Ref. 88, but for windows 4 and 5, the agreement between the experimental and calculated population densities using the present model is good and better than those presented in Ref. 88.

The emission enhancement factors $(R_B = \frac{I_B}{I_O})$ for HeI and HeII at various magnetic fields based on ratios of population densities, as reported in Ref. 11, were also calculated using the present model. Whereas the ratios of population densities are not sensitive probes to test a model, it was found that the theoretical enhancement profiles for all of the HeI lines are in agreement within 25% of the experimental profiles. A typical result for the transitions 3^1D-2^1P is shown in Figure 4.5. The HeII enhancement profile, however, was found to be quite sensitive to the ionization-excitation cross section used. This may be expected since at zero magnetic field, the dominant term determining the population density of HeII is the ionization-excitation process, whereas at all other magnetic fields, the dominant term results from the population of HeII excited states from the ground state of HeII.

Table 4.5. Comparison of experimentally observed population densities (Ref. 38) for 3^3D and 4^1D levels of HeI with the present calculations

Population Densities (cm^{-3}) for TPD Plasma Experiment Conditions

Levels	Window 3			Window 4			Window 5		
	Expt. (Ref. 38)	Ref. 88	Present Work	Expt. (Ref. 38)	Ref. 88	Present Work	Expt. (Ref. 38)	Ref. 88	Present Work
3^3D	2.0+7*	1.10+7 1.70+7	1.14+8 1.84+8	1.0+8	6.30+8 7.60+8	2.25+8 3.58+8	3.0+8	8.80+8 9.80+8	5.95+8 6.10+8
4^1D	2.1+6	1.20+6 1.40+6	1.38+7 2.10+7	2.0+7	1.10+8 1.70+8	4.70+7 5.33+7	8.5+7	7.30+8 8.20+8	2.56+8 2.59+8

* Read 2.0+7 as 2.0 x 10^7; upper value in each box corresponds to optically thin case and the lower value to partially optically thick case.

Figure 4.5. Comparison of the experimental and calculated emission enhancement profiles for the transition 3^1D-2^1P; ——, experimental profile[11]; ---, calculated profile[11]; -·-·-, present calculated profile.

The calculated population densities of n = 4 level of HeII for the conditions of TPD machine are also compared with the corresponding experimental results of Otsuka et al[38] and are presented in Table 4.6. The following equation has been used for calculating the population densities of HeII levels.

$$n^+(i) = r_o^+(i) \; n_e \; n^{++} \frac{4.14 \times 10^{-16}}{T_e^{3/2}} \; i^2 \; \exp(E_i^+/kT_e) +$$

$$r_1^+(i) \; n(1) \; 4i^2 \; \frac{n^{++}}{n^+(1)} \; \exp((E_i^+ - E_1^{\cdot})/kT_e) +$$

$$r_2^+(i) \; i^2 \; n^+(1) \; \exp((E_i^+ - E_1^+)/kT_e) \tag{4.2}$$

where E_i^+ and E_1^+ are respectively the ionization potentials of the ith state and ground state of HeII and $E_1^{\cdot}$ is the ionization potential of the ground state of HeI to the first continuum. In Table 4.6, the results of Ref. 88 are also given. For window 3 and for the partially optically thick case, the dominant contribution is made by the third term of Eq. (4.2), in contrast to the calculated results of Otsuka et al[10] where the first term is dominant. For windows 4 and 5, present calculations and the calculations of Otsuka et al[10] agree about the dominance of the first term. The n(4) population densities of HeII using the present calculations for window 3 are not in as good agreement with experiment as the corresponding value of Otsuka et al[10], but those for windows 4 and 5 are in better agreement with the experimental results than those of Refs. 10 and 88.

Therefore it may be concluded that at low electron temperatures, the results of present calculations agree with the experimental results but at high electron temperatures the matching is

Table 4.6. The first, second and third terms of Eq. (4.2) for the i = 4 level of HeII and comparisons of calculated population densities (cm^{-3}) for i = 4 with those of Refs. 10, 38 and 88

	Present Calculations							$n(4)$ Ref. 88	$n(4)$ Ref. 10	Expt. $n(4)$ Ref. 38
	r_o^+	r_1^+	r_2^+	I Term	II Term	III Term	$n(4)$			
Window 3	5.73$-$2*	1.50$-$13	1.22$-$5	1.35+4	3.22$-$3	5.39+3	1.89+4	9.62+4	1.00+5	2.10+5
	6.03$-$2	2.05$-$13	5.65$-$5	1.42+4	4.39$-$3	2.49+4	3.91+4	2.00+5	1.00+5	
Window 4	9.99$-$3	9.99$-$35	1.80$-$5	1.71+6	8.34$-$31	3.45$-$15	1.71+6	2.33+7	1.50+7	2.50+6
	1.03$-$2	1.44$-$33	8.38$-$5	1.77+6	1.25$-$29	1.61$-$14	1.77+6		1.50+7	
Window 5	5.50$-$5	$<10^{-38}$	$\leq 10^{-38}$	1.84+5	$<10^{-38}$	$<10^{-38}$	1.84+5	1.37+7	4.30+6	2.60+4
	5.60$-$5	$<10^{-38}$	$<10^{-38}$	1.88+5	$<10^{-38}$	$<10^{-38}$	1.88+5		4.30+6	

* Read 5.73$-$2 as 5.73×10^{-2}; upper value in each group corresponds to optically thin case and the lower value to partially optically thick case.

not good. The calculated results are in near agreement with the experimental results, if lower values of radiative recombination coefficients and higher values of electron impact excitation rate coefficients are used.

4.4. ROLE OF DIRECT IONIZATION-EXCITATION

Figures 3.15-3.19 show that the direct ionization-excitation process plays a significant role in determining the population densities of HeII levels, particularly at high electron temperatures (> 2 eV) and at electron densities less than 10^{12} cm^{-3}. Here we comment on the role of the ratio $n^+(1)/n^{++}$, that of $n(1)$ and the contribution of the excited states of HeI.

The second term of Eq. (3.1) presented below,

$$ n^+(i) = r_0^+(i) \, n_E^+(i) + r_1^+(i) \, \frac{n(1)}{n_E(1)} \cdot n_E^+(i) + $$

$$ r_2^+(i) \, n^+(1) \, \frac{n_E^+(i)}{n_E^+(1)} $$

is a function of the ratio $n^+(1)/n^{++}$. It is found that for $kT_e > 5$ eV, the variation of this ratio does not alter the population densities of HeII levels more than 2% in the range $n^+(1)/n^{++} = 10^2$-10^4. The values of population densities of HeII levels at $n^+(1)/n^{++} = 10^4$ are about a factor of 3 larger than those at $n^+(1)/n^{++} = 1$. This is clear from the values of population densities of HeII levels shown in Table 4.7. This table presents the population densities of HeII excited states at $kT_e = 5$, 10, 15 and 18 eV, $n_e = 10^{12}$ cm^{-3} and for the ratio $\frac{n^+(1)}{n^{++}} = 1$, 100, 1000. The ground state density of HeI is 2.25×10^{14} cm^{-3} and $n^+(1) \approx n_e$. The values of population densities of level $i = 4$ at

Table 4.7. Effect of the variation of ratio $(n^+(1)/n^{++})$ on the population densities of HeII excited states

$$(n(1) = 2.25+14 \text{ cm}^{-3}, \quad n_e = 1.0+12 \text{ cm}^{-3}, \quad n^+(1) \approx n_e)$$

HeII Levels	$n^+(1)/n^{++} = 1$ Population Densities cm^{-3}				$n^+(1)/n^{++} = 100$ Population Densities cm^{-3}				$n^+(1)/n^{++} = 10^4$ Population Densities cm^{-3}			
$kT_e =$	5 eV	10 eV	15 eV	18 eV	5 eV	10 eV	15 eV	18 eV	5 eV	10 eV	15 eV	18 eV
i=2	1.1-01*	5.8+00	2.7+01	4.7+01	1.2-01	8.1+00	4.9+01	9.7+01	1.2-01	8.1+00	5.0+01	9.9+01
3	7.2-03	1.3+00	1.2+01	2.7+01	7.7-03	2.7+00	3.1+01	7.2+01	7.7-03	2.8+00	3.1+01	7.3+01
4	2.6-03	1.1+00	1.3+01	3.1+01	3.1-03	2.7+00	3.6+01	8.8+01	3.1-03	2.7+00	3.7+01	9.0+01
5	1.6-03	1.2+00	1.6+01	4.0+01	2.2-03	3.2+00	4.6+01	1.2+02	2.2-03	3.2+00	4.7+01	1.2+02
6	1.2-03	1.4+00	2.1+01	5.2+01	2.0-03	4.0+00	6.0+01	1.5+02	2.0-03	4.0+00	6.1+01	1.5+02
7	1.1-03	1.7+00	2.6+01	6.6+01	2.0-03	4.9+00	7.6+01	1.9+02	2.1-03	5.0+00	7.8+01	2.0+02
8	1.1-03	2.1+00	3.2+01	8.2+01	2.3-03	6.0+00	9.5+01	2.4+02	2.3-03	6.2+00	9.7+01	2.4+02
9	1.1-03	2.5+00	4.0+01	1.0+02	2.5-03	7.3+00	1.2+02	2.9+02	2.6-03	7.5+00	1.2+02	3.0+02
10	1.2-03	3.0+00	4.8+01	1.2+02	2.9-03	8.8+00	1.4+02	3.5+02	2.9-03	9.0+00	1.4+02	3.6+02
11	1.3-03	3.6+00	5.6+01	1.4+02	3.3-03	1.0+01	1.7+02	4.2+02	3.3-03	1.1+01	1.7+02	4.3+02
12	1.5-03	4.1+00	6.6+01	1.7+02	3.7-03	1.2+01	1.9+02	4.9+02	3.8-03	1.2+01	2.0+02	5.0+02
13	1.6-03	4.8+00	7.6+01	1.9+02	4.2-03	1.4+01	2.2+02	5.7+02	4.3-03	1.4+01	2.3+02	5.8+02
14	1.8-03	5.5+00	8.8+01	2.2+02	4.7-03	1.6+01	2.6+02	6.6+02	4.8-03	1.6+01	2.6+02	6.7+02
15	2.0-03	6.2+00	9.9+01	2.5+02	5.3-03	1.8+01	2.9+02	7.5+02	5.4-03	1.9+01	3.0+02	7.6+02

* Read 1.1-01 as 1.1×10^{-01}.

various electron temperatures and electron densities corresponding to $\frac{n^+(1)}{n^{++}}$ = 1000 were already presented in Table 3.6.

The second term of Eq.(3.1) is a function of also the HeI ground state population density n(1).For all the levels, on taking lower values of n(1) the value of electron temperature, above which direct ionization-excitation becomes important, increases. For example, for i = 4, at n_e = 10^8 cm^{-3} and n(1) = 1.0 x 10^{14} cm^{-3}, the direct ionization-excitation is important above kT_e = 3.3 eV, while at the same electron density and for n(1) = 1.0 x 10^{12} cm^{-3} this process is important above kT_e = 6.6 eV. A decrease in HeI ground state population density results in a reduced contribution of direct ionization-excitation and in an increase in the electron temperature above which this process is important.

Present calculations also indicate that, for the conditions of calculations used in the present work, the major contribution to population densities of HeII levels is mainly from the ground state of HeI. The contribution from the excited states of HeI to the population densities of HeII levels is much less. This is because of the fact that although the ionization-excitation rate coefficients for the metastable states of HeI are much larger than the rate coefficient of the ground state of HeI (Table 3.2) but the population densities of metastable states of HeI are atleast three orders of magnitude smaller than the population density of HeI ground state. The contribution from the higher states of HeI is even less in populating the excited levels of HeII. The present calculations provide an estimate of the role of direct ionization-excitation in populating HeII excited states.

Non availability of the exact simultaneous ionization-excitation cross sections for the higher excited levels constitutes a major shortcoming. However, it was found that the results obtained about the range of electron temperature where ionization-excitation is important are not very sensitive to considerable variations in the cross sections. Hence, the results obtained in the present work should give a fairly good idea about the quantitative role of direct ionization-excitation processes in spite of uncertainties in the cross sections. Thus, it may be concluded that direct ionization-excitation process dominantly populates HeII levels at $kT_e > 2$ eV and $n_e < 10^{12}$ cm^{-3} and must be an integral part of the model under such conditions.

4.5. MECHANISM OF POPULATION OF EXCITED STATES

The procedure outlined in Chapter 2 and the results presented in Chapter 3 for evolving the mechanism of population of excited states give an idea about how the various excited states of HeI and HeII are populated and which rate coefficients and transition probabilities have major significance. The present work, perhaps for the first time, focusses a method which systematically examines the importance of individual atomic processes. It is true that the dominant mechanism that finally evolves ultimately depends on the choice of cross sections; however, for any choice of cross sections, the above procedure can be used, which is of general applicability.

It may be added here that whereas the above numerical procedure can be used for identification of the important elementary processes, an idea about the dominant processes of the

mechanism in populating various levels can be had from an analytical consideration of the form and constituents of the elements of the inverted matrix. This can be done in the following manner. The elements of an inverted matrix X ($X = A^{-1}$) pertaining to a collisional-radiative model are constructed out of the various elements a_{ij} of the original matrix A, which themselves are combinations of rate coefficients of elementary processes as described in Figure 2.2. A peculiar property of the inverted matrix is that an element x_{ij} of the inverted matrix X of dimension m x m can be written in terms of the corresponding element x'_{ij} of inverted matrix X' of dimension (m-1) x (m-1) as $x_{ij} = x'_{ij} +$ an additional term. For example, the x_{11} terms of inverted matrices of dimensions 2 x 2, 3 x 3, and 4 x 4 (obtained by using SNOBOL programme; see discussion later) are as follows:

2 x 2

$$x_{11}^{2x2} = \frac{1}{a_{11}} - \frac{a_{12}}{a_{11}} \left(- \frac{a_{21}}{a_{11}}\right) \frac{1}{a_{22} - \dfrac{a_{21} \cdot a_{12}}{a_{11}}} \tag{4.3}$$

3 x 3

$$x_{11}^{3x3} = x_{11}^{2x2} - \frac{c_{131} \cdot c_{351}}{c_{331}} \tag{4.4}$$

4 x 4

$$x_{11}^{4x4} = x_{11}^{3x3} - \left(c_{141} - \frac{c_{131} \cdot c_{341}}{c_{331}}\right) \frac{c_{451} - \dfrac{c_{431} \cdot c_{351}}{c_{331}}}{c_{441} - \dfrac{c_{431} \cdot c_{341}}{c_{331}}} \tag{4.5}$$

where

$$C_{131} = \frac{a_{13}}{a_{11}} - \frac{\dfrac{a_{12}}{a_{11}}\left(a_{23} - \dfrac{a_{21}\cdot a_{13}}{a_{11}}\right)}{a_{22} - \dfrac{a_{21}\cdot a_{12}}{a_{11}}}$$

$$C_{141} = \frac{a_{14}}{a_{11}} - \frac{\dfrac{a_{12}}{a_{11}}\left(a_{24} - \dfrac{a_{21}\cdot a_{14}}{a_{11}}\right)}{a_{22} - \dfrac{a_{21}\cdot a_{12}}{a_{11}}}$$

$$C_{331} = a_{33} - \frac{a_{31}\cdot a_{13}}{a_{11}} - \left(a_{32} - \frac{a_{31}\cdot a_{12}}{a_{11}}\right)\frac{a_{23} - \dfrac{a_{21}\cdot a_{13}}{a_{11}}}{a_{22} - \dfrac{a_{21}\cdot a_{12}}{a_{11}}}$$

$$C_{341} = a_{34} - \frac{a_{31}\cdot a_{14}}{a_{11}} - \left(a_{32} - \frac{a_{31}\cdot a_{12}}{a_{11}}\right)\frac{a_{24} - \dfrac{a_{21}\cdot a_{14}}{a_{11}}}{a_{22} - \dfrac{a_{21}\cdot a_{12}}{a_{11}}}$$

$$C_{351} = -\frac{a_{31}}{a_{11}} - \frac{a_{32} - \dfrac{a_{31}\cdot a_{12}}{a_{11}}\left(-\dfrac{a_{21}}{a_{11}}\right)}{a_{22} - \dfrac{a_{21}\cdot a_{12}}{a_{11}}}$$

$$C_{431} = a_{43} - \frac{a_{41}\cdot a_{13}}{a_{11}} - \left(a_{42} - \frac{a_{41}\cdot a_{12}}{a_{11}}\right)\frac{a_{23} - \dfrac{a_{21}\cdot a_{13}}{a_{11}}}{a_{22} - \dfrac{a_{21}\cdot a_{12}}{a_{11}}}$$

$$C_{441} = a_{44} - \frac{a_{41}\cdot a_{14}}{a_{11}} - \left(a_{42} - \frac{a_{41}\cdot a_{12}}{a_{11}}\right)\frac{a_{24} - \dfrac{a_{21}\cdot a_{14}}{a_{11}}}{a_{22} - \dfrac{a_{21}\cdot a_{12}}{a_{11}}}$$

$$C_{451} = -\frac{a_{41}}{a_{11}} - \frac{a_{42} - \dfrac{a_{41}\cdot a_{12}}{a_{11}}\left(-\dfrac{a_{21}}{a_{11}}\right)}{a_{22} - \dfrac{a_{21}\cdot a_{12}}{a_{11}}}$$

Population of a level is given by the product of matrix multiplication of a given row such as i of the inverted matrix with column matrices B, C, D, and E (as shown in Figure 2.2). That particular term x_{ij} which leads to the most significant value of the product makes the dominant contribution to the mechanism. A detailed analysis of the term structure of an inverted 4 x 4 matrix (along the lines of Eq. (4.5)) and a comparison with the numerical values of the elements of 45 x 45 inverted matrices (for various values of plasma parameters in the collisional-radiative model) indicate that, for the range of values of rate coefficients in the present work, the first term of all the elements of the inverted matrix is the dominant one. Therefore, all those processes whose rate coefficients make significant contribution to the matrix elements a_{ij}'s (of the original matrix A) which appear in the first term of x_{ij} would be important.

The process of sorting out the important terms is perhaps more conveniently accomplished by having the inverted matrix in algebraic form. For this a programme written in SNOBOL was used (see Appendix III),where the output provides the inverse of a matrix in the algebraic mode as is given in Eqs. (4.3-4.5). From this one could directly estimate the role of a particular rate coefficient in populating or depopulating a particular level. Without repetitive inversion of the original matrix, the method using SNOBOL permits direct estimates of contributions of various processes, but the computer memory requirement to completely write out the inverse of a 45 x 45 matrix in algebraic mode is substantial. The method however is potent as it permits a direct insight into the complicated processes.

From this study in simplification of the model we conclude that more than 70% of the processes used in the model could be neglected and yet population densities could be obtained within 20% of those from the elaborate models.

This method focusses attention on those atomic processes which make substantial contribution to the population densities, hence identifies the processes where knowledge of experimental cross sections would be of great value, if they are not already available.

4.6. LASER INDUCED SELECTIVE EXCITATION

In this section we critically examine the results of some recent laser induced selective excitation experiments against the predictions of the collisional-radiative model of the present work. We consider the experiments of Catherinot et al[39], Yasumaru et al[42], and Gauthier et al[90].

In the two sets of experiments of Catherinot et al[39], two different transitions are pumped. In the first set, 2^1S-3^1P transition (5016 Å) is pumped by a pulsed laser (500 Watts/pulse) at $P = 1$ torr, $T_g = 400°K$, $n_e = 10^{12}$ cm^{-3}, $kT_e = 5.17$ eV, laser pulse base width 5 nsec, spectral width 0.1 Å, and a pulse time delay of 2.1 nsec. The calculated enhanced population densities (in terms of arbitrary units) for 3^1P, 3^1D, 3^3D and 3^3P states under the above conditions along with the experimental results are presented in Figure 4.6. In the second set, the transition 2^1P-4^1D (4922 Å) is pumped with a laser pulse, time delay of 11.2 nsec. Other parameters are the same as for the first set. Experimental results for 3^1P, 4^1P and 4^3D levels along with the calculated results are shown in Figure 4.7.
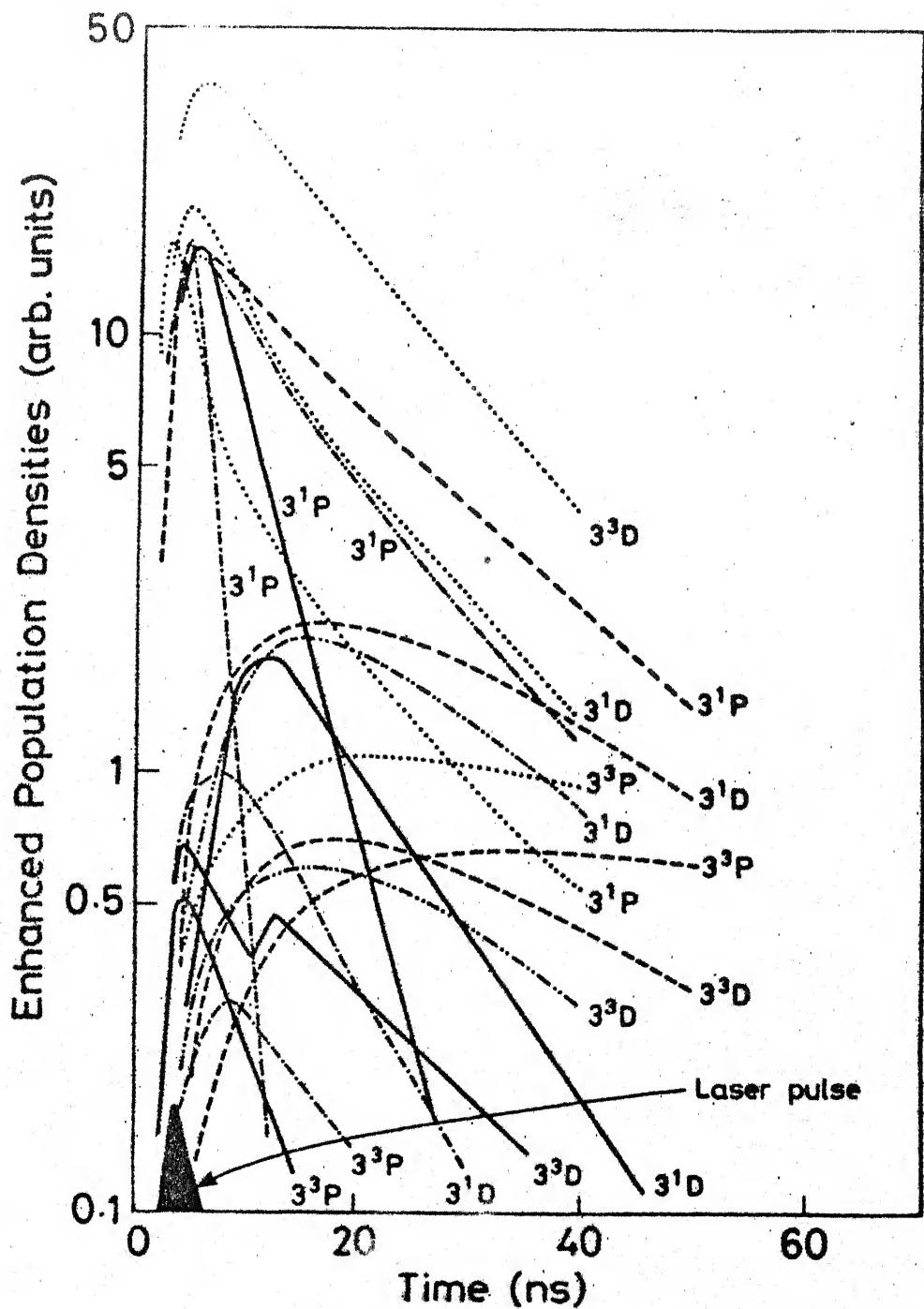
Figure 4.6.   Enhancement and decay of population densities of 3^1P,
3^1D, 3^3D and 3^3P states; _____, experiment[39]; ------,
calculated, partially optically thick and low KN(p,q)
values; ......, calculated, partially optically thick
and high KN(p,q) values[79]; -.-.-, calculated, optically
thin and low KN(p,q) values; -..-, calculated higher
(X20) optical escape factors and low KN(p,q) values.
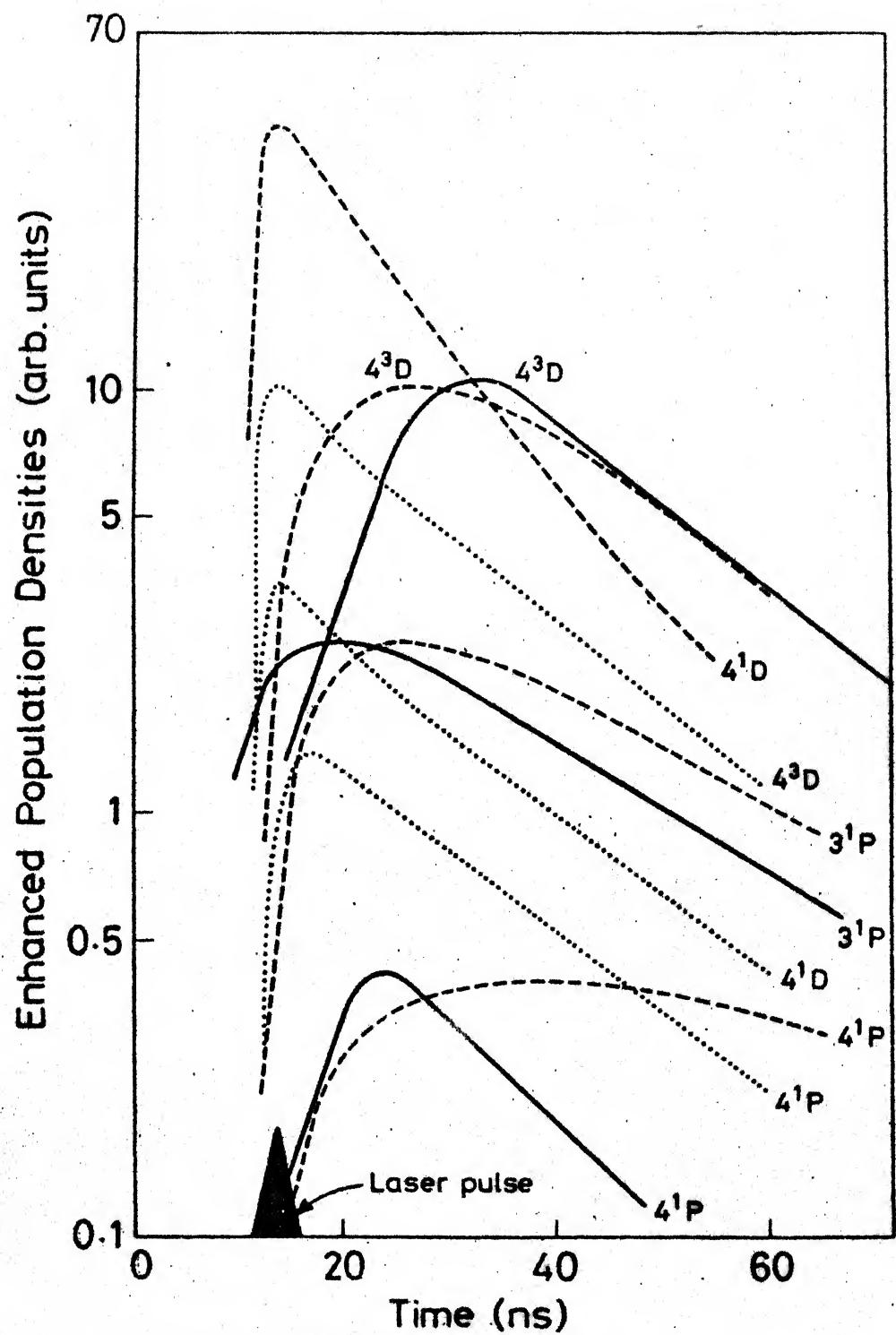
Figure 4.7. Enhancement and decay of populations of 3^1P, 4^1P and 4^3D states; ———, experiment[39]; ------, calculated, partially optically thick and low KN(p,q) values; ....., calculated, partially optically thick and high KN(p,q) values[79].

Figure 4.8 presents the calculated time dependent population densities compared with the corresponding results of Yasumaru et al[42]. In the experiment of Yasumaru et al[42], the 2^1S-3^1P transition (5016 $\overset{\circ}{A}$) is pumped with a laser pulse of width (FWHM) 5 nsec, spectral width 0.1 $\overset{\circ}{A}$, and relative population densities of the 3^1P and 3^1D levels are monitored at two pressures, 0.4 torr and 5 torr. The electron densities and electron temperatures at these two pressures respectively are n_e = 2 x 10^{10} cm^{-3} and 3 x 10^{11} cm^{-3}, and kT_e = 10.34 eV and 3.45 eV.[91] The calculated and experimental population densities at both the pressures are shown in Figure 4.8.

In the experiment of Gauthier et al[90], the triplet transition 2^3S-3^3P (3888.6 $\overset{\circ}{A}$) is pumped by a laser pulse of power 2 KW, width (FWHM) 3.5 nsec, and spectral width 0.1 $\overset{\circ}{A}$. The plasma parameters are T_e = 600°K, n_e = 2.9 x 10^{11} cm^{-3}, T_g = 300°K and the ground state population density = 4.6 x 10^{17} cm^{-3}. The fluorescence decay of 3^3P, 3^3S and 3^3D levels are monitored as a function of time. In this experiment the electron temperature (kT_e = 0.0517 eV) is quite low. At kT_e < 0.1 eV, the population densities from the present collisional-radiative model are rather uncertain because of substantial under flow in the process of computer calculations. Hence, in order to make a rough comparison, the absolute population densities as a function of time are calculated at higher electron temperatures kT_e = 0.517 eV and also at kT_e = 1 eV and the results are presented in Figure 4.9.

In none of the above laser induced selective excitation experiments, the absolute population densities are provided. Hence to compare the calculated absolute population densities
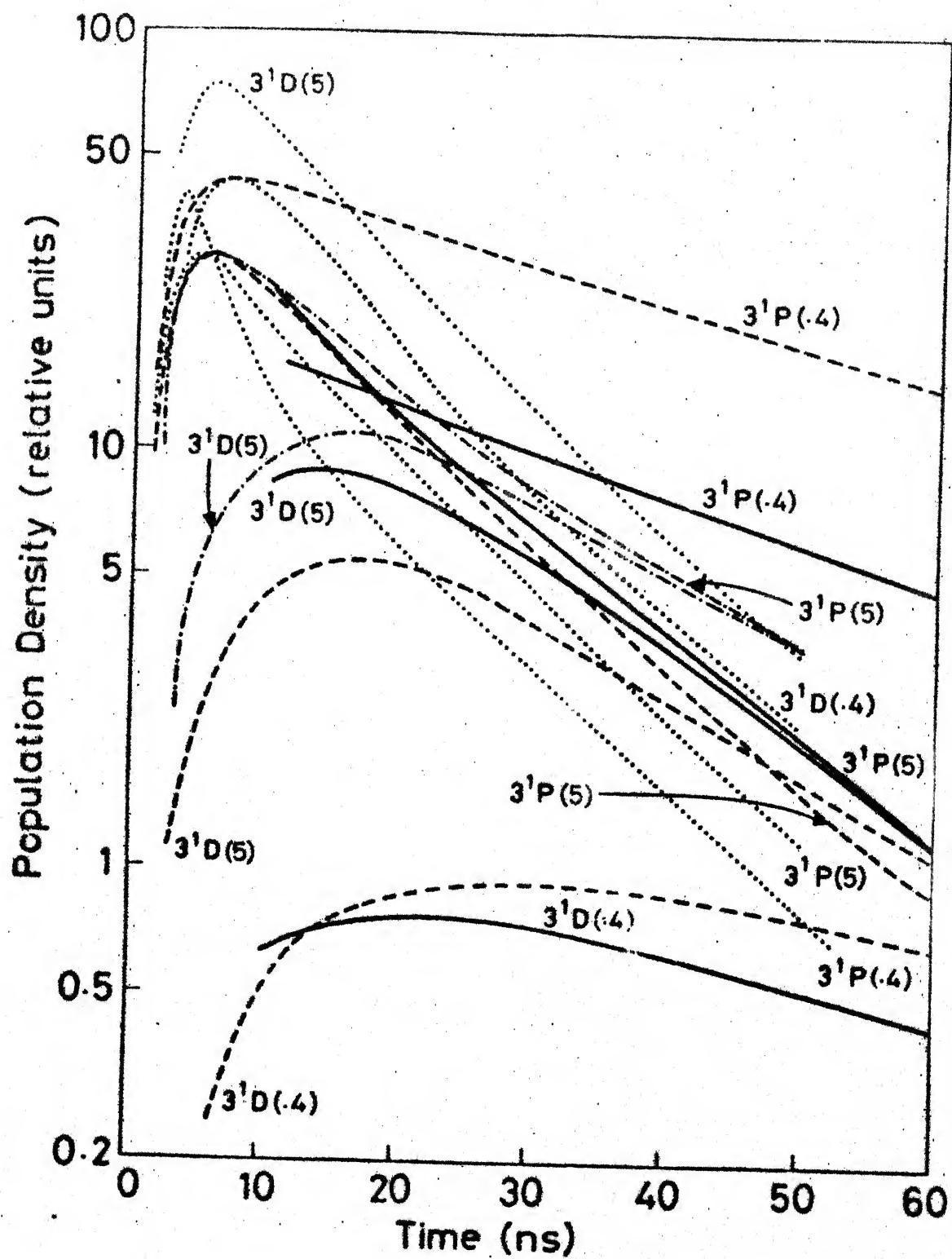
Figure 4.8. Relative population densities of 3^1P and 3^1D states at 0.4 torr and 5 torr gas pressure; _____, experiment[42]; ------, calculated, partially optically thick and low KN(p,q) values; ....., calculated, partially optically thick and high KN(p,q) values[79]; -.-.-, calculated, only one rate coefficient (3^1P-3^1D) non zero and the rest zero.
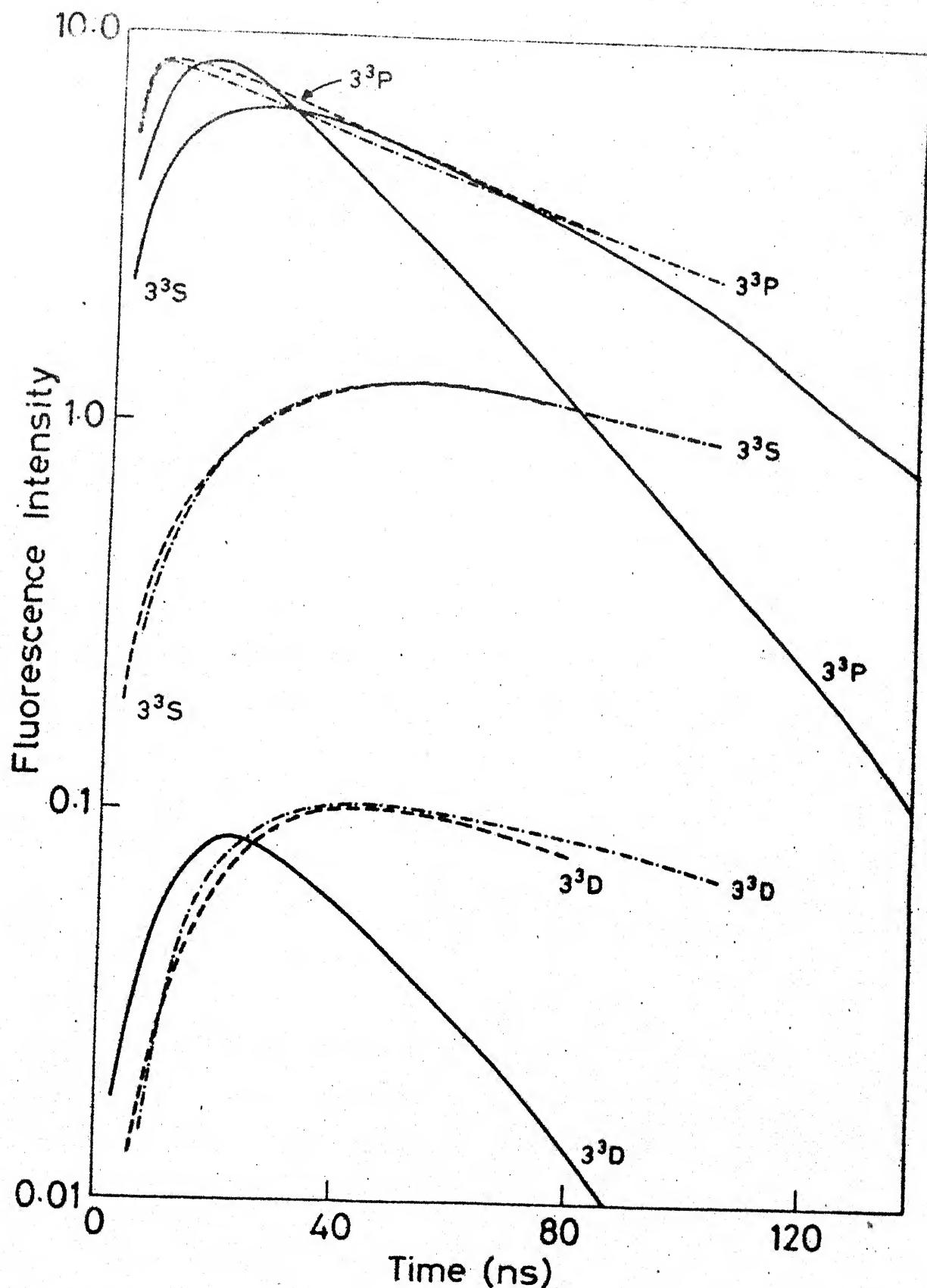
Figure 4.9. Fluorescence decay of 3^3P, 3^3S and 3^3D levels; ———, experiment[90]; -----, calculated at $kT_e = 0.517$ eV; -·-·-, calculated at $kT_e = 1$ eV.

with the experimental results, the calculated absolute population densities are converted to relative population densities by normalizing with respect to one of the experimental population densities. In Figures 4.6 and 4.7 enhanced population densities N (N = $N_{t=t}$, $N_{t=0}$) normalized with respect to respectively 3^1P and 4^3D peaks are presented. In Figure 4.8, relative population densities normalized with respect to 3^1P peak at 5 torr are shown. In Figure 4.9, the number of photons emitted cm^{-3} sec^{-1} (calculated absolute population density x transition probability, normalized with respect to 3^3P peak) against the elapsed time are plotted. The calculated absolute population densities corresponding to the data presented in Figures 4.6-4.9 are presented in Appendix II.

The derivation[85] of Einstein coefficients B involves the use of Boltzmann distribution law. Thus, strictly speaking, the term $B.\rho(\nu)$ gives the rate of induced emission or induced absorption for equilibrium situations. However, even for the non equilibrium situations, it has been used in the recent literature.[51] It has been found that a considerable variation in the numerical values of B (by an order of magnitude) does not change the relative population densities presented in Figures 4.6-4.9, and also, the peaks of enhancement curves on the time axis do not shift much. Only the absolute population densities increase or decrease with an increase or decrease in the numerical values of B.

A comparison of the magnitudes of electron impact and heavy particle collision terms in the rate expression of excited state population densities (Eq. 2.46) shows that in the pressure range of the laser induced selective excitation experiments discussed above, heavy particle collisions and the radiative

processes, and not the electron impact processes, play dominant role in populating or depopulating the levels studied. This is presented in Table 4.8 where the numerical values of all the terms of rate equation (2.46) are shown for the experimental conditions of the experiments of Catherinot et al[39] ($kT_e = 5.17$ eV, $n_e = 10^{12}$ cm^{-3} and P = 1 torr) and of Yasumaru et al[42] ($kT_e = 3.45$ eV, $n_e = 3 \times 10^{11}$ cm^{-3} and P = 5 torr) for some levels of HeI.

The calculations on temporal enhancement and decay profiles of population densities show that with rate coefficients for neutral-neutral excitation, deexcitation, ionization as well as recombination taken from Drawin and Emard[79], the calculated relative enhancements with respect to the pumped levels for the conditions of the experiment of Catherinot et al[39] and of Yasumaru et al[42] are much higher (shown by dotted lines in Figures 4.6, 4.7 and 4.8), than the experimental values. They also do not agree with the experimental peaks in terms of their positions on the time scale. It was found that the rate coefficients for heavy particle collisions given by Drawin and Emard[79] are about 1-2 orders of magnitude higher than that needed for an agreement with the experimental results and the reduction of the factor 128 (in Eq. 2.24) to 2.3 helps. Results of calculations with the factor 128 in Eq.(2.24)(Eq. 23 of Ref. 79) reduced to 2.3 are shown by dashed lines in Figures 4.6-4.8. A definite improvement in the calculated enhancements is noted. With this modified expression for heavy particle collisional rate coefficients, the deexcitation rate coefficient $KN(3^1P-3^1D)$ turns out to be 1.96×10^{-10} cm^3 sec^{-1} for the conditions of the experiment of Catherinot et al[39]. This reduction of heavy particle rate coefficients, however, is

Table 4.8 (continued)

Term	3^3P	3^3D	3^1D	3^1P	4^3D	4^1P
$\sum\limits_{q \neq p} n(q)\, A(q,p)$	1.5+18 4.4+16	4.3+17 2.4+16	2.1+17 2.5+16	8.8+16 7.7+16	1.3+16 1.5+15	1.9+16 2.7+15
$n_e\, K(p,i)\, n_E(p)$	1.1+08 5.8-07	2.0+08 1.0-06	6.8+07 3.5-07	4.1+07 2.1-07	4.9+08 2.7-06	9.9+07 5.4-07
$\dfrac{n_e^2}{\bar{X}}\, \beta(p)$	2.4+10 2.7+19	2.2+10 2.5+19	2.2+10 2.5+19	2.2+10 2.4+19	9.2+09 1.0+19	9.1+09 9.9+18

Upper value in each box corresponds to the experimental conditions of Ref. 39 and lower value to the experimental conditions of Ref. 42.

still not adequate to reproduce the decay patterns. The calculated decay curves are less steep and this departure may be attributed to the low values of the optical escape factors, used in this work. This is so because the curves represented by dotted lines and dashed lines have been obtained by using partially optically thick conditions and are broader than the experimental curves. On calculating the time dependent population densities under optically thin conditions (shown by dot-and-dash lines in Figure 4.6), the enhancement curves are found to be very sharp, in fact sharper than the experimental curves. Thus the optical escape factors used in this work are smaller than what are required to explain the experimental enhancement curves of Catherinot et al[39]. The optical escape factors used in the present calculations are calculated by using Eq.(2.32). This equation yields for the conditions of the experiment of Ref. 39 $\Lambda_{3^1P-1^1S} = 3.32 \times 10^{-3}$. By using higher (about one order of magnitude) OEF's, sharp decays of all the four curves (shown by dash-double dot lines in Figure 4.6), in near agreement with the experimental results, can be obtained. It may be added here that the optical escape factor for 3^1P-1^1S transition experimentally estimated by Dubreuil and Catherinot[41] at 0.4 torr, in the n_e range $10^{10}-10^{11}$ cm^{-3} and $T_g = 350\,^\circ K$, is $\Lambda_{3^1P-1^1S} = 0.014$. The estimated values of $\alpha_{3^1P-1^1S}$ and $\hat{\tau}_{3^1P-1^1S}$ in Ref. 41 are respectively 2.6×10^{-2} and 106. Under similar conditions Eq.(2.32)yields $\alpha_{3^1P-1^1S} = 1.99 \times 10^{-5}$, $\hat{\tau}_{3^1P-1^1S} = 107.41$ and $\Lambda_{3^1P-1^1S} = 2.75 \times 10^{-3}$. Obviously, the experiment of Catherinot et al[39] requires optical escape factors about one order of magnitude higher than those given by Eq.(2.32).

In Figure 4.8, using the reduced rate coefficients for heavy particle collisions, and taking the 3^1P peak at 5 torr as the normalized reference point, the calculated results are compared with the experimental results of Yasumaru et al[42] both at 0.4 torr and 5 torr. Under the conditions of this experiment, for the 3^1P-3^1D excitation transfer, the value for the electron impact rate coefficient $K(3^1P$-$3^1D)$ used in the model is 2.19×10^{-5} cm^3 sec^{-1} and for the heavy particle rate coefficient $KN(3^1P$-$3^1D)$ is 1.45×10^{-10} cm^3 sec^{-1}, both of which are close to the corresponding experimentally estimated values of Yasumaru et al[42]. Their corresponding values respectively are 3.5×10^{-5} and 3.5×10^{-10} cm^3 sec^{-1}. In order to explore the role of heavy particle rate coefficients, the value 3.5×10^{-10} cm^3 sec^{-1} for $KN(3^1P$-$3^1D)$ given by Yasumaru et al[42] along with all other KN's equated to zero was used. The resulting enhancement curves for 3^1P and 3^1D at 5 torr are shown by dot-dash lines in Figure 4.8. The curves thus obtained are broader than the experimental ones as well as the curves calculated earlier which considered additionally other transfer processes. This indicates that in the decay of the population densities of enhanced levels, several states make significant contribution.

It has already been mentioned that since the electron temperature in the experiment of Gauthier et al[90] is very low (0.0517 eV), the time dependent population densities were calculated at two higher electron temperatures 0.517 eV and 1 eV to have a rough idea of the matching of calculated and experimental enhancement curves, as the present calculations are rather uncertain at low electron temperatures ($kT_e < 0.1$ eV) due to

substantial underflow. Since under the conditions of this experiment the contribution of electron impact processes is relatively unimportant, it is expected that the results at relatively higher kT_e should not deviate much from those calculated at lower electron temperatures. Relative intensities for 3^3S and the decay patterns for both 3^3P and 3^3D are significantly off. A change in the optical escape factors in the singlet system has imperceptible effect on the calculated curves. Incorporation of partially optically thick condition for the 2^3S-3^3P, 2^3S-4^3P and 2^3S-5^3P transitions increases (not shown in Figure 4.9) the relative fluorescence intensities of both 3^3S (by a factor of 2) and 3^3D (by about an order of magnitude), keeping the peak shapes practically unchanged but flattening out the decay of 3^3P. Triplet states with n = 3 do contribute to the associative ionization process, a process which is not included in the present model but is expected to affect materially the triplet state population densities at high pressures. This could be a reason of the discrepancy between experimental and calculated curves of Figure 4.9. The required increase in calculated relative population density of 3^3S (in comparison with 3^3P and 3^3D in Figure 4.9) is compatible with the estimates of associative ionization cross sections in the literature: $Q_i(3^3S) = 0.06$, $Q_i(3^3P) = 2.0$, $Q_i(3^3D) = 2.9$ (Ref. 92), and $\sigma(3^3S) = 0$, $\sigma(3^3P) = 1.6$, $\sigma(3^3D) = 4.5$ (Ref. 93), all in units of 10^{-16} cm^2.

Thus from the application of the model to a range of laser excitation studies in helium plasmas, it may be concluded that the heavy particle rate coefficients from Ref. 79 used in this work should be lower by about 1-2 orders of magnitude and optical escape

factors from Ref. 83 should be larger by about one order of magnitude.

This latter conclusion if applied generally to Eq. (2.32) (Ref. 83) would come in conflict with its suitability already noted in connection with the applications to steady state helium plasmas.[11,34,35,38] The latter experiments were at low pressures with optical escape factors in the range $10^{-2}-10^{0}$. The implication here may be that whereas Eq. (2.32) is satisfactory in the low pressure range, at high pressures, the relative accuracy of the optical escape factors from Eq. (2.32) (where absolute values are small) is poor and need of appropriate corrective factors is indicated.

4.7. DETERMINATION OF ELECTRON TEMPERATURE FROM LINE INTENSITY RATIO

Both spectroscopic methods and electric probes have been used for determination of electron temperature T_e in plasmas. Spectroscopic methods have an advantage over electric probes because T_e estimates can be obtained without disturbing the plasma. Among the spectroscopic methods the one using line intensity ratios which has bearing in the collisional-radiative model has been controversial.[96-101] Since the present work involves a detailed examination of the collisional-radiative model of helium plasmas we examine here, using the results of our calculations as well as some experimental data, reliability of the method.

Cunningham[96] suggested that in non-thermal plasmas the electron temperature could be determined from the ratio of two spectral lines if they have similar excitation energies and the excitation cross sections of the emitting levels have very

different dependence on electron energy. These criteria are met in the case of singlet and triplet lines of HeI. Cunningham applied this method to HeI lines 4^3S-2^3P (4713 Å) and 4^1D-2^1P (4921 Å).

Drawin and Henning[97] also used the same pair of lines. However, in addition to processes considered by Cunningham[96] they considered ionization from the excited levels 4^1D and 4^3S and collisions of excited atoms with other plasma particles, particularly the singlet-triplet excitation transfer. They found that the line intensity ratio shows less temperature dependence than that observed by Cunningham[96], and the intensity ratio depends more strongly on gas pressure than on electron temperature. They concluded that this method is suitable for determination of electron temperature in non-thermal laboratory plasmas only if the lines lie far from one another.

Sovie[98], on the basis of a simplified collisional-radiative model, calculated the line intensity ratio of HeI lines 4^1S-2^1P (5047 Å) and 4^3S-2^3P (4713 Å). For plasmas with $n_e/n(1) < 10^2$, he considered excitations from the ground state and meta-stable states to excited levels and their radiative decays. The effect of cascading was also considered. He used the following relation to calculate the line intensity ratio:

$$X_o = \frac{N_{5047}}{N_{4713}} = \left[K(1^1S-4^1S) + B'K(2^1S-4^1S) + D'K(2^3S-4^1S) \right.$$

$$\left. + \frac{1}{n(1^1S)n_e} \sum_{r\geq4} R(r^1P)\, \bar{A}(r^1P-4^1S) \right] \bar{A}(4^1S-2^1P)/$$

$$\left[K(1^1S-4^3S) + B'K(2^1S-4^3S) + D'K(2^3S-4^3S) \right.$$

$$\left. + \frac{1}{n(1^1S)n_e} \sum_{r\geq4} R(r^3P)\, \bar{A}(r^3P-4^3S) \right] \bar{A}(4^3S-2^3P)$$

$$(4.6)$$

where K represents electron impact excitation rate coefficients; $n(1^1S)$ and n_e represent ground state population density and electron density respectively. B' and D respectively are $n(2^1S)/n(1^1S)$ and $n(2^3S)/n(1^1S)$, and $\bar{A}(a\text{-}b) = A(a\text{-}b)/A(a, tot)$ where A is the spontaneous transition probability. R(a) is the rate of production of state a. The ratio given by the above equation is a function of T_e, $n(2^1S)$ and $n(2^3S)$. To account for the cascading effects, Sovie[98] suggested that the quantity to be experimentally determined can be obtained by subtracting the product of observed $r^1P\text{-}4^1S$ transitions and $\bar{A}(4^1S\text{-}2^1P)$ from the observed number of 5047 Å $(4^1S\text{-}2^1P)$ transitions. On the basis of this premise and Eq. (4.6), one obtains

$$X_{casc} = \frac{\left[K(1^1S\text{-}4^1S) + B'K(2^1S\text{-}4^1S) + D'K(2^3S\text{-}4^1S)\right]\bar{A}(4^1S\text{-}2^1P)}{\left[K(1^1S\text{-}4^3S) + B'K(2^1S\text{-}4^3S) + D'K(2^3S\text{-}4^3S)\right]\bar{A}(4^3S\text{-}2^3P)}$$

$$(4.7)$$

From Eqs. (4.6) and (4.7), Sovie evaluated the values of X_o and X_{casc} for kT_e range 4-20 eV, both with and without the contribution from the metastable states. The ratios were found to be dependent only on T_e. However, this method is valid only when population of excited states by radiative recombination and depopulation by electronic collisions are unimportant processes.

Schieber et al[99] found that by using different cross sections, different estimates of T_e are obtained and concluded that with the available knowledge of cross sections, determination of electron temperature by this method is of little value. Eastlund et al[100] modified this method by suggesting an averaging technique to evaluate experimental data. This technique uses both relative and absolute line intensities. However, they do not take

into account the reabsorption of resonance radiation, excitation transfer and cascade processes.

In a recent work, Brenning[101] has examined the limitations of the method of determination of T_e from line intensity ratios, for various pair of lines. He found that, in general, secondary processes such as excitation from metastables, excitation transfer collisions, cascading etc., greatly influence the method and the method is restricted to only low density (n_e < 2 x 10^7 cm^{-3}), short duration (t_{exct} < 5 x 10^{-6} sec) plasmas. He suggested a method for T_e determination from absolute line intensities.

Thus the usefulness of this method has been viewed diversely. Whereas Cunningham[96] and Sovie[98] support this method with certain qualifications, Drawin and Henning[97], Schieber et al[99], Eastlund et al[100] and Brenning[101] either reject it or recommend it for a very restricted use. We examine here the validity of this method for determining T_e, by using the colli-sional-radiative model calculations of the present work.

Using Sovie's simplified model (Eqs. 4.6 and 4.7) and the rate coefficients used in the present model, we calculated the ratio I_{5047}/I_{4713}, both with and without metastables, at two electron densities $n_e = 10^{12}$ and 10^{14} cm^{-3}. In this, for the electron impact excitation 1^1S-4^1S, we used, in two separate set of calculations, cross sections given by Raan et al[68] and by Drawin[65]. The results for partially optically thick case are presented in Figure 4.10. We find that the line intensity ratio I_{5047}/I_{4713} strongly depends on the cross section for the process 1^1S-4^1S. On using Raan et al's[68] experimental cross section, the
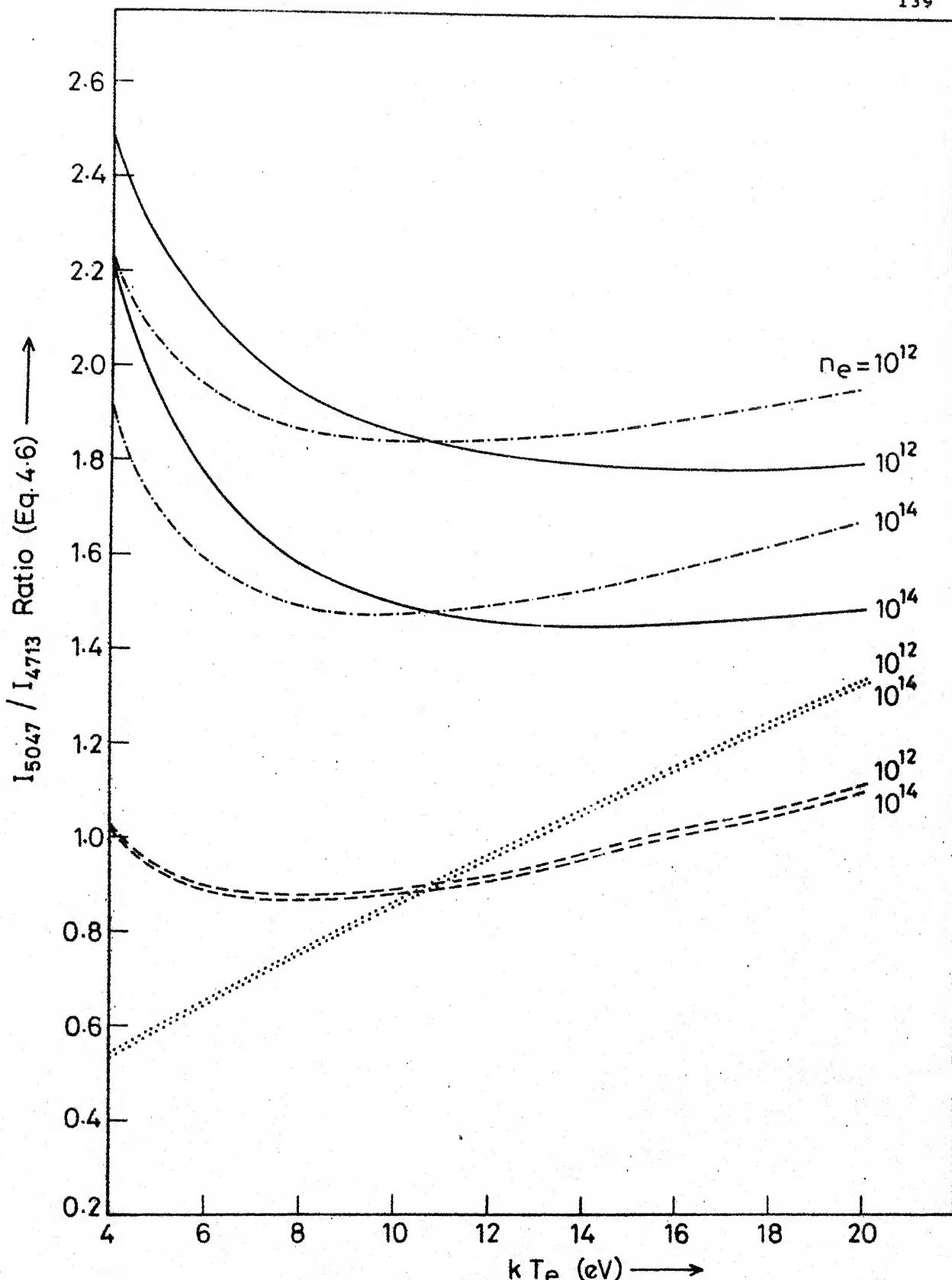
Figure 4.10. Variation of calculated (Sovie's model[98] and present rate coefficients) relative number of 5047Å and 4713Å transitions with T_e at $n_e = 10^{12}$ and 10^{14} cm^{-3} for partially optically thick case; ――――, experimental cross section[68], metastables included; ――――, experimental cross section[68], metastables excluded; -.-.-, empirical cross section[65], metastables included; ......, empirical cross section[65], metastables excluded.

intensity ratios first decrease and then gradually increase. Whereas on using Drawin's empirical cross section, the curves obtained are more steep. Whether Eq. (4.6) or Eq. (4.7) is used the results do not vary significantly. On excluding the excitations from metastable states the line intensity ratios regularly increase with increase in T_e and are independent of n_e, but still they depend on the choice of cross sections. With metastables included the line ratios are also a function of electron density as is evident from Figure 4.10. Figure 4.11 presents the results of ratio I_{5047}/I_{4713} (obtained by Sovie's method) for an optically thin plasma. By comparing the results obtained with partially optically thick conditions (Figure 4.10) and optically thin conditions (Figure 4.11), we find that absorption of resonance radiation also affects the line intensity ratios. Similar results are obtained for the ratio I_{7281}/I_{7065} presented in Figure 4.12. Thus these results show that Sovie's line intensity ratio method (neglecting secondary processes) is not valid for determination of T_e.

Sovie's[98] method does not take into account radiative recombination, electron impact deexcitation, electron impact ionization and recombination, excitation transfers, and absorption of radiations by plasma, and therefore it does not describe a realistic situation of non-LTE laboratory plasmas. Using Sovie's model and our rate coefficients we also calculated the absolute population densities of the levels 3^3S, 3^1S, 4^3S and 4^1S for the conditions of the experiments of Johnson[34], and Johnson and Hinnov[35]. Table 4.9 compares the population densities obtained by Sovie's method with the experimental results. Population densities
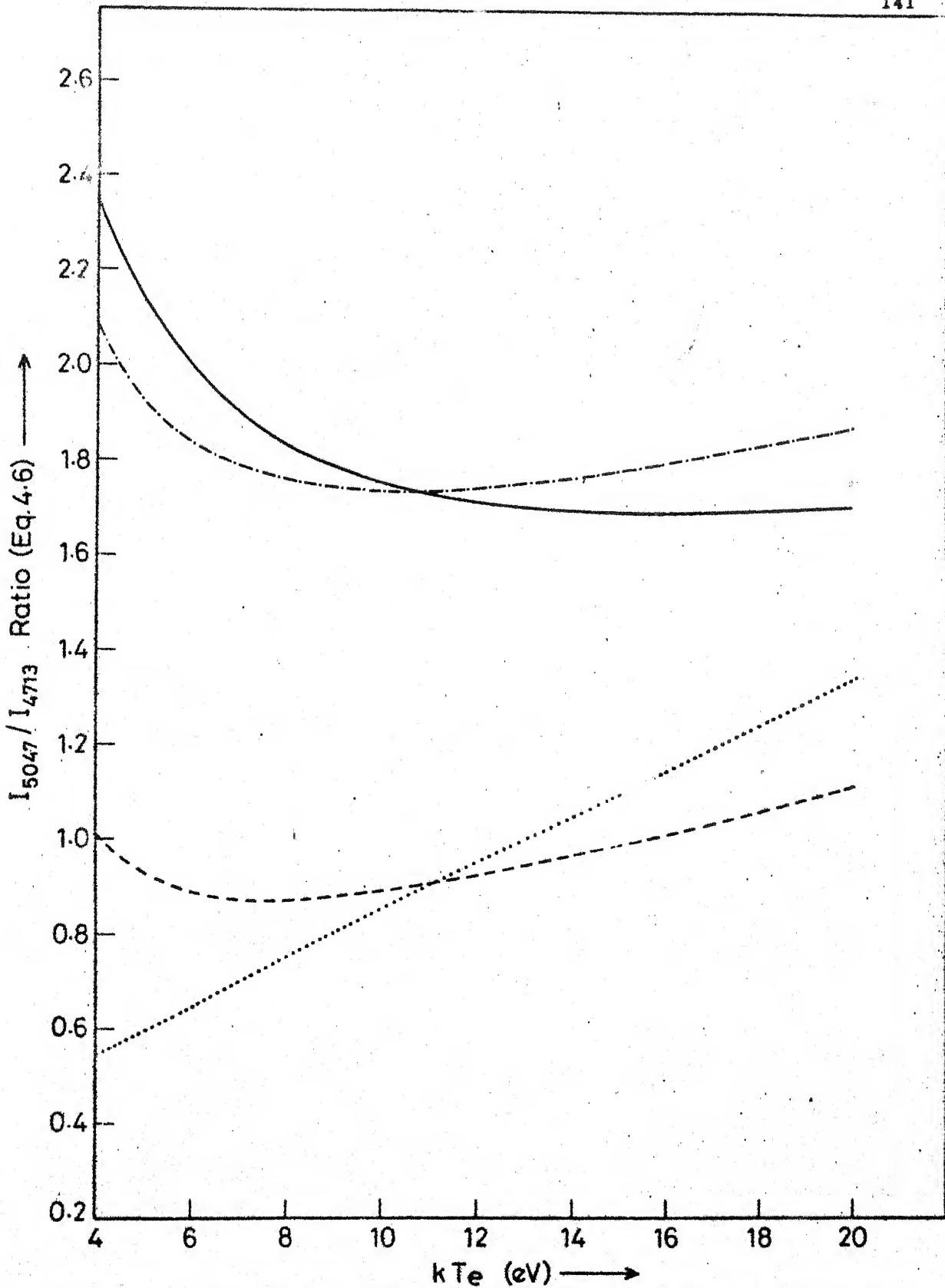
Figure 4.11. Variation of calculated (using Sovie's model[98] and present rate coefficients) I_{5047}/I_{4713} ratio with T_e at $n_e = 10^{12}$ cm^{-3} for optically thin case; ——, experimental cross section[68], metastables included; ————, experimental cross sections[68], metastables excluded; -.-.-, empirical cross section[65], metastables included; ......, empirical cross section[65], metastables excluded.
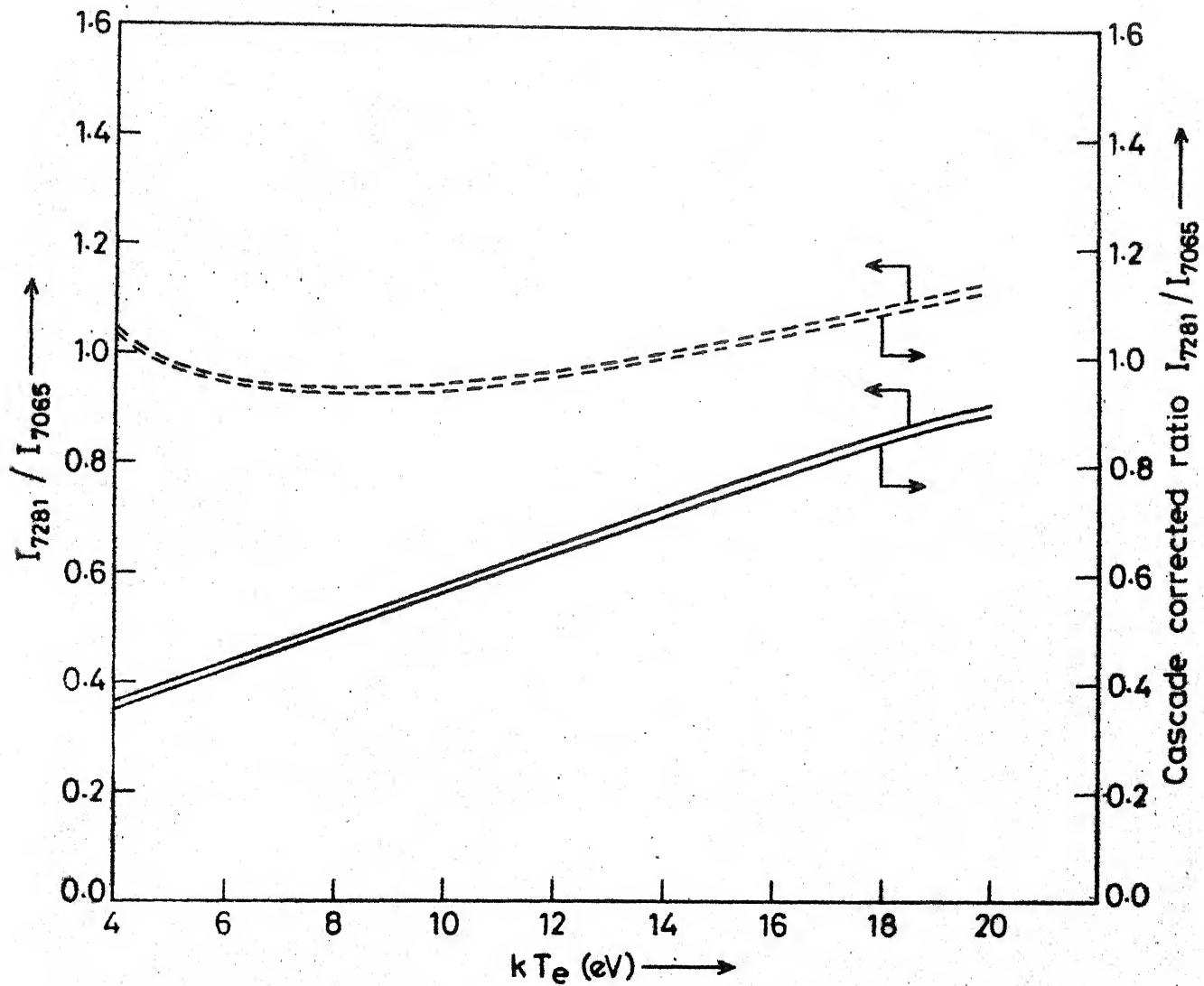
Figure 4.12. Variation of calculated (Sovie's model[98] and present rate coefficients) relative number of 7281Å and 7065Å transitions at $n_e = 10^{12}$ cm^{-3} and for partially optically thick case; -----, metastables included; ———, metastables excluded.

Table 4.9. Comparison of population densities $(n(p)/g_p \text{ cm}^{-3})$ obtained by Sovie's method[98] and present calculations with the experimental results

Experiment Ref. and Plasma Parameters	Levels	Experimental Results	Sovie's Method	Present Calculations
Ref. 34 $kT_e = 7.9$ eV, $n_e = 3.3{+}13$ cm^{-3}, $n(1) = 1.8{+}13$ cm^{-3}	3^3S 3^1S 4^3S 4^1S	2.60+07 – 4.40+06 4.80+06	2.611+08 9.52+08 1.05+08 7.36+08	3.53+07 4.15+07 1.58+07 3.27+07
Ref. 34 $kT_e = 14.4$ eV, $n_e = 5.1{+}12$ cm^{-3}, $n(1) = 4.1{+}11$ cm^{-3}	3^3S 3^1S 4^3S 4^1S	2.30+06 – 7.00+05 9.30+05	2.51+06 1.06+07 1.06+06 8.33+06	1.22+06 1.84+06 5.60+05 1.64+06
Ref. 35 $kT_e = 1.1$ eV, $n_e = 2.4{+}13$ cm^{-3}, $n(1) = 5.75{+}13$ cm^{-3}	3^3S 3^1S 4^3S 4^1S	2.6+05 – 1.35+05 9.80+4	2.90+05 2.34+06 3.90+04 1.14+06	3.34+05 3.17+05 1.63+05 2.15+05

obtained from the present model are also shown in Table 4.9. From this table, it is clear that Sovie's method explains the experimental population densities of only 3^3S level. The population densities of other levels are very far from experimental results.

The collisional-radiative model used in the present work takes into consideration deexcitation by electron impact, electron impact ionization and recombination, radiative decay, excitation transfer between excited states and absorption of radiation by plasma. From this model, taking all these processes into account, we have calculated the line intensity ratio I_{5047}/I_{4713}. The line intensity is taken to be the product of the calculated absolute population density and spontaneous transition probability of the upper level (e.g. $I_{5047} = n(4^1S) \cdot A(4^1S-2^1P)$). The plasma parameters used in these calculations are $kT_e = 1-20$ eV, $n_e = 10^6-10^{16}$ cm^{-3}, $T_g = 300°K$, $n(1) = 10^{12}-10^{16}$ cm^{-3}. Both optically thin and partially optically thick cases were considered. Figure 4.13 presents the calculated line intensity ratios for I_{5047}/I_{4713} against electron temperature. The curves represented by continuous lines correspond to $n(1) = 1.28 \times 10^{14}$ cm^{-3} and a partially optically thick case.

At low electron densities ($\leq 10^9$ cm^{-3}), the intensity ratio is a function of T_e alone but at higher electron density it becomes a function of both T_e and n_e. As the electron density increases the intensity ratio in general decreases. For a particular electron density, the variation of line ratio with electron temperature is irregular. Figure 4.13 also presents line intensity ratio data for optically thin case (shown by dashed lines)
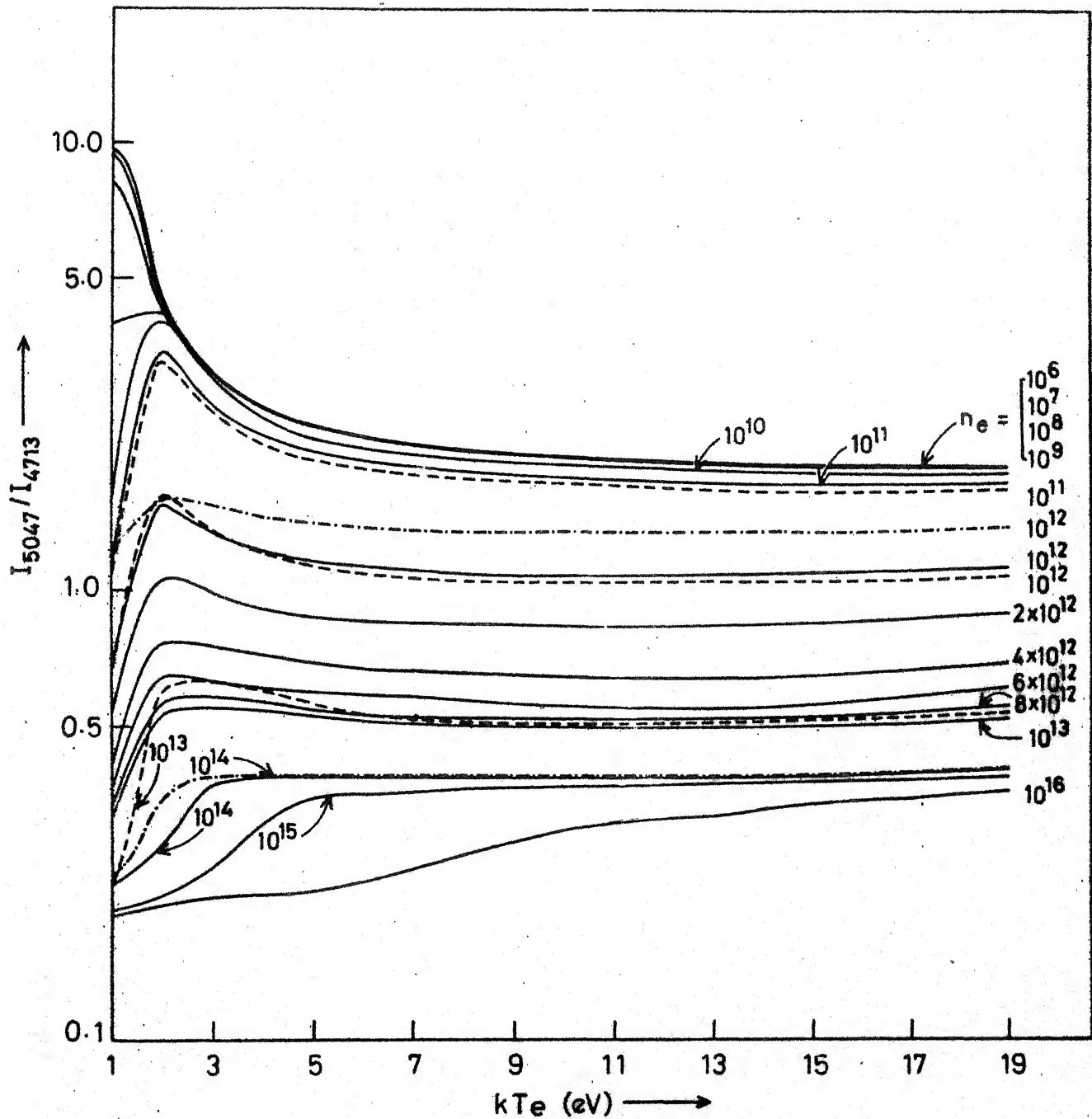
Figure 4.13. Variation of the calculated line intensity ratio I_{5047}/I_{4713} with electron temperature at $n_e = 10^6 - 10^{16}$ cm^{-3}; ———, partially optically thick, $n(1) = 1.28 \times 10^{14}$ cm^{-3}; -----, optically thin, $n(1) = 1.28 \times 10^{14}$ cm^{-3}; -.-.-, partially optically thick, $n(1) = 1.0 \times 10^{16}$ cm^{-3}.

and for high pressure $n(1) = 1.0 \times 10^{16}$ cm^{-3} (shown by dash-dot lines) case at $n_e = 10^{12}$ cm^{-3} and $n_e = 10^{14}$ cm^{-3}. A comparison of these curves with curves mentioned earlier reveals that line intensity ratios, in addition to n_e and T_e, are also functions of gas pressure and extent of absorption of radiation.

Thus, for determination of T_e from the line intensity ratio method, a knowledge of n_e, gas pressure and optical thickness is essential. Moreover, a particular value of line ratio at a particular n_e, may correspond to two or more values of electron temperature. Thus the line ratio method, even with a knowledge of n_e, $n(1)$, and optical thickness may not give correct values of T_e. However, at low electron densities $(n_e < 10^9$ cm$^{-3})$, T_e can be estimated from this method in the kT_e range 2-12 eV.

CHAPTER 5

CONCLUSION

The purpose of the present work was to improve the collisional-radiative model for low temperature non-LTE helium plasmas and gain an insight into the complicated coupled processes which contribute to observed phenomena. This was attempted through a detailed examination of the atomic processes in the model and also comparisons of predicted population densities with experimental observations. It is believed that the effort, within the inherent limitations of collisional-radiative models, has yielded some positive results.

Introduction of experimental cross sections for a number of electron impact processes, used for the first time in collisional-radiative models for helium, is believed to have significantly contributed to the near agreement with the results of several HeI, HeII experiments, viz., those of Johnson[34], Johnson and Hinnov[35], Otsuka et al[38], Hegde and Ghosh[11], involving population densities of 3^1P, 3^1D, 3^3S, 3^3P, 3^3D, 4^1S, 4^1P, 4^1D, 4^3S, 4^3P, 4^3D, 5^1S, 5^1P, 5^1D, 5^3S, 5^3P, 5^3D states. The population coefficients r_0, r_1 were compared with recently available values of Fujimoto[52] and Hess and Burrell[51]. r_1 values are in close agreement; the source of differences in r_0 at low electron densities could be settled if experimental population densities are available at low ground state densities ($< 10^9$ cm^{-3}) or at extremely low electron temperatures. The relative lack of agreement at high electron densities indicate need of lower values of

radiative recombination coefficients and higher values of electron impact excitation rate coefficients. A detailed examination of the direct ionization-excitation process[57] shows that it is dominant in populating HeII levels at $kT_e > 2$ eV and $n_e < 10^{12}$ cm^{-3}. The process is more effective in populating HeII excited states at high gas pressures. From a thorough examination of the line ratio method of determination of electron temperature, we find that in the n_e range 10^9-10^{16} cm^{-3}, kT_e range 1-20 eV the line ratios are not independent of n_e and $n(1)$, and we conclude that the method is not dependable at $n_e \geq 10^9$ cm^{-3}.

From applications of the present collisional-radiative model to recent laser induced selective excitation experiments of Catherinot et al[39], Yasumaru et al[42] and Gauthier et al[90], we find that a good agreement between the experimental enhancements and decay patterns with the calculated ones can be obtained only if the heavy particle collisional rate coefficients from Drawin and Emard[79] are *lower* by about 1-2 orders of magnitude and the optical escape factors given by Drawin and Emard[83] are

higher by about one order of magnitude. The latter conclusion and the fact that optical escape factors from Ref. 83 yield satisfactory population densities in steady state helium plasmas[11,34,35,38] might appear to be conflicting. The latter experiments, however, were at low pressures with optical escape factors in the range 10^{-2}-10^0. The implication here may be that whereas Eq. (2.32) yields satisfactory optical escape factors in the low pressure range, at high pressures, where absolute values of optical escape factors are small, the relative accuracy of

the optical escape factors from Eq. (2.32) is poor and there is need of appropriate corrective factors.

An interesting study in the present work has been the evolution of a systematic procedure[58] to sort out the important rate processes used in a collisional-radiative model. Though the method has been applied to helium plasmas, it is of general applicability. It is shown that by application of this method, it is possible to leave aside as much as 70% of the atomic processes employed in elaborate models and still predict, in the kT_e range of 4-20 eV and n_e range 10^6-10^{12} cm^{-3}, HeI population densities within 20% of the predictions of elaborate model.[56] The method yields statewise population mechanism and also focusses those processes where knowledge of experimental cross sections would be   particularly valuable in enhancing the predictive properties of a collisional-radiative model.

REFERENCES

1. H.W. Drawin, in 'Progress in Plasmas and Gas Electronics', R. Rompe and M. Steenbeck, Eds., Akademie-Verlag-Berlin, 1975.

2. H.W. Drawin, in 'Reactions Under Plasma Conditions', M. Venugopalan, Ed., Vol. 1, Wiley-Interscience, New York, 1971.

3. R.W.P. McWhirter, in 'Plasma Diagnostic Techniques', R.H. Huddlestone and S.L. Leonard, Eds., Academic, New York, 1965.

4. J. Richter, in 'Plasma Diagnostics', W. Lochte-Holtgrevin, Ed., North Holland, 1968.

5. H.W. Drawin, J. Physique $\underline{C7}$ Supplement 149 (1979).

6. D.H. Menzel, Astrophys. J. $\underline{85}$, 330 (1937).

7. D.H. Menzel and J.G. Baker, Astrophys. J. $\underline{86}$, 70 (1937).

8. T. Holstein, Phys. Rev. $\underline{83}$, 1159 (1951).

9. H.W. Drawin and F. Emard, Plasma Physik $\underline{13}$, 143 (1973).

10. M. Otsuka, R. Ikee, and K. Ishii, JQSRT $\underline{21}$, 41 (1979).

11. M.S. Hegde and P.K. Ghosh, Physica C $\underline{97}$, 275 (1979).

12. H.W. Drawin and H. Henning, Z. Naturforsch. $\underline{22a}$, 587 (1967).

13. N. Brenning, J. Phys. D $\underline{13}$, 1459 (1980).

14. B. Dubreuil and A. Catherinot, Phys. Rev. A $\underline{21}$, 188 (1980).

15. G. Baravian, J. Godart, and G. Sultan, Physica C $\underline{94}$, 275 (1978).

16. D.R. Bates, A.E. Kingston, and R.W.P. McWhirter, Proc. Roy. Soc. (Lond.) A $\underline{267}$, 297 (1962).

17. R.W.P. McWhirter and A.G. Hearn, Proc. Phys. Soc. (Lond.) $\underline{82}$, 641 (1963).

18. H.W. Drawin, Z. Naturforsch. $\underline{24a}$, 1492 (1969).

19. H.W. Drawin, JQSRT $\underline{10}$, 33 (1970).

20. L.C. Johnson and E. Hinnov, JQSRT $\underline{13}$, 333 (1973).

21. H.W. Drawin and F. Emard, Z. Physik $\underline{270}$, 59 (1974).

22. H.W. Drawin and F. Emard, Physica C $\underline{85}$, 333 (1977).

23. H.W. Drawin and F. Emard, Physica C $\underline{94}$, 134 (1978).

24. C. Park, JQSRT $\underline{8}$, 1633 (1968).

25. D.C. Cartwright, J. Geophys. Res. $\underline{83}$, 517 (1978).

26. A. Ashraf, U.K. Roychowdhury, and P.K. Ghosh, J. Physique $\underline{C7}$, 129 (1979).

27. R.J. Giannaris and F.P. Incropera, JQSRT $\underline{13}$, 167 (1973).

28. B.F.M. Pots, B. van der Sijde, and D.C. Schram, Physica C $\underline{94}$, 369 (1978).

29. B. van der Sijde, B.F.M. Pots, and D.C. Schram, J. Physique $\underline{C7}$, 23 (1979).

30. H.W. Drawin, F. Emard, and K. Katsonis, Z. Naturforsch. $\underline{28a}$, 1422 (1973).

31. E. Hinnov and J.G. Hirschberg, Proc. 5th ICPIG, Munich, 1961.

32. E. Hinnov and J.G. Hirschberg, Phys. Rev. $\underline{125}$, 795 (1962).

33. R.W. Motley and A.F. Kuckes, Proc. 5th ICPIG, Munich, 1961.

34. L.C. Johnson, Phys. Rev. $\underline{155}$, 64 (1967).

35. L.C. Johnson and E. Hinnov, Phys. Rev. $\underline{187}$, 143 (1969).

36. R. Ikee and H. Takeyama, JQSRT $\underline{15}$, 543 (1975).

37. R. Ikee and H. Takeyama, JQSRT $\underline{15}$, 701 (1975).

38. M. Otsuka, R. Ikee, and K. Ishii, JQSRT $\underline{15}$, 995 (1975).

39. A. Catherinot, B. Dubreuil, A. Bouchoule, and P. Davy, Phys. Lett. $\underline{56A}$, 469 (1976).

40. B. Dubreuil and A. Catherinot, J. Phys. D $\underline{11}$, 1043 (1978).

41. B. Dubreuil and A. Catherinot, Physica C $\underline{93}$, 408 (1978).

42. N. Yasumaru, S. Oku, T. Fujimoto, and K. Fukuda, J. Phys. Soc. Japan $\underline{49}$, 696 (1980).

43. P. Thoma, Z. Naturforsch. $\underline{35a}$, 808 (1980).

44. D.R. Bates and A.E. Kingston, Proc. Roy. Soc. A $\underline{279}$, 32 (1964).

45. D.R. Bates, K.L. Bell, and A.E. Kingston, Proc. Phys. Soc. 91, 288 (1967).

46. H.W. Drawin and F. Emard, Z. Physik 243, 326 (1971).

47. H.W. Drawin, Z. Naturforsch. 19a, 1451 (1964).

48. H.W. Drawin and F. Emard, Report EUR-CEA-FC-697, Fontenay aux-Roses, France (1973).

49. H.W. Drawin and F. Emard, Report EUR-CEA-FC-534, Fontenay aux-Roses, France (1970).

50. M.S. Hegde and P.K. Ghosh, Pramana 12, 367 (1979).

51. R. Hess and F. Burrell, JQSRT 21, 23 (1979).

52. T. Fujimoto, JQSRT 21, 439 (1979).

53. T. Fujimoto, J. Phys. Soc. Japan 47, 265 (1979).

54. A. Catherinot and B. Dubreuil, Phys. Rev. A 23, 763 (1981).

55. F. Dothan and Y.M. Kagan, J. Phys. D 14, 183 (1981).

56. H.C. Srivastava and P.K. Ghosh, JQSRT 25, 59 (1981).

57. H.C. Srivastava and P.K. Ghosh, Physica C 101, 120 (1980).

58. H.C. Srivastava and P.K. Ghosh, Proc. 15th ICPIG, Minsk, (1981).

59. M. Otsuka, private communication.

In earlier stages of this work[56], the weight factors of atomic levels were adopted from Ref. 89 with that for n = 6 taken as 288 instead of 144. These weight factors for HeI levels with principal quantum number n $\geq$ 6 are in error by a factor of 2 as pointed out by Otsuka[59]. With corrected weight factors (Table 2.1) results of calculations, however, are different by only 3% for n < 6 and by 2% for n $\geq$ 6. The error in population density results with weight factors used earlier is thus small. The difference in results is shown in Appendix I.

60. W.B. Westerveld, H.G.M. Heideman, and J. van Eck, J. Phys. B 12, 115 (1979).

61. F.G. Donaldson, M.A. Hender, and J.W. McConkey, J. Phys. B 5, 1192 (1972).

62. T. Scott and M.R.C. McDowell, J. Phys. B 9, 2235 (1976).

63. M.R. Flannery and K.J. McCann, Phys. Rev. A 12, 846 (1975).

64. D. Ton-That, S.T. Manson, and M.R. Flannery, J. Phys. B 10, 621 (1977).

65.   H.W. Drawin, Report EUR-CEA-FC-383, Fontenay aux-Roses, France (1967).

66.   W.L. Wiese, M.W. Smith, and B.M. Glennon, NSRDS-NBS 4 $\underline{1}$, 9 (1966).

67.   J.K. Rice, D.G. Truhlar, D.C. Cartwright, and S. Trajmar, Phys. Rev. A $\underline{5}$, 762 (1972).

68.   A.F.J. van Raan, J.P. De Jongh, J. van Eck, and H.G.M. Heideman, Physica $\underline{53}$, 45 (1971).

69.   A. Pochat, D. Rozuel, and J. Peresse, J. Physique $\underline{34}$, 701 (1973).

70.   R.M. St. John, F.L. Miller, and C.C. Lin, Phys. Rev. $\underline{134}$, A888 (1964).

71.   H.R. Moustafa Moussa, F.J. de Heer, and J. Schutten, Physica $\underline{40}$, 517 (1969).

72.   G.A. Khayarallah, S.T. Chen, and J.R. Rumble, Jr., Phys. Rev. $\underline{17}$, 513 (1978).

73.   J.D. Jobe and R.M. St. John, Phys. Rev. $\underline{164}$, 117 (1967).

74.   H.G.P. Lins de Barros and H.S. Brandi, Can. J. Phys. $\underline{53}$, 2289 (1975).

75.   B.L. Moisewitsch and S.J. Smith, Rev. Mod. Phys. $\underline{40}$, 238 (1968).

76.   M. Gryzinski, Phys. Rev. $\underline{138}$, A336 (1965).

77.   L.D. Weaver and R.H. Hughes, J. Chem. Phys. $\underline{47}$, 346 (1967).

78.   J.F. Sutton and R.B. Kay, Phys. Rev. A $\underline{9}$, 697 (1974).

79.   H.W. Drawin and F. Emard, Z. Physik $\underline{254}$, 202 (1972).

80.   L.C. Green, P.P. Rush, and C.D. Chandler, Astrophys. J. Suppl. Series $\underline{3}$, 37 (1957).

81.   H.A. Kramers, Phil. Mag. $\underline{46}$, 836 (1923).

82.   M.J. Seaton, Mon. Not. Roy. Astron. Soc. $\underline{119}$, 81 (1959).

83.   H.W. Drawin and F. Emard, Plasma Physik $\underline{13}$, 143 (1973).

84.   M. Abramowitz and I.A. Stegun, Hand Book of Mathematical Functions, Dover, New York, 1965.

85.   A. Yariv, Quantum Electronics, Wiley, New York, 1967.

86. A. Ralston and H.S. Wilf, <u>Mathematical Methods for Digital Computers</u>, Wiley, New York, 1960.

87. A. Ralston, <u>Runge-Kutta Methods with Minimum Error Bounds</u>, MTAC <u>16</u>, 431 (1962).

88. M.S. Hegde and P.K. Ghosh, JQSRT <u>17</u>, 635 (1977).

89. C. Park, JQSRT <u>11</u>, 7 (1971).

90. J.C. Gauthier, F. Devos, and J.F. Delpech, Phys. Rev. A <u>14</u>, 2162 (1976).

91. T. Fujimoto, private communication.

92. J.S. Cohen, Phys. Rev. A <u>13</u>, 99 (1976).

93. H.F. Wellenstein and W.W. Robertson, J. Chem. Phys. <u>56</u>, 1077 (1972).

94. L.G. Dugan, H.L. Richards, and E.E. Muschlitz, J. Chem. Phys. <u>46</u>, 346 (1967).

95. F.T. Chan and C.H. Chang, Phys. Rev. A <u>12</u>, 1383 (1975).

96. S.P. Cunningham, USAEC Report WASH-289, (1955).

97. H.W. Drawin and H. Henning, Z. Naturforsch. <u>22a</u>, 587 (1967).

98. R.J. Sovie, JQSRT <u>8</u>, 833 (1968).

99. D. Schieber, S. Gavril, and M.S. Erlicki, Plasma Phys. <u>12</u>, 897 (1970).

100. B.J. Eastlund, D. Spero, M. Johnson, P. Korn, C.B. Wharton, and E.R. Wilson, J. Appl. Phys. <u>44</u>, 4930 (1973).

101. N. Brenning, JQSRT <u>24</u>, 293 (1980).

APPENDIX I

POPULATION DENSITIES WITH CORRECTED WEIGHT FACTORS

Population densities (cm^{-3}) of HeI levels with the weight factors used in Ref. 56 ($g_n = 4n^2$ for $n < 6$, $g_n = 8n^2$ for $n \geq 6$) and with the corrected weight factors (Table 2.1, $g_n = 4n^2$) are presented in the Table I.1. Plasma parameters are $kT_e = 10$ eV, $n_e = 10^{12}$ cm^{-3}, $n(1) = 2.0 \times 10^{14}$ cm^{-3}, $T_g = 300°K$ and optically thin case.

Table I.1.   Population densities with weight factors used in
Ref. 56 and with corrected weight factors

Levels	Population densities with weight factors used in Ref. 56	Population densities with corrected weight factors	Percent change in population densities
2^3S	1.472+11	1.472+11	0
2^1P	6.754+07	6.754+07	0
3^3P	6.901+08	6.905+08	0.06
3^1D	1.243+08	1.243+08	0
3^1P	5.389+07	5.390+07	0.02
4^3S	1.770+08	1.770+08	0
4^1D	3.471+07	3.467+07	-0.1
4^1P	3.067+07	3.068+07	0.03
5^3S	4.088+07	4.110+07	0.5
5^1S	2.591+07	2.598+07	0.3
5^3P	3.146+07	3.235+07	2.8
5^3D	4.245+07	4.366+07	2.9
5^1D	1.548+07	1.590+07	2.7
5^1P	2.186+07	2.194+07	0.4
n=6	4.410+07	4.331+07	-1.8
7	2.577+07	2.554+07	-0.9
8	1.851+07	1.839+07	-0.6
9	1.587+07	1.579+07	-0.5
10	1.552+07	1.545+07	-0.5
11	1.698+07	1.691+07	-0.4
12	1.933+07	1.924+07	-0.5

APPENDIX   II

ABSOLUTE POPULATION DENSITIES FOR FIGURES 4.6-4.9

In Figures 4.6-4.9, the normalized relative population densities were presented. In the following tables, we present absolute population densities corresponding to the data given in these figures. In these tables, for a particular curve and for a particular level, the absolute population densities have been listed for the initial time (t = 0, first value in each box), for peak (second value in each box, time in nsec mentioned in parenthesis), and for t = 40 (75 in case of Figure 4.9) nsec, third value in each box).

Table   II.1.   Absolute population densities (cm^{-3}) at t = 0, peak, and t = 40 nsec corresponding to data presented in Figure 4.6

Curve	Time (nsec)	Absolute population densities (cm^{-3})			
		Level 3^1P	3^1D	3^3D	3^3P
dashed line	0 peak 40	2.8+10* 4.1+12(4.4) 6.9+11	3.3+10 6.1+11(17.2) 3.7+11	1.4+10 1.9+11(18.6) 1.3+11	3.4+10 2.0+11(35.2) 2.0+11
dotted line	0 peak 40	6.0+09 1.2+12(3.2) 4.9+10	1.6+10 1.5+12(4.4) 1.2+11	3.7+10 2.9+12(5.6) 3.5+11	3.1+10 1.1+11(23.6) 1.0+11
dash-dotted line	0 peak 40	8.7+08 4.1+11(4.2) 9.1+08	3.0+09 2.8+10(7.8) 3.3+09	4.1+09 1.2+10(7.8) 5.1+09	1.6+10 2.1+10(9.0) 1.9+10

* The absolute population densities of level 3^1P at time t = 0, at peak (which occurs at 4.4 nsec), and at t = 40 nsec respectively are 2.8 x 10^{10}, 4.1 x 10^{12}, and 6.9 x 10^{11} cm^{-3}.

Table II.2. Absolute population densities (cm^{-3}) at $t = 0$, peak, and $t = 40$ nsec corresponding to data presented in Figure 4.7

Curve	Time (nsec)	Absolute population densities (cm^{-3})			
		Level 4^1D	4^3D	3^1P	4^1P
dashed line	0	3.9+09	6.4+09	2.8+10	1.1+10
	peak	1.0+12(13.4)	2.5+11(25.7)	8.8+10(26.7)	2.0+10(38.6)
	40	1.5+11	1.9+11	7.7+10	2.0+10
dotted line	0	3.2+09	9.5+09	6.0+09	2.0+09
	peak	2.6+11(13.4)	7.7+11(14.0)	7.8+09(26.6)	1.1+11(17.0)
	40	7.8+10	2.4+11	7.5+09	4.3+10

Table II.3. Absolute population densities at $t = 0$, peak, and $t = 40$ nsec corresponding to data presented in Figure 4.8

Gas pressure	Curve	Time (nsec)	Absolute population density (cm^{-3})	
			Level 3^1P	3^1D
0.4 torr	dashed line	0	2.7+09	1.1+09
		peak	1.2+13 (6.5)	2.5+11 (29.3)
		40	6.4+12	2.4+11
	dotted line	0	3.0+08	8.9+08
		peak	3.8+12 (3.7)	4.3+12 (6.4)
		40	1.5+11	4.0+11
5 torr	dashed line	0	7.8+09	1.4+10
		peak	7.8+12 (5.6)	1.5+12 (16.0)
		40	7.9+11	7.1+11
	dash-dotted line	0	1.4+10	1.7+10
		peak	8.9+12 (5.6)	3.2+12 (15.0)
		40	1.6+12	1.6+12

Table II.4. Absolute population densities at t = 0, peak, and
t = 75 nsec corresponding to data presented in
Figure 4.9

Curve	Time (nsec)	Absolute population density (cm^{-3})		
		Level 3^3S	3^3P	3^3D
dashed line	0	5.1+02	1.2+03	2.4+02
	peak	4.1+05 (51.5)	8.2+06 (7.0)	1.3+04 (43.0)
	75	3.84+05	3.5+06	1.1+04
dash-dotted line	0	1.7+05	1.3+05	1.1+05
	peak	8.6+07 (51.5)	1.7+09 (7.1)	2.9+06 (43.1)
	75	7.8+07	6.9+08	2.4+06

APPENDIX III

SNOBOL PROGRAMME

This programme, written in SNOBOL, prints the inverse of a square matrix in algebraic mode. In the programme, N is the number of rows of the matrix. The dimension of arrays A and C should be made (N, 2N) and (N, 2N, 8) respectively. The output obtained contains the elements of inverse matrix in algebraic form in various levels of indexing. The programme itself takes care of index referencing and defines the variables used.

```
00020
00030
00040
00050
00060                Y     = 'A'
00070                BLANK =
00080                Z     = 0
00090                N     = 4
00100                M     = N * 2
00110         A     = ARRAY('4,8')
00120         C     = ARRAY('4,8,8')
00130                I     = 0
00140   THETA        I = I + 1
00150                LE(I, N)  :F(RO)
00160                J = 0
00170   ZETA         J = J + 1
00180                LE(J, N)  :F(THETA)
00190                A[I,J] = 'A' '(' I ',' J ')'  :(ZETA)
00200   RO           I = 0
00210   GAMMA        I = I + 1
00220                LE(I, N)  :F(DELTA)
00230                J = N
00240   ALPHA        J = J + 1
00250                LE(J, M)  :F(GAMMA)
00260                K = J - N
00270                EQ(I, K)  :S(BETA)
00280                A[I,J] = '0'  :(ALPHA)
00290   BETA         A[I,J] = '1'  :(ALPHA)
00300   DELTA        K = 0
00310   AA           K = K + 1
00320                LE(SIZE(A[1,(N + 1)]), 60)  :S(AZ)
00330   FR           Z = Z + 1
00340                P = 0
00350   CE           P = P + 1
00360                GT(P, N)   :S(AZ)
00370                Q = 0
00380   CF           Q = Q + 1
00390                GT(Q, M)   :S(CE)
00400                C[P,Q,Z] = A[P,Q]
00410                A[P,Q] = 'C' '(' P ',' Q ',' Z ')'  :(CF)
00420   AZ           IDENT(FULL, 'TRUE')  :S(XA)
00430                LE(K, N)  :F(AF)
00440                J = K - 1
00450
00460   AB           J = J + 1
00470                LE(J, M)  :F(AD)
00480                NE(J, K)  :F(AB)
00490                IDENT(A[K,J], '0')  :S(AE)
00500                A[K,J] = '(' A[K,J] '/' A[K,K] ')'  :(AB)
00510   AE           A[K,J] = '0'   :(AB)
00520   AD           A[K,K] = '1'
00530                I = 0
00540   AJ           I = I + 1
00550                LE(I, N)  :F(AA)
00560                NE(I, K)  :F(AJ)
00570                J = K - 1
00580   AH           J = J + 1
00590                LE(J, M)  :F(AG)
00600                NE(J, K)  :F(AH)
00610                IDENT(A[K,J], '0')  :S(AH)
00620                IDENT(A[I,K], '0')  :S(AH)
00630                IDENT(A[I,J], '0')  :F(AI)
00640                A[I,J] = '(' '-' A[I,K] '*' A[K,J] ')'  :(AH)
00650   AI           A[I,J] = '(' A[I,J] '-' A[I,K] '*' A[K,J] ')'  :(AH)
00660   AG           A[I,K] = '0'  :(AJ)
00670   AF           FULL = 'TRUE'  :(FR)
00680   XA           OUTPUT =
00690                OUTPUT = '    C'
00700                OUTPUT = '    C THE VALUES OF VARIABLES USED FOR I.R. ARE:'
00710                OUTPUT = '    C'
00720                S = 0
00730   FQ           S = S + 1
00740                P = 0
00750   OZ           P = P + 1
00760                Q = 0
00770   PZ           Q = Q + 1
00780                IDENT(C[P,Q,S], BLANK)  :S(LM)
00790                IDENT(C[P,Q,S], '1')  :S(LM)
00800                IDENT(C[P,Q,S], '0')  :S(LM)
00810                OUTPUT = '      ' 'C(' P ',' Q ',' S ')' '=' C[P,Q,S]
00820   LM           EQ(Q, M)  :F(PZ)
00830                EQ(P, N)  :F(OZ)
00840                EQ(S, Z)  :F(FQ)
00850                OUTPUT = '    C'
00860                OUTPUT = '    C VALUES OF VARIABLES'
00870                OUTPUT = '    C'
00880                I = 0
00890   AK           I = I + 1
```

```
00900              LE(I, N)  :F(RD)
00910              I = N
00920              INTER =
00930     AM       I = I + 1
00940              LE(J, N)  :F(AL)
00950              IDENT(INTER, BLANK)  :S(DOWN)
00960              INTER = INTER '+' A[I,J] '*' 'B' (J - N)   :(AM)
00970     DOWN     INTER = A[I,J] '*' 'B' (J - N) :(AM)
00980     AL       OUTPUT = '' 'X' I '=' INTER :(AK)
00990     RD       OUTPUT =
01000     END
```

APPENDIX   IV

PROGRAMME TO CALCULATE POPULATION DENSITIES

This programme, written in FORTRAN, calculates the
population densities of HeI and HeII levels for both optically
thin and partially optically thick conditions. The input
parameters (besides those defined in the programme) are as
follows:

WL   Wavelengths of HeI (1^1S-n^1P, n = 2-6) and HeII
            (1^2S-n^2P, n = 2-6) transitions.

OS   Absorption oscillator strengths for the above
            transitions

EAE, EBE,   Discrete electron energies (eV) at which the cross
ECE, EDE,   section data for various transitions are given
EEE, EFE

CS1   Cross section data at electron energies EAE for
            transitions 1^1S-4^1P, 1^1S-5^1P, 1^1S-5^1S, 1^1S-4^1S

CS2   Cross section data at electron energies EBE for
            transitions 2^1S-3^1S, 2^1S-3^1P, 2^1S-3^1D, 2^3S-4^3S

CS3   Cross section data at electron energies ECE for
            transitions 2^3S-3^3P,-3^3D,-4^3S,-4^3P,-4^3D,-4^3F,-5^3S,
            -5^3P,-5^3D,-5^3F,-2^3P

CS4   Cross section data at electron energies EDE for
            transitions 1^1S-2^3P,-2^3S

CS5   Cross section data at electron energies EEE for
            transition 1^1S-2^1S

CS6   Cross section data at electron energies EFE for
            transitions 1^1S-3^1D,-4^1D

CS7   Cross section data at electron energies EGE for
            transitions 1^1S-2^1P,-3^1P

AF   Constant $\alpha_{p,q}$ (Eq. 2.17) for transitions 1^1S-n^1P
(n = 2-5),   -n (n = 6-12)

FA   Absorption oscillator strengths for the above transitions

EA   Excitation energies (eV) of the above transitions

AP   Roots of Laguerre polynomial

H   Weight factors of Laguerre polynomial

BF   Constant $\alpha_{p,q}$ for transitions 2^1S-n^1P (n = 3-5),
2^1S-n (n = 6-12)

EB   Excitation energies (eV) of the above transitions

FB   Oscillator strengths for the above transitions

E   Energies (cm^{-1}) of HeI levels

G   Weight factors of HeI levels

AAF   Oscillator strengths for transitions 4^1S-5^1P,-6^1P;
4^1P-5^1S,-6^1S,-6^1D; 4^1D-5^1F,-5^1P,-6^1F; 4^3F-5^1D,-6^3D;
4^3S-5^3P,-6^3P; 4^3P-5^3S,-5^3D,-6^3D; 4^3D-5^3P,-5^3F,-6^3F;
4^3F-5^3D,-6^3D

AAE   Excitation energies (eV) for the above transitions

CF   Oscillator strengths for transitions 2^1P-n^1S (n =
3-5), 2^1S-n (n = 6-12)

CE   Excitation energies of the above transitions

DF   Absorption oscillator strength for transitions
2^1P-n^1D (n = 3-5), 2^1P-n (n = 6-12)

DE   Excitation energies (eV) for the above transitions

EF   Oscillator strengths for transitions 3^1S-n^1P(n = 3-5),
3^1S-n (n = 6-12)

EE   Excitation energies (eV) for the above transitions

FE   Oscillator strengths for transitions 3^1P-n^1S (n = 4,5),
3^1P-n (n = 6-12)

FE   Excitation energies (eV) for the above transitions

GF   Oscillator strengths for transitions 3^1D-n^1P (n = 3-5),
3^1D-n (n = 6-12)

GE   Excitation energies (eV) for the above transitions

HF   Oscillator strengths for transitions 3^1D-4^1F,-5^1F,-n
(n = 6-12)

HE	Excitation energies (eV) for the above transitions
OF	Oscillator strengths for transitions $3^1P-4^1D,-5^1D,-n$ (n = 6-12)
OE	Excitation energies (eV) for the above transitions
PF	Oscillator strengths for transitions 2^3S-n^3P (n = 2-5), 2^3S-n (n = 6-12)
PE	Excitation energies (eV) for the above transitions
QF	Oscillator strengths for transitions 2^3P-n^3D (n = 3-5), $-n$ (n = 6-12)
QE	Excitation energies (eV) for the above transitions
RF	Oscillator strengths for transitions 2^3P-n^3S (n = 3-5), 2^3P-n (n = 6-12)
RE	Excitation energies for the above transitions
SF	Oscillator strengths for transitions 3^3S-n^3P (n = 3-5), 3^3S-n (n = 6-12)
SE	Excitation energies for the above transitions
UF	Oscillator strengths for the transitions $3^3P-4^3S,$ $-5^3S,-n$ (n = 6-12)
UE	Excitation energies for the above transitions
VF	Oscillator strengths for transitions $3^3P-4^3D,-5^3D,-n$ (n = 6-12)
VE	Excitation energies for the above transitions
WF	Oscillator strengths for transitions $3^3D-4^3P,-5^3P,-n$ (n = 6-12)
WE	Excitation energies for the above transitions
XF	Oscillator strengths for the transitions $3^3D-4^3F,$ $-5^3F,-n$ (n = 6-12)
XE	Excitation energies for the above transitions
QEE	Values of $4Q_{p,q}$ in Eq. (2.19) for transitions $1^1S-2^1S,$ $-3^1S,-3^1D,-4^1S,-4^1D,-5^1S,-5^1D,-6^1D$
SEE	Excitation energies of above transitions
TEE	Excitation energies for transitions $1^1S-2^3S,-2^3P,-3^3S,$ $-3^3P,-3^3D,-4^3S,-4^3P,-4^3D,-5^3S,-5^3P,-5^3D$
QTE	Values of $4Q_{p,q}$ for the above transitions
CRE	Excitation energies for transitions $2^3S-2^1S,-3^1S,-4^1S;$ $3^3S-3^1S, -4^1S,-5^1S; 4^3S-4^1S,-5^1S; 2^3P-2^1P,-3^1P,-4^1P;$ 3^3P-3^1P

CRQ	Values of $4Q_{p,q}$ for the above transitions
SFE	Electron energies
SFF	Cross section data at electron energies SFE for transitions $1^1S-4^1F,-5^1F$
ES	Electron energies
QQQ	Cross section data at electron energies ES for transitions $2^3S-3^1S,-4^1S,-5^1S,-2^1P,-3^1P,-4^1P,-5^1P,$ $-3^1\Gamma,-4^1D,-5^1D,-4^1F,-5^1F$
APQ	Spontaneous transition probabilities for HeI transitions
ETT	Electron energies
QQ	Cross section data at electron energies ETT for transitions from level 2^3S

```fortran
C
C..................................................................
C     This PROGRAM calculates the population densities of HeI
C     and HeII levels for both optically thin and partially
C     optically thick conditions. Important terms involved
C     are as tellows :
C     TTP = Electron temperature in ev
C     NC = Electron density
C     DPOP = Population densities of HeI and HeII levels
C     E = Energy of levels in inverse centimeters
C     G = Weight factors
C     NG = HeI ground state population density
C     TG = Gas temperature in ev
C     OEF = Optical escape factors
C     DEGREE = n+(1)/n++
C     KPO = Electron impact excitation and deexcitation rate coeffs.
C     KNPO = Neutral-neutral excitation rate coeffs.
C     KNPC, KNCP  = Neutral neutral ionization and recomb. rate coeffs.
C     APO = Spontaneous transition probabilities
C     BETA = Radiative recombination rate coeffs
C     FPO = Oscillator strengths
C..................................................................
C
C     Variables with integer names are declared real .
      REAL NC,KNPC,KNCP,KNPO,KNSUM,NG
      REAL KPC,KPO,KPOSUM,NP,NO,KSPO,KKPO,TP,KP,NPX
C
C...... Dimensions declared for subscripted variables
      DIMENSION TTE(1),OEF(10),WL(10),OS(10)
      DIMENSION AF(11),FA(11),EA(11),AP(11),H(11),HF(11),EB(11),FB(11),
     1EE(10),FF(10),FE(10),GF(10),GE(10),HF(10),HE(10),OF(10),OE(10),
     2E(47),G(47),AAF(20),AAE(20),CF(10),CE(10),DF(10),DE(10),
     3PF(11),PE(11),QF(10),QE(10),RF(10),RE(10),SF(10),SE(10),UF(10),
     4 UE(10),VF(10),VE(10),WF(10),WE(10),XF(10),XE(10),OEF(10),SEF(10),
     5TEE(11),OTE(11),CRE(12),CRO(12),SFF(12),ES(14),OOO(12,14),FK(12),
     6ET(32),KKPO(17),OO(17,12),ETT(12)
      DIMENSION EF(12),SFF(12,14)
      DIMENSION FFP(32,32),KNPC(32),KNCP(32),KNPO(32,32)   ,KNSUM(32)
      DIMENSION HEI(15),HGI(15),HAPO(15,15),HKPO(15,15),HKPC(15)
     1,HNP(15),HNQ(15),HKPSUM(15),HAPSUM(15),HEXI(47,47),HEXSUM(47)
      DIMENSION SPK(2),KSPO(12),SKK(8),TEK(15),PK(12),QK(12),RK(12) ,
     1AK(11),BK(11),SK(10),UK(10),VK(10),WK(10),XK(10),CK(12),DK(12),
     2EK(12),GK(12),HK(12),OK(12),A(32),AAK(30),
     3APO(47,47),KPO(47,47),FPO(32,32),CRK(15),AAPO(47,47),
     4 AO(47,47),BO(47,4),ANEW(45,45),BNEW(45,4),BN(45),
     5 APOSUM(47),KPOSUM(47),NP(47),NQ(47),NERM(45),F(45),FS(45,4)
      DIMENSION BETA(47),V(32),GG(32),KPC(47)
      DIMENSION ONE(15,15),Y(15),D(24),HCK(27)
      DIMENSION NPX(47),APOP(45),BPOP(45),DPOP(45),CPOP(45)
      DIMENSION EAE(22),E4E(22),ECE(24),EDE(13),EEE(13),EFE(15),EGE(22)
      DIMENSION CS1(13,4),CS2(22,4),CS3(24,12),CS4(13,2),CS5(13,1)
      DIMENSION CS6(15,2),CS7(22,2)
      DIMENSION TUM1(12),TUM2(12),TUM3(12),TUM4(12),TUM5(12),TUM(12)
C
C...... Data for electron temperatures given. Number of these data
C       should be equal to the dimension of TTE and final value of
C       variable NTMP
      DATA TTE/10.0/
C
C...... Data for NHE(Total number of levels),NG,DEGREE.EI(Ionization
C       energy of HeI are given
      NHE=47
      NHS=NHE-2
      NG=2.00E+14
      DEGREE=1000.0
      N=32
      NST=N
      NS=N-1
      EI=198311.0
C
C...... Initialization of subscripted variables
      DO 4000 I=1,NHE
      KPC(I)=0.0
      NP(I)=0.0
      NO(I)=0.0
      APOSUM(I)=0.0
      HEXSUM(I)=0.0
      KPOSUM(I)=0.0
      DO 4000  J=1,NHE
      APO(I,J)=0.0
      KPO(I,J)=0.0
      HEXI(I,J)=0.0
      AO(I,J)=0.0
4000  CONTINUE
C
C...... Other data (see Appendix IV)are read from a data file and normalized
      READ 821,(WL(I),I=1,10)
      READ 821,(OS(I),I=1,10)
821   FORMAT(10F8.4)
```

```
          READ 561,(AAE(I),I=1,13)
          READ 561,(SHE(I),I=1,22)
          READ 561,(WCE(I),I=1,24)
          READ 561,(PDE(I),I=1,13)
          READ 561,(HED(I),I=1,13)
          READ 561,(PPE(I),I=1,15)
          READ 562,(PGE(I),I=1,22)
  561     FORMAT(15F5.1)
  562     FORMAT(13F6.1)
          READ 564,((CS1(I,J),I=1,13),J=1,4)
          READ 564,((CS2(I,J),I=1,22),J=1,4)
          READ 564,((CS3(I,J),I=1,24),I=1,12)
          READ 564,((CS4(I,J),I=1,13),J=1,2)
          READ 564,((CS5(I,J),I=1,13),I=1,1)
          READ 564,((CS6(I,J),I=1,15),J=1,2)
          READ 936,((CS7(I,J),I=1,22),J=1,2)
  564     FORMAT(13F6.3)
  936     FORMAT(11F7.3)
          READ 61,(AF(I),I=1,11)
          READ 62,(FA(I),I=1,11)
          READ 63,(EA(I),I=1,11)
          READ 67,(AP(I),I=1,11)
          READ 67,(H(I),I=1,11)
          READ 61,(RF(I),I=1,11)
          READ 63,(FB(I),I=1,11)
          READ 63,(FB(I),I=1,11)
  61      FORMAT(11F4.1)
  62      FORMAT(11F7.5)
  63      FORMAT(11F7.4)
  67      FORMAT(6F12.5)
          READ 40,(E(I),I=1,N)
          READ 50,(G(I),I=1,N)
  40      FORMAT(10F8.1)
  50      FORMAT(10F6.1)
          READ 81,(AAF(I),I=1,20)
          READ 81,(AAE(I),I=1,20)
          READ 81,(CF(I),I=1,10)
          READ 81,(CE(I),I=1,10)
  81      FORMAT(10F7.4)
          READ 81,(DF(I),I=1,10)
          READ 81,(DE(I),I=1,10)
          READ 81,(EF(I),I=1,10)
          READ 81,(EE(I),I=1,10)
          READ 101,(FF(I),I=1,9)
          READ 101,(FE(I),I=1,9)
          READ 81,(GF(I),I=1,10)
          READ 81,(GE(I),I=1,10)
          READ 101,(HF(I),I=1,9)
          READ 101,(HE(I),I=1,9)
          READ 101,(OF(I),I=1,9)
          READ 101,(OE(I),I=1,9)
          READ 11,(PF(I),I=1,11)
          READ 11,(PE(I),I=1,11)
          READ 81,(QF(I),I=1,10)
          READ 81,(QE(I),I=1,10)
          READ 81,(RF(I),I=1,10)
          READ 81,(RE(I),I=1,10)
          READ 81,(SF(I),I=1,10)
          READ 81,(SE(I),I=1,10)
          READ 101,(UF(I),I=1,9)
          READ 101,(UE(I),I=1,9)
          READ 101,(VF(I),I=1,9)
          READ 101,(VE(I),I=1,9)
          READ 101,(WF(I),I=1,9)
          READ 101,(WE(I),I=1,9)
          READ 101,(XF(I),I=1,9)
          READ 101,(XE(I),I=1,9)
          READ 301,(OEE(I),I=1,8)
          READ 300,(SEE(I),I=1,8)
  101     FORMAT(9F7.4)
  301     FORMAT(8F7.3)
  300     FORMAT(8F7.4)
          READ 309,(TEE(I),I=1,11)
          READ 315,(OTE(I),I=1,11)
  309     FORMAT(11F7.4)
  315     FORMAT(11F7.2)
          READ 81,(CRE(I),I=1,12)
          READ 400,(CRO(I),I=1,12)
  400     FORMAT(10E8.1)
          READ 31,(SFE(I),I=1,12)
  31      FORMAT(12F5.1)
          DO 41    J=1,2
          READ 42,(SFF(I,J),I=1,12)
  42      FORMAT(12F4.1)
          DO 41    I=1,12
  41      SFF(I,J)=SFF(I,J)*1.0E-06
          READ 47,(ES(I),I=1,14)
  47      FORMAT(14F5.1)
          DO 48    I=1,12
```

```
  48       READ  49,((QG(I,J),I=1,14)
  49       FORMAT(11F5.2)
           DO 18 J=1,?
           READ 19,(APQ(I,J),I=1,T)
  19       FORMAT(10F8.5)
  18       CONTINUE
  11       FORMAT(11F7.1)
           DO 822 I=1,13
           QG(I)=QG(I)*1.0E-08
  822      QS(I)=QS(I)*1.0E-02
           DO 565 J=1,2
           DO 565 I=1,13
  565      CS1(I,J)=CS1(I,J)*1.0E-02
           DO 566 J=3,4
           DO 566 I=1,13
  566      CS1(I,J)=CS1(I,J)*1.0E-04
           DO 567 J=3,5
           DO 567 I=1,24
  567      CS3(I,J)=CS3(I,J)*1.0E-01
           DO 568 J=5,10
           DO 568 I=1,24
  568      CS3(I,J)=CS3(I,J)*1.0E-02
           DO 569 I=1,24
  569      CS3(I,11)=CS3(I,11)*1.0E-03
           DO 570 I=1,24
  570      CS3(I,12)=CS3(I,12)*1.0E-01
           DO 571 J=1,2
           DO 571 I=1,13
  571      CS4(I,J)=CS4(I,J)*1.0E-02
           DO 572 I=1,13
  572      CS5(I,1)=CS5(I,1)*1.0E-02
           DO 22 I=1,N
           DO 22  J=1,I
  22       APQ(I,J)=APQ(I,J)*1.0E+08
           DO 5633 I=1,32
  5633     AAPQ(I,1)=APQ(I,1)
  21       FORMAT(1X,10F13.5)
           READ 24,(ETT(I),I=1,12)
  24       FORMAT(12F5.1)
           DO 26  I=1,17
  26       READ 25,(QQ(I,J),J=1,12)
  25       FORMAT(12F5.2)
           DO 555 I=1,8
  555      QEE(I)=QEE(I)*1.0E-04
           DO 556 I=1,11
  556      QTE(I)=QTE(I)*1.0E-04
           DO 51 J=1,14
           QQQ(1,J)=QQQ(1,J)*1.0E-01
           QQQ(2,J)=QQQ(2,J)*1.0E-02
           QQQ(3,J)=QQQ(3,J)*1.0E-03
           QQQ(5,J)=QQQ(5,J)*1.0E-01
           QQQ(6,J)=QQQ(6,J)*1.0E-02
           QQQ(7,J)=QQQ(7,J)*1.0E-02
           QQQ(8,J)=QQQ(8,J)*1.0E-01
           QQQ(9,J)=QQQ(9,J)*1.0E-02
           QQQ(10,J)=QQQ(10,J)*1.0E-02
           QQQ(11,J)=QQQ(11,J)*1.0E-02
           QQQ(12,J)=QQQ(12,J)*1.0E-03
  51       CONTINUE
           DO 28 I=1,3
           DO 28 J=1,12
  28       QQ(I,J)=QQ(I,J)*1.0E-01
           DO 29 J=1,12
           QQ(4,J)=QQ(4,J)*1.0E-02
  29       QQ(5,J)=QQ(5,J)*1.0E-02
           DO 32 I=6,9
           DO 32 J=1,12
  32       QQ(I,J)=QQ(I,J)*1.0E-01
           DO 34 J=1,12
  34       QQ(10,J)=QQ(10,J)*1.0E-03
           DO 33 I=12,17
           DO 33 J=1,12
  33       QQ(I,J)=QQ(I,J)*1.0E-01
C
C...... Electron temperature loop starts . The final value of NTMP
C       should be equal to number of TTE data
           DO 5000 NTMP=1,1
           TE=TTE(NTMP)
           TEMP=11600.0*TE
           TGAS=1000.0
           TG=TGAS/11600.0
           PRINT 12,TE,TG
  12       FORMAT(10X,'ELECTRON TEMP=',E12.3,10X,'GAS TEMP=',E12.3/)
C
C...... In the following section electron impact excitation rate coeffs.
C       are calculated by using Simpson's rule for those transitions for
C       which cross sections are available at discrete electron energies
C       and are stored in array HCK
           DO 579 II=1,4
```

```
              DO 573 I=1,9
573           D(I)=CS1(I,I1)*EAE(I)*EXP(-EAE(I)/TE)
              J=1
              SUMP=D(J)
574           J=J+2
              SUMP=SUMP+2.0*D(J)
              IF(J.LT.7) GO TO 574
              J=2
              SUMQ=D(J)*4.0
575           J=J+2
              SUMQ=SUMQ+4.0*D(J)
              IF(J.LT.8) GO TO 575
              J=9
              TUM1(I1)=(SUMP+SUMQ+D(J))*10.0/3.0
              DO 576 I=9,13
576           D(I)=CS1(I,I1)*EAE(I)*EXP(-EAE(I)/TE)
              J=9
              SUMX=D(J)
577           J=J+2
              SUMX=SUMX+2.0*D(J)
              IF(J.LT.11) GO TO 577
              J=10
              SUMY=D(J)*4.0
578           J=J+2
              SUMY=SUMY+4.0*D(J)
              IF(J.LT.12) GO TO 578
              J=13
              TUM2(I1)=(SUMX+SUMY+D(J))*100.0/3.0
              TUM(I1)=TUM1(I1)+TUM2(I1)
579           HCK(I1)=7.3587E-03*TUM(I1)/(TEMP**1.5)
              DO 589 I1=1,4
              DO 580 I=1,9
580           D(I)=CS2(I,I1)*EBE(I)*EXP(-EBE(I)/TE)
              J=1
              SUMP=D(J)
581           J=J+2
              SUMP=SUMP+2.0*D(J)
              IF(J.LT.7) GO TO 581
              J=2
              SUMQ=D(J)*4.0
582           J=J+2
              SUMQ=SUMQ+4.0*D(J)
              IF(J.LT.8) GO TO 582
              J=9
              TUM1(I1)=(SUMP+SUMQ+D(J))*1.0/3.0
              DO 583 I=9,17
583           D(I)=CS2(I,I1)*EBE(I)*EXP(-EBE(I)/TE)
              J=9
              SUMX=D(J)
584           J=J+2
              SUMX=SUMX+2.0*D(J)
              IF(J.LT.15) GO TO 584
              J=10
              SUMY=D(J)*4.0
585           J=J+2
              SUMY=SUMY+4.0*D(J)
              IF(J.LT.16) GO TO 585
              J=17
              TUM2(I1)=(SUMX+SUMY+D(J))*10.0/3.0
              DO 586 I=18,22
586           D(I)=CS2(I,I1)*EBE(I)*EXP(-EBE(I)/TE)
              J=18
              SUMX1=D(J)
587           J=J+2
              SUMX1=SUMX1+2.0*D(J)
              IF(J.LT.20) GO TO 587
              J=19
              SUMY1=D(J)*4.0
588           J=J+2
              SUMY1=SUMY1+4.0*D(J)
              IF(J.LT.21) GO TO 588
              J=22
              TUM3(I1)=(SUMX1+SUMY1+D(J))*100.0/3.0
              EX=EBE(18)-EBE(17)
              TUM4(I1)=(D(18)+D(17))*EX/2.0
              TUM(I1)=TUM1(I1)+TUM2(I1)+TUM3(I1)+TUM4(I1)
              I2=I1+4
589           HCK(I2)=7.3587E-03*TUM(I1)/(TEMP**1.5)
              DO 599 I1=1,12
              DO 590 I=1,7
590           D(I)=CS3(I,I1)*ECE(I)*EXP(-ECE(I)/TE)
              J=1
              SUMP=D(J)
591           J=J+2
              SUMP=SUMP+2.0*D(J)
              IF(J.LT.5) GO TO 591
              J=2
              SUMQ=D(J)*4.0
592           J=J+2
```

```
          SUMP=SUMQ+1.0*D(J)
          IF(J.LT.5) GO TO 592
          J=7
          TUM1(I1)=(SUMP+SUMQ+D(J))*1.0/3.0
          DO 593 I=7,15
593       D(I)=CS3(I,I1)*ECE(I)*EXP(-ECE(I)/TE)
          J=7
          SUMX=D(J)
594       J=J+2
          SUMX=SUMX+2.0*D(J)
          IF(J.LT.13) GO TO 594
          J=8
          SUMY=D(J)
595       J=J+2
          SUMY=SUMY+4.0*D(J)
          IF(J.LT.14) GO TO 595
          J=15
          TUM2(I1)=(SUMX+SUMY+D(J))*10.0/3.0
          DO 596 I=16,24
596       D(I)=CS3(I,I1)*ECE(I)*EXP(-ECE(I)/TE)
          J=16
          SUMX1=D(J)
597       J=J+2
          SUMX1=SUMX1+2.0*D(J)
          IF(J.LT.22) GO TO 597
          J=17
          SUMY1=D(J)*4.0
598       J=J+2
          SUMY1=SUMY1+4.0*D(J)
          IF(J.LT.23) GO TO 598
          J=24
          TUM3(I1)=(SUMX1+SUMY1+D(J))*100.0/3.0
          EX=ECE(16)-ECE(15)
          TUM4(I1)=(D(16)+D(15))*EX/2.0
          TUM(I1)=TUM1(I1)+TUM2(I1)+TUM3(I1)+TUM4(I1)
          I2=I1+8
599       HCK(I2)=7.3587E-03*TUM(I1)/(TEMP**1.5)
          DO 907 I1=1,2
          DO 901 I=1,7
901       D(I)=CS4(I,I1)*EDE(I)*EXP(-EDE(I)/TE)
          J=1
          SUMP=D(J)
902       J=J+2
          SUMP=SUMP+2.0*D(J)
          IF(J.LT.5) GO TO 902
          J=2
          SUMQ=D(J)*4.0
903       J=J+2
          SUMQ=SUMQ+4.0*D(J)
          IF(J.LT.6) GO TO 903
          J=7
          TUM1(I1)=(SUMP+SUMQ+D(J))*2.0/3.0
          DO 904 I=7,13
904       D(I)=CS4(I,I1)*EDE(I)*EXP(-EDE(I)/TE)
          J=7
          SUMX=D(J)
905       J=J+2
          SUMX=SUMX+2.0*D(J)
          IF(J.LT.11) GO TO 905
          J=8
          SUMY=D(J)*4.0
906       J=J+2
          SUMY=SUMY+4.0*D(J)
          IF(J.LT.12) GO TO 906
          J=13
          TUM2(I1)=(SUMX+SUMY+D(J))*10.0/3.0
          TUM(I1)=TUM1(I1)+TUM2(I1)
          I2=I1+20
907       HCK(I2)=7.3587E-03*TUM(I1)/(TEMP**1.5)
          DO 914 I1=1,1
          DO 908 I=1,9
908       D(I)=CS5(I,I1)*EEE(I)*EXP(-EEE(I)/TE)
          J=1
          SUMP=D(J)
909       J=J+2
          SUMP=SUMP+2.0*D(J)
          IF(J.LT.7) GO TO 909
          J=2
          SUMQ=D(J)*4.0
910       J=J+2
          SUMQ=SUMQ+4.0*D(J)
          IF(J.LT.8) GO TO 910
          J=9
          TUM1(I1)=(SUMP+SUMQ+D(J))*5.0/3.0
          DO 911 I=9,13
911       D(I)=CS5(I,I1)*EEE(I)*EXP(-EEE(I)/TE)
          J=9
          SUMX=D(J)
912       J=J+2
```

```
      SUMX=SUMX+(12.0*D(I)
      IF(J.LT.11) GO TO 912
      I=10
      SUM1=D(J)*4.0
913   I=I+2
      SUM1=SUMY+4.0*D(I)
      IF(J.LT.12) GO TO 913
      I=13
      TUM2(I1)=(SUMX+SUMY+D(J))*10.0/3.0
      TUM(I1)=TUM1(I1)+TUM2(I1)
      I2=I1+22
914   HCK(I2)=7.3587E-03*TUM(I1)/(TEMP**1.5)
      DO 921 I1=1,2
      DO 915 I=1,7
915   D(I)=CS6(I,I1)*EFE(I)*EXP(-EFE(I)/TE)
      I=1
      SUMP=D(J)
916   I=I+2
      SUMP=SUMP+2.0*D(J)
      IF(J.LT.5) GO TO 916
      J=2
      SUMQ=D(J)*4.0
917   I=I+2
      SUMQ=SUMQ+4.0*D(J)
      IF(J.LT.6) GO TO 917
      I=7
      TUM1(I1)=(SUMP+SUMQ+D(J))*10.0/3.0
      DO 918 I=7,15
918   D(I)=CS6(I,I1)*EFE(I)*EXP(-EFE(I)/TE)
      I=7
      SUMX=D(J)
919   I=I+2
      SUMX=SUMX+2.0*D(J)
      IF(J.LT.13) GO TO 919
      I=8
      SUMY=D(J)*4.0
920   I=J+2
      SUMY=SUMY+4.0*D(J)
      IF(J.LT.14) GO TO 920
      J=15
      TUM2(I1)=(SUMX+SUMY+D(J))*100.0/3.0
      TUM(I1)=TUM1(I1)+TUM2(I1)
      I2=I1+23
921   HCK(I2)=8.3703E-07*TUM(I1)/(TEMP**1.5)
      DO 933 I1=1,2
      DO 922 I=1,7
922   D(I)=CS7(I,I1)*EGE(I)*EXP(-EGE(I)/TE)
      J=1
      SUMP=D(J)
923   J=J+2
      SUMP=SUMP+2.0*D(J)
      IF(J.LT.5) GO TO 923
      J=2
      SUMQ=D(J)*4.0
924   I=J+2
      SUMQ=SUMQ+4.0*D(J)
      IF(J.LT.6) GO TO 924
      J=7
      TUM1(I1)=(SUMP+SUMQ+D(J))*5.0/3.0
      DO 925 I=8,12
925   D(I)=CS7(I,I1)*EGE(I)*EXP(-EGE(I)/TE)
      J=8
      SUMX=D(J)
926   I=J+2
      SUMX=SUMX+2.0*D(J)
      IF(J.LT.10) GO TO 926
      J=9
      SUMY=D(J)*4.0
927   I=J+2
      SUMY=SUMY+4.0*D(J)
      IF(J.LT.11) GO TO 927
      J=12
      TUM2(I1)=(SUMX+SUMY+D(J))*10.0/3.0
      DO 928 I=12,20
928   D(I)=CS7(I,I1)*EGE(I)*EXP(-EGE(I)/TE)
      J=12
      SUMX1=D(J)
929   J=J+2
      SUMX1=SUMX1+2.0*D(J)
      IF(J.LT.18) GO TO 929
      J=13
      SUMY1=D(J)*4.0
930   J=J+2
      SUMY1=SUMY1+4.0*D(J)
      IF(J.LT.19) GO TO 930
      J=20
      TUM3(I1)=(SUMX1+SUMY1+D(J))*50.0/3.0
      DO 931 I=20,22
      D(I)=CS7(I,I1)*EGE(I)*EXP(-EGE(I)/TE)
```

```
            I=2J
            SUMX2=D(1)
            I=21
            SUMI2=D(1)*4.0
            I=22
932         TUM1(I1)=(SUMX2+SUMY2+D(J))*500.0/3.0
            EZ=EGE(8)-EGE(7)
            TUM5(I1)=(D(8)+D(7))*EZ/2.0
            TUM(I1)=TUM1(I1)+TUM2(I1)+TUM3(I1)+TUM4(I1)+TUM5(I1)
            I2=I1+25
933         HQ(I2)=8.3703E-06*TUM(I1)/(TEMP**1.5)
C
C...... Electron impact excitation rate coeffs. are calculated ov
C       integrating the cross section expression using Laguerre
C       integration method and are stored in different arrays .
935         FORMAT(1X,10E13.4/1X,10E13.4/1X,7E13.4/)
            DO 65 I=1,11
            AL=EA(I)/TE
            ACON=5.436273*AF(I)*FA(I)*EXP(-AL)/(AL*(TEMP**1.5))
            SUM=0.0
            DO 66 J=1,11
            Z=AP(J)/AL
            AG=1.25*(Z+1.0)
            AFUN=Z*ALOG(AG)/(Z+1.0)
            ASUM=AFUN*H(J)
            SUM=SUM+ASUM
66          CONTINUE
            AK(I)=SUM*ACON
65          CONTINUE
            DO 75  I=1,11
            AL=EB(I)/TE
            BCON=5.436273*BF(I)*FB(I)*EXP(-AL)/(AL*(TEMP**1.5))
            SUM=0.0
            DO 76 J=1,11
            Z=AP(J)/AL
            AM=1.25*(Z+1.0)
            BSUM=Z*ALOG(AM)/(Z+1.0)
            FUM=BSUM*H(J)
            SUM=SUM+FUM
76          CONTINUE
            BK(I)=SUM*BCON
75          CONTINUE
            RY=109677.0
            E1=198311.0
            A(1)=(RY/E1)**0.5
            DO 80  I=2,N
            A(I)=(RY/(E1-E(1)))**0.5
80          CONTINUE
            DO 90  I=12,25
            DO 98  J=27,N
            AN=A(I)
            AM=A(J)
            A1=1.0/(AN*AN)
            A2=1.0/(AM*AM)
            A3=1.0/(((A1-A2)*AN*AM)**3)
98          FPQ(I,J)=1.9603*A3/(AN*AN)
90          CONTINUE
            DO 105  I=12,25
            DO 105 J=27,N
            AL=(E(J)-E(I))/(TE*8064.0)
            ALCON=5.436273*FPQ(I,J)*EXP(-AL)/(AL*(TEMP**1.5))
            CALL FINT(AP,H,AL,SUM)
105         KPQ(I,J)=ALCON*SUM
            DO 110 I=26,N
            DO 120 J=I,N
            IF (I.EQ.J) GO TO 120
            AN=A(I)
            AM=A(J)
            A5=1.0/(AN*AN)
            A6=1.0/(AM*AM)
            A7=1.0/(((A5-A6)*AN*AM)**3)
            FPQ(I,J)=1.9603*A7/(AN*AN)
            AL=(E(J)-E(I))/(8064.0*TE)
            ALC=5.436273*FPQ(I,J)*EXP(-AL)/(AL*(TEMP**1.5))
            CALL FINT(AP,H,AL,SUM)
            KPQ(I,J)=ALC*SUM
120         CONTINUE
110         CONTINUE
            DO 213  I=1,20
            AL=AAE(I)
            AL=AL/TE
            AACON=5.436273*AAE(I)*EXP(-AL)/(AL*(TEMP**1.5))
            CALL FINT(AP,H,AL,SUM)
            AAK(I)=SUM*AACON
213         CONTINUE
            DO 223  I=19,25
            AL=(E(26)-E(I))/(8064.0*TE)
            ACN=5.436273*EXP(-AL)/(AL*(TEMP**1.5))
            CALL FINT(AP,H,AL,SUM)
```

```
223      KPD(I,25)=SUM*ACN
         DO 85 I=1,10
         AL=CF(I)/TE
         CCON=5.436273*CF(I)*EXP(-AL)/(AL*(TEMP**1.5))
         CALL FINT(AP,H,AL,COF)
85       CK(I)=CCON*COF
         DO 88 I=1,10
         AL=DF(I)/TE
         DCON=5.436273*DF(I)*EXP(-AL)/(AL*(TEMP**1.5))
         CALL FINT(AP,H,AL,DOF)
88       DK(I)=DOF*DCON
         DO 91 I=1,10
         AL=EF(I)/TE
         ECON=5.436273*EF(I)*EXP(-AL)/(AL*(TEMP**1.5))
         CALL FINT(AP,H,AL,EOF)
91       EK(I)=EOF*ECON
         DO 103  I=1,9
         AL=FF(I)/TE
         FCON=5.436273*EXP(-AL)*FF(I)/(AL*(TEMP**1.5))
         CALL FINT(AP,H,AL,FOF)
103      FK(I)=FOF*FCON
         DO 111 I=1,10
         AL=GF(I)/TE
         GCON=5.436273*GF(I)*EXP(-AL)/(AL*(TEMP**1.5))
         CALL FINT(AP,H,AL,GOF)
111      GK(I)=GOF*GCON
         DO 113  I=1,9
         AL=HF(I)/TE
         HCON=5.436273*HF(I)*EXP(-AL)/(AL*(TEMP**1.5))
         CALL FINT(AP,H,AL,HOF)
113      HK(I)=HCON*HOF
         DO 123  I=1,9
         AL=OF(I)/TE
         OCON=5.436273*OF(I)*EXP(-AL)/(AL*(TEMP**1.5))
         CALL FINT(AP,H,AL,OOF)
123      OK(I)=OOF*OCON
         DO 133  I=1,11
         AL=PF(I)/TE
         PCON=5.436273*PF(I)*EXP(-AL)/(AL*(TEMP**1.5))
         CALL FINT(AP,H,AL,POF)
133      PK(I)=POF*PCON
         DO 143 I=1,10
         AL=QF(I)/TE
         QCON=5.43623*QF(I)*EXP(-AL)/(AL*(TEMP**1.5))
         CALL FINT(AP,H,AL,QOF)
143      QK(I)=QOF*QCON
         DO 153 I=1,10
         AL=RF(I)/TE
         RCON=5.436273*RF(I)*EXP(-AL)/(AL*(TEMP**1.5))
         CALL FINT(AP,H,AL,ROF)
153      RK(I)=ROF*RCON
         DO 163   I=1,10
         AL=SF(I)/TE
         SCON=5.436273*SF(I)*EXP(-AL)/(AL*(TEMP**1.5))
         CALL FINT(AP,H,AL,SOF)
163      SK(I)=SOF*SCON
         DO 173 I=1,9
         AL=UF(I)/TE
         UCON=5.436273*UF(I)*EXP(-AL)/(AL*(TEMP**1.5))
         CALL FINT(AP,H,AL,UOF)
173      UK(I)=UOF*UCON
         DO 183  I=1,9
         AL=VF(I)/TE
         VCON=5.436273*VF(I)*EXP(-AL)/(AL*(TEMP**1.5))
         CALL FINT(AP,H,AL,VOF)
183      VK(I)=VOF*VCON
         DO 193  I=1,9
         AL=WF(I)/TE
         WCON=5.436273*WF(I)*EXP(-AL)/(AL*(TEMP**1.5))
         CALL FINT(AP,H,AL,WOF)
193      WK(I)=WOF*WCON
         DO 203 I=1,9
         AL=XF(I)/TE
         XCON=5.436273*XF(I)*EXP(-AL)/(AL*(TEMP**1.5))
         CALL FINT(AP,H,AL,XOF)
203      XK(I)=XOF*XCON
         DO 303   I=1,8
         AL=SEE(I)/TE
         SSCN=7.358721E-3*SEE(I)*SEE(I)*QEE(I)*EXP(-AL)/(AL*(TEMP**1.5))
         CALL SINT(AP,H,AL,SUM)
303      SKK(I)=SUM*SSCN
         DO 360 I=1,11
         AL=TEE(I)/TE
         TECON=7.358721E-3*TEE(I)*TEE(I)*QTE(I)*EXP(-AL)/(AL*(TEMP**1.5))
         CALL FINT(AP,H,AL,SUM)
360      TEK(I)=SUM*TECON
C
C...... The electron impact excitation rate coeffs. stored in different
C       arrays are transferred to array KPD of dimnsion 45X45
```

```
              KPO(1,5)=CK(25)
              KPO(1,11)=CK(27)
              KPO(1,18)=CK(1)
              KPO(1,25)=HCK(2)
              DO  497   I=5,11
              II=I+21
497           KPO(1,II)=AK(I)
              KPO(3,5)=BK(1)
              KPO(3,11)=HCK(6)
              KPO(3,18)=AK(3)
              KPO(3,25)=BK(4)
              DO  104   I=5,11
              II=I+21
104           KPO(3,II)=BK(I)
              KPO(5,7)=CK(1)
              KPO(5,13)=CK(2)
              KPO(5,20)=CK(3)
              KPO(5,1)=DK(1)
              KPO(5,16)=DK(2)
              KPO(5,23)=DK(3)
              DO  407   I=4,10
              II=I+22
407           KPO(5,II)=DK(I)+CK(I)
              KPO(7,11)=EK(1)
              KPO(7,18)=EK(2)
              KPO(7,25)=EK(3)
              DO  409   I=4,10
              II=I+22
409           KPO(7,II)=EK(I)
              KPO(11,13)=FK(1)
              KPO(11,20)=FK(2)
              KPO(10,11)=GK(1)
              KPO(10,18)=GK(2)
              KPO(10,25)=GK(3)
              KPO(10,17)=HK(1)
              KPO(10,24)=HK(2)
              DO  415   I=3,9
              II=I+23
415           KPO(10,II)=HK(I)
              KPO(11,16)=OK(1)
              KPO(11,23)=OK(2)
              DO  417   I=3,9
              II=I+23
417           KPO(11,II)=OK(I)
              KPO(2,4)=HCK(20)
              KPO(2,8)=HCK(9)
              KPO(2,14)=HCK(12)
              KPO(2,21)=HCK(16)
              DO  419  I=5,11
              II=I+21
419           KPO(2,II)=PK(I)
              KPO(4,9)=QK(1)
              KPO(4,15)=QK(2)
              KPO(4,22)=QK(3)
              DO  421   I=4,10
              II=I+22
421           KPO(4,II)=QK(I)+RK(I)
              KPO(4,6)=RK(1)
              KPO(4,12)=RK(2)
              KPO(4,19)=RK(3)
              KPO(6,8)=SK(1)
              KPO(6,14)=SK(2)
              KPO(6,21)=SK(3)
              KPO(6,26)=SK(4)
              KPO(8,12)=UK(1)
              KPO(8,19)=UK(2)
              KPO(8,15)=VK(1)
              KPO(8,22)=VK(2)
              DO  429  I=3,9
              II=I+23
              KPO(8,II)=VK(I)
429           CONTINUE
              KPO(9,14)=WK(1)
              KPO(9,21)=WK(2)
              DO 433 I=3,9
              II=I+23
433           KPO(9,II)=WK(I)
              KPO(9,17)=XK(1)
              KPO(9,24)=XK(2)
              KPO(13,25)=AAK(1)
              KPO(13,26)=AAK(2)
              KPO(18,20)=AAK(3)+AAK(4)
              KPO(8,26)=AAK(5)
              KPO(8,24)=AAK(6)
              KPO(6,25)=AAK(7)
              KPO(6,26)=AAK(8)
              KPO(17,23)=AAK(9)
              KPO(12,21)=AAK(11)
              KPO(12,26)=AAK(12)
```

```
        KPD(14,19)=AAK(13)
        KPD(14,22)=AAK(14)
        KPD(14,26)=AAK(15)
        KPD(15,21)=AAK(16)
        KPD(15,24)=AAK(17)
        KPD(15,26)=AAK(18)
        KPD(17,22)=AAK(19)
        KPD(17,26)=AAK(20)
        KPD(1,3)=HCK(23)
        KPD(1,7)=SK(2)
        KPD(1,13)=HCK(4)
        KPD(1,20)=HCK(3)
        KPD(1,10)=HCK(24)
        KPD(1,16)=HCK(25)
C
C.....  Oscillator strengths for Hei transitions, read and stored
C       separately are restored in array FFP of dimension 32X32
        DO 6585 I=1,32
        DO 6585 J=1,32
6585    FFP(I,J)=0.0
        FFP(8,11)=0.01
        FFP(9,11)=0.00742
        FFP(15,16)=5.1396E-07
        FFP(16,18)=5.01E-04
        FFP(1,5)=FA(1)
        FFP(1,11)=FA(2)
        FFP(1,18)=FA(3)
        FFP(1,25)=FA(4)
        DO 6581 I=5,11
        II=I+21
        FFP(1,II)=FA(1)
        FFP(3,II)=FB(I)
        FFP(2,II)=PF(1)
6581    CONTINUE
        FFP(3,5)=FB(1)
        FFP(3,11)=FB(2)
        FFP(3,18)=FB(3)
        FFP(3,25)=FB(4)
        FFP(13,25)=AAF(1)
        FFP(13,26)=AAF(2)
        FFP(18,20)=AAF(3)
        FFP(18,26)=AAF(5)
        FFP(16,24)=AAF(6)
        FFP(16,25)=AAF(7)
        FFP(16,26)=AAF(8)
        FFP(17,23)=AAF(9)
        FFP(12,21)=AAF(11)
        FFP(12,26)=AAF(12)
        FFP(14,19)=AAF(13)
        FFP(14,22)=AAF(14)
        FFP(14,26)=AAF(15)
        FFP(15,21)=AAF(16)
        FFP(15,24)=AAF(17)
        FFP(15,26)=AAF(18)
        FFP(17,22)=AAF(19)
        FFP(17,26)=AAF(20)
        FFP(5,7)=CF(1)
        FFP(5,13)=CF(2)
        FFP(5,20)=CF(3)
        DO 6582 I=4,10
        II=I+22
        FFP(4,II)=OF(I)
        FFP(5,II)=DF(I)
        FFP(6,II)=SF(I)
        FFP(7,II)=EF(I)
6582    CONTINUE
        FFP(5,10)=DF(1)
        FFP(5,16)=DF(2)
        FFP(5,23)=DF(3)
        FFP(7,11)=EF(1)
        FFP(7,18)=EF(2)
        FFP(7,25)=EF(3)
        FFP(11,13)=FF(1)
        FFP(11,20)=FF(2)
        DO 6583 I=3,9
        II=I+23
        FFP(11,II)=OF(I)
        FFP(10,II)=HF(I)
        FFP(8,II)=VF(I)
        FFP(9,II)=XF(I)
6583    CONTINUE
        FFP(10,11)=GF(1)
        FFP(10,18)=GF(2)
        FFP(10,25)=GF(3)
        FFP(10,17)=HF(1)
        FFP(10,24)=HF(2)
        FFP(11,16)=OF(1)
        FFP(11,23)=OF(2)
        FFP(2,4)=PF(1)
```

```
      FPP(2,8)=PF(2)
      FPP(2,11)=PF(3)
      FPP(2,21)=PF(4)
      FPP(4,9)=QF(1)
      FPP(4,15)=QF(2)
      FPP(4,22)=QF(3)
      FPP(4,6)=RF(1)
      FPP(4,12)=RF(2)
      FPP(4,19)=RF(3)
      FPP(6,8)=SF(1)
      FPP(6,14)=SF(2)
      FPP(6,21)=SF(3)
      FPP(8,12)=UF(1)
      FPP(8,19)=UF(2)
      FPP(8,15)=VF(1)
      FPP(8,22)=VF(2)
      FPP(9,14)=WF(1)
      FPP(9,21)=WF(2)
      FPP(9,17)=XF(1)
      FPP(9,24)=XF(2)
C
C...... Subroutine ATOM is called to calculate neutral-neutral exc.,
C       deexcitation, ionization and recombination rate coeffs.
      CALL ATOM(E,G,PA,N,ET,TG,TE,FPP,KNPC,KHCP,KNPQ)
C...... KNPQ,s are summed
      DO 466  I=1,32
      SUM=0.0
      DO 467 J=1,32
      IF(I.EQ.J)  GO TO 467
      SUM=SUM+KNPQ(I,J)
467   CONTINUE
466   KNSUM(I)=SUM
C
C...... Remaining electron impact exc. rate coeffs. are stored in
C       array KPO
      KPO(1,23)=SKK(7)
      KPO(1,2)=HCK(22)
      KPO(1,4)=HCK(21)
      KPO(1,6)=TEK(3)
      KPO(1,12)=TEK(6)
      KPO(1,19)=TEK(9)
      KPO(1,8)=TEK(4)
      KPO(1,9)=TEK(5)
      KPO(1,12)=TEK(6)
      KPO(1,14)=TEK(7)
      KPO(1,15)=TEK(8)
      KPO(1,19)=TEK(9)
      KPO(1,21)=TEK(10)
      KPO(1,22)=TEK(11)
      DO  403   I=1,12
      AL=CRE(I)/TE
403   CRK(I)=7.358721E-3*EXP(-AL)*CRO(I)*CRE(I)*CRE(I)/(AL*(TEMP**1.5))
      KPO(2,3)=CRK(1)
      KPO(2,7)=CRK(2)
      KPO(2,13)=CRK(3)
      KPO(6,7)=CRK(4)
      KPO(6,13)=CRK(5)
      KPO(6,20)=CRK(6)
      KPO(12,13)=CRK(7)
      KPO(12,20)=CRK(8)
      KPO(4,5)=CRK(9)
      KPO(4,11)=CRK(10)
      KPO(4,18)=CRK(11)
      KPO(8,11)=CRK(12)
      KPO(1,26)=KPO(1,26)+SKK(8)
      COR=7.358721E-03/(TEMP**1.5)
      DO  45   J=1,2
      SUM=0.0
      DO  46   I=1,11
      II=I+1
      RX=SFE(II)-SFE(I)
      PO=-SFE(I)/TE
      TERM=SFE(I)*RX*SFF(I,J)*EXP(PO)
46    SUM=SUM+TERM
45    SPK(J)=SUM*COR
      KPO(1,17)=SPK(1)
      KPO(1,24)=SPK(2)
      DO  53  I=1,12
      SUM=0.0
      DO  54 J=1,13
      ESS=-ES(J)/TE
      J1=J+1
      ES1=ES(J1)-ES(J)
      TERM=ES(J)*ES1*EXP(ESS)*OQO(I,J)
54    SUM=SUM+TERM
53    KSPO(I)=SUM*7.358721E-03/(TEMP**1.5)
      DO  36   I=1,17
      SUM=0.0
      DO  37  J=1,11
```

```
      JJ=J+1
      PN=ETI(JJ)-ETI(J)
      RAM=-ETI(J)/TE
      TERM2=ETI(JJ)*RN*EXP(RAM)*LQ(I,J)
37    SUM=SUM+TERM2
30    KKPO(I)=SUM*7.358721E-03/(TEMP**1.5)
      KPO(2,20)=KSPO(3)
      KPO(2,5)=KSPO(4)
      KPO(2,11)=KSPO(5)
      KPO(2,18)=KSPO(6)
      KPO(2,25)=KSPO(7)
      KPO(2,10)=KSPO(8)
      KPO(2,16)=KSPO(9)
      KPO(2,23)=KSPO(10)
      KPO(2,17)=HCK(14)
      KPO(2,24)=HCK(18)+HCK(19)

      KPO(2,6)=HCK(8)
```

```
        KPO(2,12)=HCK(11)
        KPO(2,14)=HCK(15)
        KPO(2,9)=HCK(10)
        KPO(2,15)=HCK(13)
        KPO(3,7)=HCK(5)
        KPO(3,10)=HCK(7)
        KPO(2,22)=HCK(17)
C
C...... Saha equilibrium population densities (normalized) are calculated
      DO  150  I=1,N
      CONST=4.14250bE-16/(TEMP**1.5)
      TP=EI/8064.0
      IF(I.EQ.1)  GO  TO  455
      TP=(EI-E(I))/8064.0
455   TP=TP/TE
      NP(I)=G(I)*CONST*EXP(TP)/4.0
      NP(I)=NP(I)*1.0E+10
450   NO(I)=NP(I)
C
C...... Electron impact deexcitation rate coeffs. are calculated by
C       using priciple of detailed balancing
      DO  888  J=1,N
      DO  888  I=1,J
888   KPO(J,I)=KPO(I,J)*NP(I)/NO(J)
C
C......Calculation of electron impact ionization rate coeffs.
      X=EI/8064.0
      DO  240  I=1,N
      IF(I.EQ.1)  GO  TO  235
      X=(EI-E(I))/8064.0
235   CONTINUE
      X=X/TE
      CONST=10.90007*EXP(-X)/(X*(TEMP**1.5))
      SUM=0.0
      DO  250  J=1,11
      Z=AP(J)/X
      D1=(Z/(Z+2.0))**1.5
      D2=(1.0-(1.0/(2.0*(Z+1.0))))*2.0/3.0
      D3=2.7+Z**0.5
      D5=ALOG(D3)
      D6=H(J)*D1*(1.0+D2*D5)
250   SUM=SUM+D6
240   KPC(I)=SUM*CONST
C
C...... For a particular level KPO's are summed
      DO  460  I=1,N
      SUM=0.0
      DO 470  J=1,N
      IF(I.EQ.J)  GO  TO  470
      SUM=SUM+KPO(I,J)
470   CONTINUE
460   KPOSUM(I)=SUM
C
C...... Radiative recombination rate coeffs. for HeI and HeII calculated
      C1=16.0*6.7682E+04
      F(1)=198311.0
      C2=3.0E+10
      DO  5051  I=1,N
      XA1=1.0/((A(I)**3)*C2*E(I))
5051  BETA(I)=C1*XA1/(TEMP**0.5)
      DO  5052  I=1,N
      VOO=C2*E(I)
      VKK=4.175E+15
      VO1=VOO+VKK/(A(I)**3)
      V(I)=VO1*((VKK/VOO)**0.5)/VOO
      P=-0.66666666
5052  GG(I)=1.0-0.218*(V(I)**P)
      DO  5053  I=1,N
5053  BETA(I)=BETA(I)*GG(I)*1.0E+10
      DO 251 I=1,15
      II=I+32
      P=I
      Y(I)=157890.0*4.0/(TEMP*(P**2))
      SUM=0.0
      DO 252 J=1,11
      Z=AP(J)/Y(I)
      Z1=1.0+(0.1728*(Z-1.0)/(P**0.666*(Z+1.0)**0.666))
      Z2=(0.0496*(Z**2+Z*4.0/3.0+1.0))/(P*(Z+1.0))**1.333
      Z3=(Z1-Z2)/(Z+1.0)
      Z4=Z3*H(J)
252   SUM=SUM+Z4
      BETA(II)=5.197E-14*2.0*Y(I)**1.5*SUM
251   BETA(II)=BETA(II)*1.0E+10
C
C......Electron density loop starts
      DO 500  NNN=1,11
      NC=1.0E+11*(10.0**NNN)
      PRINT 5054,NC
5054  FORMAT(20X,'ELECTRON DENSITY=',E13.3/)
```

```
C
C......  Optical escape fectors for resonance transitions of Hef and HeII
C        are calculated. TI = Ion temperature, WL = wave length
C        OS = Oscillator strength, XL = Diareter of plasma tube
         TI=1540
         DO 824 I=1,5
         P=T
         P=T+1.0
         T=TGAS
         XN=NC
         WL1=WL(I)
         OS1=OS(I)
         CALL OEFAC(P,T,NC,WL1,XL,OS1,OPF)
         OEF(I)=OPF
824      CONTINUE
         DO 825 I=1,5
         J=I+5
         P=T
         P=P+1.0
         T=TI
         XN=NC
         WL1=WL(J)
         OS1=OS(J)
         CALL OEFAC(P,T,NC,WL1,XL,OS1,OPF)
         OEF(J)=OPF
825      CONTINUE
         PRINT 833,(OEF(I),I=1,10)
833      FORMAT(1X,10E13.4/)
C
C......  For partially optically thick case, transition probabilities are
C        multiplied by optical escape fectors. For optically thin case
C        these statements should be removed
         APO(5,1)=AAPO(5,1)*OEF(1)
         APO(11,1)=AAPO(11,1)*OEF(2)
         APO(18,1)=AAPO(18,1)*OEF(3)
         APO(25,1)=AAPO(25,1)*OEF(4)
         APO(26,1)=AAPO(26,1)*OEF(5)
C
C......  Transition probabilities are summed
         DO 480 I=1,N
         SUM=0.0
         DO 490 J=1,I
         SUM=SUM+APO(I,J)
490      CONTINUE
480      APOSUM(I)=SUM
C
C......Suproutine HeII is called to calculate energies, wieght fectors,
C      electron impact excitation,ionization rate coeffs., and
C      transition probabilties for HeII
         OEF1=OEF(6)
         OEF2=OEF(7)
         OEF3=OEF(8)
         OEF4=OEF(9)
         OEF5=OEF(10)
         CALL HEIT(TE,HEI,HGI,HAPO,HKPQ,HKPC,HNP,HNO,HKPSUM,HAPSUM,OEF1,
        1OEF2,OEF3,OEF4,OEF5)
         DO 164 I=1,15
         TI=I+N
         E(TI)=HEI(I)
         G(TI)=HGI(I)
         KPC(TI)=HKPC(1)
         NP(TI)=HNP(I)
         NO(TI)=HNO(I)
         KPOSUM(TI)=HKPSUM(I)
         APOSUM(TI)=HAPSUM(I)
         DO 164 J=1,15
         JJ=J+N
         KPO(TI,JJ)=HKPO(I,J)
         APO(TI,JJ)=HAPO(I,J)
164      CONTINUE
C
C......  Direct ionization-excitation rate coeffs. calculated
         E(1)=0.0
         DO 166 I=1,N
         SUM=0.0
         DO 168 J=33,NHE
         AL=(E(J)-E(I))/(8064.0*TE)
         CONST=6.2541E-03*EXP(-AL)/(AL*(TEMP**1.5))
         CALL TION(AP,H,AL,SUM)
168      HEXI(I,J)=SUM*CONST
166      CONTINUE
         DO 169 I=1,N
         SUM=0.0
         DO 171 J=34,NHE
171      SUM=SUM+HEXI(I,J)
169      HEXSUM(I)=SUM
C
```

```
         II=I-1
         IF(I.EQ.1) GO TO 601
         DO 610 JJ=1,II
610      AD(I,JJ)=-NC*KPC(I,JJ)
601      CONTINUE
         AD(I,I)=NC*(KEC(I)+KPOSUM(I))+APOSUM(I)
         II=I+1
         IF (I.EQ.NHE)  GO TO 621
         DO 620  JJ=II,NHE
620      AD(I,JJ)=-NC*KPO(I,JJ)-APO(JJ,I)*NO(I,I)/NP(I)
621      CONTINUE
         RO(I,1)=NC*KPC(I)
         RO(I,2)=BETA(I)/NP(I)
600      CONTINUE
         DO 6001 I=1,32
6001     AD(I,I)=NC*(KPC(I)+HEXSUM(I)+KPOSUM(I))+APOSUM(I)
         DO 616  I=1,32
         II=I-1
         IF(I.EQ.1)  GO TO 617
```

```
        DO  618   I=1,11
618     AD(I,J)=AD(I,J)-NG*NO(J)*KNPO(I,I)/NP(I)
617     CONTINUE
        AD(I,I)=AD(I,I)+NG*(KNPC(I)+N.SUM(I))
        TI=I+1
        IF(J.EQ.32)  GO TO 616
        DO 623   I=1,32
623     AD(I,J)=AD(I,J)-NO(J)*KNPO(J,I)*NG/NP(I)
616     CONTINUE
        DO 176 J=33,NHS
        DO 176 I=1,J
176     AD(J,I)=-NP(I)*HEXI(I,J)*DEGREE*NC/NO(J)
C
C...... From matrix AD, a new matrix ANEW(45X45)is formed which does
C       not contain first and thirty third rows, and first and thirty
C       third columns of AD. Similarly first and thirty third rows of
C       matrix BD are removed and the remaining matrices are stored
C       in a new array BNEW(45X45). The first and thirty third columns
C       of AD are brought in third and fourth columns of BNEW (see Fig. 2.3)
        DO 700   I=1,NS
        DO 750   J=1,NS
        II=I+1
        JJ=J+1
750     ANEW(I,J)=AD(II,JJ)
        DO 802   J=1,2
802     BNEW(I,J)=BD(II,J)
        BNEW(I,4)=0.0
        BNEW(I,3)=-AD(II,1)
700     CONTINUE
        DO 752   I=32,NHS
        DO 752   J=32,NHS
        II=I+2
        JJ=J+2
752     ANEW(I,J)=AD(II,JJ)
        DO 753   I=32,NHS
        II=I+2
        BNEW(I,1)=BD(II,1)
        BNEW(I,2)=BD(II,2)
        BNEW(I,3)=-AD(II,1)
        BNEW(I,4)=-AD(II,33)
753     CONTINUE
        DO  408   J=32,NHS
        DO  408   I=1,NS
        JJ=J+2
        II=I+1
408     ANEW(J,I)=AD(JJ,II)
C
C...... Subroutine FSOLVE is called to solve the system of linear
C       simultaneous equations. The array FS contains the final solution.
C       Population Coeff. r0 = (FS(I,1)+FS(I,2)), r1 = FS(I,3), r2 = FS(I,4)
C       The elements of first row of FS correspond to level 2, and the
C       elements of 32nd row correspond to level 34 (level i=2 of HeII).
        L=1
        DO 715 J=1,4
        DO 716 I=1,NHS
716     BN(I)=BNEW(I,J)
        CALL FSOLVE(ANEW,BN,F,NERM,NHS,L)
        DO 2222 I=1,NHS
2222    FS(I,J)=F(I)
        L=2
715     CONTINUE
C
C...... Population coeffs. printed
        PRINT 815,((FS(I,J),I=1,NHS),J=1,3)
815     FORMAT(1X,10E13.4/1X,10E13.4/1X,10E13.4/1X,10E13.4/1X,5E13.4/)
        PRINT 815,(FS(I,4),I=32,NHS)
C...... From population coeffs. the population densities of HeI levels
C       are calculated and stored in array DPOP. DPOP(I) corresponds to
C       the population density of HeI level I+1. NPX are the actual
C       Saha equilibrium population densities.
        DO 505 I=1,31
        II=I+1
        NPX(I)=NP(I)*(NC**2)/1.0E+10
        NPX(II)=(NP(II)*NC**2)/1.0E+10
        APOP(I)=(FS(I,1)+FS(I,2))*NPX(II)
        BPOP(I)=(FS(I,3)*NG*NPX(II))/NPX(1)
        DPOP(I)=APOP(I)+BPOP(I)
505     CONTINUE
C
C...... Population densities of HeII levels are calculated and stored in
C       array DPOP. DPOP(32) corresponds to the population density of
C       HeII level 2.
        DO 506 I=33,47
506     NPX(I)=(NP(I)*NC**2)/(1.0E+10*(DEGREE+2.0))
        DO 507 I=32,45
        II=I+2
        APOP(I)=(FS(I,1)+FS(I,2))*NPX(II)
        BPOP(I)=(FS(I,3)*NG*NPX(II))/NPX(1)
        DPOP(I)=(FS(I,4)*NC*NPX(II))/NPX(33)
```

```
          DPOP(I)=APOP(I)+BPOP(I)+CPOP(I)
507      CONTINUE
C
C...... Population densities and Saha eq. population densities of HeI
C       and HeII levels printed
         PRINT 57
57       FORMAT(10X,'POPULATION DENSITIES OF HEI AND HEII LEVELS'/)
         PRINT 815,(DPOP(I),I=1,45)
         PRINT 59
59       FORMAT(10X,'SAHA EQUILIBRIUM POPULATION DENSITIES'/)
         PRINT 815,(NPX(I),I=1,45)
500      CONTINUE
5000     CONTINUE
         STOP
         END
C
C...... Subroutine FSOLVE solves a system of linear cupled simultaneous
C       equations by Gauss elimination method. IInput parameters are:
C       A = Matrix of dimension NXN
C       B = Column vector of dimension N
C       N = Number of equations
C       L = 1 for first execution, 2 for further executions
C       F = Output parameter containing the final solution
         SUBROUTINE  FSOLVE(A,B,F,NERM,N,L)
         DIMENSION  A(45,45),B(45),NERM(45),F(45)
         GO TO (17,43),L
17       N1=N-1
         DO 4  I=1,N1
         X=0.0
         K=0
         DO 2  J=I,N
         A1=A(J,I)
         IF(ABS(A1).LE.X)  GO TO 2
         X=ABS(A1)
         K=J
2        CONTINUE
         NERM(I)=K
         DO  3  J=1,N
         Y=A(I,J)
         A(I,J)=A(K,J)
3        A(K,J)=Y
         II=I+1
         DO 4 J=II,N
         A(J,I)=A(J,I)/A(I,I)
         DO 4 M=II,N
4        A(J,M)=A(J,M)-A(I,M)*A(J,I)
43       DO 5 I=1,N1
         NN=NERM(I)
         Y=B(NN)
         B(NN)=B(I)
         B(I)=Y
         II=I+1
         DO 5 J=II,N
5        B(J)=B(J)-A(J,I)*B(I)
         F(N)=B(N)/A(N,N)
         DO 8 II=1,N1
         I=N1-II+1
6        II=I+1
         DO 7 J=II,N
7        B(I)=B(I)-A(I,J)*F(J)
8        F(I)=B(I)/A(I,I)
         RETURN
         END
C       Subroutines FINT, SINT, TINT, TION evaluate the integrals by
C       Gauss quadrature method (see page 37). Input parameters are:
C       AP = Roots of Laguerre polynomial
C       H = Weight factors of Laguerre polynomial
C       AL = ED.g/Te
         SUBROUTINE FINT(AP,H,AL,SUM)
         DIMENSION AP(11),H(11)
         SUM=0.0
         DO 10 J=1,11
         Z=AP(J)/AL
         CM=1.25*(Z+1.0)
         CFUN=Z*ALOG(CM)/(Z+1.0)
         CFUN=CFUN*H(J)
10       SUM=SUM+CFUN
         RETURN
         END
         SUBROUTINE SINT(AP,H,AL,SUM)
         DIMENSION AP(11),H(11)
         SUM=0.0
         DO 30 I=1,11
         Z=AP(I)/AL
         FUN=H(I)*Z/(Z+1.0)
         SUM=SUM+FUN
30       CONTINUE
         RETURN
         END
```

```
      SUBROUTINE FINT(AP,H,AL,SUM)
      DIMENSION AP(11),H(11)
      SUM=0.0
      DO 80 J=1,11
      Z=AP(J)/AL
      FUNT=Z*(Z+2.0)/((Z+1.0)**3)
      SUM=SUM+FUNT*H(J)
80    CONTINUE
      RETURN
      END
      SUBROUTINE FION(AP,H,AL,SUM)
      DIMENSION AP(11),H(11)
      SUM=0.0
      DO 10 J=1,11
      Z=AP(J)/AL
      D1=Z/(Z+1.0)
      D2=10.0*(Z+1.0)
      D6=H(J)*D1*ALOG(D2)
10    SUM=SUM+D6
      RETURN
      END
C
C..... Subroutine ATOM calculates neutral-neutral excitation, deexcitation
C      ionization and recombination rate coeffs. Input parameters are:
C      E = Energy of levels
C      G = Weight factors
C      N = Number of levels
C      EI = Ionization energy
C      TG = Gas Temperature
C      FFP = Oscillator strength
      SUBROUTINE ATOM(E,G,FA,N,EI,TG,TE,FFP,KNPC,KNCP,KNPQ)
      DIMENSION E(32),G(32),FA(11),FFP(32,32),KNPC(32),KNCP(32),
     1KNPQ(32,32),FAA(32)
      REAL KNPC,KNCP,KNPQ
      TEMP=TE*11600.0
      TGAS=TG*11600.0
      DO 5 I=4,11
      II=I+21
5     FAA(II)= FA(I)
      DO 10 I= 25,N
      EN=(EI-E(I))/(8064.0)
      WN= EN/TG
      CONT=1.0/(1.0+(2.7414E-04/WN)**2)
      CONT=CONT*(1.0+(2.0/WN))
      CONT=CONT*(1.0+(2.0/WN))
      CONST=FAA(I)/(EN**2)
      CONST=CONST*(TGAS**0.5)
      CONST1=G(I)*CONT*CONST*EXP(-WN)
      KNPC(I)=2.9085E-12*CONST1
      BON=4.144E-16/4.0
      UN=EN/TE
      XP=-UN+2.0*(UN*WN)**0.5
10    KNCP(I)=EXP(XP)*BON*KNPC(I)*G(I)/((TGAS**0.5)*TEMP)
      DO 50 I=1,32
      II=I+1
      DO 50 J=II,32
      EKN=(E(J)-E(I))/8064.
      WKN=EKN/TG
      BONT=1.0/(1.0+(2.7414E-04/WKN)**2)
      BONT=BONT*(1.0+(2.0/WKN))
      BONT1=FFP(I,J)/(EKN**2)
      BONT1=BONT1*(TGAS**0.5)
      BONT2=BONT*BONT1*EXP(-WKN)
      KNPQ(I,J)=5.2262E-14*BONT2
      KNPQ(J,I)=KNPQ(I,J)*EXP(WKN)*G(I)/G(J)
50    CONTINUE
      RETURN
      END
C
C..... Subroutine HEII calculates energies, weight factors, electron
C      impact excitation, deexcitation, ionization rate coeffs., and
C      Saha eq. population densities of HeII levels. Input parameters are:
C      TE = Electron temperature
C      E = Energies of levels
C      G = Weight factors
C      APO = Transition probabilities
C      DEF1-DEF5 = Optical escape factors for HeII transitions
      SUBROUTINE HEII(TE,E,G,APO,KPO,KPC,NP,NO,KPOSUM,APOSUM,DEF1,
     1DEF2,DEF3,DEF4,DEF5)
      DIMENSION A(15),E(15),G(15),KPO(15,15),APO(15,15),KPC(15),NP(15),
     1NO(15),FPO(15,15),GPO(15,15),APOSUM(15),KPOSUM(15),F(15),DEF(10)
      REAL KPO,KPC,NP,NO,KPOSUM,IP      ,NC
      ZZ=4.0
      DEGREE=1000.0
      N=15
      TEMP=11600.0*TE
      DO 1 I=1,N
      KPC(I)=0.0
      DO 1 J=1,N
```

```
      APO(I,J)=0.0
      FPO(I,J)=0.0
      KPO(I,J)=0.0
      GPO(I,J)=0.0
    1 CONTINUE
      R=109677.0
      E(1)=109331.0
      DO 5 I=2,N
      P=I
    5 E(I)=ZZ*R*(1.0-(1.0/(P*P)))+E(1)
      DO 10 I=1,N
      P=I
      G(I)=2.0*P*P
   10 A(I)=E(I)/8064.0
      EI=ZZ*R+E(1)
      AI=EI/8064.0
      DO 50 I=1,N
      AL=(AI-A(I))/TE
   50 KPC(I)=1.4E-05*G(I)*EXP(-AL)/(ZZ*(TEMP**0.5))
      DO 70 I=1,N
      CON=4.142500E-16/(TEMP**1.5)
      IP=(AI-A(I))/TE
      NP(I)=G(I)*CON*EXP(IP)/2.0
      NP(I)=NP(I)*1.0E+10
   70 NO(I)=NP(I)
      BON=8.0*3.14*3.14*4.803*4.803/27.324
      BON =BON*1.09677*1.09677*1.0E+08
      BX1=64.0/(3.0*SQRT(3.0)*4.0*ATAN(1.0))
      DO 90 J=1,N
      DO 95 I=J,N
      P=I
      Q=J
      IF(I.EQ.J) GO TO 95
      AX1=(P*Q)**2/(P*P-Q*Q)
      GPO(I,J)=1.0-0.1728*((1.0/AX1)**0.3333)*((2.0/(Q*Q))*AX1-1.0)
      GPO(J,I)=GPO(I,J)
      FPO(I,J)=BX1*(1.0/(2.0*(Q*Q)))*(AX1**3)+GPO(I,J)/((P*Q)**3)
      FPO(J,I)=FPO(I,J)
      APO(I,J)=(Q/P)**2*(1.0/AX1)*BON*FPO(I,J)*ZZ*ZZ*0.7
      APO(J,I)=APO(I,J)
   95 CONTINUE
   90 CONTINUE
C
C...... For optically thin case following five statements should be removed
      APO(2,1)=APO(2,1)*OEF1
      APO(3,1)=APO(3,1)*OEF2
      APO(4,1)=APO(4,1)*OEF3
      APO(5,1)=APO(5,1)*OEF4
      APO(6,1)=APO(6,1)*OEF5
      DO 55 I=1,N
      DO 56 J=I,N
      P=I
      Q=J
      AL=(A(J)-A(I))/TE
      IF(I.EQ.J) GO TO 56
      KPO(I,J)=4.75E-05*P*P*Q*Q*EXP(-AL)/(Q*Q-P*P)
      KPO(I,J)=KPO(I,J)*FPO(I,J)/(ZZ*(TEMP**0.5))
   56 CONTINUE
   55 CONTINUE
      DO 80 J=1,N
      DO 80 I=1,J
   80 KPO(J,I)=KPO(I,J)*NP(I)/NO(J)
      DO 460 I=1,N
      SUM=0.0
      DO 470 J=1,N
      IF(I.EQ.J) GO TO 470
      SUM=SUM+KPO(I,J)
  470 CONTINUE
  460 KPOSUM(I)=SUM
      DO 480 I=1,N
      SUM=0.0
      DO 490 J=1,I
      SUM=SUM+APO(I,J)
  490 CONTINUE
  480 APOSUM(I)=SUM
      RETURN
```

```fortran
                END

C......    Subroutine DEFAC calculates optical escape factors. Input
C          parameters are:
C          P = Number of level
C          T = Gas temperature
C          NC = Electron density
C          WL = Wave length
C          OS = Oscillator strength
C          XN = Ground state population density
          SUBROUTINE DEFAC(P,T,NC,WL,XN,OS,OPF)
          REAL NC
          PI=3.14593
          XL=0.01
          ALP=3.72E-22*NC*(P**3)*(P-1.0)/(SQRT(T)*WL)
          BRA1=(SQRT(PI))*(1.0+(PI*(ALP*ALP)))
          BRA2=ALP/BRA1
          BRA3=1.0-BRA2
          BRA=BRA3/BRA1
          TO=4.11E-06*XN*XL*OS*WL*BRA/(SQRT(T))
          TO1=1.0+(TO/(2.0+TO**2))
          TO2=TO1/(1.0+SQRT(PI*TO))
          IF (ALP.GT.3.0) GO TO 10
          TO3=ALP*TO*100.0
          TO4=TO3/(1.0+100.0*(SQRT(ALP)*TO+ALP*SQRT(TO)))
          TO5=1.0-(ALP/(SQRT(PI)*(1.0+PI*ALP**2)))
          TO6=TO5/SQRT(PI*(1.0+PI*ALP**2))
          TO7=SQRT(PI*TO6)
          TO8=TO7*TO4*TO2
          TO9=TO1/(1.0+TO*SQRT(PI*ALOG(1.0+TO)))
          OPF=TO9+TO8
          GO TO 11
10        OPF=TO2
C     11  IF(OPF.GT.1) OPF=1.0
11        RETURN
          END
```

APPENDIX V

SUBROUTINE TO SOLVE THE LINEAR SYSTEM OF COUPLED FIRST-ORDER
DIFFERENTIAL EQUATIONS

```
C.......................................................................
C
C       Subroutine HPCL, taken from IBM Subroutine Package, solves a system
C       of first order differential equations by Hamming's predictor corrector
C       method. As this method is not self starting, the starting values
C       are calculated by a special Runge-Kutta method. The input
C       parameters are as follows:
C       PRMT(1) = Lower bound of the interval
C       PRMT(2) = Upper bound of the interval
C       PRMT(3) = Initial increment of the independent variable
C       PRMT(4) = Upper error bound
C       Y = Input vector of initial values. Later on array Y contains
C           the values of dependent variables calculated at intermediate
C           point X.
C       DERY = Vector of error weights. Later on DERY contains the values
C              of derivatives
C       NDIM = Number of equations in the system
C       AFCT = An external subroutine which computes the matrix of
C              dimension NDIM X NDIM at given values of independent variable
C       FCT = An external subroutine to compute the vector on the right
C             right hand side of the system at given values of independent
C             variable.
C       OUTP = An external subroutine which prints the calculated values
C              at given values of independent variable.
C.......................................................................
C
        SUBROUTINE HPCL(PRMT,Y,DERY,NDIM,IHLF,AFCT,FCT,OUTP,AUX,A)
        DIMENSION PRMT(1),Y(1),DERY(1),AUX(16,1),A(1)
        NL1=1
C
C       NL2 stands for the number of steps after which the results are
C       desired to be printed
        NL2=25
        GO TO 100
1       CALL AFCT(X,A)
        CALL FCT(X,DERY)
        DO 3 M=1,NDIM
        LL=M-NDIM
        HS=0.0
        DO 2 L=1,NDIM
        LL=LL+NDIM
2       HS=HS+A(LL)*Y(L)
3       DERY(M)=HS+DERY(M)
        GO TO(105,202,204,206,115,122,125,308,312,327,329,128),ISW2
100     N=1
        IHLF=0
        X=PRMT(1)
        H=PRMT(3)
        PRMT(5)=0.0
        DO 101 I=1,NDIM
        AUX(16,I)=0.
        AUX(15,I)=DERY(I)
101     AUX(1,I)=Y(I)
        IF(H*(PRMT(2)-X))103,102,104
102     IHLF=12
        GO TO 104
103     IHLF=13
104     ISW2=1
        GO TO 1
105     NL1=NL2
        CALL OUTP(X,Y,DERY,IHLF,NDIM,PRMT,NL1,NL2)
        IF(NL1.EQ.NL2) NL1=1
        IF(PRMT(5))107,106,107
106     IF(IHLF)108,108,107
107     RETURN
108     DO 109 I=1,NDIM
109     AUX(8,I)=DERY(I)
        ISW1=1
        GO TO 200
110     X=X+H
        DO 111 I=1,NDIM
111     AUX(2,I)=Y(I)
112     IHLF=IHLF+1
        X=X-H
```

```
113       AUX(4,I)=AUX(2,I)
          T=0.5*H
          I=1
          ISW1=2
          GO TO 200
114       X=X+T
          ISW2=5
          GO TO 1
115       N=2
          DO 116 I=1,NDIM
          AUX(2,I)=Y(I)
116       AUX(9,I)=DERY(I)
          ISW1=3
          GO TO 200
117       DELT=0.0
          DO 118 I=1,NDIM
118       DELT=DELT+AUX(15,I)*ABS(Y(I)-AUX(4,I))
          DELT=0.06666667*DELT
          IF(DELT-PRMT(4))121,121,119
119       IF(IHLF-10)112,120,120
120       IHLF=11
          X=X+H
          GO TO 104
121       X=X+H
          ISW2=6
          GO TO 1
122       DO 123 I=1,NDIM
          AUX(3,I)=Y(I)
123       AUX(10,I)=DERY(I)
          N=3
          ISW1=4
          GO TO 200
124       N=1
          X=X+H
          ISW2=7
          GO TO 1
125       X=PRMT(1)
          DO 126 I=1,NDIM
          AUX(11,I)=DERY(I)
126    0Y(I)=AUX(1,I)+H*(0.375*AUX(8,I)+0.7916667*AUX(9,I)
          1-0.2083333*AUX(10,I)+0.04166667*DERY(I))
127       X=X+H
          N=N+1
          ISW2=12
          GO TO 1
128       NL1=NL1+1
          CALL OUTP(X,Y,DERY,IHLF,NDIM,PRMT,NL1,NL2)
          IF(NL1.EQ.NL2) NL1=1
          IF(PRMT(5))107,129,107
129       IF(N-4)130,300,300
130       DO 131 I=1,NDIM
          AUX(N,I)=Y(I)
131       AUX(N+7,I)=DERY(I)
          IF(N-3)132,134,300
132       DO 133 I=1,NDIM
          DELT=AUX(9,I)+AUX(9,I)
          DELT=DELT+DELT
133       Y(I)=AUX(1,I)+0.3333333*H*(AUX(8,I)+DELT+AUX(10,I))
          GO TO 127
134       DO 135 I=1,NDIM
          DELT=AUX(9,I)+AUX(10,I)
          DELT=DELT+DELT+DELT
135       Y(I)=AUX(1,I)+0.375*H*(AUX(8,I)+DELT+AUX(11,I))
          GO TO 127
200       Z=X
          DO 201 I=1,NDIM
          X=H*AUX(N+7,I)
          AUX(5,I)=X
201       Y(I)=AUX(N,I)+0.4*X
          X=Z+0.4*H
          ISW2=2
          GO TO 1
202       DO 203 I=1,NDIM
          X=H*DERY(I)
          AUX(6,I)=X
203       Y(I)=AUX(N,I)+0.2969776*AUX(5,I)+0.1587596*X
          X=Z+0.4557372*H
          ISW2=3
          GO TO 1
204       DO 205 I=1,NDIM
          X=H*DERY(I)
          AUX(7,I)=X
205       Y(I)=AUX(N,I)+0.2181004*AUX(5,I)-3.050965*AUX(6,I)+3.832865*X
          X=Z+H
          ISW2=4
          GO TO 1
206       DO 207 I=1,NDIM
207    0Y(I)=AUX(N,I)+0.1747603*AUX(5,I)-0.5514807*AUX(6,I)
```

```
              X=7
              GO TO(113,115,117,121),ISW1
300           ISTEP=3
301           IF(J-8)314,322,304
302           DO 303 N=2,7
              DO 303 I=1,NDIM
              AUX(N-1,I)=AUX(N,I)
303           AUX(N+6,I)=AUX(N+7,I)
              I=7
304           N=I+1
              DO 305 I=1,NDIM
              AUX(N-1,I)=Y(I)
305           AUX(N+6,I)=DERY(I)
              X=X+H
306           ISTEP=ISTEP+1
              DO 307 I=1,NDIM
       ODELT=AUX(N-4,I)+1.333333*H*(AUX(N+6,I)+AUX(N+6,I)-AUX(N+5,I)+
      1AUX(N+4,I)+AUX(N+4,I))
              Y(I)=DELT-0.925b198*AUX(16,I)
307           AUX(16,I)=DELT
              ISW2=8
              GO TO 1
308           DO 309 I=1,NDIM
       ODELT=0.125*(9.0*AUX(N-1,I)-AUX(N-3,I)+3.*H*(DERY(I)+AUX(N+6,I)+
      1AUX(N+6,I)-AUX(N+5,I)))
              AUX(16,I)=AUX(16,I)-DELT
309           Y(I)=DELT+0.07438017*AUX(16,I)
              DELT=0.0
              DO 310 I=1,NDIM
310           DELT=DELT+AUX(15,I)*ABS(AUX(16,I))
              IF(DELT-PRMT(4))311,324,324
311           ISW2=9
              GO TO 1
312           NL1=NL1+1
              CALL OUTP(X,Y,DERY,IHLF,NDIM,PRMT,NL1,NL2)
              IF(NL1.EQ.NL2) NL1=1
              IF(PRMT(5))314,313,314
313           IF(IHLF-11)315,314,314
314           RETURN
315           IF(H*(X-PRMT(2)))316,314,314
316           IF(ABS(X-PRMT(2))-0.1*ABS(H))314,317,317
317           IF(DELT-0.02*PRMT(4))318,318,301
318           IF(IHLF)301,301,319
319           IF(N-7)301,320,320
320           IF(ISTEP-4)301,321,321
321           IMOD=ISTEP/2
              IF(ISTEP-IMOD-IMOD)301,322,301
322           H=H+H
              IHLF=IHLF-1
              ISTEP=0
              DO 323 I=1,NDIM
              AUX(N-1,I)=AUX(N-2,I)
              AUX(N-2,I)=AUX(N-4,I)
              AUX(N-3,I)=AUX(N-6,I)
              AUX(N+6,I)=AUX(N+5,I)
              AUX(N+5,I)=AUX(N+3,I)
              AUX(N+4,I)=AUX(N+1,I)
              DELT=AUX(N+6,I)+AUX(N+5,I)
              DELT=DELT+DELT+DELT
323    0AUX(16,I)=8.962963*(Y(I)-AUX(N-3,I))-3.361111*H*(DERY(I)+DELT
      1+AUX(N+4,I))
              GO TO 301
324           IHLF=IHLF+1
              IF(IHLF-10)325,325,311
325           H=0.5*H
              ISTEP=0
              DO 326 I=1,NDIM
       0Y(I)=0.00390625*(80.*AUX(N-1,I)+135.*AUX(N-2,I)+40.*AUX(N-3,I)+
      1AUX(N-4,I))-.1171875*(AUX(N+6,I)-6.*AUX(N+5,I)-AUX(N+4,I))*H
       0AUX(N-4,I)=.00390625*(12.*AUX(N-1,I)+135.*AUX(N-2,I)+
      108.*AUX(N-3,I)+AUX(N-4,I))-.0234375*(AUX(N+6,I)+18.*AUX(N+5,I)
      2-9.*AUX(N+4,I))*H
              AUX(N-3,I)=AUX(N-2,I)
326           AUX(N+4,I)=AUX(N+5,I)
              DELT=X-H
              X=DELT-(H+H)
              ISW2=10
              GO TO 1
327           DO 328 I=1,NDIM
              AUX(N-2,I)=Y(I)
              AUX(N+5,I)=DERY(I)
328           Y(I)=AUX(N-4,I)
              X=X-(H+H)
              ISW2=11
              GO TO 1
329           X=DELT
              DO 330 I=1,NDIM
              DELT=AUX(N+5,I)+AUX(N+4,I)
```

```
      0AUX(15,1)=2.962963*(AUX(N+10,1))-3.361111*H*(AUX(N+5,1)+DERI
      1+DERV(T))
330   AUX(N+3,T)=DERV(T)
      GO TO 305
      END
```

190